

# **Water balance and productivity of a Mediterranean oak woodland**

**Quantifying understory vegetation impacts by development of a  
stable oxygen isotope partitioning approach**



Dissertation

zur Erlangung des Grades Doktor der Naturwissenschaften (Dr. rer. nat.)  
an der Fakultät Biologie / Chemie / Geowissenschaften der Universität Bayreuth

vorgelegt von:

**Maren Dubbert**

Bayreuth, März 2014



Die vorliegende Arbeit wurde in der Zeit vom Januar 2010 bis zum März 2014 – in Bayreuth am Lehrstuhl für Agrarökosystemforschung und in Bielefeld am Lehrstuhl für Experimentelle Ökologie und Ökosystembiologie – unter der Betreuung von Frau Prof. Dr. Christiane Werner angefertigt.

Vollständiger Abdruck der von der Fakultät für Biologie, Chemie und Geowissenschaften der Universität Bayreuth genehmigten Dissertation zur Erlangung des akademischen Grades eines Doktors der Naturwissenschaften (Dr. rer. nat.).

Dissertation eingereicht: 12.3.2014

Zugelassen durch die Prüfungskommission: 19.3.2014

Wissenschaftliches Kolloquium: 25.7.2014

Amtierender Dekan: Prof. Dr. Rhett Kempe

1. Prof. Dr. Christiane Werner (Erstgutachterin)
2. Prof. John Tenhunen, Ph. D. (Zweitgutachter)
3. Prof. Dr. Ludwig Zöller (Vorsitz)
4. Prof. Dr. Bernd Huwe





## TABLE OF CONTENTS

TABLE OF CONTENTS.....	I
ACKNOWLEDGEMENTS .....	X
LIST OF FIGURES .....	XII
LIST OF TABLES .....	XIX
ABBREVIATIONS .....	XXI
SUMMARY .....	XXII
ZUSAMMENFASSUNG .....	XXIV
EXTENDED SUMMARY .....	1
1. VEGETATION AND DROUGHT EFFECTS ON WATER BALANCE AND ITS IMPACT ON CARBON GAIN IN SEMI-ARID ECOSYSTEMS .....	3
2. OBJECTIVES OF THE PRESENT WORK .....	5
3. STUDY SITE AND EXPERIMENTAL DESIGN .....	9
4. MAIN RESULTS OF THIS THESIS .....	11
4.1. VALIDATION OF OXYGEN ISOTOPE MODELING APPROACHES ( <i>STUDY I, II, V</i> ).....	11
4.2. IMPACT OF SCALE HETEROGENEITY DUE TO SPARSE TREE COVER ON UNDERSTORY VEGETATION DYNAMICS AND FLUXES ( <i>STUDY III, IV</i> ) .....	13
4.3. IMPACT OF THE HERBACEOUS LAYER ON ECOSYSTEM WATER BUDGET, INFILTRATION CAPACITY AND PRODUCTIVITY ( <i>STUDY IV, V</i> ) .....	15
4.4. EFFECTS OF EXTREME DROUGHT ON ECOSYSTEM CARBON GAIN, CORK-OAK AND HERBACEOUS LAYER DEVELOPMENT ( <i>STUDY VI, VII</i> ).....	18
4.5. CONCLUSIONS.....	21
5. LITERATURE .....	22
6. STUDY OVERVIEW, PUBLICATION STATUS AND CONTRIBUTIONS.....	26
CUMULATIVE STUDIES .....	31
1. STUDY I: OXYGEN ISOTOPE SIGNATURES OF TRANSPIRED WATER VAPOR – THE ROLE OF ISOTOPIC NON-STEADY-STATE TRANSPIRATION UNDER NATURAL CONDITIONS .....	33
1.1. SUMMARY .....	34

## Table of Contents

---

1.2.	INTRODUCTION .....	35
1.3.	MATERIALS AND METHODS .....	37
1.3.1.	STUDY SITE .....	38
1.3.2.	ENVIRONMENTAL VARIABLES .....	38
1.3.3.	CRDS BASED MEASUREMENTS .....	39
1.3.4.	MEASUREMENT OF THE ISOTOPIC COMPOSITION OF XYLEM WATER .....	40
1.3.5.	CALCULATION OF ISOTOPIC SIGNATURES .....	41
1.3.6.	STATISTICAL ANALYSIS.....	43
1.4.	RESULTS AND DISCUSSION.....	43
1.4.1.	ISOTOPIC NON-STEADY-STATE TRANSPIRATION UNDER NATURAL CONDITIONS AND COMPARISON WITH MODELED $\Delta_T$ .....	44
1.4.2.	RELATIONSHIP BETWEEN $\Delta_E - \Delta_C$ AND $\Delta_T$ AND IMPACT ON ATMOSPHERIC VAPOR .....	49
1.5.	ACKNOWLEDGEMENTS .....	53
1.6.	LITERATURE .....	53
1.7.	SUPPORTING INFORMATION .....	56
2.	STUDY II: PARTITIONING EVAPOTRANSPIRATION – TESTING THE CRAIG AND GORDON MODEL WITH FIELD MEASUREMENTS OF OXYGEN ISOTOPE RATIOS OF EVAPORATIVE FLUXES .....	59
2.1.	ABSTRACT.....	60
2.2.	ABBREVIATIONS .....	61
2.3.	INTRODUCTION .....	62
2.4.	THE CRAIG AND GORDON EQUATION .....	63
2.5.	MATERIALS AND METHODS .....	66
2.5.1.	STUDY SITE .....	66
2.5.2.	ENVIRONMENTAL VARIABLES .....	66
2.5.3.	SAMPLING AND MEASUREMENT OF $\Delta^{18}O_s$ .....	67
2.5.4.	CRDS BASED MEASUREMENTS OF $\Delta^{18}O_E$ AND UNDERSTORY $\Delta^{18}O_{ET}$ AND THEIR RESPECTIVE FLUXES .....	67

## Table of Contents

2.5.5.	ESTIMATION OF $\Delta^{18}\text{O}_E$ , $\Delta^{18}\text{O}_E$ , AND $\Delta^{18}\text{O}_T$ AND FT .....	68
2.6.	RESULTS .....	71
2.6.1.	ENVIRONMENTAL CONDITIONS .....	71
2.6.2.	PROFILES OF SOIL TEMPERATURE, VOLUMETRIC WATER CONTENT AND $\Delta^{18}\text{O}$ .....	72
2.6.3.	MEASURED AND MODELED $\Delta^{18}\text{O}_E$ .....	74
2.6.4.	MEASURED $\Delta^{18}\text{O}$ OF EVAPOTRANSPIRATION .....	75
2.6.5.	CALCULATING $\Delta^{18}\text{O}_E$ AND $\Delta^{18}\text{O}_T$ FOR VEGETATION PLOTS .....	77
2.6.6.	CALCULATING THE CONTRIBUTION OF T TO ET .....	78
2.7.	DISCUSSION .....	78
2.7.1.	$\Delta^{18}\text{O}_E$ AND UNCERTAINTIES IN REGARD TO CHANGES IN $\Delta^{18}\text{O}_E$ , TEMPERATURE AND $A_K$ .....	78
2.7.2.	MODELING $\Delta^{18}\text{O}_E$ , $\Delta^{18}\text{O}_E$ AND $\Delta^{18}\text{O}_T$ ON VEGETATION PLOTS .....	83
2.7.3.	PARTITIONING EVAPOTRANSPIRATION .....	84
2.8.	CONCLUSIONS .....	87
2.9.	ACKNOWLEDGEMENTS .....	87
2.10.	LITERATURE .....	87
3.	STUDY III: INFLUENCE OF WOODY TISSUE AND LEAF CLUMPING ON VERTICALLY RESOLVED LEAF AREA INDEX AND ANGULAR GAP PROBABILITY ESTIMATES .....	91
3.1.	ABSTRACT .....	92
3.2.	INTRODUCTION .....	93
3.3.	MATERIALS AND METHODS .....	95
3.3.1.	THEORY .....	95
3.3.2.	SITE DESCRIPTION .....	99
3.3.3.	SAMPLING DESIGN AND MEASUREMENTS .....	99
3.3.4.	DATA PROCESSING AND ANALYSIS .....	100
3.4.	RESULTS AND DISCUSSION .....	102
3.4.1.	LAI-2000 BAD READINGS HANDLING .....	102
3.4.2.	GAP PROBABILITY DISTRIBUTION .....	104
3.4.3.	LEAF PROJECTION FUNCTION .....	106

## Table of Contents

3.4.4.	CLUMPING INDEX .....	107
3.4.5.	CUMULATIVE LEAF AREA INDEX HEIGHT DISTRIBUTION .....	109
3.4.6.	INFLUENCE OF VIEW ANGLE SPAN ON DCP RESULTS .....	111
3.4.7.	EXCLUSION OF WOODEN TISSUE .....	112
3.4.8.	AUXILIARY DATA DERIVED HEIGHT DISTRIBUTIONS.....	114
3.5.	CONCLUSIONS.....	115
3.6.	ACKNOWLEDGEMENTS .....	116
3.7.	APPENDIX A: NOMENCLATURE .....	117
3.8.	APPENDIX B: IMAGE OBJECT CLASSIFICATION CRITERIA.....	118
3.9.	REFERENCES.....	119
4.	STUDY IV: INFLUENCE OF TREE COVER ON HERBACEOUS LAYER DEVELOPMENT AND CARBON AND WATER FLUXES IN A PORTUGUESE CORK-OAK WOODLAND .....	125
4.1.	ABSTRACT.....	126
4.2.	INTRODUCTION .....	127
4.3.	MATERIALS AND METHODS .....	129
4.3.1.	STUDY SITE .....	129
4.3.2.	ENVIRONMENTAL PARAMETERS .....	130
4.3.3.	VEGETATION COVER AND ABOVEGROUND BIOMASS.....	131
4.3.4.	SOIL NITRATE CONTENT .....	131
4.3.5.	GAS-EXCHANGE MEASUREMENTS.....	132
4.3.6.	STATISTICAL ANALYSIS.....	133
4.4.	RESULTS .....	133
4.4.1.	DEVELOPMENT OF MICROCLIMATIC CONDITIONS AND SOIL NITRATE CONTENT .....	133
4.4.2.	HERBACEOUS LAYER SPECIES DISTRIBUTION AND ABOVEGROUND BIOMASS.....	135
4.4.3.	HERBACEOUS LAYER EVAPOTRANSPIRATION, WATER LOSS IN THE SOIL AND TOTAL CONDUCTANCE .....	138
4.4.4.	NET CO <sub>2</sub> EXCHANGE OF THE HERBACEOUS LAYER.....	140
4.5.	DISCUSSION.....	142

4.5.1.	INFLUENCE OF TREE COVER ON HERBACEOUS LAYER PRODUCTIVITY AND THE DEVELOPMENT OF DISTINCT FUNCTIONAL GROUPS .....	143
4.5.2.	COMPETITION FOR WATER DURING LATE SPRING BETWEEN HERBACEOUS LAYER AND TREES .....	145
4.6.	CONCLUSIONS.....	147
4.7.	ACKNOWLEDGEMENTS .....	147
4.8.	LITERATURE .....	148
5.	STUDY V: STABLE OXYGEN ISOTOPE AND FLUX PARTITIONING DEMONSTRATES UNDERSTORY OF AN OAK SAVANNA CONTRIBUTES UP TO HALF OF ECOSYSTEM CARBON AND WATER EXCHANGE .....	151
5.1.	ABSTRACT.....	152
5.2.	INTRODUCTION .....	153
5.3.	MATERIALS AND METHODS .....	155
5.3.1.	STUDY SITE AND EXPERIMENTAL DESIGN .....	155
5.3.2.	ENVIRONMENTAL VARIABLES AND HERBACEOUS BIOMASS .....	156
5.3.3.	EDDY-COVARIANCE MEASUREMENTS .....	157
5.3.4.	CAVITY RING-DOWN SPECTROMETER BASED MEASUREMENTS OF $\Delta^{18}\text{O}_\text{E}$ AND UNDERSTORY $\Delta^{18}\text{O}_\text{ET}$ , AND GAS-EXCHANGE FLUX MEASUREMENTS.....	158
5.3.5.	SAMPLING AND MEASUREMENT OF $\Delta^{18}\text{O}$ OF SOIL WATER AND PRECIPITATION.....	159
5.3.6.	CALCULATION OF $\Delta^{18}\text{O}$ OF SOIL EVAPORATION.....	160
5.3.7.	MODELING $\Delta^{18}\text{O}$ OF PLANT LEAF WATER AT THE EVAPORATING SITES AND TRANSPIRATION .....	161
5.3.8.	WATER AND CARBON PARTITIONING.....	162
5.3.9.	STATISTICAL ANALYSIS .....	163
5.4.	RESULTS .....	164
5.4.1.	ENVIRONMENTAL CONDITIONS AND NET ECOSYSTEM CARBON AND WATER FLUXES .....	164
5.4.2.	VEGETATION EFFECTS ON RAINFALL INFILTRATION .....	165
5.4.3.	SEASONAL DEVELOPMENT OF $\Delta^{18}\text{O}$ WITHIN THE ECOSYSTEM .....	166

---

5.4.4.	SEASONAL DEVELOPMENT OF HERBACEOUS ET AND NEE COMPONENTS .....	170
5.4.5.	CONTRIBUTION OF UNDERSTORY VEGETATION AND SOIL TO THE ECOSYSTEM CARBON AND WATER FLUXES .....	173
5.5.	DISCUSSION.....	174
5.6.	ACKNOWLEDGEMENTS .....	179
5.7.	LITERATURE .....	179
5.8.	SUPPORTING INFORMATION .....	185
6.	STUDY VI: EFFECTS OF AN EXTREME DRY WINTER ON <i>Q. SUBER</i> WOODLAND: NET ECOSYSTEM EXCHANGE AND TREE PHENOLOGY ADJUSTMENTS .....	191
6.1.	ABSTRACT.....	192
6.2.	INTRODUCTION .....	193
6.3.	MATERIAL AND METHODS.....	195
6.3.1.	SITE DESCRIPTION .....	195
6.3.2.	ENVIRONMENTAL PARAMETERS .....	195
6.3.3.	PHENOLOGICAL AND ECOPHYSIOLOGICAL MEASUREMENTS .....	196
6.3.4.	SOIL ANALYSIS .....	197
6.3.5.	ECOSYSTEM FLUX MEASUREMENTS .....	197
6.3.6.	DATA AND STATISTICAL ANALYSIS .....	198
6.4.	RESULTS .....	199
6.4.1.	METEOROLOGY AND SOIL WATER AVAILABILITY .....	199
6.4.2.	ECOSYSTEM CARBON FLUXES .....	201
6.4.3.	RADIATION USE EFFICIENCY .....	203
6.4.4.	TREE LEAF WATER POTENTIALS .....	204
6.4.5.	TREE LITTER FALL AND PHENOLOGICAL DEVELOPMENT .....	205
6.4.6.	LEAF AREA INDEX .....	206
6.4.7.	TREE DIAMETER INCREMENT .....	207
6.5.	DISCUSSION.....	208
6.5.1.	ECOSYSTEM CARBON FLUXES AND SEASONAL PATTERNS .....	208

## Table of Contents

---

6.5.2.	EXTREME DRY WINTER EFFECTS ON CARBON FLUXES .....	210
6.5.3.	EXTREME DRY WINTER EFFECTS IN TREE GROWTH AND PHENOLOGY .....	212
6.5.4.	CONCLUSION .....	215
6.6.	ACKNOWLEDGEMENTS .....	215
6.7.	REFERENCES.....	215
7.	STUDY VII: DROUGHT IMPACT ON CARBON AND WATER CYCLING IN A MEDITERRANEAN <i>QUERCUS SUBER</i> L. WOODLAND DURING THE EXTREME DROUGHT EVENT IN 2012 .....	221
7.1.	ABSTRACT.....	222
7.2.	INTRODUCTION .....	223
7.3.	MATERIAL AND METHODS .....	225
7.3.1.	SITE DESCRIPTION .....	225
7.3.2.	CLIMATE CONDITIONS.....	226
7.3.3.	OVERSTOREY TOWER EDDY COVARIANCE MEASUREMENTS .....	226
7.3.4.	UNDERSTOREY TOWER EDDY COVARIANCE MEASUREMENTS .....	227
7.3.5.	SOIL TEMPERATURE AND MOISTURE .....	228
7.3.6.	DATA TREATMENT.....	228
7.3.7.	PHOTOSYNTHESIS AND STOMATAL CONDUCTANCE MODELLING .....	229
7.4.	RESULTS AND DISCUSSION.....	230
7.4.1.	METEOROLOGICAL AND ENVIRONMENTAL CONDITIONS .....	230
7.4.2.	DROUGHT INUENCE ON ECOSYSTEM WATER BALANCE.....	233
7.4.3.	UNDERSTOREY GROWTH INHIBITION.....	235
7.4.4.	ECOSYSTEM PRODUCTIVITY REDUCTION .....	236
7.4.5.	NET ECOSYSTEM CARBON EXCHANGE REDUCTION.....	238
7.4.6.	DROUGHT IMPACT ON TREE PHYSIOLOGY .....	239
7.4.7.	FUTURE DEVELOPMENT .....	245
7.5.	CONCLUSIONS.....	246
7.6.	APPENDIX A – NOMENCLATURE.....	247
7.7.	APPENDIX B PHOTOSYNTHESIS MODEL .....	248

## Table of Contents

---

7.8.	ACKNOWLEDGEMENTS.....	251
7.9.	REFERENCES.....	252
	CURRICULUM VITAE AND PUBLICATIONS .....	I
	DECLARATION .....	VII





## **ACKNOWLEDGEMENTS**

Many thanks go to all the people who supported me throughout this dissertation.

First of all I would like to thank Christiane for her personal and scientific support from my very first scientific steps throughout this dissertation. She has always provided me with a great working environment and sent me out into the world, enabling my Portuguese adventures and numerous conference trips. I cannot imagine a better mentor.

Matthias for trying to teach me some fundamental theoretical background, the great atmosphere he brought into this project and also for the laser! I really appreciate the patience he had with my excel sheets.

Prof. Joao Santos Pereira for allowing me access to his labs and field equipment, providing the field site and for his contribution to this project.

Arndt for the great company and moral support throughout all the stages of this project. It still amazes me how calm he stays when everything falls apart! The only things killing his patience are unprofessional electrical installations.

Stephan for his help with field site installations and language issues and for his moral support in the cursed first year!

The DFG (WATERFLUX Project: # WE 2681/6-1; # CU 173/2-1) and DAAD for financial support of this project.

Many thanks to all co-authors of manuscripts contained in this dissertation for the collaborative effort!

In Portugal: I would specifically like to thank Alexandra, Filipe, Rodrigo, Marjan, Stephan, Fabio, Patricia, and Jan for their company in Portugal and their assistance in the field and lab; the Ferreira family at Herdade da Machoqueira for help with field site establishment, technical support and

especially for repairing my tires! Also many thanks go to Cristina for access to her labs and ecophysiological equipment. Also for the car until it finally expired after a very long life.

In Bielefeld: thanks go to Katrin, Ingo, Stephan, Freddy, Katie, Tine, and Alex for the great times inside and outside the office in Bielefeld. Prof. Beyschlag and the Experimental and Systems Ecology group for the great working surroundings and atmosphere in Bielefeld. Special thanks to Babsi and Elke for night time measurements and keeping my plants healthy. And to Tom for allowing me near continuous access to the old and new transporter!

In Bayreuth: The Michi's and Mario for including me into the family in Bayreuth! It meant a lot. The entire AgroEcosystem Research group and associates for the great atmosphere in the working group. Especially to Ilse, because she is the soul of this working group and tolerates the chaos I create in her store rooms.

My friends, especially Sabrina and Chrissie for their unwavering moral support regardless of the situation, the long nights and their friendship since a very long time!

My mom and dad and also my brother Flo, who supported me both morally and financially since my childhood and never stopped believing in me. Without your love, this would never have been possible!

Finally, David for his unwavering love and support and for moving to Bayreuth to end those endless travels! You were celebrating all the highs with me and comforted me through all the lows of the past two years and I cannot say how much it means to me!

## LIST OF FIGURES

### Extended summary

**Figure 1:** a) Satellite image of the study site (© Google Maps, 2011) with 1 position of the experimental understory sites; 2 position of the ecosystem tower and 3 position of the understory tower. b, c) Picture of the open and tree site, respectively and d, e) vegetation and bare soil plots.

**Figure 2:** Schematic overview of the experimental setup for measuring soil evaporation and understory evapotranspiration and its isotopic composition in the field. Insets 13 show pictures of the chamber and laser spectrometer (L2120-i, Picarro, Santa Clara, USA).

**Figure 3:** a) Oxygen isotope signatures of soil evaporation on bare soil plots calculated with the Craig and Gordon equation versus measured values for the open (white circles) and tree site (black circles) of every measurement point (mean values  $\pm$  SD;  $n=3$ ), the grey and black line denote regression lines for the open and tree site, respectively (adapted from Dubbert *et al.*, 2014c, see also Dubbert *et al.*, 2013).

**Figure 4:** Diel measurements in spring (a-c), summer (d-f) and fall (g-i) of the oxygen isotope signature of transpired vapor ( $\delta^{18}O_T$ , black circles,  $n=3$ , mean values  $\pm$  SE) and modeled  $\delta^{18}O_T$  (red lines). Grey squares show measured oxygen isotope signatures of ambient air and grey triangles indicate  $\delta^{18}O$  of source water, i.e. xylem (from Dubbert *et al.*, 2014a).

**Figure 5:** a-h) Relative vegetation cover in % of distinct functional groups of the herbaceous layer (Poaceae, N-fixing and other forbs) in spring and fall 2011 on the open (a-e) and tree site (f-h; mean values;  $n=5$ ). From Dubbert *et al.*, 2014b.

**Figure 6:** Dependency of gap probability  $P_{gap}$  on zenith view angle  $\theta$ . Black symbols: DCP method at 3, 6 and 8 m height. Grey symbols: LAI-2000 method at 3 m height (6 and 8 m heights not shown). Solid lines: Beer's law with effective leaf area index  $L_e$ . Dashed lines: Beer's law with angular dependent leaf clumping  $\Omega(\theta)$  (see chapter III). From Piayda *et al.*, under review Ecology.

**Figure 7:** Daytime integrated net understory  $CO_2$  exchange ( $NEE$ ,  $g\ C\ m^{-2}\ d^{-1}$ , white circles; mean values  $\pm$  SE,  $n=3$ ), herbaceous gross primary production ( $GPP$ , dashed green line, mean values,  $n=3$ ) and respiration ( $R$ , blue line and circles, mean values,  $n=3$ ) on the open (a-d) and tree site (e-h); daytime integrated understory evapotranspiration ( $ET$ ,  $mm\ d^{-1}$ , mean values  $\pm$  SD,  $n=3$ ), which is the sum of herbaceous layer transpiration ( $T$ , green bars) and soil evaporation ( $E$ , blue bars) at the open (i-l) and tree site (m-p). Adapted from Dubbert *et al.*, 2014c.

**Figure 8:** a) Daytime integrated ecosystem evapotranspiration ( $ET$ , sum of the stacked bars) and its components cork-oak transpiration ( $T_o$ , dark green), herbaceous transpiration ( $T_u$ , green) and soil evaporation ( $E$ , blue, all  $mm\ d^{-1}$ ). b) Daytime integrated  $GPP$  of cork-oaks ( $GPP_o$ , dark green) and understory ( $GPP_u$ , green), ecosystem respiration ( $R_{eco}$ ; blue), and net ecosystem  $CO_2$  exchange ( $NEE$ , black squares, all in  $g\ C\ m^{-2}\ d^{-1}$ ). From Dubbert *et al.*, 2014c.

**Figure 9:** Rainfall and infiltration into the soil following rain events  $> 2\ mm$  at a, b) the open and c, d) tree site on understory plots (green circles), bare soil plots (blue circles, all in  $mm\ d^{-1}$ ;  $n=4$ , mean values  $\pm$  SE) and rainfall (grey bars). Insets present differences in infiltration between understory and bare soil versus rain amount at the open and tree site. Regression line, coefficient of regression and p-value are given. From Dubbert *et al.*, 2014c.

**Figure 10:** a) Ecosystem net carbon exchange ( $NEE_o$ ), b) ecosystem gross primary production ( $GPP_o$ ) and c) understory gross primary production ( $GPP_u$ ) for 2011 (black) and 2012 (grey). Dots mark daily sums, lines are kernel regressions. a) Ecosystem evapotranspiration  $ET_o$  and b) understory evapotranspiration  $ET_u$  for 2011 (black) and 2012 (grey). Dots mark daily sums, lines are kernel regressions. Adapted from Piayda *et al.*, 2014.

**Figure 11:** Tree diameter increment (mm) during 2011 and 2012. Values are means  $\pm$  se (n=9). From Costa e Silva *et al.*, under review in AFM.

### Study I

**Figure 1:** a) Schematic overview and pictures of the experimental setup for measuring leaf transpiration, its isotopic composition and micrometeorological parameters within the chamber in the field.

**Figure 2:** Environmental conditions and ecophysiological parameters observed with the chamber setup in late spring (a-c), late summer (d-f) and fall (g-i; date format: day.month.year): relative humidity corrected to leaf temperature ( $h$ , [%], black lines), leaf temperature ( $^{\circ}\text{C}$ ], dashed grey lines), transpiration rate ( $E$ , [ $\text{mmol m}^{-2} \text{s}^{-1}$ ], n=3, mean  $\pm$  SE, green circles), and total leaf conductance ( $g_{\text{tw}}$ , [ $\text{mmol m}^{-2} \text{s}^{-1}$ ], black circles).

**Figure 3:** Measurements in spring (a-c), summer (d-f) and fall (g-I; date format: day.month.year) of the oxygen isotope signatures of transpired vapor ( $\delta_E$ , black circles, n=3, mean values  $\pm$  SE) and modeled  $\delta_E$  considering non-steady state with varying observed leaf water volume  $V_m$  and  $\alpha_k$  between 1.018 and 1.0265 (grey uncertainty band). The dark grey uncertainty band indicates modeled  $\delta_E$  with  $\alpha_k = 1.018$  and varying leaf temperature from observed values to  $+6^{\circ}\text{C}$ . The solid red line is modeled  $\delta_E$  with constant leaf water volume  $V_m$  of the observed mean value and  $\alpha_k = 1.018$ . Grey squares show measured oxygen isotope signatures of ambient air and white triangles are oxygen isotope signatures of xylem (n=3, mean values  $\pm$  SE). Please note different scales for positive and negative values..

**Figure 4:** Diurnal cycles of modeled and measured oxygen isotope signatures of leaf mesophyll water ( $\delta_m$ ; a) and modeled versus measured  $\delta_m$  (b) on 4.6. (circles; black line); 6.6. (up triangles; black dotted line); 10.6. (squares; black dashed line) and 11.11.2011 (down triangles; grey line).

**Figure 5:** Modeled oxygen isotope signatures of transpiration and observed oxygen isotope signatures of xylem (grey dotted line; n=3, mean values) at June 4 (a), September 18 (b) and November 11 (c; date format: day.month.year). Red lines indicate modeled  $\delta_E$  with observed leaf water residence time (see Fig. 2), black dotted and solid lines are  $\delta_E$  with  $\frac{1}{2}$  and  $\frac{1}{4}$  of the observed leaf water residence time and black dashed lines are  $\delta_E$  with twice the observed leaf water residence time.

**Figure 6:** Spring (a, d), summer (b, e) and fall (c, f) deviations of the oxygen isotope signature of transpired vapor from xylem water ( $\Delta_E$ , [‰]) against deviation of leaf water isotopic composition at the evaporating sites from isotopic steady-state ( $\Delta_e - \Delta_C$ , [‰]; a-c), and against  $\Delta_e - \Delta_C$  amplified by  $1/(1-h)$  (d-f). The black lines indicate significant linear regressions and dashed black lines the 95% confident bands. The 1:1 line is indicated in black; coefficients of determination  $R^2$  and significance level  $p$  are shown inside the plots.

**Figure 7:** Isoforcing of transpiration on the atmosphere [ $I_E$ ;  $\text{mol m}^{-2} \text{s}^{-1} \text{‰}$ ] for each measurement day assuming isotopic steady-state (ss, black solid lines) or non-steady-state (nss, red dashed lines). Nighttime transpiration rates and conductances were taken from Dawson *et al.* (2007). 24h means  $\pm$  SE are given for each measurement day (date format: day.month.year); errors were calculated from bootstrap re-sampling.

**Figure S1:** Concentration dependencies of the Cavity Ring-Down Spectrometer at six different oxygen (a) and deuterium (b) isotopic signatures. Each sample with distinct signature (I-VI; see Table S1) was measured from 5000 to 30000 ppmv  $\text{H}_2\text{O}$  concentration.

**Figure S2:** H<sub>2</sub>O (ppm),  $\delta^{18}\text{O}$  and  $\delta\text{D}$  (‰) observed with the Cavity Ring-Down Spectrometer of ambient air and blank branch chamber (a-c) and of ambient air and branch chamber with branch enclosed (d-f). Arrows denote switch from ambient air going into the branch chamber to air coming out of the branch chamber.

## Study II

**Figure 1:** Environmental conditions from April 6 to May 3, 2011. a) Photosynthetic photon flux density (PPFD,  $\mu\text{mol m}^{-2} \text{s}^{-1}$ , black lines), b) air temperature ( $^{\circ}\text{C}$ , black lines), c) relative humidity (% , black lines), d) vapor pressure deficit (VPD, kPa, black lines), e) soil temperature in 5 cm soil depth on vegetation (black lines), roots (black dotted lines) and bare soil plots (black dashed lines), and f) soil volumetric water content in 5 cm soil depth ( $\theta_s$ ,  $\text{m}^3 \text{m}^{-3}$ ) on vegetation (black lines), roots (black dotted lines) and bare soil plots (black dashed lines) as well as rainfall ( $\text{mm d}^{-1}$ , black bars). Black arrows indicate measurement dates (April 8, 12, 18, 26, and May 2, 2011).

**Figure 2:** Soil profiles of volumetric water content ( $\theta_s$ , dashed black lines and grey squares; mean  $\pm$  SD,  $n=3-4$ ; depths 5, 15, 30, and 60 cm) temperature (dotted black lines and dark grey up triangles; mean  $\pm$  SD,  $n=3-4$ ; depths 0, 5, 15, 30, and 60 cm), and soil  $\delta^{18}\text{O}$  (black solid lines and circles; mean  $\pm$  SD,  $n=3-4$ ; depths 0, 2, 5, 10, 15, 20, and 40 cm) on roots, soil and vegetation plots on 5 days between April 8 and May 2, 2011.

**Figure 3:** Measured  $\delta^{18}\text{O}_E$  on root and bare soil plots (black circles) and calculated with the Craig and Gordon equation using approach I (solid black lines), II (long dashed black lines) and III (dotted black lines) according to Table 1. Measured  $\delta^{18}\text{O}_E$  are shown as mean values  $\pm$  SD ( $n=3$ ).

**Figure 4:** a-e) Measured evapotranspiration (ET, black squares) and  $\delta^{18}\text{O}_{ET}$  (grey circles, ‰) based on CRDS measurements from April 8 to May 2, 2011 (mean  $\pm$  SD,  $n = 3$ ). f-j) Modeled isotopic signature of leaf water at the evaporating sites in steady state ( $\delta^{18}\text{O}_{e-ss}$ , dashed black lines) and non-steady state ( $\delta^{18}\text{O}_{e-nss}$ , solid black lines) and measured  $\delta^{18}\text{O}$  of leaf mesophyll water at midday (grey circles, mean values  $\pm$  SD,  $n=5$ ). k-o) Modeled isotopic composition of leaf transpired water ( $\delta^{18}\text{O}_T$ ) in steady-state ( $\delta^{18}\text{O}_{T-ss}$ , black dashed lines) and non-steady state ( $\delta^{18}\text{O}_{T-nss}$ , black solid lines) and isotopic composition of soil evaporated water  $\delta^{18}\text{O}_E$  using different formulations for the kinetic fractionation factor on vegetation plots. p-t) Contribution of plant transpiration to total understory evapotranspiration ( $ft$ ) using all combinations of  $\delta^{18}\text{O}_T$  and  $\delta^{18}\text{O}_E$  of k-o). No values for  $ft$  are displayed if  $ft < 0$  or  $ft > 1$ .

**Figure 5:** Regressions of measured against modeled  $\delta^{18}\text{O}_E$  on soil plots varying a) the oxygen isotope composition of the evaporating surface ( $\delta^{18}\text{O}_e$ ); b) temperature and c) the formulation for  $\alpha_k$ . a)  $\delta^{18}\text{O}_e$  was varied relative to the nominal values at the evaporating front by +1‰ (grey dashed line), +3‰ (dark grey dashed line), -1‰ (light grey dashed line), -3‰ (grey dotted line) and as obtained at the evaporating front (black line). b) temperature ( $t_e$ ) was equally varied relative to values obtained at the evaporating front by +2  $^{\circ}\text{C}$  (grey dashed line), +5 $^{\circ}\text{C}$  (black dashed line), -2 $^{\circ}\text{C}$  (light grey dashed line), -5 $^{\circ}\text{C}$  (grey dotted line) and as obtained at the evaporating front (black line). c) In order to test the sensitivity of the modeled  $\delta^{18}\text{O}_E$  in regard to  $\alpha_k$  we obtained  $\delta^{18}\text{O}_E$  by using the formulations for  $\alpha_k$  as follows: diffusivity coefficient of Merlivat et al. (1978) in combination with  $nk=\text{MB96}$  (black line), in combination with  $nk=1$  (grey dotted line) and the diffusivity coefficient of Cappa et al. (2003) in combination with  $nk=\text{MB96}$  (black dashed line) and  $nk=0.5$  (grey dashed line). Black circles are measured ( $\pm$  SD,  $n = 3$ ) against modeled values with the nominal values of  $\delta^{18}\text{O}_e$  and temperature at the evaporative front and  $\alpha_k = \text{Me78}^{\text{MB96}}$ .

## Study III

**Figure 1:** Rectangular transect grid (white squares) with 100 observation points of  $100 \times 100$  m extend. Background: aerial photograph of study site in central Portugal with *Q. suber* trees (Google, 2013).

**Figure 2:** Sketches of crown models: ellipsoidal  $Se(h)$ , asymmetric ellipsoidal  $Se9/10(h)$  and triangular model  $St(h)$ .  $ht$  = crown top height,  $hb$  = crown bottom height,  $rc$  = crown radius.

**Figure 3:** Histogram of angular averaged transmittance deviations from unity  $P_{gap} - 1$ . Light grey: values set to 1 and kept for further analysis. Black: considered operational errors and excluded from further analysis with MAD filter based on 2.5 standard deviations.

**Figure 4:** Dependency of gap probability  $P_{gap}$  on zenith view angle  $\theta$ . Black symbols: DCP method at 3, 6 and 8 m height. Grey symbols: LAI-2000 method at 3 m height (6 and 8 m heights not shown). Solid lines: Beer's law with effective leaf area index  $Le$ . Dashed lines: Beer's law with angular dependent leaf clumping  $\Omega(\theta)$  of Fig. 6.

**Figure 5:** a) Empirical leaf inclination angle  $\alpha$  distribution (bars,  $n=281$ ), non-parametric kernel smooth distribution function (dashed line), two-parameter Beta-distribution (solid line). The abscissa displays angle of the leaf normal to zenith: 0=horizontal aligned leaves, 1 = vertical aligned leaves. b) Leaf projection function  $G(\theta)$  over view zenith angle  $\theta$  derived from kernel smooth (dashed line) and Beta-distribution (solid line). Uncertainty bands present standard error.

**Figure 6:** Change of clumping index  $\Omega$  with zenith view angle  $\theta$  at 3, 6 and 8 m height. Solid lines: fitted third degree polynomials.

**Figure 7:** a) Height distribution of cumulative effective leaf area index  $\sum Le$  for LAI-2000 and DCP derived from  $P_{gap}$  ( $53^\circ$ ). b) Same for cumulative leaf area index  $\sum L$ .

**Figure 8:** a, b) change of mean gap probability  $\overline{P_{gap}}$  and standard error  $\sigma_{\overline{P_{gap}}}$  with view angle span  $\theta_v$ . c, d) change of mean leaf area index  $\overline{L}$  and standard error  $\sigma_{\overline{L}}$  with view angle span  $\theta_v$ . All plots display observations at zenith view angles of  $0^\circ$ ,  $53^\circ$ ,  $68^\circ$  and 3 m height above ground for LAI 2000 and DCP.

**Figure 9:** a) height distribution of leaf area index  $L$  estimated with the ellipsoidal ( $Se$ , solid line), asymmetric ellipsoidal ( $Se\ 9/10$ , dashed line) and triangular ( $St$ , dotted-dashed line) crown model from crown parameters and leaf area index  $L$  derived from  $P_{gap}$  ( $53^\circ$ ) at 3 m height. b) height distribution of cumulative leaf area index  $\sum L$ . Dots: measured cumulative height distribution with DCP. Lines: estimated cumulative height distribution by integration of  $Se$ ,  $Se\ 9/10$  and  $St$  from a).

## Study IV

**Figure 1:** Environmental conditions during 2011; a) daily mean air temperature (black line), vapor pressure deficit (VPD; black long dashed line) and daily rainfall (black bars) observed in the open area; b) soil temperature in the open and tree plots (grey and black lines, respectively). The lighter grey lines indicate daily means; c) soil volumetric water content ( $\Theta$ ) in 5 cm soil depth in the open and tree plots (grey and black lines, resp.) and d) daily sums of photosynthetic photon flux density (PPFD) in the open (grey line) and tree plots (black line).

**Figure 2:** a-h) Relative vegetation cover in % of living biomass of distinct functional groups of the herbaceous layer (Grasses, N-fixing and other forbs) in early spring, late spring and fall 2011 on the open (a-e) and tree plots (f-h; mean values;  $n = 5$ ).

**Figure 3:** a) Renkonen index showing the relative (0-1) similarity between the open and the tree site from April to June. b-g) Relative vegetation cover in % of each species of the three functional groups of the herbaceous layer (Grasses, N-fixing and other forbs) on the open (left) and the tree site (right) from April to June (mean values;  $n = 5$ ).

**Figure 4:** a-h) Total daily water reduction in the upper 60 cm of the soil in the open and the tree plots (grey and black bars, respectively) as well as total herbaceous evapotranspiration ( $ET$ ) during daylight on the open (a-d) and tree plots (e-h; white and black circles, respectively). Results are presented as mean values ( $\pm$  SD in case of  $ET$ ;  $n=3-4$ ) and i-l) relative water use of the herbaceous layer [%] on the open (grey circles) and tree plots (black circles), between April 4 and November 22, 2011: early spring (a, e, i), late spring (b, f, j), summer (c, g, k), and fall (d, h, l).

**Figure 5:** a-d) Total net  $CO_2$  exchange during daylight on the open and tree site (grey and black cycles) during the four measurement campaigns between April 24 and November 22, 2011: early spring (a), late spring (b), summer (c), and fall (d). Results are mean values  $\pm$  SD ( $n=3$ ).

**Figure 6:** a-b) Open and tree site (white and black circles, respectively) net  $CO_2$  exchange during daylight ( $NEE$ ) in spring (April-June) versus open and tree site photosynthetic photon flux density (a, PPFD), and soil water content in 5 cm depth (b). c-d) Difference between open and tree site in spring ( $\Delta$ open – tree site; April-June) net  $CO_2$  exchange during daylight ( $NEE$ ) versus difference between open and tree site photosynthetic photon flux density (c, PPFD), and water use (d). Sites specific differences could only be calculated for measurements on consecutive days. Black lines depict linear regressions between  $NEE$  and  $SWC$  (b) and non-linear regressions between  $\Delta NEE$  and  $\Delta$ soil water use (d).

### Study V

**Figure 1:** Environmental conditions from March to December 2011; a) daily averages of air temperature (grey line), vapor pressure deficit (VPD; grey long dashed line) and rainfall (black bars); b-de) daily sums of environmental conditions at the open (grey) and tree site (black) of: photosynthetic photon flux density (PPFD), soil temperature in 5 cm soil depth (lighter lines denote running averages), soil volumetric water content ( $\Theta$ ) in 5 and 60 cm soil depth. e) daytime integrated net ecosystem fluxes of: net  $CO_2$  exchange ( $NEE$ ,  $g\ C\ m^{-2}\ d^{-1}$ ) and evapotranspiration ( $ET$ ,  $mm\ d^{-1}$ , black bars) from March to December 2011.

**Figure 2:** Rainfall and infiltration into the soil following rain events  $> 2\ mm$  at a, b) the open and c, d) tree site on understory plots (green circles), bare soil plots (blue circles, all in  $mm\ d^{-1}$ ;  $n=4$ , mean values  $\pm$  SE) and rainfall (grey bars). Insets present differences in infiltration between understory and bare soil versus rain amount at the open and tree site. Regression line, coefficient of regression and p-value are given.

**Figure 3:** Development of midday oxygen isotope signatures within the ecosystem from April to November 2011; a-d) atmospheric  $\delta^{18}O$  at 9 m height (grey diamonds); e-h)  $\delta^{18}O$  of rainfall (black circles) and  $\delta^{18}O$  of soil water at the evaporating site on vegetation plots at the open (white triangles) and tree site (grey triangles, mean values  $\pm$  SD,  $n=3$ ); i-l) measured  $\delta^{18}O$  of evapotranspiration on the open (white circles) and tree site (grey circles, mean values  $\pm$  SD,  $n=3$ ); m-p) modeled  $\delta^{18}O$  of evaporated vapor from vegetation plots on the open (white triangles) and the tree site (grey triangles) and modeled  $\delta^{18}O$  of herbaceous leaf transpired vapor at the open (white circles) and the tree site (grey circles).

**Figure 4:** a) Oxygen isotope signatures of soil evaporation on bare soil plots calculated with the Craig and Gordon equation versus measured values for the open (white circles) and tree sites (black circles) of all measurements (mean values  $\pm$  SE;  $n=3$ ); the grey and black line denote regression lines for the open and tree sites, respectively. b) Modeled against measured values during midday only (14:00 h). c) Modeled  $\delta^{18}O$  of leaf water at the evaporating sites in the non steady state versus measured oxygen isotope signatures of bulk leaf water for the open (white circles) and tree site (black circles) for all available data points of measured leaf water  $\delta^{18}O$  throughout the study period. Regression equations (observed vs. modeled), correlation coefficients are given below the plots. p-values were less than 0.001 for all regressions.

**Figure 5:** Daytime integrated understory evapo-transpiration ( $ET$ ,  $mm\ d^{-1}$ , mean values  $\pm$  SD,  $n=3$ ),



which is the sum of herbaceous layer transpiration ( $T$ , green bars) and soil evaporation ( $E$ , blue bars) at the open (i-l) and tree site (m-p); daytime integrated net understory  $\text{CO}_2$  exchange ( $NEE$ ,  $\text{g C m}^{-2} \text{d}^{-1}$ , white circles; mean values  $\pm$  SE,  $n=3$ ), herbaceous gross primary production ( $GPP$ , dashed green line, mean values,  $n=3$ ) and respiration ( $R$ , blue line, mean values,  $n=3$ ) on the open (a-d) and tree site (e-h). q-x) Inherent water-use efficiency ( $iWUE$ ) of the whole understory ( $GPP \cdot VPD/ET$ , white circles), and understory vegetation ( $GPP_u \cdot VPD/T$ , green circles).  $iWUE$  was calculated from daytime integrated values of  $ET$ ,  $T$  and  $GPP_u$  for the open site (q-t) and the tree site (u-x).

**Figure 6:** a) Daytime integrated ecosystem evapotranspiration ( $ET$ , sum of the stacked bars) and its components cork-oak transpiration ( $T_o$ , dark green), herbaceous transpiration ( $T_u$ , green) and soil evaporation ( $E$ , blue, all  $\text{mm d}^{-1}$ ). b) Daytime integrated  $GPP$  of cork oaks ( $GPP_o$ , dark green) and understory ( $GPP_u$ , green), ecosystem respiration ( $R_{eco}$ ; blue), and net ecosystem  $\text{CO}_2$  exchange ( $NEE$ , black squares, all in  $\text{g C m}^{-2} \text{d}^{-1}$ ).

**Figure 7:** Inherent water-use efficiency ( $iWUE$ ,  $GPP \cdot VPD/(E)T$ ) of the ecosystem (white circles), the black line represents the running average, cork oaks (dark green) and understory vegetation (green circles).

**Figure S1:** Typical diurnal courses of understory  $ET$ ,  $\delta^{18}O_{ET}$ ,  $NEE$  and its components on 23. and 24. May 2011. a,d) of oxygen isotope signatures of measured  $ET$  (grey circles,  $n=3 \pm \text{SD}$ ) and modeled  $E$  and  $T$  (blue line and green dashed line) at the open (a) and tree site (d); b, e) of fluxes of measured  $ET$  (grey circles,  $n=3 \pm \text{SD}$ ) and modeled  $E$  and  $T$  (blue line and green dashed line) on the open (b) and tree site (e). c, f) Fluxes of measured net understory  $\text{CO}_2$  exchange ( $NEE_u$ ; grey circles,  $n=3 \pm \text{SD}$ ) and understory respiration ( $R_u$ ; blue circles,  $n=3 \pm \text{SD}$ ) and estimated understory plant  $\text{CO}_2$  uptake ( $GPP_u$ ; green dashed line) at the open (c) and tree site (f).

## Study VI

**Figure 1:** Meteorological data during 2011 and 2012. (a) 10-day average air temperatures ( $^{\circ}\text{C}$ ) and 10-day sum of precipitation (mm). (b) 10 day average of total incident photosynthetically active radiation (PAR,  $\text{mol m}^{-2} \text{d}^{-1}$ ). (c) 10-day average of maximum vapour pressure deficit ( $VPD_{max}$ , hPa).

**Figure 2:** Daily mean values of soil water content (%) at 2 and 40 cm depth.

**Figure 3:** Daily values of net ecosystem exchange ( $NEE$ ,  $\text{g C m}^{-2} \text{day}^{-1}$ ) during 2011 (a) and 2012 (b). Negative values represent carbon sequestration in the ecosystem while positive values represent carbon emissions to the atmosphere. The black line indicates a 10-day running average.

**Figure 4:** Linear regressions between gross primary productivity ( $GPP$ ) and daily-integrated incident photosynthetically active radiation (PAR) over the seasons in 2011 and 2012. Radiation use efficiency (RUE) expressed in  $\text{g C MJ}^{-1}$ . (a) Winter, 2011:  $y = 0.31x + 1.11$ ,  $r^2 = 0.57$ ,  $n=56$ ; 2012:  $y = 0.25x + 1.06$ ,  $r^2 = 0.62$ ,  $n=71$ . (b) Spring, 2011:  $y = 0.26x + 2.74$ ,  $r^2 = 0.20$ ,  $n=32$ ; 2012:  $y = 0.28x + 2.0$ ,  $r^2 = 0.46$ ,  $n=44$ . (c) Summer, 2011:  $y = 0.42x + 0.02$ ,  $r^2 = 0.58$ ,  $n=96$ ; 2012:  $y = 0.21x + 0.24$ ,  $r^2 = 0.22$ ,  $n=62$ . (d) Autumn, 2011:  $y = 0.33x + 0.67$ ,  $r^2 = 0.55$ ,  $n=61$ ; 2012:  $y = 0.33x + 0.83$ ,  $r^2 = 0.71$ ,  $n=57$ .

**Figure 5:** Total cumulative leaf fall during 2011 and 2012 in  $\text{g DM m}^{-2}$  and time interval of different phenological stages. Values are means  $\pm$  se ( $n=6$ ).

**Figure 6:** Tree leaf area index ( $LAI$ ) during 2011 (a) and 2012 (b). The dash line represents  $LAI$  of old leaves matured in the previous spring.

**Figure 7:** Tree diameter increment (mm) during 2011 and 2012. Values are means  $\pm$  se ( $n=9$ ).

## Study VII

**Figure 1:** Satellite image of the study site (© Google Maps, 2013). 1: position of the overstorey tower.

2: position of the understorey tower.

**Figure 2:** a) Daily sum of precipitation  $P$  for 2011 (black) and 2012 (grey). b) Cumulative precipitation  $P$  for 2011 (black) and 2012 (grey) based on half hourly data.

**Figure 3:** Quantile-quantile plot of important climate and environmental parameters for the years 2011 and 2012 based on daily averages. Black dots represent the 0.01, 0.05, 0.1, 0.2, 0.3, 0.4, 0.6, 0.7, 0.8, 0.9, 0.95, and 0.99 quantiles of the respective distribution. Grey dots represent the 0.5 quantile. a) air temperature  $T$ , b) precipitation  $P$ , and c) vapour pressure deficit of the air  $vpd$ , each measured at 20 m height above ground. d) soil moisture in the first 20 cm  $\theta_{20\text{ cm}}$  (root zone of understorey vegetation).

**Figure 4:** a) Maximum daily vapour pressure deficit  $vpd_{max}$ , b) daily sum of ecosystem evapotranspiration  $ET_o$  and c) daily sum of understorey transpiration + soil evaporation  $ET_u$  for 2011 (black) and 2012 (grey). Lines mark kernel regressions.

**Figure 5:** Box plot of monthly volumetric soil moisture a) down to 20 cm depth  $\theta_{20\text{ cm}}$  (root zone of understorey vegetation) and b) down to 60 cm depth  $\theta_{60\text{ cm}}$  for the years 2011 (black) and 2012 (grey). Central line marks the median, box marks the 0.25 and 0.75 quantiles. Dashed lines mark the 0.05 and 0.95 quantiles. Data within a two day interval after a rain event were excluded.

**Figure 6:** a) Ecosystem net carbon exchange  $NEE_o$ , b) ecosystem gross primary production  $GPP_o$ , c) understorey gross primary production  $GPP_u$  for 2011 (black) and 2012 (grey). Dots mark daily sums, lines are kernel regressions.

**Figure 7:** a) Apparent maximum carboxylation rate  $V_{cmax}$ , b) stomatal conductance parameter  $m$ , c) vapour pressure deficit sensitivity parameter  $D_o$ , d) fraction  $m/(1 + (\overline{vpd}/D_o))$  relating assimilation  $A$  and stomatal conductance  $g_s$ , e) daily median stomatal conductance for water vapour  $g_{sh}$  and f) optimal temperature of carboxylation  $T_{opt}$ . The model is fitted to median daily cycles of gross primary production  $GPP_o$  and evapotranspiration  $ET_o$  of the *Q. suber* trees in a day long moving window for the summer period of 2011 (black) and 2012 (grey).

## LIST OF TABLES

### Extended summary

**Table 1:** Overview of titles, objectives and Conclusions of the individual studies of this work.

#### Study I

**Table 1:** Used symbols and descriptions.

**Table S1:** Equations,  $R^2$  and p values for the Concentration dependencies of the Cavity Ring-Down Spectrometer at six different oxygen and deuterium isotopic signatures as shown in Fig. S1.

#### Study II

**Table 1:** Description of the three approaches used in this study to calculate  $\delta^{18}O_E$  varying the soil depth used to derive the isotopic signature and temperature at the evaporating site ( $\delta^{18}O_e$  and  $T_e$ ) and the kinetic fractionation factor ( $\alpha_k$ ).

#### Study III

**Table 1:** Relative bias of gap probability  $P_{gap}$  and leaf area index  $L$  when wooden tissue is not excluded.  $h$  = height above ground,  $\varepsilon P_{gap}(\theta)$  = relative bias of gap probability at  $0^\circ$ ,  $53^\circ$  and  $71^\circ$  view zenith angle,  $\varepsilon L$  = relative bias of leaf area index  $L$  derived from  $P_{gap}$  ( $53^\circ$ ).

#### Study IV

**Table 1:** List of herbaceous species growing in the open and tree site in 2011.

**Table 1:** Nitrate content in different soil depths in May, September and November 2011 (mean values  $\pm$  SD;  $n = 3$ ). \* denote statistic significant differences between the open and the tree site ( $p < 0.05$ ).

**Table 2:** Living aboveground biomass [ $g\ m^{-2}$ ] of distinct functional groups of the herbaceous layer (Grasses, N-fixing and other forbs) in spring and fall 2011 on the open and tree site (mean values  $\pm$  SD;  $n=5$ ).

#### Study V

**Table 1:** List of herbaceous species growing in the open and tree plots in 2011.

**Table 2:** Living aboveground biomass ( $g\ m^{-2}$ ) of the herbaceous layer in spring and fall 2011 on the open and tree site (mean values  $\pm$  SD;  $n=5$ ).

**Table 3:** Daytime mean conductance ( $mmol\ m^{-2}\ s^{-1}$ ) of the herbaceous layer during spring, late spring and fall (mean values  $\pm$  SE) at the open and tree site. Site specific differences are indicated at  $p < 0.05$  (Mann-Whitney U-test).

**Table S1:** Oxygen isotope signatures of soil water [‰] in 0.5, 2, 5, 10, 15, 20 and 40 cm depth on bare soil and vegetation plots at the open and tree site between 7.4. and 21.11.2011.

#### Study VI

**Table 1:** General soil, climate and vegetation characteristics in 2011 and 2012. Values are means  $\pm$  se.

**Table 2:** Predawn ( $\Psi_{pd}$ ) and midday ( $\Psi_{md}$ ) tree leaf water potential (MPa, n=6) measured during 2011 and 2012 in the early summer and summer end. Values are means  $\pm$  se. Different letters represent statistical significance at  $P < 0.05$ , no letters means no differences

**Table 3:** Total annual litter fall and litter fall components during 2011 and 2012 in  $\text{g m}^{-2} \text{ year}^{-1}$ . Values are means  $\pm$  se (n=6). Different letters represent statistical significance at  $P < 0.05$ , no letters means no differences.

### **Study VII**

**Table 1:** Parameters used in the photosynthesis - stomatal conductance model. Parameters with the source 'site average' were estimated with an optimization on the entire data set.

## ABBREVIATIONS

$\alpha_k$	kinetic fractionation factor
$\alpha^+$	equilibrium fractionation factor
$\delta^{18}O$	stable oxygen isotope signature (‰)
$\Theta$	volumetric water content
$E$	soil evaporation
$ET$	evapotranspiration
$ft$	fraction of $T$ contributing to $ET$
$GPP$	gross primary productivity
$g_t$	total leaf conductance to water vapor ( $\text{mol m}^{-2} \text{s}^{-1}$ )
$h$	relative humidity
$LAI$	leaf area index
$NEE$	net ecosystem $\text{CO}_2$ exchange
$o$	overstory
$P_{gap}$	gap probability
$R$	ratio of $[^{18}\text{O}]/[^{16}\text{O}]$
$R_{eco}$	ecosystem respiration
$s$	<i>soil</i>
$T$	plant transpiration
$V_{cmax}$	maximum carboxylation rate
$w$	$\text{H}_2\text{O}$ concentration
$T$	temperature
$t$	trees
$u$	understory

## SUMMARY

Semi-arid ecosystems cover large areas world-wide and contribute about 40% to global gross primary production (*GPP*). The major driving factor of *GPP* in these ecosystems is water availability; since annual precipitation pattern show periodical summer droughts and evapotranspiration losses are high. Hence, understanding seasonal vegetation-soil-water feedbacks is vitally important. This thesis aims at disentangling vegetation impacts on water and carbon cycling of a Mediterranean savanna-type oak woodland. Special focus was laid on the seasonal understory impact on net ecosystem fluxes, soil water distribution and tree-understory interactions. Moreover, the impact of altered precipitation pattern and drought intensity on ecosystem functioning was assessed, as these phenomena are predicted to increase by climate change scenarios in these ecosystems.

To achieve these aims, classical ecophysiological measurements, plant community and structural observations as well as eddy-covariance technique were combined with a novel stable oxygen isotope partitioning approach.

Stable oxygen isotopes are valuable tracers for water movements within the ecosystem, but due to methodological restrictions in the past, it was necessary to validate modeling approaches and derive field sampling protocols for model input parameters. Therefore, a measurement set-up was developed coupling branch and soil chambers with an H<sub>2</sub>O laser spectrometer, enabling direct, high frequent measurements of  $\delta^{18}O$  signatures of evaporative fluxes and, to my best knowledge, the first validation of the Craig and Gordon model under heterogeneous field conditions. Thereby it was possible to assess multiple effects of understory vegetation on ecosystem water cycle and productivity. Although understory transpiration strongly contributed to ecosystem evapotranspiration, beneficial effects of the understory vegetation were dominant as herbaceous biomass strongly increased rain infiltration, diminished soil evaporation and significantly added to the ecosystem carbon sink strength. However, the understory was also vulnerable towards drought: development, species composition, transpiration and carbon gain of the understory plants were strongly influenced by competition for water with cork-oak trees which shortened the understory longevity and reduced the overall understory productivity in spring.

The years 2011 and 2012, contrasting in annual precipitation amount and pattern, offered an ideal opportunity to study effects of drought on ecosystem functioning. The pronounced winter/spring drought and reduced precipitation in 2012 led to strongly reduced development of the understory layer. Ecosystem carbon sink strength and net ecosystem evapotranspiration were severely reduced and more water was used by the ecosystem through evapotranspiration than was introduced by precipitation in 2012. Decreased ecosystem productivity was caused by stomatal regulations and decreased maximum carboxylation rate ( $V_{cmax}$ ) of cork-oaks. Moreover, the drought in 2012 led to strong alterations in tree phenology: annual tree diameter increment and fruit production were severely reduced.

These findings suggest that the herbaceous understory, although vulnerable to drought, plays a vitally important role for ecosystem fluxes, rain infiltration and hence also cork-oak productivity and ecosystem resilience towards drought. At the same time, the increased drought and altered precipitation pattern predicted in future climate change scenarios for the Mediterranean basin does not only threaten understory development and annual cork growth. It also very likely decreases rain infiltration and ground water recharge, which in turn can severely affect cork-oak productivity and the resilience of the ecosystem towards drought.

## ZUSAMMENFASSUNG

Semiaride Ökosysteme tragen etwa 40% zur globalen Brutto-Primär-Produktion (*GPP*) bei und bedecken große Teile der weltweiten Landmasse. Wasserverfügbarkeit ist einer der wichtigsten limitierenden Faktoren für *GPP*; insbesondere, da die jahreszeitlichen Niederschlagsdynamiken zu periodischen Sommerdürren führen und die Wasserverluste durch Evapotranspiration hoch sind. Daher ist ein Verständnis saisonaler Wechselwirkungen zwischen Vegetation, Boden und Wasser von fundamentaler Bedeutung. Das Hauptziel dieser Doktorarbeit ist die Aufschlüsselung von Vegetationseinflüssen auf den Wasser- und Kohlenstoffhaushalt eines mediterranen savannenartig strukturierten Eichenwaldes. Ein spezieller Fokus liegt dabei auf dem saisonalen Einfluss des Unterwuchses auf Ökosystemflüsse, Bodenwasserverteilung und auf Wechselwirkungen mit der Baumschicht. Außerdem wurde der Einfluss veränderter Niederschlagsdynamiken auf Nettoflüsse und Produktivität des Ökosystems untersucht, da eine Zunahme von Trockenstressperioden durch Klimawandelmodellen vorhergesagt wird.

Um diese Fragen zu untersuchen, wurden klassische ökophysiologische Messungen, pflanzengesellschaftliche und strukturelle Vegetationsaufnahmen und die Eddy-Kovarianz-Technik kombiniert und basierend auf den Eigenschaften stabiler Sauerstoff-Isotopen ein neuartiger Partitionierungsansatz entwickelt.

Stabile Sauerstoff-Isotope sind wertvolle Indikatoren für Wasserbewegungen innerhalb eines Ökosystems. Bisher unterlag der Einsatz stabiler Sauerstoff-Isotope für ökologische Untersuchungen technischen Einschränkungen. Deshalb wurden im Zuge dieser Arbeit verbreitete Modellansätze validiert und Freiland-Messprotokolle für deren Eingangsparameter erarbeitet. In einem ersten Schritt wurde dafür ein Messaufbau entwickelt, bei dem Gaswechselkammern auf verschiedenen Ebenen mit einem H<sub>2</sub>O-Laser-Spektrometer gekoppelt wurden, um eine direkte, hochfrequente Messung der  $\delta^{18}O$  Signaturen evaporativer Flüsse zu ermöglichen und die erste Validierung des Craig-und-Gordon-Modells unter heterogenen Freilandbedingungen durchzuführen. So konnten verschiedener Effekte der Unterwuchsvegetation auf den Wasserhaushalt und die Produktivität des Ökosystems ermittelt werden. Insgesamt trug die Transpiration des Unterwuchses stark zur Evapotranspiration des Ökosystems bei. Dennoch waren vorteilhafte Effekte dominant: die Biomasse des krautigen



Unterwuchses erhöhte in starkem Ausmaß die Niederschlagsinfiltration, unterdrückte die Bodenevaporation und trug signifikant zur Funktion des Ökosystems als Kohlenstoffsенke bei. Andererseits zeigte die Unterwuchsvegetation eine starke Sensitivität gegenüber Trockenheit, da ihr Biomassezuwachs, ihre Artenzusammensetzung, Transpiration und Kohlestoffaufnahme durch Wasserkonkurrenz mit Korceichen limitiert war. Dies führte zu einer verkürzten Vegetationsperiode und reduzierte die Kohlenstoffaufnahme im gesamten Frühjahr.

Die Jahre 2011 und 2012 unterschieden sich signifikant hinsichtlich der absoluten Niederschlagsmenge und -verteilung, so dass diese Zeit eine ideale Gelegenheit bot, den Einfluss von Trockenheit und veränderten Niederschlagsdynamiken auf das Ökosystem zu untersuchen. Die Winter/Frühjahrstrockenheit in 2012 verhinderte die Entwicklung des Unterwuchses und die Kohlenstoffaufnahme und Evapotranspiration des Ökosystems waren stark vermindert. Zudem verlor das Ökosystem im trockenen Jahr 2012 mehr Wasser durch Evapotranspiration als durch Niederschläge zugeführt wurde. Die verminderte Ökosystem-Produktivität im Sommer 2012 wurde hauptsächlich durch stomatäre Regulation und verminderte maximale Carboxilierungsrate ( $V_{max}$ ) der Korceichen verursacht, während die gesamte Blattfläche stabil geblieben ist. Desweiteren zeigten sich starke Einbußen in Fruchtproduktion und Stammzuwachs, was für die Korkproduktion von wirtschaftlicher Bedeutung ist.

Die Ergebnisse dieser Arbeit weisen darauf hin, dass der krautige Unterwuchs, trotz seiner Dürreanfälligkeit, eine entscheidende Rolle für die Entwicklung der Kohlenstoff- und Wasserflüsse des Ökosystems und für die Niederschlagsinfiltration spielt, was wiederum die Produktivität der Korceichen und die Resilienz des Ökosystems gegenüber Trockenheit beeinflusst. Gleichzeitig, schädigen verstärkte Trockenheit und veränderte Niederschlagsverteilung, wie sie durch Klimawandelprognosen für den Mittelmeerraum vorausgesagt werden, nicht nur die Entwicklung des Unterwuchses und die Korkproduktion. Vielmehr sind negative Auswirkungen auf die Niederschlagsinfiltration und die Grundwasserneubildung sehr wahrscheinlich, was zu langfristigen und anhaltenden Konsequenzen für die Produktivität und die Resilienz des Ökosystems gegenüber Trockenheit führen kann.

# **Water balance and productivity of a Mediterranean oak woodland**

**Quantifying understory vegetation impacts by development of a  
stable oxygen isotope partitioning approach**

## **EXTENDED SUMMARY**





## **1. VEGETATION AND DROUGHT EFFECTS ON WATER BALANCE AND ITS IMPACT ON CARBON GAIN IN SEMI-ARID ECOSYSTEMS**

Semi-arid ecosystems contribute to ca. 40% global net primary productivity (Grace *et al.*, 2006), although water availability is the major factor limiting carbon dioxide uptake (Pereira *et al.*, 2006). Annual precipitation pattern show periodical summer droughts and evapotranspiration (*ET*) losses are high accounting up to 95% of the water input (Huxman *et al.*, 2005). At the same time, *ET* has two distinct components: soil evaporation and plant transpiration, which may need to be further separated in contributions of different plant functional types. These fluxes are not necessarily controlled by the same mechanisms (Cavanaugh *et al.*, 2011; Raz-Yaseef *et al.*, 2012; Yepez *et al.*, 2007; Zhang *et al.*, 2011). Thus a separation of these component fluxes is needed to gain functional understanding on the development of net ecosystem water fluxes and their coupling with carbon cycling.

In addition, climate change is expected to cause substantial changes in water availability due to increasing air temperature and changed rainfall pattern, which might lead to a prolonged dry season and to more frequent drought spells but also significant increases in heavy precipitation events (Costa *et al.*, 2012; IPCC, 2007; Trigo *et al.*, 2013; Xu *et al.*, 2013). Annual precipitation pattern of the recent past already show a significant decrease of rain amount in February and March as well as a decrease of total annual rainfall on the Iberian Peninsula (Guerreiro *et al.*, 2013; Garcia-Barron *et al.*, 2013; Pereira *et al.*, 2007; Paredes *et al.*, 2006). While well adapted to a prolonged summer drought, species in semi-arid Mediterranean ecosystems rely on winter recharge and sufficient water supply during spring, as this is their main growth period. Consequently, a functional understanding of the impact of increased drought and altered precipitation pattern on ecosystem functioning is vitally important for predictions of ecosystem resilience towards ongoing climate change.

In the Mediterranean Basin evergreen savannah type oak woodlands (called 'Montado' in Portugal and 'Dehesa' in Spain) form such semi-arid ecosystems. In Portugal and Spain they cover 1.5 million hectares (2.5 million hectares in the Mediterranean Basin) and form the predominant land-cover type in the south-western Iberian Peninsula. They are commonly exploited as pastoral agro-forestry ecosystems, mainly for cork-production but also for grain harvest or pastures. Moreover, they are

highly diverse and considered a habitat of high conservation value (Moreno *et al.*, 2005; Perez-Ramos *et al.*, 2008). Therefore, their sustainability is vitally important for agronomical and biodiversity aspects and is currently being threatened by unbalanced management practices (Bugalho *et al.*, 2011). The ‘Montado’ is a multi-layered ecosystem consisting of a widely spaced tree cover usually composed of *Quercus suber* L. sometimes mixed with *Quercus ilex* La. and an understory layer comprised of grasslands, shrub formations and/or cereal crops (Perez-Ramos *et al.*, 2008). While trees have access to deeper soil layers and/or ground water, shallow rooted herbaceous plants are vulnerable to drought and die back at the onset of summer drought (Paço *et al.*, 2009). Consequently, the contribution of the herbaceous layer to ecosystem productivity varies intra-annually and can be remarkably high, especially in spring, contributing up to more than 50% of total gross primary productivity (*GPP*; Unger *et al.*, 2009, 2010).

While the impact of understory plants on carbon and also nitrogen cycling (Hussain *et al.*, 2009; Otieno *et al.*, 2011; Unger *et al.*, 2009, 2010) in the Montado is relatively well characterized, less is known concerning its role in the ecosystem water cycle. Paço *et al.* (2009) gave first insights that at least in times of high water availability (October-May/June) understory evapotranspiration can be equal to and sometimes exceeds tree transpiration, but due to methodological difficulties soil evaporation and understory transpiration have so far not been analyzed separately. The functional understanding of soil evaporation dynamics and vegetation-soil-feedbacks within the water cycle, however, remains a main challenge in semi-arid regions, as diminishing the unproductive water loss from the soil has been addressed a high priority (Wang *et al.*, 2012a; Raz-Yaseef *et al.*, 2012). Moreover, the presence of understory vegetation has various other impacts on soil water relations than sheer reduction of soil evaporation. Transpiration of active vegetation causes great water losses which are dependent in their amount on water availability, plant functional type and stomatal regulation as well as leaf area index (*LAI*). Also, rainfall might be intercepted while at the same time hydraulic redistribution might be altered depending on rooting depths and structure (Tromble, 1988; Bhark & Small, 2003; Huxman *et al.*, 2005; Dawson, 1993; Schwinning & Ehleringer, 2001; Devitt & Smith, 2002). Thus, more research is needed to disentangle the complex interplay between vegetation-soil-atmosphere feedbacks and ecological functioning.

## 2. OBJECTIVES OF THE PRESENT WORK

The overall aim of this dissertation is a detailed mechanistic evaluation of the water balance and carbon cycling in a Mediterranean savannah-type oak woodland with a focus on understory vegetation impact. Moreover, this dissertation aims at disentangling impacts of drought and altered precipitation regime on ecosystem functioning.

Gaining a complete picture of these complex processes requires a combination of multiple methods. Consequently, this thesis combines classical ecophysiological measurements (i.e. gas exchange, leaf water potentials), eddy-covariance technique and plant community assessments and stand structural observations. Moreover, new methods were developed, namely a digital cover based approach obtaining leaf areas index in heterogeneous stands and a novel partitioning approach based on coupling of gas-exchange chambers with a stable oxygen isotope laser spectrometer.

Using oxygen isotope signatures as a tool to partition ecosystem evapotranspiration: fractionation processes and model evaluations (study I, II)

Separating net fluxes into their components enhances functional understanding regarding the seasonal dynamics of ecosystem water and carbon fluxes. Traditionally, partitioning water into its component fluxes, transpiration ( $T$ ) and evaporation ( $E$ ), can be done with combinations of lysimeter, porometer, Bowen ratio, eddy-covariance and sap flow measurements (e.g. Haverd *et al.*, 2011; Lai *et al.*, 2006). However, these methods have limitations in multi-layered ecosystems; requiring a separation between soil evaporation and transpiration of a dense grass layer (Dubbart *et al.*, 2013) and an additional tree layer (Yepez *et al.*, 2007). A solution in such a case can be the partitioning by means of stable oxygen isotopes, as soil evaporation and plant transpiration differ in their oxygen isotope signatures. Hence, evapotranspiration can be separated knowing the net  $ET$  flux and oxygen isotope compositions of  $ET$ , soil  $E$  and plant  $T$  (Yakir & Sternberg, 2000).

Evaporation from the soil modifies the isotopic composition of source water (Craig and Gordon, 1965), due to kinetic (lighter isotopologues  $H_2^{16}O$  diffuse faster) and equilibrium (lighter isotopologues evaporate more easily) fractionation effects. While soil evaporation is depleted compared to the  $\delta^{18}O$  signature of source/soil water,  $\delta^{18}O$  of plant transpiration is supposed to be in an

isotopic steady-state, which means that it equals the isotope signature of source water, at least during daytime (Dawson, 1993), although steady-state conditions are not always found due to the transient changes in atmospheric conditions (Lai *et al.*, 2006). The large differences between evaporative  $\delta^{18}O$  (depleted compared to source water) and transpirational  $\delta^{18}O$  (equal to source water) provide the basis for using stable isotopes to separate soil evaporation and plant transpiration fluxes (e.g. Williams *et al.*, 2004; Lai *et al.*, 2006; Yezpez *et al.*, 2007). This requires the use of modeling approaches, estimating  $\delta^{18}O$  of soil evaporation and plant transpiration. However, field studies validating  $\delta^{18}O$  modeling approaches with direct estimates of  $\delta^{18}O$  of transpiration and evaporation are still scarce (Wang *et al.*, 2012b, 2013, Simonin *et al.*, 2013) specifically under field conditions, since only recent developments in laser spectroscopy enable the measurement of  $\delta^{18}O_{ET}$  and its components directly (Werner *et al.*, 2012b). Therefore, I developed and implemented a flow-through gas-exchange systems at ground and branch level coupled to a H<sub>2</sub>O Cavity-Ring-Down Spectrometer enabling high frequent measurements of fluxes and oxygen isotopic signatures of evaporation, transpiration and evapotranspiration.

The specific tasks were:

- Validate modeling approaches calculating  $\delta^{18}O$  of transpired vapor (Dongmann *et al.*, 1974) or soil evaporation (Craig and Gordon, 1965) with direct estimates (study I, II).
- Determine field sampling protocols for important input parameters of the model based on sensitivity analyses (study I and II) and determine the impact of isotopic non-steady-state of transpiration on  $\delta^{18}O$  of atmospheric vapor (study II).
- Develop a partitioning approach using stable oxygen isotopes separating understory T and soil E (study II)

#### Assessing small scale heterogeneity due to sparse, heterogeneous tree cover (study III, IV)

In cork-oak woodlands, tree cover is sparse and not uniformly distributed, creating distinct patches where the herbaceous layer grows under the tree-crown projected area or in clearings. It can thus be expected that the microclimate is significantly influenced by the patchy cover of oak trees, probably

creating small scale heterogeneity within the understory vegetation (Scholes & Archer, 1997; Cubera & Moreno, 2007; Moreno, 2008). Therefore, it is important to characterize the interactions between trees and understory vegetation throughout the seasons to answer the question:

- How does tree cover influences overall herbaceous layer yield, species abundance and understory longevity (study IV)?

Such possible small scale heterogeneity in herbaceous layer development and fluxes need to be considered when up-scaling to a higher level. Estimates of stand leaf area index ( $LAI$ ) and gap probability ( $P_{gap}$ ) can be used to upscale small scale observations to ecosystem level. However, common indirect approaches estimating stand  $LAI$  and  $P_{gap}$ , for example the  $LAI-2000$  instrument (Li-Cor, 1992), often do not account for leaf clumping and wooden tissue effects, which can have a large influence on the estimate of  $LAI$  and  $P_{gap}$  specifically in open, heterogeneous stands such as savanna-type ecosystems.

Therefore, it was necessary to:

- Develop and validate a method to obtain oak-tree leaf area index ( $LAI$ ) and gap probability ( $P_{gap}$ ) in distinct seasons accounting for effects of leaf clumping and wooden tissue (study III).

#### Understory impact on soil water distribution, water cycling and productivity (study IV, V)

In general, introducing dense herbaceous layers to maximize the productive and minimize the unproductive water loss by reducing open soil patches (Wang *et al.*, 2010; Raz-Yaseef *et al.* 2012) has been addressed a major goal in dry-lands (Wang *et al.*, 2012a). However, the presence of vegetation has various impacts on soil water relations than sheer reduction of soil evaporation. Rainfall might be intercepted while at the same time hydraulic redistribution might be altered (Tromble, 1988; Dawson, 1993; Schwinning & Ehleringer, 2001; Devitt & Smith, 2002; Bhark & Small, 2003; Huxman *et al.*, 2005; Scott *et al.*, 2014). Similar to the findings regarding its impact for carbon cycle (Unger *et al.*, 2009, 2010), I hypothesize that the herbaceous understory layer, although vulnerable to drought, plays an important role in the water cycle and particularly for soil water redistribution.



Consequently the method developed in *studies I, II, III and IV* will be used to:

- *Disentangle the impact and environmental controls of herbaceous vegetation and soil fluxes on ecosystem evapotranspiration, productivity and water-use efficiency with special respect to understory heterogeneity (study IV, V).*
- *Quantify vegetation effects on unproductive soil water loss and rain infiltration (study V).*

Drought impact on development of cork-oak and ecosystem carbon and water cycle (study VI, VII)

Species in semi-arid environments have developed vast structural and functional adaptations to regulate carbon assimilation and respiratory water loss (e.g. Tenhunen et al., 1987, Werner et al., 1999; and literature therein). Considerable knowledge has been acquired on physiological processes in the last three decades (Beyschlag et al., 1986; Sala and Tenhunen, 1996; Tenhunen et al., 1985, 1990; Werner et al., 2001), emphasizing the role of ecophysiological adaptations to summer drought in Mediterranean climate conditions. However, winter recharge and sufficient water supply during spring are important in these ecosystems, as this is their most active period.

However, in the Mediterranean basin, reduced and altered precipitation pattern are already observed in previous studies and expected to continue with ongoing climate change (Hulme *et al.*, 1999; Costa *et al.*, 2012; Garcia-Barron *et al.*, 2013; Guerreiro *et al.*, 2013; Trigo *et al.*, 2013). Consequently, a functional understanding of the impact of increased drought and altered precipitation pattern on ecosystem functioning is vitally important for predictions of ecosystem resilience towards ongoing climate change.

Therefore, the following questions were addressed:

- *How does altered precipitation pattern and drought intensity impact net ecosystem exchange, evapotranspiration and cork-oak phenology (Study VI, VII)?*
- *What are the environmental drivers and physiological responses (study VII)?*

### 3. STUDY SITE AND EXPERIMENTAL DESIGN

Measurements were conducted in 2011 and 2012 in an open cork-oak woodland (*Quercus suber* L.) in central Portugal, approximately 100 km north-east of Lisbon (N39°8'17.84'' W8°20'3.76''; Herdade de Machoqueira do Grou). The trees are widely spaced (209 individuals ha<sup>-1</sup>) with a leaf area index of 1.1 and a gap probability of 0.7. The oak trees are managed for cork production, were planted approximately 50 years ago and have a mean maximum crown height of 10 m and diameter at breast height of 25 cm. It is a bi-layered system containing a herbaceous layer dominated by native annual forbs and grasses, with a growth peak in spring (April-May) and senescence occurring between late May and early June with the onset of summer drought. In autumn 2009 the site was ploughed, limed and then seeded with a legume-rich seed mixture of native species, a common practice in agro-silvopastoral systems in Portugal to improve productivity and soil fertility (Crespo, 2006). The soil is a cambisol, with 81% sand, 14% silt and 5% clay. The site is characterized by a Mediterranean climate, with wet spring conditions and hot, dry summers. Long-term mean annual temperature is approximately 15.9 °C and long-term mean annual precipitation is 680 mm (Instituto de Meteorologia, Lisbon).

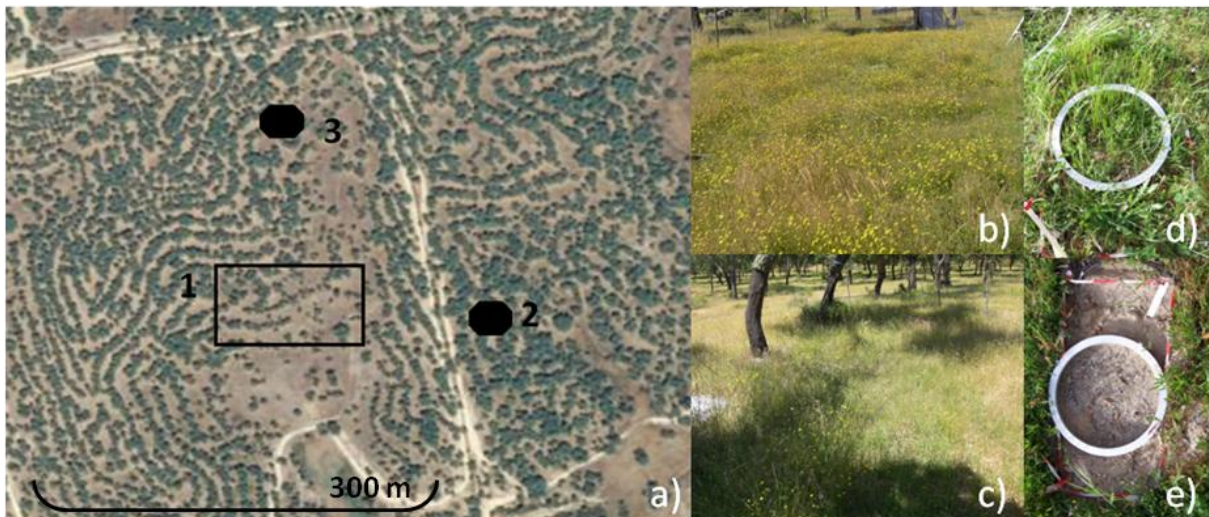


**Figure 1:** a) Satellite image of the study site (© Google Maps, 2011) with 1 position of the experimental understory sites; 2 position of the ecosystem tower and 3 position of the understory tower. b, c) Picture of the open and tree site, respectively and d, e) vegetation and bare soil plots.

Two experimental sites were established (Fig. 1a): one directly under the oak crown projected area (Fig. 1c) and another one in an adjacent open area, 5-7 m distant from any tree canopy cover (Fig. 1b).

Two types of plots were installed at each site: bare soil plots with total exclusion of above-ground biomass and root in-growth by inserting trenching meshes (Fig. 1e) and understory plots with undisturbed herbaceous understory vegetation (Fig. 1d).

An ecosystem and an understory eddy-covariance flux tower were set up both within approximately 150 m distance of the experimental field site (see Fig. 1a). Flow-through soil and branch chambers were developed, and connected to a Cavity Ring-Down Spectrometer (CRDS, Picarro; Fig. 2, a picture of the branch chamber set-up can be found in [study I](#)), to measure fluxes and isotopic signatures of evaporation and transpiration. To develop a new method indirectly estimating height and angle dependent  $LAI$  and  $P_{gap}$  based on digital cover photography a height adjustable tripod was equipped with a digital camera mounted on a tiltable rack that can be inclined to different zenith view angles.

- 1) Cylindrical Plexiglas chamber (height: 60 cm; diameter: 35 cm) coated with isotope inert FEP-foil
- 2) Metalring
- 3) Permanent soil-ring
- 4) Inlet-pipe, leads to diffuse Inlet within the metalring (2)
- 5) Outlet-pipe
- 6) Plexiglas lid
- 7) Mixing vents
- 8) Inlet and Outlet, to CRDS
- 9) Ventilator
- 10) Massflowcontroller
- 11) Clamps
- 12) Sensors: Photosynthetic active radiation, temperatur, pressure
- 13) Pictures of CRDS and chamber set-up

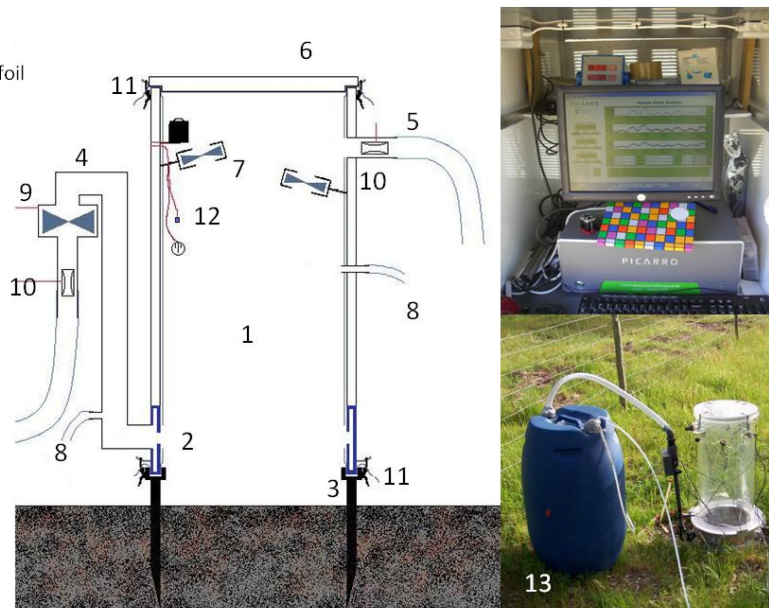


**Figure 2:** Schematic overview of the experimental setup for measuring soil evaporation and understory evapotranspiration and its isotopic composition in the field. Insets 13 show pictures of the chamber and laser spectrometer (L2120-i, Picarro, Santa Clara, USA).

## 4. MAIN RESULTS OF THIS THESIS

### 4.1. Validation of oxygen isotope modeling approaches (*study I, II, V*)

Although the Craig and Gordon (1965) model of evaporation was often used for  $ET$  partitioning in the past, its validation with direct estimates of  $\delta^{18}O_E$  in the field remained challenging (see Williams *et al.*, 2004, Yepez *et al.*, 2007; Wang *et al.*, 2013). It could be demonstrated for the first time that predicting  $\delta^{18}O$  of evaporation by the Craig and Gordon equation led to good agreement with measured  $\delta^{18}O_E$  based on CRDS measurements under very contrasting environmental conditions in the field (see Fig. 3; Dubbert *et al.*, 2013; *study II, V*). This is promising since the limiting data to test theoretical assumptions incorporated into modeling frameworks typically are direct estimates of  $\delta^{18}O_E$ .

However, special care must be taken concerning key parameters of the Craig and Gordon equation since  $\delta^{18}O_E$  is sensitive to even small uncertainties in  $\delta^{18}O$  and temperature at the evaporating sites ( $\delta^{18}O_e$  and  $T_e$ ) and the kinetic fractionation factor ( $\alpha_k$ ). The results of *study II* highlight the need for thorough characterization of the soil profile isotopic and climatic properties for correct estimations of  $\delta^{18}O_E$ . In *study II* also formulations of  $\alpha_k$  of soil evaporation were tested and it is recommended to account for variations in the kinetic fractionation factor depending on soil water availability in field studies that deal with broad changes in volumetric soil water content near the soil surface.

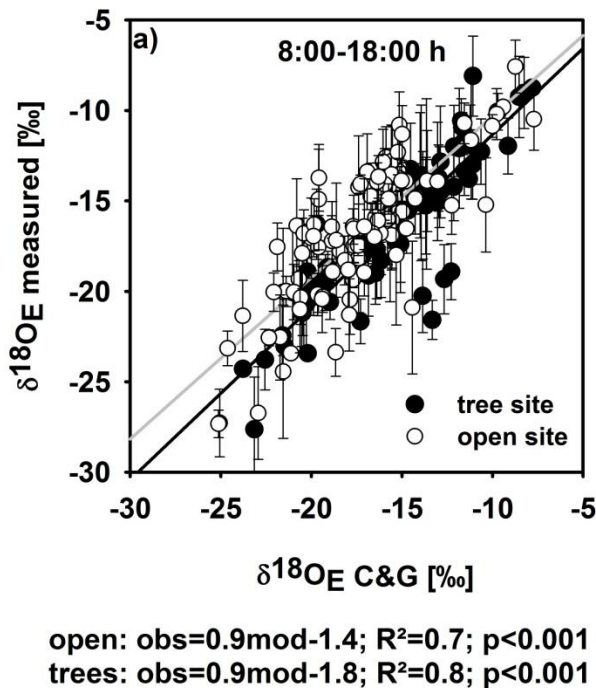


**Figure 3:** a) Oxygen isotope signatures of soil evaporation on bare soil plots calculated with the Craig and Gordon equation versus measured values for the open (white circles) and tree site (black circles) of every measurement point (mean values  $\pm$  SD;  $n=3$ ), the grey and black line denote regression lines for the open and tree site, respectively (adapted from Dubbert *et al.*, 2014c, see also Dubbert *et al.*, 2013)

Similar to validations of modeled  $\delta^{18}O$  of soil evaporation, *study I* underlined that direct estimates of  $\delta^{18}O$  of transpiration fit very well with indirect estimates of  $\delta^{18}O_T$  via modeling of  $\delta^{18}O$  of leaf water at the evaporating sites. Moreover, results of *study I* revealed that diurnal development of  $\delta^{18}O_T$  was largely driven by the strong diurnal changes in relative air humidity (see also recent findings under controlled conditions of Simonin *et al.*, 2013).

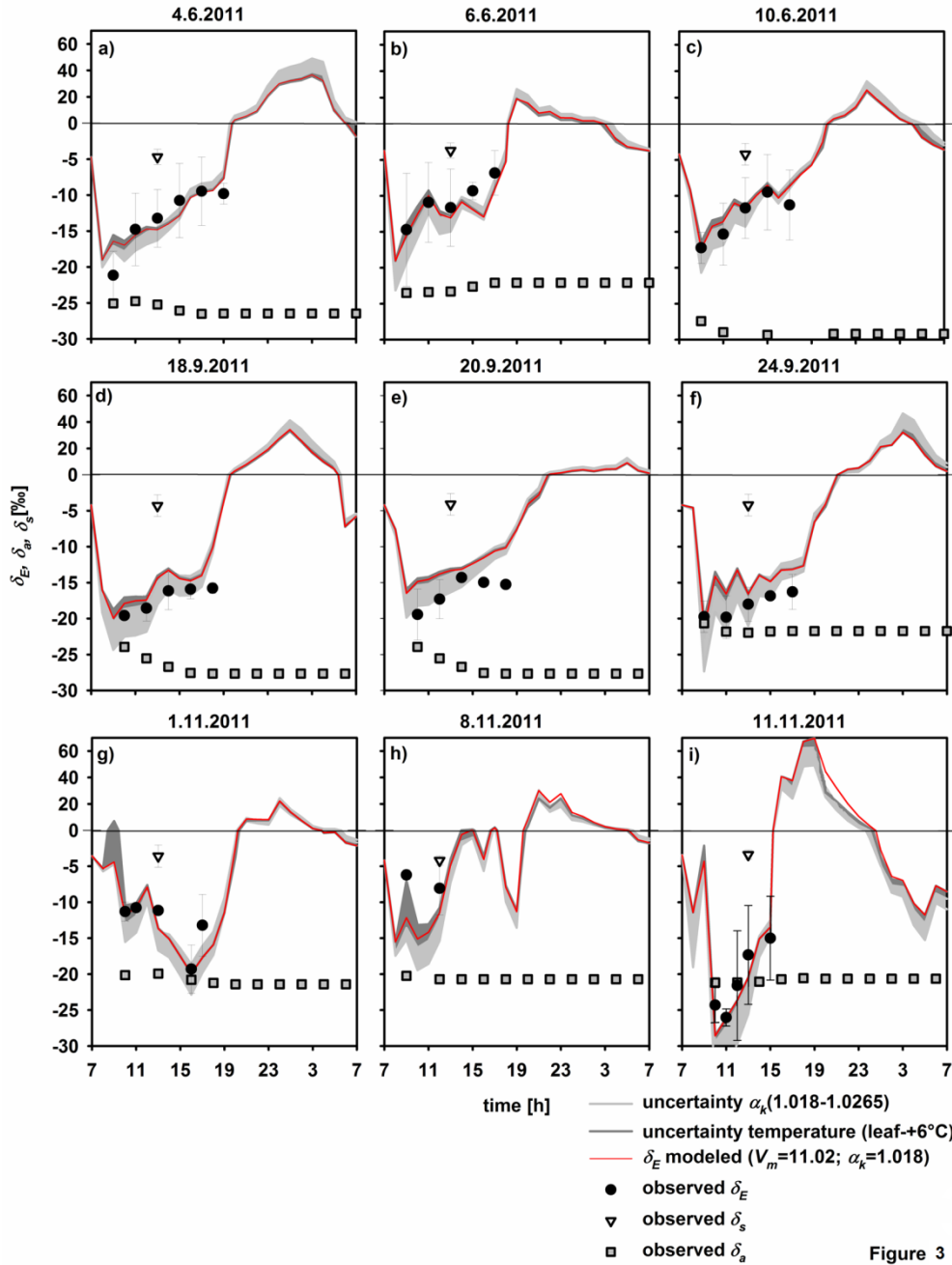


**Figure 4:** Diel measurements in spring (a-c), summer (d-f) and fall (g-i) of the oxygen isotope signature of transpired vapor ( $\delta^{18}O_T$ , black circles,  $n=3$ , mean values  $\pm$  SE) and modeled  $\delta^{18}O_T$  (red lines). Grey squares show measured oxygen isotope signatures of ambient air and grey triangles indicate  $\delta^{18}O$  of source water, i.e. xylem (from Dubbert *et al.*, 2014a).

It has generally been expected that plant transpiration reaches isotopic steady-state during large parts of the day, which means that  $\delta^{18}O_T$  is equal to source/xylem water (Dawson, 1993; see dotted line in Fig. 4). In contrast, here  $\delta^{18}O_T$  strongly deviated from steady-state predictions, specifically when leaf conductance was low (Fig. 4; compare measured and modeled  $\delta^{18}O_T$  with xylem isotopic values, dotted line).

The results obtained with this new method strongly suggest that non-steady-state transpiration very likely plays an important role under natural conditions. Finally, strong differences between isoforcing on the atmosphere considering isotopic steady-state vs. non-steady-state imply that non-steady-state effects of plant transpiration have likely consequences for partitioning ecosystem evapotranspiration using  $\delta H_2^{18}O$  or carbon fluxes using  $\delta C^{18}O^{16}O$ , or satellite-based applications (*study I, II*).

#### **4.2. Impact of scale heterogeneity due to sparse tree cover on understory vegetation dynamics and fluxes (*study III, IV*)**

In *study IV* significant interactions between trees and understory vegetation could be observed, leading to small scale heterogeneity within the understory vegetation development. By the end of the understory growing period (the last 6 weeks before senescence) a significant impact of tree cover on herbaceous plants development and net  $CO_2$  and water fluxes was detected. This led to 1) a niche segregation regarding the dominance of distinct functional groups on both sites, and 2) an earlier and faster senescence of the herbaceous layer under the trees due to a strong competition for water (*study IV, V*; Fig. 5, 7). This was unexpected as previous studies often found a beneficial effect of tree presence on herbaceous development (Joffre & Rambal, 1993; Cubera & Moreno, 2007). This even influenced total ecosystem sink strength in spring, as it reduced the overall understory productivity by 21.5% on average during the late spring (*study IV, V*, Fig. 7).

As tree cover in this ecosystem is sparse and heterogeneously distributed, the conclusions gained in *study IV* must be considered when net water and carbon fluxes of this ecosystem are separated into tree, understory and soil fluxes with the approach developed in *chapter I and II*. Therefore, partitioning of water and carbon fluxes at the understory level was done site specifically in an open area as well as under tree crowns. Estimates of vertical and angular gap probability  $P_{gap}$  distributions



(*study III*) can then be used to quantify the amount of open and tree crown covered ground area and used for up-scaling to ecosystem level.

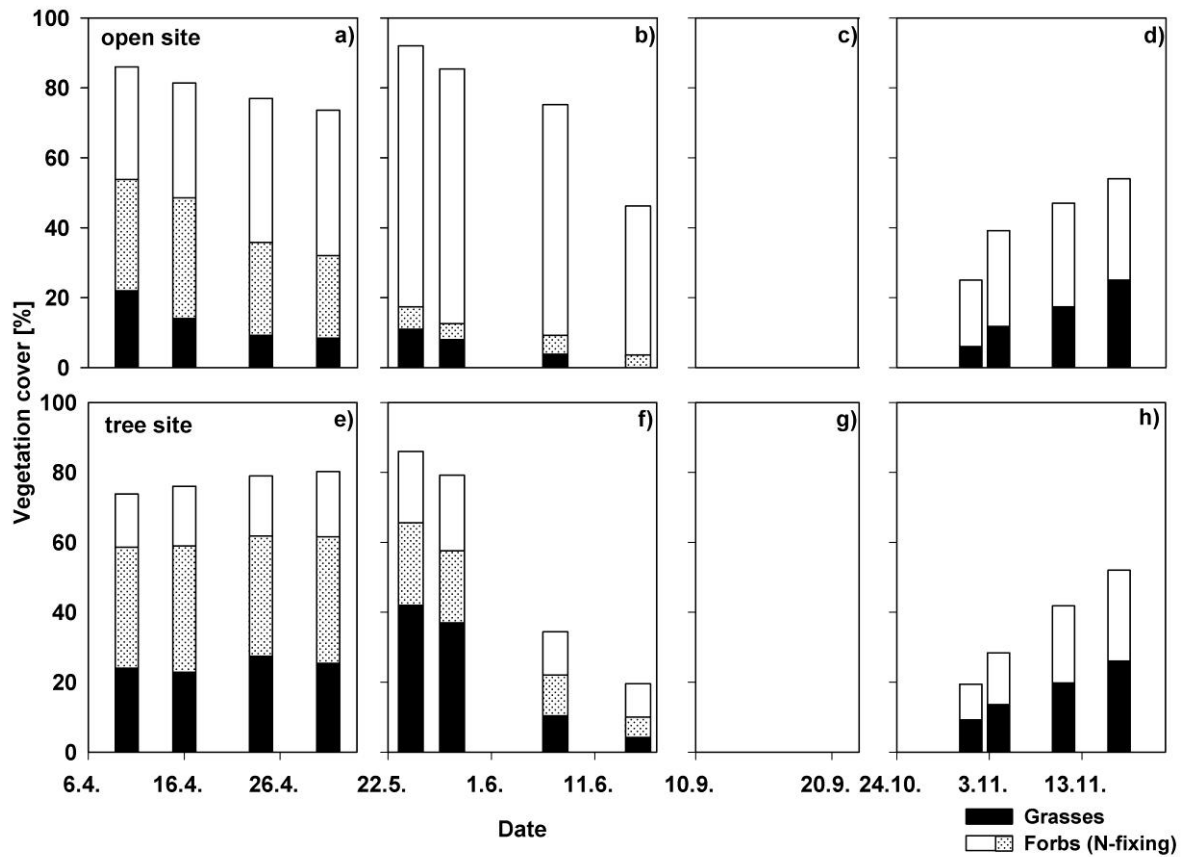


**Figure 5:** a-h) Relative vegetation cover in % of distinct functional groups of the herbaceous layer (Poaceae, N-fixing and other forbs) in spring and fall 2011 on the open (a-e) and tree site (f-h; mean values;  $n = 5$ ). From Dubbert *et al.*, 2014b.

$P_{gap}$  and  $LAI$  are important ecosystem parameters that are needed in soil-vegetation-atmosphere transfer modeling (De Pury and Farquhar, 1997; Sellers and Dorman, 1987) or radiative transfer schemes (Jacquemoud *et al.*, 2000; Haverd *et al.*, 2012). Since recent model development head towards high-resolution multi layer models (Baldocchi, 1997), the demand for vertically resolved and repeated measures of  $P_{gap}$  and  $LAI$  will increase in the future. Height and angularly distributed digital cover photography (*DCP*) could successfully be applied here for the first time and delivers similar gap probability  $P_{gap}$  and effective leaf area index  $LAI$  as the established  $LAI$ -2000. Notably, the appliance compared to the  $LAI$ -2000 is much easier and better (*study III*, Fig. 6). Regarding the present work, measurements of  $P_{gap}$  allowed a flux partitioning on ecosystem level without neglecting important information on ecosystem heterogeneity yielded through site specific measurements at the understory level (*study V*).

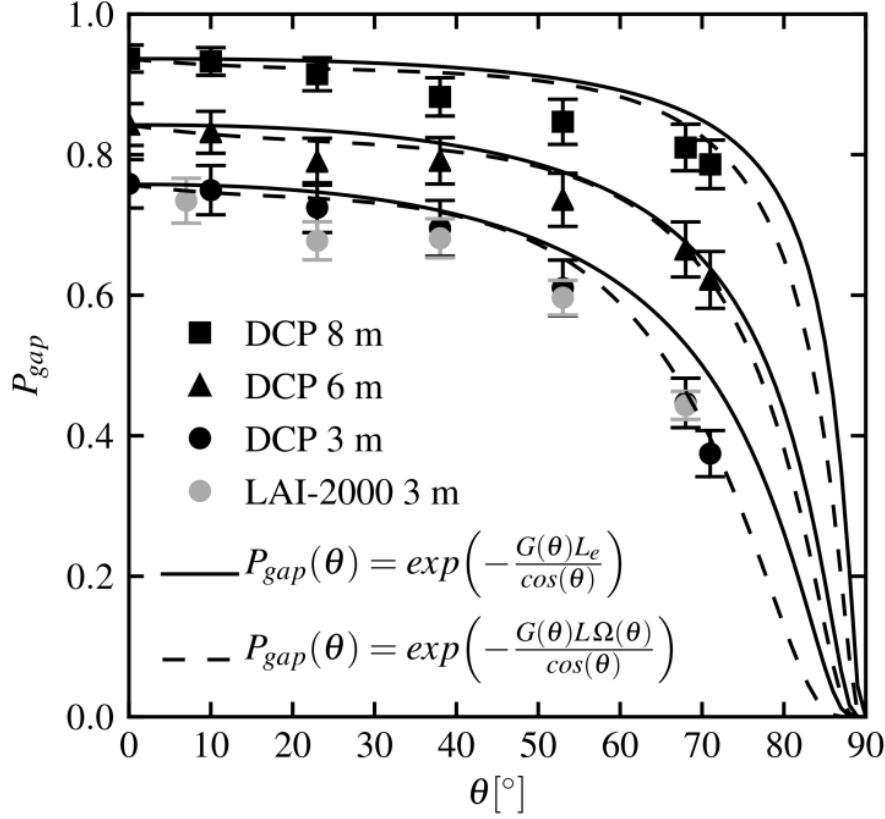


**Figure 6:** Dependency of gap probability  $P_{gap}$  on zenith view angle  $\theta$ . Black symbols: DCP method at 3, 6 and 8 m height. Grey symbols: LAI-2000 method at 3 m height (6 and 8 m heights not shown). Solid lines: Beer's law with effective leaf area index  $L_e$ . Dashed lines: Beer's law with angular dependent leaf clumping  $\Omega(\theta)$  (see chapter III). From Piayda *et al.*, under review Ecology.

#### 4.3. Impact of the herbaceous layer on ecosystem water budget, infiltration capacity and productivity (*study IV, V*)

Based on the insights from *studies I, II, III and IV* ecosystem water fluxes were separated into tree, understory and soil components. One main observation was the very distinct responses of understory  $T$  and soil  $E$  to changes in environmental conditions. While  $E$  was significantly correlated with top soil  $\theta_s$  ( $R^2=0.55$ ,  $p<0.001$ ), understory  $T$  was independent from  $\theta_s$  but correlated with  $VPD$  instead ( $R^2=0.57$ ,  $p<0.001$ ). This highlights that considering herbaceous understory  $E$  and  $T$  separately is crucial for understanding changes in net  $ET$ , as they are controlled by different environmental drivers (*study V*, Fig. 7; see also Cavanaugh *et al.*, 2011; Raz-Yaseef *et al.*, 2012).



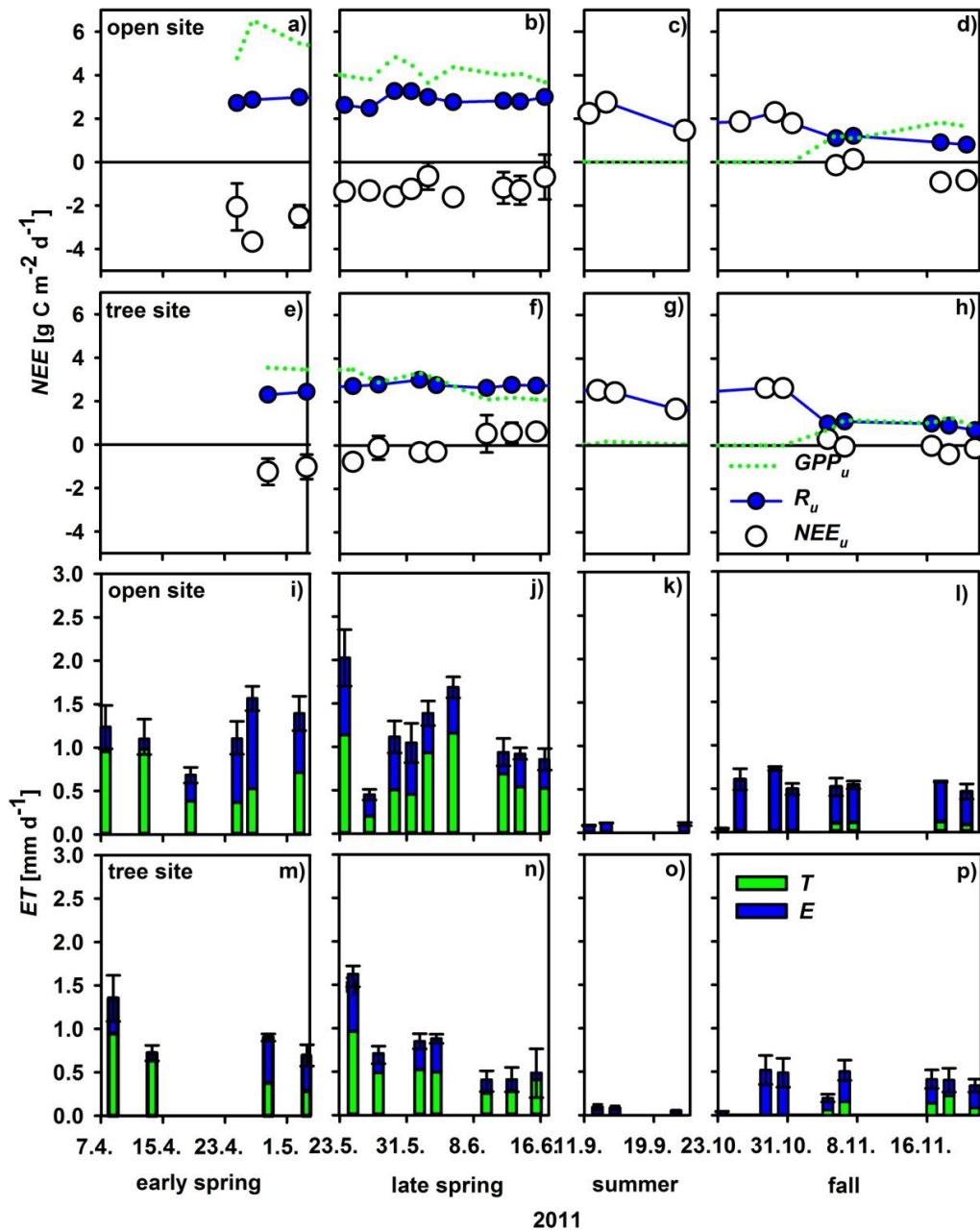


**Figure 7:** Daytime integrated net understory CO<sub>2</sub> exchange ( $NEE$ , g C m<sup>-2</sup> d<sup>-1</sup>, white circles; mean values  $\pm$  SE,  $n=3$ ), herbaceous gross primary production ( $GPP$ , dashed green line, mean values,  $n=3$ ) and respiration ( $R$ , blue line and circles, mean values,  $n=3$ ) on the open (a-d) and tree site (e-h); daytime integrated understory evapotranspiration ( $ET$ , mm d<sup>-1</sup>, mean values  $\pm$  SD,  $n=3$ ), which is the sum of herbaceous layer transpiration ( $T$ , green bars) and soil evaporation ( $E$ , blue bars) at the open (i-l) and tree site (m-p). Adapted from Dubbert *et al.*, 2014c.

Moreover, both components considerably contributed to overall ecosystem water loss (max. 43 and 55%, Fig. 8). Still, soil  $E$  did not play a major role limiting ecosystem productivity and water-use efficiency, since it decreased rapidly with drying top-soil and was low during dry periods where water availability was limiting ecosystem productivity. Moreover, the understory water-use efficiency

matched that of the cork-oaks during spring and fall and the herbaceous layer substantially added to the ecosystem carbon sink strength (see Unger *et al.*, 2009).

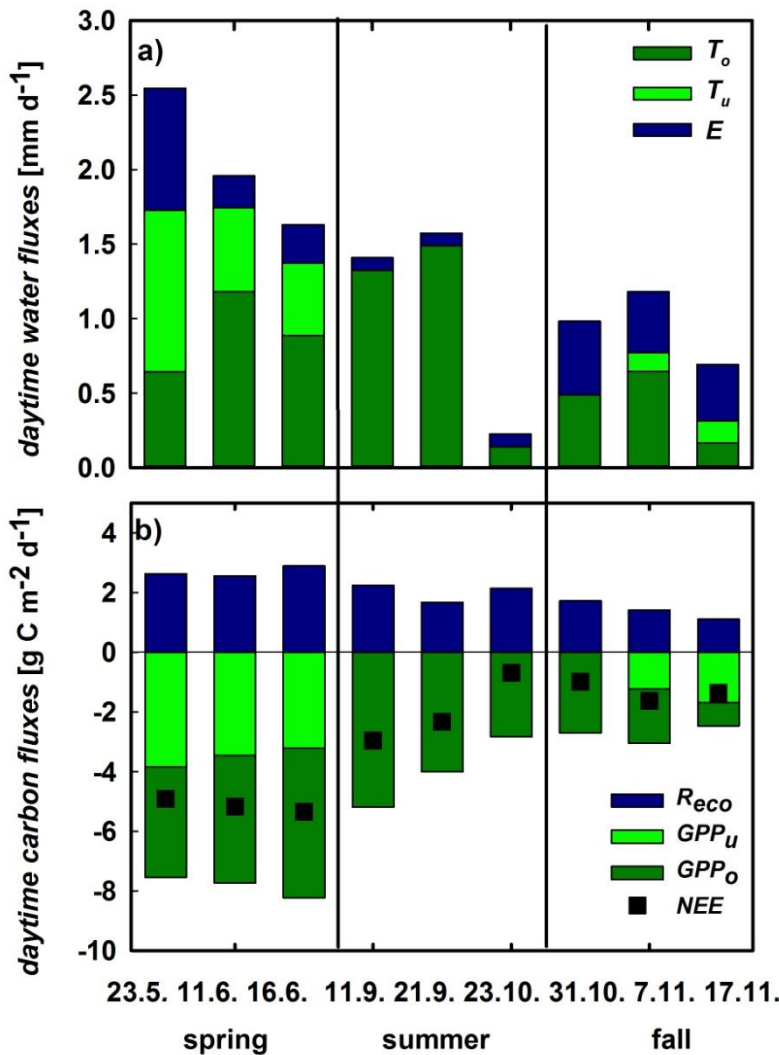


**Figure 8:** a) Daytime integrated ecosystem evapotranspiration ( $ET$ , sum of the stacked bars) and its components cork-oak transpiration ( $T_o$ , dark green), herbaceous transpiration ( $T_u$ , green) and soil evaporation ( $E$ , blue, all  $\text{mm d}^{-1}$ ). b) Daytime integrated  $GPP$  of cork-oaks ( $GPP_o$ , dark green) and understory ( $GPP_u$ , green), ecosystem respiration ( $R_{eco}$ ; blue), and net ecosystem  $\text{CO}_2$  exchange ( $NEE$ , black squares, all in  $\text{g C m}^{-2} \text{d}^{-1}$ ). From Dubbert *et al.*, 2014c.

Furthermore, herbaceous biomass strongly increased rain infiltration and also diminished  $E$ . A significant relation was found between amount of rain fall and difference in infiltration between bare soil and vegetated patches, the higher the amount of rain the higher the differences in infiltration between bare soil and vegetated soil (Fig. 9). This indicates that the presence of a fully developed herbaceous layer should be even more important with an altered, more heterogeneous precipitation pattern, with longer dry periods and heavy rain events, predicted by climate change scenarios for the Mediterranean basin (*study VII*, Fig. 9; see also Bhark *et al.*, 2003; Thompson *et al.*, 2010).

Finally, changes in ecosystem  $NEE$  and  $ET$ , especially between spring and summer, can largely be attributed to understory vegetation dynamics, since cork-oak, soil and respiratory flux components remained comparatively stable throughout the year. Thus the herbaceous layer, although itself

vulnerable to drought plays an important role for ecosystem flux dynamics, rain infiltration and hence indirectly cork-oak productivity and ecosystem resilience towards drought.

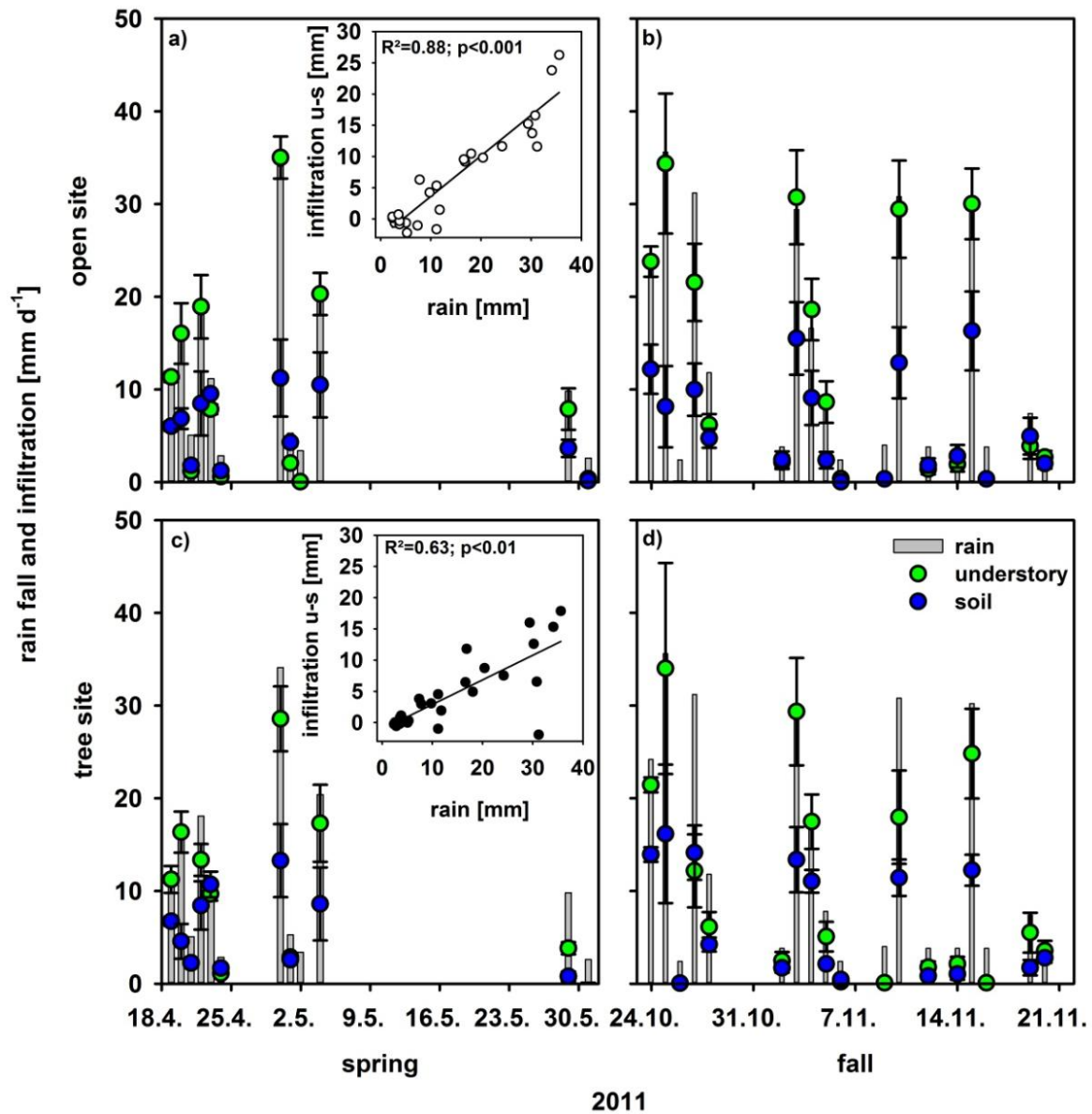


**Figure 9:** Rainfall and infiltration into the soil following rain events > 2 mm at a, b) the open and c, d) tree site on understory plots (green circles), bare soil plots (blue circles, all in mm d<sup>-1</sup>; n=4, mean values ± SE) and rainfall (grey bars). Insets present differences in infiltration between understory and bare soil versus rain amount at the open and tree site. Regression line, coefficient of regression and p-value are given. From Dubbert *et al.*, 2014c.

#### 4.4. Effects of extreme drought on ecosystem carbon gain, cork-oak and herbaceous layer development (*study VI, VII*)

Cork-oak savannas are well adapted to a prolonged summer drought, but winter recharge and sufficient water supply during spring is important in these ecosystems, as this is their most active period. Hence, a functional understanding of the impact of increased drought and altered precipitation

pattern on ecosystem functioning, as predicted by climate change scenarios (Costa *et al.*, 2012; IPCC, 2007), is important.

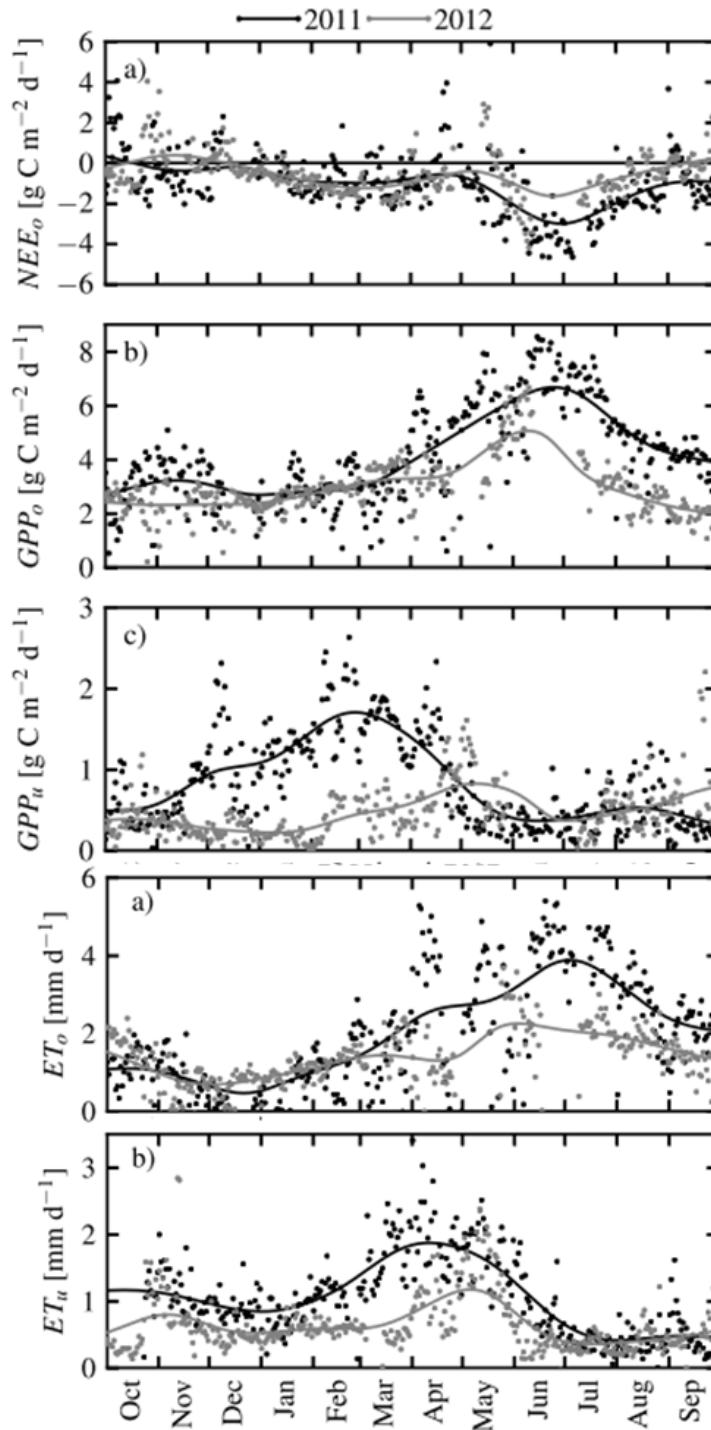


**Figure 10:** a) Ecosystem net carbon exchange ( $NEE_o$ ), b) ecosystem gross primary production ( $GPP_o$ ) and c) understory gross primary production ( $GPP_u$ ) for 2011 (black) and 2012 (grey). Dots mark daily sums, lines are kernel regressions. a) Ecosystem evapotranspiration  $ET_o$  and b) understory evapotranspiration  $ET_u$  for 2011 (black) and 2012 (grey). Dots mark daily sums, lines are kernel regressions. Adapted from Piayda *et al.*, 2014.

The years 2011 and 2012, contrasting in annual precipitation amount as well as pattern, offered an ideal opportunity to study effects of drought. Here, it could be demonstrated that in the exceptionally dry year 2012 (2<sup>nd</sup> driest year since 1950, Caldeira *et al.*, unpublished; Trigo *et al.*, 2013) ecosystem carbon sink strength and net ecosystem evapotranspiration were reduced by 34 and 26 %, respectively (*study VI, VII*; Fig. 10).

Ecosystem productivity was mainly diminished by reduced stomatal conductance and decrease of  $V_{cmax}$  of cork-oaks, while  $LAI$  was maintained (*study VI, VII*). Moreover, the severe drought in 2012 led to strong alterations in tree phenology: annual tree diameter increment was reduced by 64% and fruit production was severely depressed by water stress showing a reduction of 54% during the dry year of 2012 (*study VI, VII*; Fig. 11). Enhanced understanding of cork productivity (i.e. tree diameter growth) with ongoing climate change is particularly important for farmers. Further, understory growth was strongly diminished due to drought induced late germination in fall and a pronounced drought during the main growth period. The findings of *study VII* indicate that the timing of precipitation and drought is very important for herbaceous layer development.

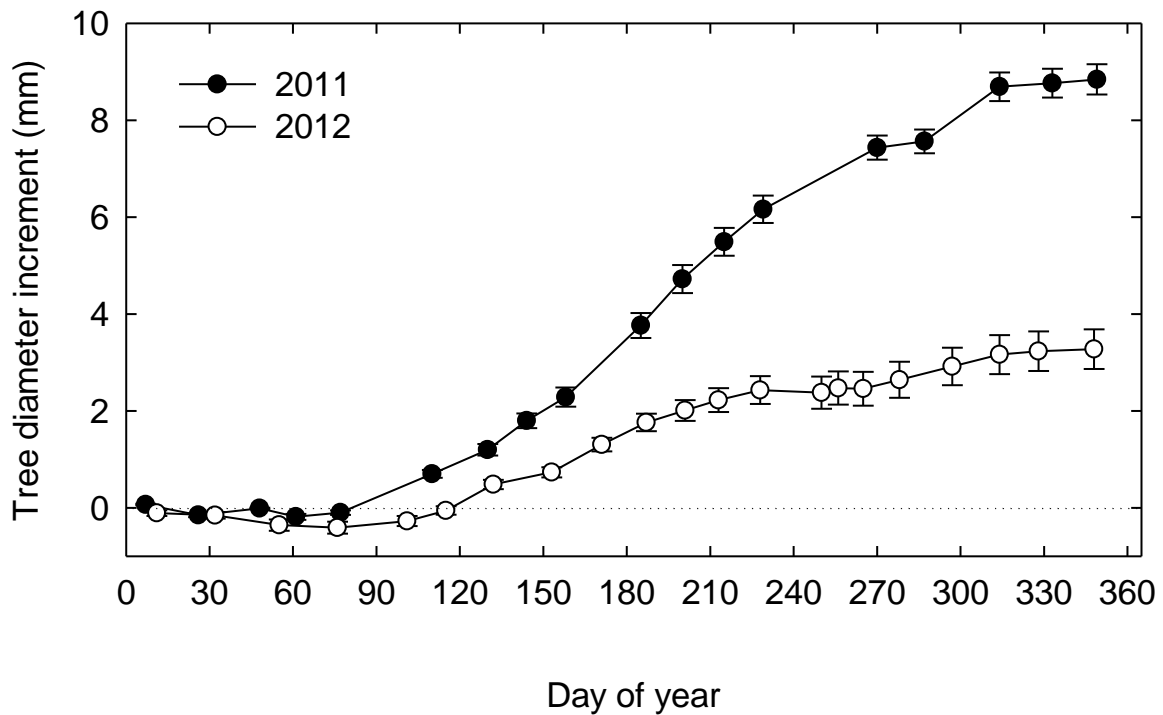


**Figure 11:** Tree diameter increment (mm) during 2011 and 2012. Values are means  $\pm$  se (n=9). From Costa e Silva *et al.*, under review in AFM.

Finally, it could be shown that in a dry year the Montado ecosystem uses more water through evapotranspiration than is introduced into the ecosystem by precipitation: the ratio  $ET/P$  increased to 122% in 2012 compared to 86% in 2011 (*study VII*). The resulting depletion of deep/groundwater reservoirs could prove fatal for the resilience of this ecosystem, as cork-oak trees rely on their access to water in deep soil layers (Kurz-Besson *et al.*, 2006).

## 4.5. Conclusions

This thesis aimed at a detailed mechanistic evaluation of the water balance and carbon cycling in a Mediterranean savannah-type oak woodland with a focus on understory vegetation impact.

To achieve this, a combined flux and  $\delta^{18}O$  partitioning approach was developed coupling flow through soil chambers to a Cavity Ring-Down Spectrometer (CRDS). It could be demonstrated for the first time that predicting  $\delta^{18}O$  of evaporation and transpiration led to good agreement with measured  $\delta^{18}O_E$  and  $\delta^{18}O_T$  based on CRDS measurements under contrasting environmental conditions in the field. The established field protocols strongly enhance the significance of  $\delta^{18}O$  as a tracer for water movement within the ecosystem and help avoiding previous pitfalls such as transpirational isotopic steady-state assumption and uncertainties related to model input parameter estimates. The developed  $\delta^{18}O$  partitioning approach proved to be a very good tool separating ecosystem water fluxes, specifically in ecosystems with dense herbaceous layers, preventing approaches solely based on flux measurements.

Thereby, it could be demonstrated that the understory, despite its high transpirational water loss, played a vitally important role for ecosystem functioning, as it enhanced rain infiltration, diminished soil  $E$  and contributed significantly to ecosystem sink strength. Moreover, altered precipitation pattern and extreme drought as observed in the extreme dry year 2012 severely reduced ecosystem net fluxes, inhibited understory development and influenced cork-oak productivity and phenological development.

In conclusion, the insights gained in this thesis enhance a mechanistic understanding of the processes regulating net water fluxes and productivity in semi-arid ecosystems. Moreover, they can help to adapt management practices maintaining a sustainable and productive land-use in the face of increased drought intensity and altered precipitation pattern.

## 5. LITERATURE

- Baldocchi DD, Vogel CA, Hall B (1997) Seasonal variation of carbon dioxide exchange rates above and below a boreal jack pine forest. *Agricultural and Forest Meteorology*, 83, 147-170.
- Beyschlag W, Lange OL, Tenhunen JD (1986) Photosynthesis and water relations of the Mediterranean sclerophyll *Arbutus unedo* L. Throughout the year at a site in Portugal. 1. Diurnal courses of CO<sub>2</sub> gas exchange and transpiration under natural conditions, *FLORA*, 178, 409-444.
- Bhark EW, Small EE (2003) Association between plant canopies and spatial pattern of infiltration in shrubland and grassland of the Chihuahuan Desert, New Mexico., *Ecosystems*, 6, 185-196.
- Bugalho MN, Caldeira MC, Pereira JS, Aronson J, Pausas JG (2011) Mediterranean cork-oak savannas require human use to sustain biodiversity and ecosystem services. *Frontiers of Ecology and Environments*, 9, 278-286.
- Cavanaugh ML, Kurc SA, Scott RL (2011) Evapotranspiration partitioning in semiarid shrubland ecosystems: a two-site evaluation of soil moisture control on transpiration. *Ecohydrology*, 4, 671-681.
- Craig H, Gordon LI (1965) Deuterium and oxygen-18 variations in the ocean and the mairitme atmosphere. Paper presented at the Stable Isotopes in Oceanographic Studies and Paleotemperatures, Spoleto, Italy.
- Crespo DG (2006) The role of pasture improvement in the rehabilitation of the “montado/dehesas” system and in developing its traditional products. In: *Animal products from the Mediterranean area* (eds. Ribeiro JMCR, Horta AEM, Mosconi C, Rosati A) 100pp., Wageningen Acad. Publ., Wageningen, NL.
- Costa AC, Santos JA, Pinto JG (2012) Climate change scenarios for precipitation extremes in Portugal. *Theoretical and applied climatology*, 108, 217-234.
- Cubera E, Moreno G (2007) Effect of single *Quercus ilex* trees upon spatial and seasonal changes in soil water content in Dehesas of central western Spain. *Annals for Forest Science*, 64, 355 – 364.
- Dawson T (1993) Hydraulic lift and water transport to, through and from roots. *Plant Physiology*, 102, 29.
- DePury DGG, Farquhar, GD (1997) Simple scaling of photosynthesis from leaves to canopies without errors of big-leaf models. *Plant, Cell and Environment*, 20, 537-557.
- Devitt DA, Smith SD (2002) Root channel macropores enhance downward movement of water in a Mojave Desert ecosystem. *Journal of arid environments*, 50, 99-108.
- Dongmann G, Nurnberg HW, Forstel H, Wagener K (1974) On the enrichment of H<sub>2</sub><sup>18</sup>O in the leaves of transpiring plants. *Radiation and Environmental Biophysics*, 11, 41-52.
- Dubbert M, Cuntz M, Piayda A, Maguas C, Werner C (2013) Partitioning evapotranspiration – Testing the Craig and Gordon model with field measurements of oxygen isotope ratios of evaporative fluxes. *Journal of Hydrology*, 496, 142-153.
- Dubbert M, Piayda A, Cuntz M, Werner C (2014a) Oxygen isotope signatures of transpired water vapor – the role of non-steady-state transpiration under natural conditions. *New Phytologist*.
- Dubbert M, Mosen A, Piayda A, Cuntz M, Correia A, Pereira J S, Werner C (2014b) Influence of tree cover on herbaceous layer development and carbon and water fluxes in a Portuguese cork oak woodland. *Acta Oecologica*.
- Dubbert M, Piayda A, Cuntz M, Correia A, Costa e Silva F, Pereira J S, Werner C (2014c) Stable oxygen isotope and flux based partitioning demonstrates understory vegetation of an oak savanna contributes up to half of ecosystem carbon and water exchange, reduces soil evaporation and increases infiltration. In press *Frontiers in Plant Science*.
- Garcia-Barron L, Morales J, Sousa A (2013) Characterisation of the intra-annual rainfall and its evolution (1837-2010) in the southwest of the Iberian Peninsula. *Theoretical and Applied*



- Climatology, pp. 1–13.
- Grace J, Jose JS, Meir P, Miranda HS, Montes RA (2006) Productivity and carbon fluxes of tropical savannas. *Journal of Biogeography*, 33, 387–400.
- Guerreiro SB, Kilsby CG, Serinaldi F (2013) Analysis of time variation of rainfall in transnational basins in Iberia: abrupt changes or trends? *International Journal of Climatology*.
- Haverd V, Cuntz M, Griffith D, Keitel C, Tados C, Twining J (2011) Measured deuterium in water vapour concentration does not improve the constraint on the partitioning of evapotranspiration in a tall forest canopy, as estimated using a soil vegetation atmosphere transfer model. *Agricultural and forest Meteorology*, 151, 645–654.
- Haverd V, Lovell J, Cuntz M, Jupp D, Newnham G, Sea W (2012) The canopy semi-analytic *Pgap* and radiative transfer (canspart) model: Formulation and application. *Agricultural and Forest Meteorology*, 160 (0), 14 – 35.
- Hulme M, Mitchell J, Ingram W, Lowe J, Johns T, New M, Viner D (1999) Climate change scenarios for global impacts studies. *Global Environmental Change*, 9, Supplement 1, S3 – S19.
- Hussain M, Otieno D, Mirzae H, Li Y, Schmidt M, Siebke L, Foken T, Ribeiro N, Pereira J, Tenhunen J (2009) CO<sub>2</sub> exchange and biomass development of the herbaceous vegetation in the Portuguese montado ecosystem during spring. *Agriculture, Ecosystems and Environment*, 132: 143–152.
- Huxman TE, Wilcox BP, Breshears DD *et al.* (2005) Ecohydrological implications of woody plant encroachment. *Ecology*, 86, 308–319.
- IPCC (2007) Climate change 2007: synthesis report. In: Contribution of Working Groups I, II and III to the Fourth Assessment Report of the Intergovernmental Panel on Climate change (eds. Core Writing Team, Pachauri RK, Reisinger A), 104pp. IPCC, Geneva, Switzerland.
- Jacquemoud S, Bacour C, Poilve H, Frangi J-P (2000) Comparison of four radiative transfer models to simulate plant canopies reflectance: Direct and inverse mode. *Remote Sensing of Environment*, 74 (3), 471 – 481.
- Joffre R, Rambal S (1993) How Tree Cover Influences the Water Balance of Mediterranean Rangelands. *Ecology*, 74: 570–582.
- Lai CT, Ehleringer JR, Bond BJ, U K (2006) Contributions of evaporation, isotopic non-steady state transpiration and atmospheric mixing on the delta O-18 of water vapor in Pacific Northwest coniferous forests. *Plant, Cell and Environment*, 29, 77–94.
- Moreno G, Obrador JJ, Cubera E, Dupraz C (2005) Fine root distribution in Dehesas of Central-Western Spain. *Plant and Soil*, 277, 153–162.
- Moreno G, (2008) Response of understorey forage to multiple tree effects in Iberian dehesas. *Agriculture, Ecosystems and Environment*, 123: 239–244.
- Otieno D, Mirzaei H, Hussain M, Li Y, Schmidt M, Wartinger M, Jung E, Ribeiro N, Pereira J, Tenhunen J (2011) Herbaceous layer development during spring does not deplete soil nitrogen in the Portuguese Montado. *Journal of Arid Environments*, 75, 231–238.
- Paço TA, David TS, Henriques MO *et al.* (2009) Evapotranspiration from a Mediterranean evergreen oak savannah: The role of trees and pasture. *Journal of Hydrology*, 369, 98–106.
- Paredes D, Trigo RM, Garcia-Herrera R, Trigo IF (2006) Understanding Precipitation Changes in Iberia in 590 Early Spring: Weather Typing and Storm-Tracking Approaches, *J. Hydrometeorol*, 7, 101–113.
- Pereira JS, Chaves M-M, Caldeira M-C, Correia AV (2006) Water availability and production. In: Plant growth and climate change (eds. Morison JIL, Morecroft MD). Blackwell Publishing Ltd., Oxford.
- Pereira JS, Mateus JA, Aires LM *et al.* (2007) Net ecosystem carbon exchange in three contrasting Mediterranean ecosystems – the effect of drought. *Biogeosciences*, 4, 791–802.
- Perez-Ramos I, Zavala M, Maranon T, Diaz-Villa M, Valladares F (2008) Dynamics of understorey



- herbaceous plant diversity following shrub clearing of cork-oak forests: A five-year study. *Forest Ecology and Management*, 255, 3242-3253.
- Piayda A, Dubbert M, Rebmann C, Kolle O, Costa e Silva F, Correia A, Pereira J S, Werner C, Cuntz M (2014) Drought impact on carbon and water cycling in a Mediterranean *Quercus suber* L. woodland during the extreme drought event in 2012. *Biogeosciences Discussions*.
- Raz-Yaseef N, Yakir D, Schiller G, Cohen S (2012) Dynamics of evapotranspiration partitioning in a semi-arid forest as affected by temporal rainfall pattern. *Agricultural and Forest Meteorology*, 157, 77-85.
- Sala A and Tenhunen J (1996) Simulations of canopy net photosynthesis and transpiration in *Quercus ilex* L. under the influence of seasonal drought, *Agricultural and Forest Meteorology*, 78, 203 – 222.
- Scholes RJ, Archer SR (1997) Tree-grass interactions in savannas. *Annual Review of Ecology and Systematics*, 28, 517-544.
- Scott RL, Huxman TE, Barron-Gafford GA, Jenerette GD, Young JM, Hammerlynck EP (2014) When vegetation change alters ecosystem water availability. *Global Change Biology*, online first.
- Schwinning S, Ehleringer J (2001) Water use trade-offs and optimal adaptations to pulse-driven arid ecosystems. *Journal of Ecology*, 89, 464–48.
- Sellers PJ, Dorman JL, May (1987) Testing the simple biosphere model (sib) using point micrometeorological and biophysical data. *Journal of Climate and applied Meteorology* 26 (5), 622–651.
- Simonin KA, Roddy AB, Link P, Apodaca R, Tu KP, Hu J, Dawson TE, Barbour MM (2013) Isotopic composition of transpiration and rates of change in leaf water isotopologue storage in response to environmental variables. *Plant, Cell and Environment* 36: 2190-2206.
- Tenhunen JD, Lange OL, Harley PC, Beyschlag W, Meyer A (1985) Limitations due to water-stress on leaf net photosynthesis of *Quercus coccifera* in the Portuguese evergreen scrub, *Oecologia*, 67, 23-30.
- Tenhunen JD, Pearcy RW, Lange OL (1987) diurnal variations in leaf conductance and gas exchange in natural environments, in *Stomatal function: Meeting Honolulu, Hawaii, USA, April 1983*, edited by Zeiger, E., Farquhar, G.D., Cowan, I.R., Stanford University press, California, USA.
- Tenhunen JD, Serra AS, Harley PC, Dougherty RL, Reynolds JF (1990) Factors influencing carbon fixation and water-use by Mediterranean sclerophyll shrubs during summer drought, *Oecologia*, 82, 381-393.
- Thompson SE, Harman CJ, Heine P, Katul GG (2010) Vegetation-infiltration relationships across climatic and soil type gradients. *Journal of geophysical Research*, 115, 1-12.
- Trigo RM, Añel JA, Barriopedro D, García-Herrera R, Gimeno L, Nieto R, Castillo R, Allen MR, Massey N (2013) THE RECORD WINTER DROUGHT OF 2011–12 IN THE IBERIAN PENINSULA. *AMERICAN METEOROLOGICAL SOCIETY, BAMS*, S41.
- Tromble JM (1988) Water interception by 2 arid land shrubs. *Journal of arid environments*, 15: 65-70.
- Unger S, Máguas C, Pereira JS, Aires LM, David TS, Werner C (2009) Partitioning carbon fluxes in a Mediterranean oak forest to disentangle changes in ecosystem sink strength during drought. *Agricultural and Forest Meteorology*, 149, 949–961.
- Unger S, Maguas C, Pereira JS, Aires LM, David TS, Werner C (2010) Disentangling drought-induced variation in ecosystem and soil respiration using stable carbon isotopes. *Oecologia*, 163, 1043-1057.
- Wang L, Caylor KK, Villegas JC, Barron-Gafford GA, Breshears DD, Huxman TE (2010) Partitioning evapotranspiration across gradients of woody plant cover: Assessment of a stable isotope technique. *Geophysical Research Letters*, 37.
- Wang L, D'Odorico P, Evans JP, Eldridge DJ, McCabe MF, Caylor KK, King EG (2012a) Dryland ecohydrology and climate change: critical issues and technical advances. *Hydrological Earth System Science*, 16, 2585-2603.

- Wang L, Good SP, Caylor KK, Cernusak LA (2012b) Direct quantification of leaf transpiration isotopic composition. *Agricultural and Forest Meteorology* 154, 127-135.
- Wang L, Niu S, Good SP, Soderberg K, McCabe M, Sherry RA, Luo Y, Zhou X, Xia J, Caylor KK (2013) The effect of warming in grassland evapotranspiration partitioning using laser-based isotope monitoring techniques. *Geochimica et Cosmochimica Acta*, in press.
- Werner C, Correia O, Beyschlag W (1999) Two different strategies of Mediterranean macchia plants to avoid photoinhibitory damage by excessive radiation levels during summer drought, *Acta Oecologia*, 20, 15-35.
- Werner C, Ryel R, Correia O, Beyschlag W (2001) Effects of photoinhibition on whole-plant carbon gain assessed with a photosynthesis model. *Plant, Cell and Environment*, 24: 27-40.
- Werner C, Schnyder H, Cuntz M *et al.* (2012) Progress and challenges in using stable isotopes to trace plant carbon and water relations across scales. *Biogeosciences*, 9, 3083-3111.
- Williams DG, Cable W, Hultine K *et al.* (2004) Evapotranspiration components determined by stable isotope, sap flow and eddy-covariance techniques. *Agricultural and Forest Meteorology*, 125, 241-258.
- Xu X, Sherry RA, Niu S, Li D, Luo Y (2013) Net primary productivity and rain-use efficiency as affected by warming, altered precipitation, and clipping in mixed-grass prairie. *Global Change Biology*, 19, 2753-2764.
- Yakir D, Sternberg LDL (2000) The use of stable isotopes to study ecosystem gas exchange. *Oecologia*, 123 (3), 297-311.
- Yepez EA, Scott RL, Cable WL, Williams DG (2007) Intraseasonal variation in water and carbon dioxide flux components in a semiarid riparian woodland. *Ecosystems*, 10, 1100-1115.
- Zhang Y, Shen Y, Sun H, Gates JB (2011) Evapotranspiration and its partitioning in an irrigated winter wheat field: A combined isotopic and micrometeorological approach. *Journal of Hydrology*, 40, 203-211.

## 6. STUDY OVERVIEW, PUBLICATION STATUS AND CONTRIBUTIONS

The publications and manuscripts included in this dissertation were prepared in cooperation with various co-authors. An overview over the objectives and the main outcome of the individual studies is presented in Table 1.

**Table 1:** Overview of titles, objectives and Conclusions of the individual studies of this work.

Study	Objectives	Conclusions
I	<ul style="list-style-type: none"> <li>Validating modeling approaches for estimating <math>\delta^{18}O_T</math> and quantify the impact of non-steady-state transpiration</li> </ul>	<ul style="list-style-type: none"> <li>Good agreement between modeled <math>\delta^{18}O_T</math> and measured <math>\delta^{18}O_T</math> based on CRDS</li> <li>Strong impact of isotopic non-steady-state on atmospheric <math>\delta^{18}O</math></li> </ul>
II	<ul style="list-style-type: none"> <li>Validating the Craig and Gordon model for soil evaporation</li> <li>Impact of isotopic steady-state assumption of transpiration on <math>ET</math> partition (<math>ft</math>)</li> </ul>	<ul style="list-style-type: none"> <li>Good agreement between modeled <math>\delta^{18}O_E</math> and measured <math>\delta^{18}O_E</math> based on CRDS</li> <li>Strong impact of isotopic non-steady-state assumption to <math>ft</math></li> </ul>
III	<ul style="list-style-type: none"> <li>Develop a DCP based method to obtain <math>LAI</math> and <math>P_{gap}</math> in an open, heterogeneous woodland and comparison with LAI-2000</li> </ul>	<ul style="list-style-type: none"> <li>Better appliance compared to established LAI-2000</li> <li>Development of field measurement and analysis protocol</li> </ul>
IV	<ul style="list-style-type: none"> <li>Determine the heterogeneity created by the patchy tree cover</li> <li>Determine possible interaction between trees and understory and their impact</li> </ul>	<ul style="list-style-type: none"> <li>Sparse tree cover leads to strong understory small scale heterogeneity regarding dominance of functional groups</li> <li>Earlier senescence of the understory under trees, due to competition for water</li> </ul>
V	<ul style="list-style-type: none"> <li>Disentangle understory impact on:               <ol style="list-style-type: none"> <li>ecosystem water fluxes</li> <li>rain water infiltration</li> </ol> </li> <li>Quantify the role of the herbaceous layer for ecosystem productivity</li> </ul>	<ul style="list-style-type: none"> <li>Understory accounted for max. 43% of <math>ET</math> and 51% of <math>GPP</math></li> <li>Soil <math>E</math> is high during wet periods but does limit ecosystem <math>WUE</math> during drought</li> <li>Beneficial understory effects are dominant: increased infiltration and reduced <math>E</math></li> </ul>
VI	<ul style="list-style-type: none"> <li>Quantify the effect of contrasting seasonal water availabilities on oak phenology and carbon cycle</li> </ul>	<ul style="list-style-type: none"> <li><math>NEE</math> reductions under drought are not caused by leaf area reductions</li> <li>Tree diameter growth and fruit production severely affected by drought</li> </ul>
VII	<ul style="list-style-type: none"> <li>Effect of winter/spring drought on net ecosystem carbon exchange (<math>NEE</math>) and evapotranspiration (<math>ET</math>)</li> <li>Identify the responsible environmental parameters and physiological responses</li> </ul>	<ul style="list-style-type: none"> <li>In a drought year more water evaporates from the ecosystem than is introduced</li> <li>Understory growth is completely inhibited in the drought year and ecosystem sink-strength strongly diminished by 34%</li> </ul>

The co-authors listed in these publications and manuscripts contributed as follows:

**Study I: OXYGEN ISOTOPE SIGNATURES OF TRANSPIRED WATER VAPOR – THE ROLE OF ISOTOPIC NON-STEADY-STATE TRANSPIRATION UNDER NATURAL CONDITIONS**

Status: published in New Phytologist, 203: 1242-1252; accepted: 9. June 2014

Contributors:

<u>Maren Dubbert</u>	development of experimental design, accomplishment of field work, modeling and laboratory analyses, preparation of the manuscript
Arndt Piayda	suggestions to improve the manuscript, help with field work
Matthias Cuntz	discussions on results, help with model development, suggestions to improve the manuscript
Christiane Werner	discussions on experimental design and results, suggestions to improve the manuscript

**Study II: PARTITIONING EVAPOTRANSPIRATION – TESTING THE CRAIG AND GORDON MODEL WITH FIELD MEASUREMENTS OF OXYGEN ISOTOPE RATIOS OF EVAPORATIVE FLUXES**

Status: published in Journal of Hydrology, 496: 142-153; accepted: 19. May 2013

Contributors:

<u>Maren Dubbert</u>	development of experimental design, accomplishment of field work, modeling and laboratory analyses, preparation of the manuscript
Matthias Cuntz	discussions on the results, help with model development, suggestions to improve the manuscript
Arndt Piayda	suggestions to improve the manuscript, help with field work
Cristina Maguas	laboratory analyses
Christiane Werner	discussions on experimental design and results, suggestions to improve the manuscript

**Study III: INFLUENCE OF WOODEN TISSUE AND LEAF CLUMPING ON VERTICALLY RESOLVED LEAF AREA INDEX AND ANGULAR GAP PROBABILITY ESTIMATES**

Status: under review at Ecology, date of submission: 11. September.2014, #14-1753

Contributors:

Arndt Piayda	development of experimental design, accomplishment of field work, preparation of the manuscript
<u>Maren Dubbert</u>	accomplishment of field work, discussions on results, suggestions to improve

	the manuscript
Christiane Werner	discussions on results, suggestions to improve the manuscript
Alexandra Correia	help with field work
Joao Santos Pereira	suggestions to improve the manuscript
Matthias Cuntz	discussions on experimental design and the results, suggestions to improve the manuscript

#### **Study IV: INFLUENCE OF TREE COVER ON HERBACEOUS LAYER DEVELOPMENT AND CARBON AND WATER FLUXES IN A PORTUGUESE CORK-OAK WOODLAND**

Status: published in Acta Oecologica, 59: 35-46; accepted: 20. May 2014

Contributors:

<u>Maren Dubbert</u>	development of experimental design, accomplishment of field work and laboratory analyses, preparation of the manuscript
Alexander Mosena	accomplishment of field work and laboratory analyses, preparation of the manuscript (Material & Methods, parts of results)
Arndt Piayda	help with field work, discussions on the results, comments on the manuscript
Matthias Cuntz	suggestions to improve the manuscript
Alexandra Correia	suggestions to improve the manuscript
Joao Santos Pereira	suggestions to improve the manuscript
Christiane Werner	discussion on experimental design and results, suggestions to improve the manuscript

#### **Study V: STABLE OXYGEN ISOTOPE AND FLUX PARTITIONING DEMONSTRATES UNDERSTORY OF AN OAK SAVANNA CONTRIBUTES UP TO HALF OF ECOSYSTEM CARBON AND WATER EXCHANGE**

Status: in press at Frontiers in Plant Science, in press; accepted: 18. September 2014

Contributors:

<u>Maren Dubbert</u>	development of experimental design, field work, modeling and laboratory analyses, preparation of the manuscript
Arndt Piayda	help with field work, suggestions to improve the manuscript
Alexandra Correia	suggestions to improve the manuscript
Filipe Costa e Silva	suggestions to improve the manuscript
Joao Santos Pereira	suggestions to improve the manuscript
Matthias Cuntz	suggestions to improve the manuscript, help with model development

Christiane Werner	discussion on experimental design and results, suggestions to improve the manuscript
-------------------	--

**Study VI: EFFECTS OF AN EXTREME DRY WINTER ON *Q. SUBER* WOODLAND: NET ECOSYSTEM EXCHANGE AND TREE PHENOLOGY ADJUSTMENTS**

Status: under review at Agricultural and Forest Meteorology, date of submission: 2. June 2014, AGRFORMET-D-14-00374

Contributors:

Filipe Costa e Silva	accomplishment of experimental design and field work, preparation of the manuscript
Alexandra Correia	field work, discussions on the results, suggestions to improve the manuscript
<u>Maren Dubbert</u>	accomplishment environmental and water potential measurements, discussion on results, help with manuscript preparation
Arndt Piayda	treatment of Eddy-covariance data, discussion on results, suggestions to improve the manuscript
Christiane Werner	discussions on results, suggestions to improve the manuscript
Matthias Cuntz	suggestions to improve the manuscript
Jorge Soares David	suggestions to improve the manuscript
Joao Santos Pereira	discussions on experimental design and the results, suggestions to improve the manuscript

**Study VII: DROUGHT IMPACT ON CARBON AND WATER CYCLING IN A MEDITERRANEAN *QUERCUS SUBER* L. WOODLAND DURING THE EXTREME DROUGHT EVENT IN 2012**

Status: published in Biogeosciences Discussions, accepted: 17. June 2014

Contributors:

Arndt Piayda	development of experimental design, field work and modeling, preparation of the manuscript
<u>Maren Dubbert</u>	help with field work, discussions on results, help with manuscript preparation
Corinna Rebmann	discussions on results, help with field site establishment
Olaf Kolle	help with field site establishment
Filipe Costa e Silva	help with field work, suggestions to improve the manuscript
Alexandra Correia	help with field work, suggestions to improve the manuscript
Joao Santos Pereira	suggestions to improve the manuscript
Christiane Werner	discussion on results, suggestions to improve the manuscript
Matthias Cuntz	model development, discussion on results, comments on the manuscript



# **Water balance and productivity of a Mediterranean oak woodland**

**Quantifying understory vegetation impacts by development of a stable oxygen isotope partitioning approach**

## **CUMULATIVE STUDIES**







# **1. STUDY I: OXYGEN ISOTOPE SIGNATURES OF TRANSPIRED WATER VAPOR – THE ROLE OF ISOTOPIC NON-STEADY-STATE TRANSPIRATION UNDER NATURAL CONDITIONS**

Maren Dubbert<sup>1,✉</sup>; Matthias Cuntz <sup>2</sup>; Arndt Piayda<sup>2</sup>; and Christiane Werner <sup>1</sup>

<sup>1</sup>Agroecosystem Research, BAYCEER, University of Bayreuth, Universitätsstraße 30, 95447 Bayreuth, Germany

<sup>2</sup>UFZ – Computational Hydrosystems, Helmholtz Centre for Environmental Research, Permoserstraße 15, 04318 Leipzig, Germany

✉ Corresponding author: Maren Dubbert ([maren.dubbert@uni-bayreuth.de](mailto:maren.dubbert@uni-bayreuth.de))



## 1.1. Summary

- The oxygen isotope signature of water is a powerful tracer of water movement from plants to the global scale. However, little is known on the short-term variability of oxygen isotopes leaving the ecosystem via transpiration as high-frequency measurements are lacking.
- A laser spectrometer was coupled to a gas-exchange chamber directly estimating branch-level fluxes in order to evaluate the short-term variability of the isotopic composition of transpiration ( $\delta_E$ ) and to investigate the role of isotopic non-steady-state under natural conditions in cork-oak trees (*Quercus suber* L.) during distinct Mediterranean seasons.
- Measured  $\delta^{18}\text{O}$  of transpiration ( $\delta_E$ ) deviated from isotopic steady-state throughout most of the day even when leaf water at the evaporating sites was near isotopic steady-state. High agreement was found between estimated and modeled  $\delta_E$  assuming non-steady-state enrichment of leaf water.
- Isoforcing, i.e. the influence of the transpirational  $\delta^{18}\text{O}$  flux on atmospheric values, deviated from steady-state calculations but daily means were similar between steady-state and non-steady-state. However, strong daytime isoforcing on the atmosphere imply that short-term variations in  $\delta_E$  have likely consequences for large-scale applications, e.g. partitioning of ecosystem fluxes or satellite-based applications.

**Table 1:** Used symbols and descriptions.

Symbol	Description
$\alpha_k$	kinetic fractionation factor
$\alpha^+$	equilibrium fractionation factor
$\delta^{18}O$	oxygen stable isotope signature (‰)
$\delta$	shortened for oxygen stable isotope signature (‰)
$\Delta$	deviation of a given isotopic signature from source water
$\phi$	Péclet number
$\theta$	volumetric soil water content ( $m^3 m^{-3}$ )
$C$	the molar water concentration ( $mol m^{-3}$ )
$D/D_i$	differences in molecular diffusivity ( $D$ ) between the major and the minor isotopologue
$E$	plant transpiration ( $mmol m^{-2} s^{-1}$ )
$ET$	Evapotranspiration ( $mmol m^{-2} s^{-1}$ )
$f_{l,2}$	factors for estimating $R_l$
$f_{em}$	factor for estimating $R_m$
$g_{tw}$	total conductance for water vapour
$h$	relative humidity normalized to leaf temperature (%)
$I$	Isoforcing ( $mol m^{-2} s^{-1} \text{‰}$ )
$L_{eff}$	effective length of water movement in the leaf mesophyll (m)
$n$	exponent relating $D/D_i$ to apparent kinetic fractionation
$rh$	relative air humidity (%)
$R$	isotope ratio of ( $^{18}O$ )/( $^{16}O$ )
$T$	temperature ( $^{\circ}C$ )
$u$	flow rate ( $mol(air) s^{-1}$ )
$V_m$	leaf water volume ( $mol(H_2O) m^{-2}$ ),
$w$	mole fraction ( $mol(H_2O) mol(air)^{-1}$ )
Subscript	Description
$a$	atmospheric air
$C$	Craig and Gordon steady-state prediction at the evaporating (‰)
$e$	evaporating site
$e(t)$	leaf-water at the evaporating sites at time $t$ (‰)
$e(t+dt)$	leaf-water at the evaporating sites at time plus a time step $t+dt$ (‰)
$h$	relative humidity
$i$	stomatal cavity
$in$	chamber air
$l$	leaf
$m$	liquid mesophyll water
$out$	background air
$p$	precipitation
$s$	source water; i.e. xylem water

## 1.2. Introduction

Oxygen isotope signatures ( $\delta^{18}O$ ) of water can reveal important information on the impact of distinct pathways of water from ecosystem to global scale (Dongmann *et al.*, 1974; Yakir & Sternberg, 2000;

Williams *et al.*, 2004). At ecosystem level for example they can be used to partition net water fluxes into their constituent fluxes (Yakir and Sternberg, 2000). The largest water output flux of an ecosystem is transpiration, associated with an isotopic composition ( $\delta_E$ ), participating strongly in the local (isotopic) water cycle.  $\delta_E$  is mostly assumed to be in isotopic steady-state, i.e. has the same composition as the supplying water, because an increase in the isotopic composition of terrestrial waters is not observed in the long-term. It became clear, though, in recent years that leaf water, which feeds transpiration, is isotopically not in steady-state most of the time in many of different ecosystems (Dongmann *et al.*, 1974; Cernusak *et al.*, 2002; and others). Consequently,  $\delta_E$  should also deviate from isotopic steady-state. It was, however, difficult to determine  $\delta_E$  in the past since measurements of water vapor isotopes were difficult to obtain using cold-trap methods (Helliker *et al.*, 2002), delivering data with low time resolution (Harwood *et al.*, 1998). Alternatively,  $\delta_E$  can be estimated indirectly by modeling the isotopic signature of leaf water at the evaporating sites of the leaves under the assumption of non-steady-state transpiration, i.e.  $\delta_E \neq \delta^{18}O$  of xylem/source water ( $\delta_s$ ; Dongmann *et al.*, 1974). Thereafter  $\delta_E$  can be determined by the equation of Craig & Gordon (1965). Nevertheless, ecosystem partitioning studies still often assumed transpiration to be in isotopic steady-state, i.e. being equal to  $\delta^{18}O$  of xylem water ( $\delta_s$ , e.g. Yepez *et al.*, 2003).

More information is available on isotopic non-steady-state effects on the oxygen isotope enrichment of leaf water itself ( $\delta_l$ ) and associated mechanistic processes at leaf- and canopy-scale (Cuntz *et al.*, 2007; Farquhar & Cernusak, 2005; Lai *et al.*, 2008; Seibt *et al.*, 2006; Xiao *et al.*, 2012). In contrast, the diurnal development of  $\delta_E$  and the relation between non-steady-state leaf water and the consequent non-steady-state effect of transpired vapor has gained little attention. The latter can, however, be estimated indirectly by measurements of ambient vapor isotopic composition inside the canopy (Xiao *et al.*, 2010), whereas field studies estimating the temporal development of  $\delta_E$  directly, i.e. by coupling gas-exchange systems to laser spectrometers, are still scarce (but see Haverd *et al.*, 2011; Wang *et al.*, 2012). The recent developments in laser spectroscopy now enable direct measurements of the isotopic composition of atmospheric water vapor ( $\delta_a$ ), evapotranspiration ( $\delta_{ET}$ ), and its components with high temporal resolution in the field (minute to hourly scale, Werner *et al.*, 2012 and literature therein). Consequently, emerging studies using continuous high-frequency measurements of  $\delta_a$  combined with

land surface models have gained new insights into fractionation processes occurring during isotopic water vapor and carbon dioxide exchange ( $C^{18}O^{16}O$ ; e.g. Berkelhammer *et al.*, 2013; Lee *et al.*, 2012; Welp *et al.*, 2012; Xiao *et al.*, 2010; 2012). In this context, it is important to quantify and disentangle the impact of isotopic non-steady-state transpiration on ecosystem flux partitioning and atmospheric vapor under natural conditions.

Moreover, direct estimates of  $\delta_E$  bear the novel opportunity to validate and improve common modeling, for example the Craig and Gordon equation isotopes of soil evaporation (Craig & Gordon, 1965; Good, *et al.*, 2012; Dubbert *et al.*, 2013; Hu *et al.*, 2014) and resolve the role of non-steady-state transpiration under natural conditions on a diurnal basis at high resolution (Simonin *et al.*, 2013). At present hardly anything is known about the impact of environmental factors or differences between plant functional groups on i) temporal variations of  $\delta_E$  on a diurnal time scale, ii) the proportion of non-steady-state transpiration under natural conditions and iii) the isoforcing of non-steady-state transpiration on the atmosphere. This knowledge is crucial, since  $\delta_E$  is widely used to partition ecosystem fluxes (Yakir & Sternberg, 2000) or in water balance modeling from regional to global scales (e.g. Farquhar & Lloyd, 1993; Jasechko *et al.*, 2013; Schlesinger *et al.*, 2014).

To fill this gap, a novel approach was used, combining a custom build flow-through gas-exchange branch chamber with a Cavity Ring-Down Spectrometer. We present here, to our knowledge, the first data-set on daytime cycles of direct estimates of  $\delta_E$  in key environmental periods: spring, summer drought, and the beginning of autumn. Particularly, we compare direct with indirect estimates of the isotopic composition of transpired water vapor ( $\delta_E$ ) of cork-oak trees (*Quercus suber* L.). Furthermore, we quantify the role of non-steady-state transpiration and determine the driving factors for the deviation of  $\delta_E$  from the isotopic composition of source water  $\delta_s$ , i.e. isotopic steady-state, as well as the isoforcing of isotopic non-steady-state transpiration on the atmosphere.

### 1.3. Materials and Methods

Isotopic compositions are reported here as ratios  $R$  between the concentrations of rare and common isotopes, and expressed as  $\delta$ -notation, i.e. relative to Vienna Standard Mean Ocean Water (V-SMOW; Gonfiantini, 1978):  $\delta = R/R_{V-SMOW} - 1$ , or in  $\Delta$ -notation, i.e. relative to source water  $R_s$ :  $\Delta = R/R_s - 1$ .

The latter facilitates a comparison between different ecosystems. A list of all abbreviations is given in Table 1.

#### 1.3.1. *Study site*

Measurements were conducted between June and November 2011 in an open cork-oak woodland in central Portugal (N39° 8' 17.84'' W8° 20' 3.76''; Herdade de Machoqueira do Grou). The trees are widely spaced (209 individuals ha<sup>-1</sup>) with a leaf area index of 1.1 and mean maximum height of 10 m. Mean annual temperature is approximately 15.9 °C and mean annual precipitation is 680 mm (last 30-years average, Instituto de Meteorologia, Lisbon). For further information see Dubbert *et al.* (2013).

#### 1.3.2. *Environmental variables*

Air temperature and relative humidity (*rh*, CS-215 Temperature and Relative Humidity Probe, Campbell Scientific, Logan, UT, USA) were stored as 30 min averages in a data logger (Cr10x, CR1000, Campbell Scientific, Logan, UT, USA). Volumetric soil water content ( $\theta_s$ , 10hs, Decagon, Washington, USA) in 5 and 60 cm depth were measured and 60 min averages were stored in a datalogger (CR1000, Campbell Scientific, Logan, UT, USA; 4 sensors per depth). Leaf temperature was recorded simultaneously with gas-exchange measurements (see below). Relative humidity corrected to leaf temperature *h* and leaf vapor pressure deficit *VPD* ([Pa]) were calculated from relative humidity and leaf and air temperature.

### 1.3.3. CRDS based measurements

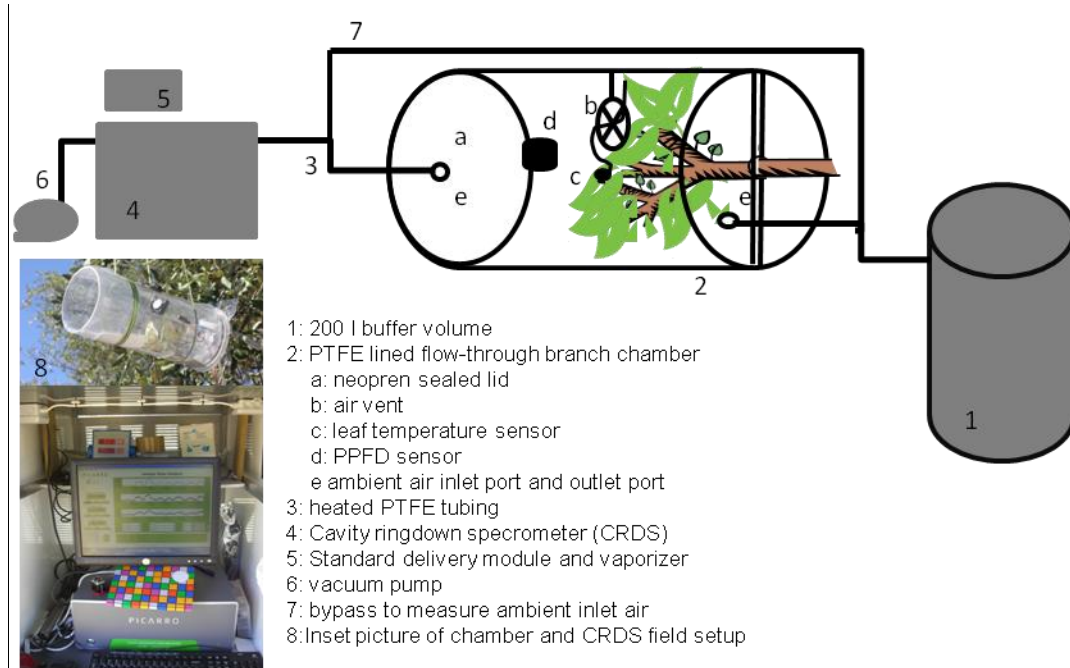


**Figure 1:** a) Schematic overview and pictures of the experimental setup for measuring leaf transpiration, its isotopic composition and micrometeorological parameters within the chamber in the field.

Fluxes and isotopic composition of cork-oak transpiration were measured using a Cavity Ring-Down Spectrometer (CRDS, L2120-i, Picarro, Santa Clara, USA) in combination with custom-built branch chambers in an open gas exchange system ( $n=3$  per treatment, Fig. 1). A transparent cylindrical acrylic chamber with a total volume of 2.5 L was coated with an FEP foil (4PTFE, Stühr, Germany) to avoid isotopic fractionation. The background air inlet port and the sampling air outlet port were located at opposite sides of the chamber. The background air was sampled above crown height and buffered with a 200 L volume. The flow through the chamber was adjusted between 1 and  $2.5 \text{ L min}^{-1}$ . The CRDS was calibrated three times a day using a standards delivery module and vaporizer (Picarro, Santa Clara, USA) with two laboratory standards that were regularly calibrated against V-SMOW and SLAP (IAEA, Vienna). Measurement precision was  $< 0.2\text{‰}$ . The concentration dependency of the instrument was determined according to the procedure of Schmidt *et al.* (2010, Figure S1 and Table S1).  $\text{H}_2\text{O}$  mole fractions (ppmv) of the CRDS were calibrated prior to each measurement campaign in the laboratory using a dew point generator (Walz, Effeltrich, Germany). During field measurements the precision of the instrument was regularly cross-checked using an equally calibrated infrared gas



analyzer (Li840, Licor Biosciences, Lincoln, USA). The precision of the CRDS was < 100 ppmv throughout the measurement period; blank measurements of the chamber were obtained and did not reveal differences connected with air passing the chamber (Fig. S2). Background and sampling air were measured alternately until stable values were reached and a five minutes interval average was recorded for calculation of transpiration ( $E$ ) and  $\delta_E$  (see Fig. S2). The observed increase in air temperature in the chamber above ambient was ca. 2 °C after 5 min and stable thereafter.

Fluxes of  $E$  as well as total leaf conductance ( $g_{tw}$ ) were calculated based on von Caemmerer & Farquhar (1981). Gas-exchange was not measured during the night, because transpiration ceases almost completely and calculations of fluxes are very error prone. Therefore nighttime values of transpiration and conductance needed for modeling nighttime  $\delta_E$  and  $\delta_e$  were taken from published data of a comparative Mediterranean oak system (Dawson *et al.*, 2007). Isotope signatures of transpired vapor were calculated by mass balance:

$$\begin{aligned}\delta_E &= \frac{u_{out} w_{out} \delta_{out} - u_{in} w_{in} \delta_{in}}{u_{out} w_{out} - u_{in} w_{in}} \\ &= \frac{w_{out} \delta_{out} - w_{in} \delta_{in}}{w_{out} - w_{in}} - \frac{w_{in} w_{out} (\delta_{out} - \delta_{in})}{w_{out} - w_{in}}\end{aligned}\quad (1)$$

where  $u$  is flow rate [mol(air) s<sup>-1</sup>],  $w$  is mole fraction [mol(H<sub>2</sub>O) mol(air)<sup>-1</sup>] and  $\delta$  is isotope ratio of the incoming (*in*) and outgoing (*out*) air stream of the chamber. Flow rates are measured with humid air so that conservation of dry air gives  $u_{in}(1-w_{in}) = u_{out}(1-w_{out})$ , and it follows the second line of Eq. (1). This is equivalent to the equation given by Simonin *et al.* (2013) therein cited as Evans and von Caemmerer (personal communication). The second term in Eq. (1) corrects for the increased air flow in the chamber due to addition of water by transpiration  $E$ .

#### 1.3.4. Measurement of the isotopic composition of xylem water

Xylem samples of terminal branches (n=4) were collected at noon. Leaf samples (n = 2-4) were collected at 12 time points throughout the measurement campaign. Xylem and leaf water was extracted on a custom build vacuum line by cryogenic distillation. Samples were heated at approximately 95 °C for 90 min under vacuum of 0.04 to 0.08 mbar and vapor was trapped in liquid N<sub>2</sub> cooled water traps.

Samples were stored in sealed glass vials at 4 °C until analysis. Water  $\delta^{18}\text{O}$  was analyzed after headspace equilibration for 24 hours at 20 °C on an Isoprime IRMS (Elementar, Hanau, Germany) coupled via open split to a  $\mu$ gas auto sampler (Elementar, Hanau, Germany). Within every batch of 44 samples three replicates of three different laboratory standards were analyzed for  $\delta^{18}\text{O}$  calibration versus V-SMOW. Laboratory standards were regularly calibrated against V-SMOW, SLAP, and GISP water standards (IAEA, Vienna). Analytical precision was  $< 0.1\text{‰}$ .

### 1.3.5. Calculation of isotopic signatures

The isotopic ratio of transpiration  $R_E$  is linked to the isotopic ratios of water at the evaporating sites  $R_e$  and ambient vapour  $R_a$  (Craig & Gordon, 1965; Farquhar & Lloyd, 1993):

$$R_E = \frac{1}{\alpha_k \alpha^+ (1-h)} (R_e - \alpha^+ h R_a) \quad (2)$$

with  $\alpha_k$  and  $\alpha^+$  being the kinetic and equilibrium fractionation factors ( $> 1$ ), respectively, and  $h$  the relative humidity corrected for leaf temperature. The Craig and Gordon steady-state requires that the isotopic composition of vapour departing from the leaf must be the same as the isotopic composition of incoming water, i.e.  $R_E = R_s$ , which leads to:

$$R_C = \alpha_k \alpha^+ (1-h) R_s + \alpha^+ h R_a \quad (3)$$

where  $R_C$  is the isotopic composition of leaf water at the evaporating site in steady-state. Subtracting Eq. (3) from Eq. (2) gives:

$$R_e - R_C = \alpha_k \alpha^+ (1-h) (R_E - R_s) \quad (4)$$

which leads to a linear relationship in  $\Delta$ -notation between the isotopic composition of evaporation  $R_E$  or expressed as deviation from source values as  $\Delta_E$  and the deviation from steady-state of the isotopic composition at the evaporating sites  $\Delta_e$ :

$$\Delta_E = \frac{\Delta_e - \Delta_C}{\alpha_k \alpha^+ (1-h)} \quad (5),$$

with  $\Delta_C$  as the deviation of leaf water at the evaporating site in steady-state from source water.  $1-h$  in the denominator emphasizes the fact that if humidity approaches saturation the pure water flux  $E$

diminishes, while in the Isoflux term  $E\Delta_E$ , consequently  $\Delta_E$  approaches infinity; because

$$E\Delta_E = \frac{g_{tw}w_i}{\alpha_k\alpha^+}(\Delta_e - \Delta_c) \quad (6)$$

with  $g_{tw}$  being the total conductance for water vapour from the stomatal cavity to the point of observation, and  $w_i$  the humidity in the stomatal cavity, i.e. vapour saturation at leaf temperature expressed as mole fraction [ $\text{mol}(\text{H}_2\text{O}) \text{ mol}(\text{air})^{-1}$ ]. The flux from the vegetation to the atmosphere in  $\delta$ -terms is not simply an isotope flux  $E\delta_E$  but rather the isoforcing  $I_E$  (Cuntz *et al.*, 2003; Lee *et al.*, 2009):

$$I_E = \frac{E}{w_a}(\delta_E - \delta_a) \quad (6)$$

with  $w_a$  being the atmospheric humidity in mole fraction [ $\text{mol}(\text{H}_2\text{O}) \text{ mol}(\text{air})^{-1}$ ].

The non-steady-state isotopic composition of leaf water  $R_l$  can be written in an iterative form, if leaf water volume  $V_m$  [ $\text{mol}(\text{H}_2\text{O}) \text{ m}^{-2}$ ] is constant (Dongmann *et al.*, 1974; Cuntz *et al.*, 2007):

$$R_l(t + dt) = f_1 R_c + (R_l(t) - f_1 R_c) e^{-\frac{g_{tw}w_i}{\alpha_k\alpha^+V_m f_2} dt} \quad (7)$$

where  $R_l$  at a time  $t+dt$  is calculated from  $R_l$  at an earlier time  $t$  with constant environmental conditions during the time step  $dt$ . The factors  $f_1$  and  $f_2$  depend on the water pool of interest. To calculate the isotopic composition of total mesophyll water  $R_m$ , i.e.  $R_l \equiv R_m$ , the factors are  $f_1 = f_2 = f_{em}$ , with

$$f_{em} = \frac{1 - e^{-\wp_m}}{\wp_m} \text{ with the Péclet number } \wp_m = \frac{EL_{eff}}{CD} \quad (8),$$

where  $C=10^6/18=55.6 \cdot 10^3 \text{ mol m}^{-3}$  is the molar water concentration,  $D \text{ (m}^2 \text{ s}^{-1}\text{)}$  is the tracer diffusivity in liquid water and  $L_{eff} \text{ (m)}$  is the effective length of water movement in the leaf mesophyll. To calculate the isotopic composition at the evaporating sites  $R_e$ , i.e.  $R_l \equiv R_e$ , the factors are  $f_1 = 1, f_2 = f_{em}$ . We follow Cuntz *et al.* (2007), who argued that  $f_1 = f_2 = 1$  is sufficient in this case.

Notably, isotope signatures of leaf water at the evaporating site in the non-steady-state can be modeled independent from observations of  $R_E$  and can then be used to predict  $R_E$  and inversely, observations of  $R_E$  can be used to predict  $R_l$  at the evaporating site.

### 1.3.6. Statistical analysis

Linear relationships were tested between measured and modeled estimates of  $\delta_E$ , and between  $\Delta_E$  and  $(\Delta_e - \Delta_c)$  or  $(\Delta_e - \Delta_c)/(1-h)$  separately for days in spring, summer and fall. Statistical analyses were carried out with Statistica (Statistica 6.0, StatSoft, Inc., Tulsa, USA).

## 1.4. Results and discussion

The laser spectrometer coupled to gas-exchange chambers enabled high time resolved estimates of  $\delta_E$  in the field (Fig. 1). To evaluate how changes in environmental factors impact temporal variations of  $\delta_E$  on a diurnal time scale measurements were conducted in three distinct climatic periods: 1) moist and warm spring (11.4% mean soil moisture  $\theta_s$ ) with high transpiration rates (max.  $0.49 \text{ mmol m}^{-2} \text{ s}^{-1}$ ), 2) dry, warm summer (4.5%  $\theta_s$ ), with reduced leaf conductance, and 3) wet, cold fall with maximum transpiration rate dropping to  $0.18 \text{ mmol m}^{-2} \text{ s}^{-1}$  (Fig. 2).

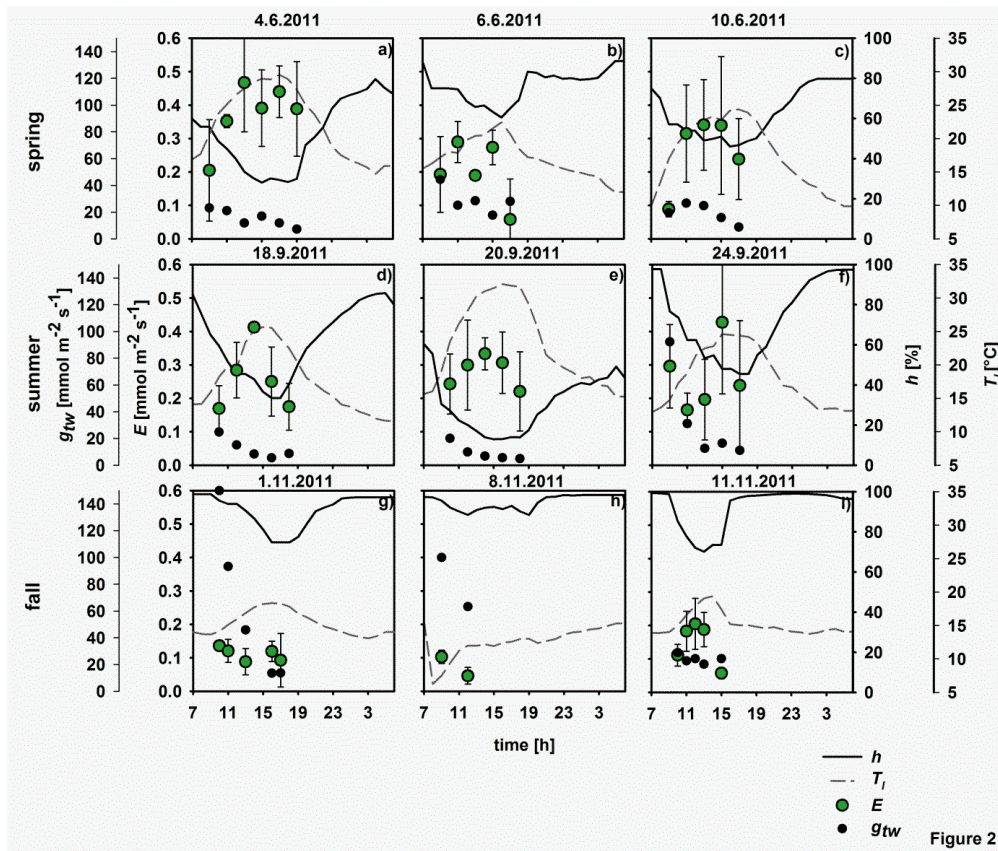


**Figure 2:** Environmental conditions and ecophysiological parameters observed with the chamber setup in late spring (a-c), late summer (d-f) and fall (g-i; date format: day.month.year): relative humidity corrected to leaf temperature ( $h$ , [%], black lines), leaf temperature ([°C], dashed grey lines), transpiration rate ( $E$ , [mmol m<sup>-2</sup> s<sup>-1</sup>],  $n=3$ , mean  $\pm$  SE, green circles), and total leaf conductance ( $g_{tw}$ , [mmol m<sup>-2</sup> s<sup>-1</sup>], black circles).

In the following we quantify the deviation of  $\delta_E$  from xylem water ( $\delta_s$ ), validate a commonly used modeling approach (3.1.) and analyze the relationship between the occurrence of isotopic non-steady-state at the leaf level and the extent of depletion of  $\delta_E$ . Finally, we quantify the isoforcing of isotopic non-steady-state transpiration on atmospheric  $\delta^{18}\text{O}$  (3.2.).

#### 1.4.1. *Isotopic non-steady-state transpiration under natural conditions and comparison with modeled $\delta_T$*

Observed plant transpirational isotope signatures ( $\delta_E$ ) never reached xylem values (i.e. steady-state,  $\delta_s$ ) during daytime on any day and varied between  $-26.1\text{‰}$  and  $-6.2\text{‰}$  (Fig. 3). Consequently, the deviation of  $\delta_E$  from  $\delta_s$  ( $\Delta_E$ ), varied strongly within a day and was generally most negative in the morning.  $\delta_E$  mainly increased throughout the day towards the end of the light period (Fig. 3). During the dark period  $\delta_E$  could not be measured due to high methodological uncertainties during very low nocturnal flux rates ( $E$ ). However, modeled  $\delta_E$  values (eq. 2 and 7) indicate that the negative  $\delta_E$  values during the day are counterbalanced during the night (Fig. 3). The diurnal development of  $\delta_E$  thus differs from the dome-shaped pattern of oxygen isotope signatures of leaf mesophyll water ( $\delta_m$ ) with highest enrichment corresponding to peak temperature and low  $h$  in the afternoon and lowest  $\delta_m$  around sunrise (Fig. 4, see also Lai *et al.*, 2006; 2008; Yopez *et al.*, 2007). The peak  $\delta_m$  enrichment shifted to latter afternoon/evening hours with increasing day length and higher temperatures. Notably, modeled and observed  $\delta_m$  fit very well ( $\delta_{m,obs} = 0.96 \cdot \delta_{m,model} + 0.33$ ,  $R^2 = 0.91$ ,  $p < 0.001$ ; Fig. 4).

In general, measured plant transpirational isotope signatures ( $\delta_E$ ) ranged between xylem water  $\delta_s$  ( $-3.4$  to  $-4.7\text{‰}$ ) and ambient vapor  $\delta_a$  ( $-19.9$  to  $-30.2\text{‰}$ ; Fig. 3). If  $\delta_a$  can assumed to be in equilibrium with precipitation during a rain event and fractionation associated with condensation is around  $-10\text{‰}$  at  $20\text{ °C}$  (Majoube, 1971) the  $\delta_a$  values observed correspond to isotope signatures of precipitation  $\delta_p$  of about  $-10\text{‰}$  (but note the shifts to very negative  $\delta_a$  on June 11, September 18 and 20). Indeed, observed  $\delta_p$  varied between  $-7$  and  $-10\text{‰}$  at this site (Dubbert *et al.*, unpublished). Somewhat higher values in xylem ( $\delta_s$ ) indicate that  $\delta_s$  and hence soil water isotopes were not in full equilibrium with  $\delta_p$ , which is mainly caused by the relatively hot and dry environment leading to strong evaporative

enrichment and isotopic gradients within the top 20 cm of the soil profile of more than 10‰ within few days after a rain event (Dubbert *et al.*, 2013). Moreover, atmospheric vapour is transported towards the site from north to north-east (mainly continental air masses) and is thus not expected to be in isotopic equilibrium with local xylem water on each day.

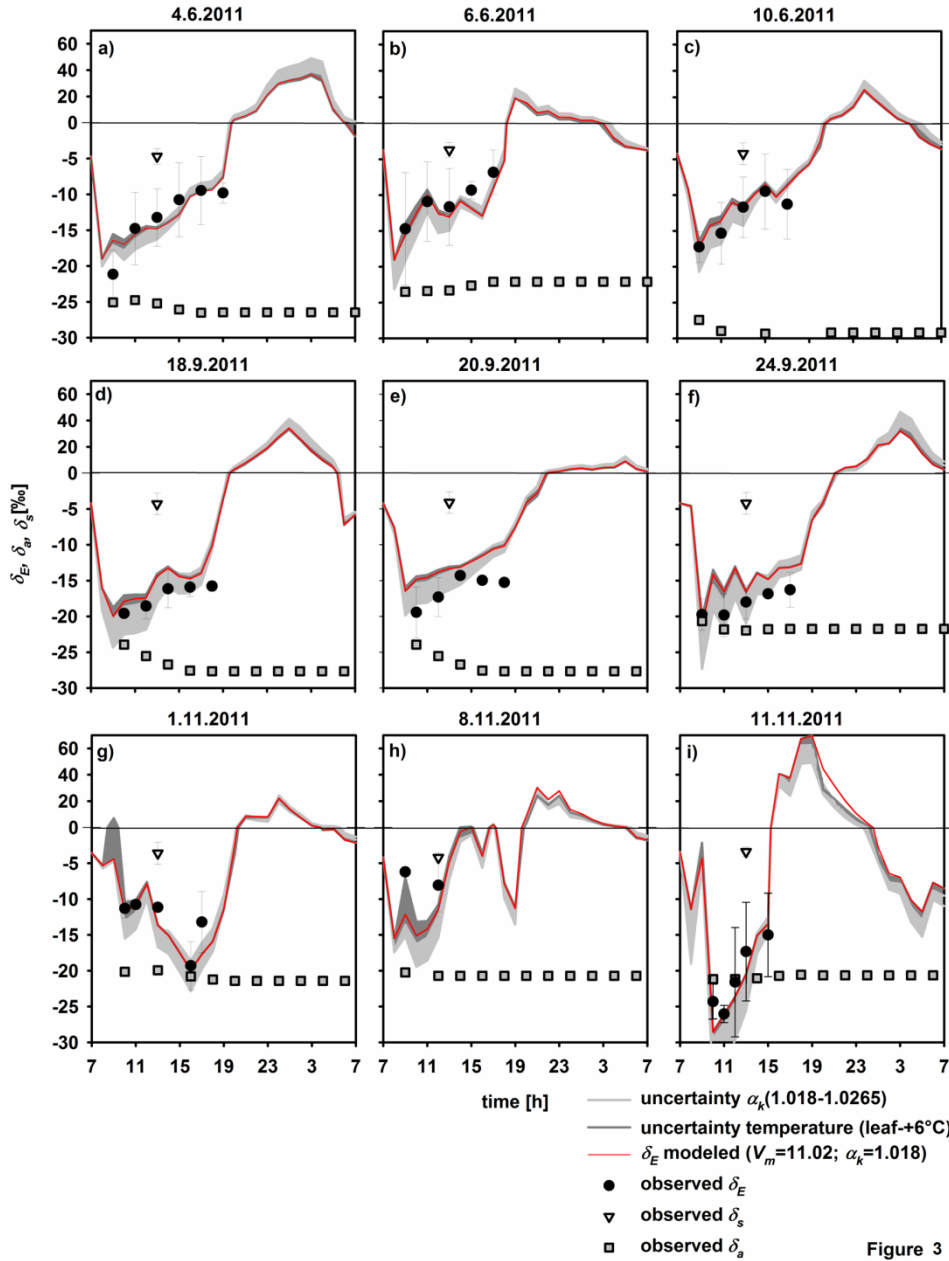
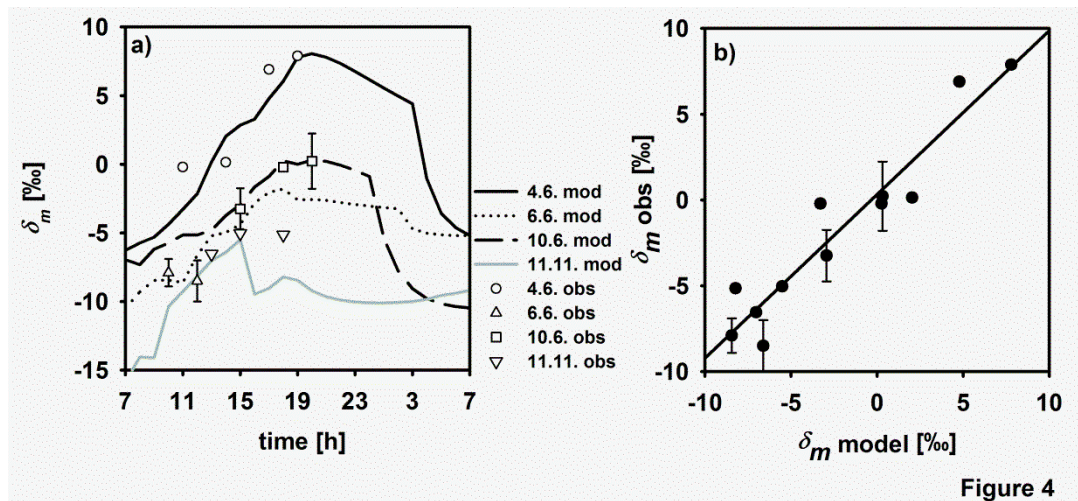


Figure 3

**Figure 3:** Measurements in spring (a-c), summer (d-f) and fall (g-i; date format: day.month.year) of the oxygen isotope signatures of transpired vapor ( $\delta_E$ , black circles,  $n=3$ , mean values  $\pm$  SE) and modeled  $\delta_E$  considering non-steady state with varying observed leaf water volume  $V_m$  and  $\alpha_k$  between 1.018 and 1.0265 (grey uncertainty band). The dark grey uncertainty band indicates modeled  $\delta_E$  with  $\alpha_k = 1.018$  and varying leaf temperature from observed values to  $+6^\circ\text{C}$ . The solid red line is modeled  $\delta_E$  with constant leaf water volume  $V_m$  of the observed mean value and  $\alpha_k = 1.018$ . Grey squares show measured oxygen isotope signatures of ambient air and white triangles are oxygen isotope signatures of xylem ( $n=3$ , mean values  $\pm$  SE). Please note different scales for positive and negative values.



Variations in  $\delta_E$  can be caused by changes in abiotic or biotic conditions, i.e. relative humidity or stomatal conductance, and are expected to persist until sufficient time has passed under constant environmental or physiological conditions to allow for  $\delta_E$  to approach  $\delta_s$ . Most isotope models assume that the leaf consists of a single water pool supplying the transpiration stream (bulk leaf water =  $V_m$ ; eq. 7; Dongmann *et al.*, 1974; Farquhar & Cernusak, 2005) and leaf water residence time can be calculated as  $V_m$  divided by the one way flux of water out of the leaf ( $g_{tw}w_i$ ; eq. 7). This leads to mean leaf water residence times of  $4.6 \pm 2.3$  h,  $5.4 \pm 1.9$  h, and  $3.6 \pm 1.6$  h in spring, summer and fall, respectively, indicating that in our case the residence time of the water supporting the transpirational flux is always much longer than periods during which environmental or physiological conditions remain constant (Fig. 2 and 3; Simonin *et al.*, 2013). However, we can expect that leaf water residence times differ strongly between different plant functional groups (Simonin *et al.*, 2013; Kahmen *et al.*, 2009), i.e. between crop plants and drought-adapted species with high stomatal control as *Q. suber*. Indeed, comparing modeled  $\delta_E$  with theoretical leaf water residence times of doubling or reducing (to  $\frac{1}{2}$  and  $\frac{1}{4}$ ) the observed leaf water residence time (Fig. 5), it becomes clear that the observed pattern of strong depletion of  $\delta_E$  relative to  $\delta_s$  during the day cannot equally be expected in ecosystems dominated by species with small leaf water residence times either due to low stomatal control or low leaf water contents (see for example the differences in leaf water residence time and depletion of  $\delta_E$  from isotopic steady-state between Citrus and Tobacco observed by Simonin *et al.* (2013).



**Figure 4:** Diurnal cycles of modeled and measured oxygen isotope signatures of leaf mesophyll water ( $\delta_m$ ; a) and modeled versus measured  $\delta_m$  (b) on 4.6. (circles; black line); 6.6. (up triangles; black dotted line); 10.6. (squares; black dashed line) and 11.11.2011 (down triangles; grey line).

Moreover, due to its influence on leaf water residence time (see Eqn. 2) the leaf water content ( $V_m$ ) represents an important model input parameter. However, measuring  $V_m$  of leaves from remote field sites is not straight forward, and is therefore often assumed to be stable (e.g. Yepez *et al.*, 2003). Here,  $V_m$  of cork-oak leaves was measured once in each season (spring, summer and fall) during morning and afternoon, and ranged between 8.4 and 12.8 mol m<sup>-2</sup>. Comparing the use of measured changes in  $V_m$  with the assumption of a fixed mean value (Fig. 3, upper boarder of grey areas and solid red lines, respectively) shows that the measured range of  $V_m$  is either not large enough to strongly influence  $\delta_E$  predictions or modeling  $\delta_E$  is not sensitive in regard to changes in  $V_m$ . Accordingly, Cernusak *et al.* (2002; 2003) found considerable variations in  $V_m$  in lupin and blue gum and still found no significant impact on the prediction of  $\delta_E$  (see also Cuntz *et al.*, 2007).

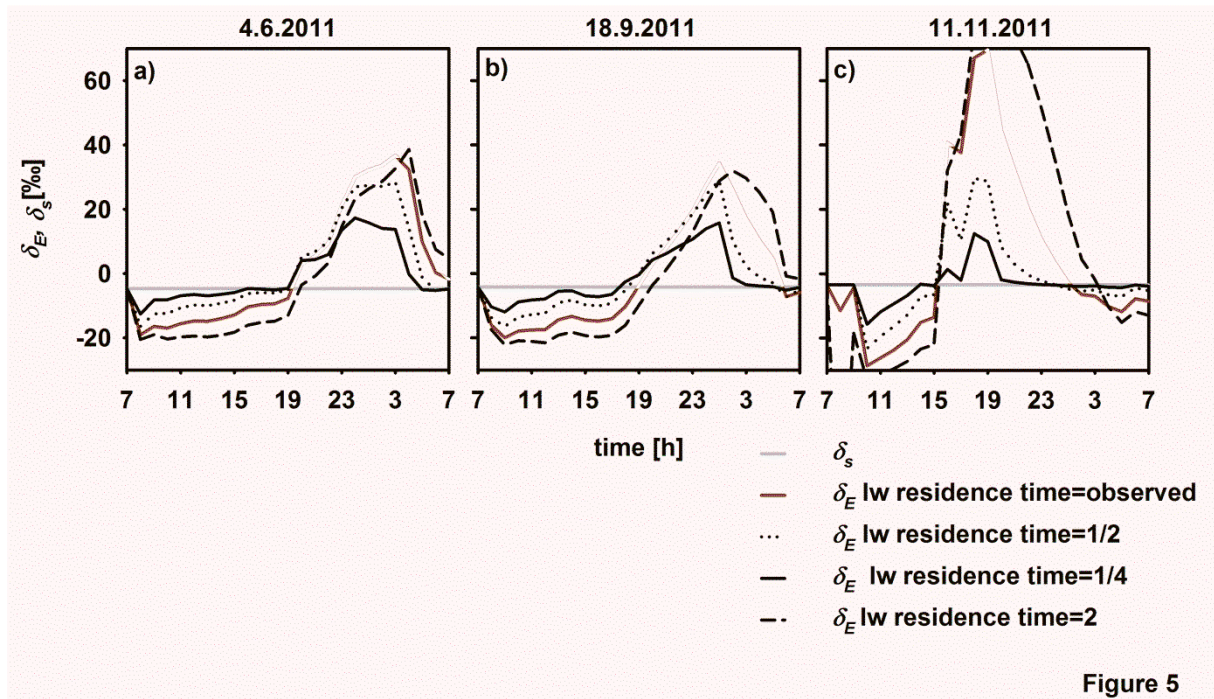


**Figure 5:** Modeled oxygen isotope signatures of transpiration and observed oxygen isotope signatures of xylem (grey dotted line; n=3, mean values) at June 4 (a), September 18 (b) and November 11 (c; date format: day.month.year). Red lines indicate modeled  $\delta_E$  with observed leaf water residence time (see Fig. 2), black dotted and solid lines are  $\delta_E$  with  $\frac{1}{2}$  and  $\frac{1}{4}$  of the observed leaf water residence time and black dashed lines are  $\delta_E$  with twice the observed leaf water residence time.

In general, we found a good agreement between measured and modeled  $\delta_E$  when first modeling the isotopic enrichment of leaf water at the evaporating sites of the leaves under the assumption of non-steady-state transpiration ( $\delta_e$ ), and second calculating the depletion of  $\delta_E$  compared to isotopic



signatures of xylem water ( $\delta_s$ ) using the Craig and Gordon equation (Fig. 3; equation 2 and 7). However, changes in the kinetic fractionation factor in the model, i.e. from morning to evening or between days strongly alter predicted  $\delta_E$  (Fig. 3d-f). Kinetic fractionation describes the effect of differences in molecular diffusivity ( $D$ ) between the major and the minor isotopologue ( $D/D_i$ ). It can be expressed as  $\alpha_k = (D/D_i)^n$ , where  $n$  equals 0 under fully turbulent conditions, 2/3 for diffusion through leaf laminar boundary layer and 1 for fully molecular diffusion (Farquhar & Lloyd, 1993). Lee *et al.* (2009) suggested that apparent  $\alpha_k$  differs between scales (i.e. leaf vs. canopy). At the leaf scale,  $\alpha_k$  should always be close to the molecular value (1.028, Merlivat 1978) as stomatal resistance is usually much greater than boundary layer resistance. In contrast at the canopy scale  $\alpha_k$  can vary much stronger: Lee *et al.* (2009) found canopy  $\alpha_k$  values between 1.012 and 1.031. In chamber applications  $\alpha_k$  should likewise be a weighted average between boundary layer, stomatal and aerodynamic resistances due to the ventilation of the chamber. Boundary layer resistance in gas exchange chambers is often determined with heat plates or alike (Brenner *et al.*, 1995). However, this determines a combined boundary and aerodynamic resistance and we argue that the boundary layer resistance determined from heat measurements cannot be taken directly for weighting boundary layer fractionation in total  $\alpha_k$ . Boundary layer and aerodynamic resistances depend on wind speed, thus using the formulations of the two resistances at canopy scale and with wind speeds of 1 to 2.5 m s<sup>-1</sup> in the chamber (i.e. range of ventilation within the chamber due to orientation of the van relative to leaves)  $\alpha_k$  was estimated to range between 1.018 and 1.0265. Notably overall very good fits between measured and modeled  $\delta_E$  and  $\delta_m$  were found with  $\alpha_k = 1.018$  ( $\delta_{E,obs} = 0.82 \cdot \delta_{E,model} - 2.9$ ;  $R^2 = 0.68$ ;  $p < 0.001$ , Fig. 3), although our results suggest that  $\alpha_k$  was larger in summer (Fig. 3d-f).

Another critical issue is the correct estimation of leaf temperature. Temperature measurements were obtained from the surface of a single leaf in this study but the increase of leaf temperature above air temperature can be in-homogeneous in branch bags specifically with high radiation as leaves might shade each other (Mott & Peak, 2011). Variations in temperature influence modeled  $\delta_E$  indirectly as they are used to calculate the equilibrium fractionation factor and to normalize  $h$  to leaf temperature values. Therefore we tested the sensitivity of temperature on modeled  $\delta_E$  by assuming a maximum deviation from observed leaf temperature during day-time of 6 °C (without incoming radiation during

night temperatures should be homogeneous). Clearly variations in temperature can have an influence on modeled  $\delta_E$  in certain situations: a high influence of temperature changes on modeled  $\delta_E$  could be observed during wet conditions in fall in the early morning (Fig. 3 dark grey areas). During all other days, modeled  $\delta_E$  was, however, not very sensitive to temperature and the uncertainty does not compromise our findings regarding the strong deviation of  $\delta_E$  from isotopic steady-state. Another aspect is the increase in air temperature inside the closed chamber, which was comparatively small here (Pape *et al.*, 2009; on average 2 °C). We did not measure the difference between leaf surface temperatures of leaves inside and outside the chamber, but could not detect an increase in leaf temperature within the app. 10 min while the chamber was closed. Thus, the increase of temperature due to the chamber application had supposedly only little impact on measured  $\delta_E$ .

#### 1.4.2. Relationship between $\Delta_e - \Delta_C$ and $\Delta_T$ and impact on atmospheric vapor

Deviations from isotopic steady state at the leaf level,  $\Delta_e - \Delta_C$ , and of transpired vapor,  $\Delta_E$ , have not been considered separately in the past. However, transpiration ( $E$ ) is a two-way flux, with  $E/(1-h)$  of water vapor diffusing out of the stomata and  $E \cdot h/(1-h)$  of vapor diffusing into the leaf (Farquhar & Cernusak, 2005) and likewise the isotopic composition of transpiration has also two parts. Denoting  $\Delta_E$  as in Eq. (5) reveals that  $\Delta_E$  is not simply a mirror of  $\Delta_e - \Delta_C$  but that the non-steady-state effect of leaf water at the evaporating sites is amplified by the factor  $1/(1-h)$  for  $\Delta_E$ . The deviation of leaf water isotopic composition at the evaporating sites from isotopic steady state ( $\Delta_e - \Delta_C$ ) was well correlated with  $\Delta_E$  in fall (and to lesser degree in spring) when  $h$  was high (Fig. 6a, c) and thus the denominator in eq. 4 is small. Still during spring and also fall, the non-steady-state effect of leaf water at the evaporating sites is amplified by up to 15‰ for  $\Delta_E$ . During dry and hot days in summer no correlation between  $\Delta_e - \Delta_C$  and  $\Delta_E$  could be found at all, although the variability of  $\Delta_e - \Delta_C$  was not small (between -4.1 to -8.8‰, Fig. 6b). In contrast,  $(\Delta_e - \Delta_C)/(1-h)$  was well correlated with  $\Delta_E$  and near to the 1:1 line also during summer (Fig. 6d-f). These results suggest that  $\delta_E$  can strongly deviate from  $\delta_s$ , even when  $\Delta_e - \Delta_C$  is small (Fig. 6). So far, the relation between the non-steady-state effects of leaf water and of transpired vapour has gained little attention. Comparing  $\Delta_e - \Delta_C$  and  $\Delta_E$  of previous studies seems to support our findings though (e.g. Lai *et al.*, 2006; Yepez *et al.*, 2007). Notably, the deviations

of observed vs. modeled  $\Delta_E$  from the 1:1 line are not caused by the exclusion of the term  $\alpha^+ \alpha_k$ , which has a very small overall effect on  $\Delta_E$  even in summer where diurnal temperature fluctuations were high (Fig. 6d-f).

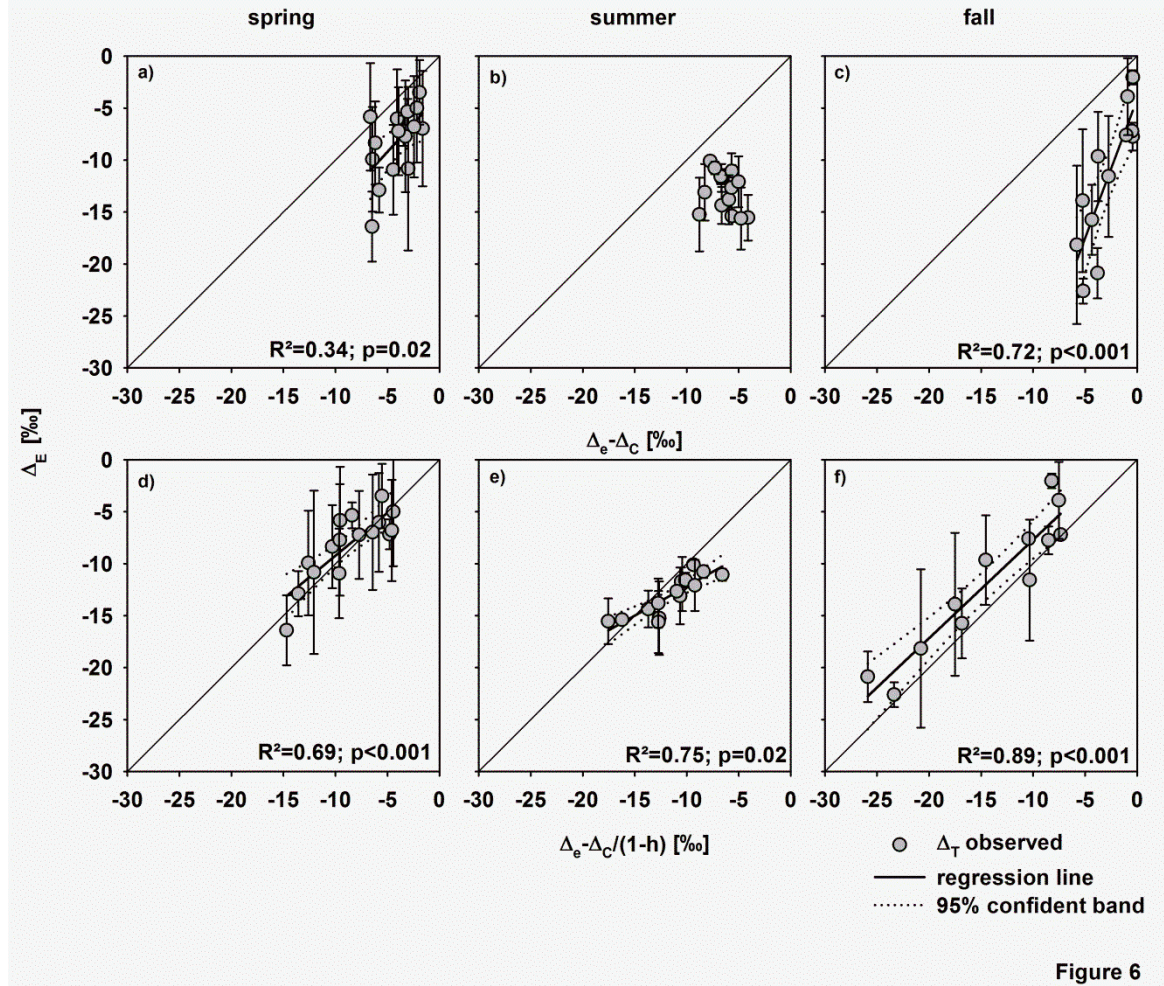


**Figure 6:** Spring (a, d), summer (b, e) and fall (c, f) deviations of the oxygen isotope signature of transpired vapor from xylem water ( $\Delta_E$ , ‰) against deviation of leaf water isotopic composition at the evaporating sites from isotopic steady-state ( $\Delta_e - \Delta_C$ , ‰; a-c), and against  $\Delta_e - \Delta_C$  amplified by  $1/(1-h)$  (d-f). The black lines indicate significant linear regressions and dashed black lines the 95% confident bands. The 1:1 line is indicated in black; coefficients of determination  $R^2$  and significance level  $p$  are shown inside the plots.

Oxygen isotope signatures of transpiration are used in applications differing in spatial (plant to global) and temporal (minute to annual) scales and it is thus crucial to assess where large errors can be expected by assuming steady-state transpiration at larger scales. Accordingly, isoforcing of transpiration on the atmosphere ( $I_E$ ; Lee *et al.*, 2009) was estimated assuming transpiration to be in steady-state vs. non-steady-state (Fig. 7). Notably, isoforcing of the transpirational flux on atmospheric vapor is mostly positive here, as despite its depletion relative to xylem values  $\delta_E$  is

enriched relative to ambient vapour.  $I_E$  was large during daytime in spring and summer (up to  $1.05 \text{ mol m}^{-2} \text{ s}^{-1} \text{ ‰}$ ), when fluxes were high. Looking at daytime values only,  $I_E$  assuming steady-state transpiration was significantly higher than assuming non-steady-state  $\delta_E$  on all days during spring and summer but not during fall, when the transpiration flux was small (Fig. 2 and 7g-i). This implies that assuming plant transpiration to be in the steady-state can have a large impact for applications that assess relatively short time intervals (e.g. partitioning studies: Williams *et al.*, 2004; Yakir & Sternberg, 2000; Yepez *et al.*, 2003; Zhang *et al.*, 2011; Hu *et al.*, 2014). Dubbert *et al.* (2013) found in a Mediterranean grassland community that assuming  $E$  in isotopic steady-state can lead to offsets of up to 70% in the estimation of the fraction of transpiration on total evapotranspiration. Moreover on larger spatial scales disregarding diurnal variation may still be affected by the sampling period during daytime, e.g. satellite based water isotope assessments looking at the atmospheric boundary layer (Lee *et al.*, 2012). Consequently, recent studies investigated the influence of (isotopic non-steady-state)  $E$  on canopy-air exchange of oxygen isotopes of  $\text{H}_2\text{O}$  and  $\text{CO}_2$  (Xiao *et al.*, 2010; Berkelhammer *et al.*, 2013) or on water vapor deuterium excess (Welp *et al.*, 2012) using continuous observations of  $\delta_a$  and including a non-steady-state formulation for leaf water enrichment into a land surface model (SiLSM). Interestingly, Xiao *et al.* (2010; for soybean) found that the isotopic non-steady-state of transpiration has a greater impact on leaf-water enrichment than the Péclet effect. Xiao *et al.* (2012) on the other hand suggest also that the isotopic steady-state assumption determines plant  $\text{C}^{18}\text{O}^{16}\text{O}$  exchange quite well during daytime.

Notably, modeling  $\delta_E$  with a broad range of leaf water residence times (Fig. 5) indicates that the effect of considering isotopic steady-state of transpiration will be strongly dependent on plant functional type. Therefore, a survey on species from distinct functional groups with different leaf morphological and structural traits, leaf water residence times and transpiration rates might be indicative for a thorough characterization of the role of non-steady-state transpiration. It would be particularly interesting to investigate how different plant functional groups differ in the diurnal development of  $\delta_E$  in regard to environmental stresses such as drought (Lai *et al.*, 2008; Simonin *et al.*, 2013).

In the long run, deviations from isotopic steady-state must be compensated for as accumulation of heavy water can only occur over short time-scales, i.e. hours or in extreme cases days. Consequently,



considering whole day mean  $I_E$ , the deviation during daytime was compensated during the night by larger  $I_E$  considering isotopic non-steady-state transpiration. Only in two out of nine measurement days 24h mean isoforcing was significantly smaller considering non-steady-state compared to steady-state (Fig. 7). It would thus be interesting to determine the maximum time period that  $I_E$  can deviate from the steady-state prediction.

Concluding, we found strong deviations from isotopic steady-state in plant transpiration during daytime that should be considered carefully when using  $\delta_E$  to trace the impact of fluxes of the water or carbon cycle.

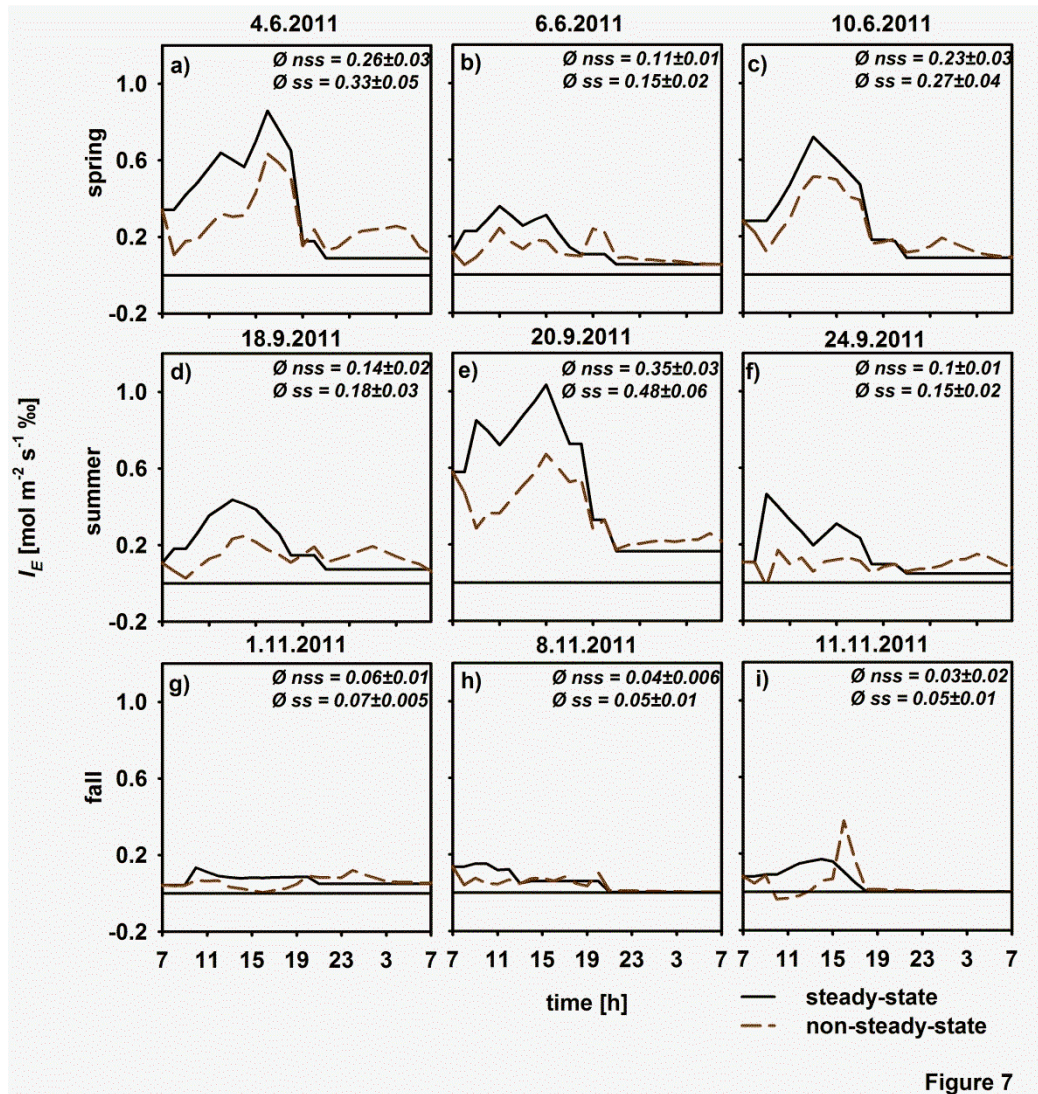


**Figure 7:** Isoforcing of transpiration on the atmosphere [ $I_E$ ;  $\text{mol m}^{-2} \text{s}^{-1} \text{‰}$ ] for each measurement day assuming isotopic steady-state (ss, black solid lines) or non-steady-state (nss, red dashed lines). Nighttime transpiration rates and conductances were taken from Dawson *et al.* (2007). 24h means  $\pm$  SE are given for each measurement day (date format: day.month.year); errors were calculated from bootstrap re-sampling.

## 1.5. Acknowledgements

Funding was provided by the DFG (WATERFLUX Project: # WE 2681/6-1; # CU 173/2-1) and DAAD. We thank the Herdade da Machoqueira and Joao S. Pereira for the possibility to use the field site as well as logistical support and Alexandra Correia and Babsi Teichner for help in the field and laboratory. Finally, we thank three anonymous reviewers for their helpful comments on this manuscript.

## 1.6. Literature

- Berkelhammer M, Hu H, Bailey A, Noone DC, Still CJ, Barnard H, Gochis D, Hsiao GS, Turnipseed A. 2013. The nocturnal water cycle in an open canopy forest. *Journal of Geophysical Research: Atmospheres* **118**: 10.225 – 10242.
- Brenner AJ, Jarvis PG. 1995. A heated leaf replica technique for determination of leaf boundary layer conductance in the field. *Agricultural and Forest Meteorology* **72**: 261-275.
- Cernusak LA, Pate JS, Farquhar GD. 2002. Diurnal variation in the stable isotope composition of water and dry matter in fruiting *Lupinus angustifolius* under field conditions. *Plant, Cell & Environment* **25**, 893–907. doi: 10.1046/j.1365-3040.2002.00875.x.
- Cernusak LA, Wong S-C, Farquhar GD. 2003. Oxygen isotope composition of phloem sap in relation to leaf water in *Ricinus communis*. *Functional Plant Biology* **30**, 1059–1070. doi: 10.1071/FP03137.
- Craig H, Gordon, LI. 1965. Deuterium and oxygen-18 variations in the ocean and the marine atmosphere. Paper presented at the Stable Isotopes in Oceanographic Studies and Paleotemperatures, Spoleto, Italy.
- Cuntz M, Ciais P, Hoffmann G, Allison CE, Francey RJ, Knorr W, Tans PP, White JWC, Levin I. 2003. A comprehensive global three-dimensional model of  $\delta^{18}\text{O}$  in atmospheric  $\text{CO}_2$ : 2. Mapping the atmospheric signal. *Journal of Geophysical Research* **108**.
- Cuntz M, Ogee J, Farquhar GD, Peylin P, Cernusak LA. 2007. Modelling advection and diffusion of water isotopologues in leaves. *Plant, Cell and Environment* **30**: 892-909.
- Dawson TE, Burgess SSO, Tu KP, Oliveira RS, Santiago LS, Fisher JB, Simonin KA, Ambrose AR. 2007. Nighttime transpiration in woody plants from contrasting ecosystems. *Tree Physiology* **27**: 561-575.
- Dongmann G, Nurnberg HW, Forstel H, Wagener K. 1974. On the enrichment of  $\text{H}_2^{18}\text{O}$  in the leaves of transpiring plants. *Radiation and Environmental Biophysics* **11**:41-52.
- Dubbert M, Cuntz M, Piayda A, Máguas C, Werner C. 2013. Partitioning evapotranspiration – Testing the Craig and Gordon model with field measurements of oxygen isotope ratios of evaporative fluxes. *Journal of Hydrology* **496**: 142-153.
- Farquhar GD, Lloyd J. 1993. Carbon and oxygen isotope effects in the exchange of carbon dioxide between terrestrial plant and the atmosphere. In: Ehleringer JD, ed., *Carbon and oxygen isotope effects in the exchange of carbon dioxide between terrestrial plant and the atmosphere*. San Diego, Academic, 47-70.
- Farquhar GD, Cernusak LA. 2005. On the isotopic of leaf water in the non-steady-state. *Functional Plant Biology* **32**: 293-303.

- Gonfiantini, R. 1978.** Standards for stable isotope measurements in natural compounds. *Nature* **271**: 534-536.
- Good SP, Soderberg K, Wang L, Caylor KK. 2012.** Uncertainties in the assessment of the isotopic composition of surface fluxes: a direct comparison of techniques using laser-based water vapor isotope composition. *Plant, Cell and Environment* **15**: 329-344.
- Haverd V, Cuntz M, Griffith D, Keitel C, Tardos C, Twining J. 2011.** Measured deuterium in water vapour concentration does not improve the constraint on the partitioning of evapotranspiration in a tall forest canopy, as estimated using a soil vegetation atmosphere transfer model. *Agricultural and forest Meteorology* **151**: 645-654.
- Harwood KG, Gillon JS, Griffiths H, Broadmeadow MSJ. 1998.** Diurnal variation of  $\Delta^{13}\text{CO}_2$  and  $\Delta\text{C}^{18}\text{O}^{16}\text{O}$  and evaporative site enrichment of  $\delta\text{H}_2^{18}\text{O}$  in *Piper aduncum* under field conditions in Trinidad. *Plant, Cell and Environment* **21**: 269-283.
- Helliker BR, Ehleringer JR. 2002.** Differential O-18 enrichment of leaf cellulose in C-3 versus C-4 grasses. *Functional Plant Biology* **29**: 435-442.
- Hu Z, Wen X, Sun X, Li L, Yu G, Lee X, Li S. 2014.** Partitioning evapotranspiration through oxygen isotopic measurements of water pools and fluxes in a temperate grassland. *Journal of Geophysical Research: Biogeosciences* **119**: 10.1002/2013JG002367.
- Kahmen A, Simonin K, Tu K, Goldsmith GR, Dawson TE. 2009.** The influence of species and growing conditions on the 18-O enrichment of leaf water and its impact on 'effective path length'. *New Phytologist* **184**: 619-630.
- Jasechko S, Sharp ZD, Gibson JJ, Birks SJ, Yi Y, Fawcett PJ. 2013.** Terrestrial water fluxes are dominated by transpiration. *Nature* **496**: 347
- Lai CT, Ehleringer JR, Bond BJ, U K. 2006.** Contributions of evaporation, isotopic non-steady-state transpiration and atmospheric mixing on the delta O-18 of water vapor in Pacific Northwest coniferous forests. *Plant, Cell and Environment* **29**: 77-94.
- Lai C-T, Ometto JPHB, Berry JA, Martinelli LA, Domingues TF, Ehleringer JR. 2008.** Life form-specific variations in leaf water oxygen-18 enrichment in Amazonian vegetation. *Oecologia* **157**: 197-210.
- Lee X, Griffis TJ, Baker JM, Billmark JM, Kim K, Welp LR. 2009.** Canopy-scale kinetic fractionation of atmospheric carbon dioxide and water vapor isotopes. *Global Biogeochemical cycles* **23**.
- Lee X, Huang J, Patton EG. 2012.** A Large-Eddy simulation study of water vapour and carbon dioxide isotopes in the atmospheric boundary layer. *Boundary-Layer Meteorology* **145**: 229-248.
- Majoube M. 1971.** Oxygen-18 and Deuterium Fractionation between Water and Steam. *Journal of Chemical Physics* **68**: 1423.
- Mott KA, Peak D. 2011.** An alternative perspective on the control of transpiration by radiation. *Proceedings of the National Academy of Science* **49**: 19820-19823.
- Pape L, Ammann, C, Nyfeler-Brunner A, Spirig C, Hens K, Meixner FX. 2009.** An automated dynamic chamber system for surface exchange measurement of non-reactive and reactive trace gases of grassland ecosystems. *Biogeosciences* **6**:405-429.
- Schlesinger WH, Jasechko S. 2014.** Transpiration in the global water cycle. *Agricultural and Forest Meteorology* **189**: 115-117.
- Schmidt M, Maseyk K, Lett C, Biron P, Richard P, Bariac T, Seibt U. 2010.** Concentration effects on laser-based  $\delta^{18}\text{O}$  and  $\delta^2\text{H}$  measurements and implications for the calibration of vapour measurements with liquid standards. *Rapid Communications in Mass Spectrometry* **24**: 3553-3561.
- Seibt U, Wingate L, Berry JA. 2006.** Non-steady state effects in diurnal O-18 discrimination by

- Picea sitchensis* branches in the field. *Plant, Cell and Environment* **29**: 928-939.
- Simonin KA, Roddy AB, Link P, Apodaca R, Tu KP, Hu J, Dawson TE, Barbour MM. 2013.** Isotopic composition of transpiration and rates of change in leaf water isotopologue storage in response to environmental variables. *Plant, Cell and Environment* **36**: 2190-2206.
- Von Caemmerer S, Farquhar GD. 1981.** Some relationships between the biochemistry of photosynthesis and the gas-exchange of leaves. *Planta* **153**: 376-387.
- Wang L, Good SP, Caylor KK, Cernusak LA. 2012.** Direct quantification of leaf transpiration isotopic composition. *Agricultural and Forest Meteorology* **154**:127-135.
- Welp LR, Lee X, Griffis TJ, Wen X-F, Xiao W, Li S, Sun X, Hu Z, Martin MV, Huang J. 2012.** A meta-analysis of water vapor deuterium-excess in the midlatitude atmospheric surface layer. *Global Biogeochemical cycles* **26**: 10.1029/2011gb004246.
- Werner C, Schnyder H, Cuntz M, Keitel C, Zeeman MJ, Dawson TE, Badeck F-W, Brugnoli E, Ghashghaie J, Grams TEE, *et al.* 2012.** Progress and challenges in using stable isotopes to trace plant carbon and water relations across scales. *Biogeosciences* **9**: 3083-3111.
- Williams DG, Cable W, Hultine K, Hoedjes JCB, Yepez EA, Simonneaux V, Er-Raki S, Boulet G, de Bruin HAR, Chehbouni A *et al.* 2004.** Evapotranspiration components determined by stable isotope, sap flow and eddy covariance techniques. *Agricultural and Forest Meteorology*, **125**: 241-258.
- Xiao W, Lee X, Griffis TJ, Kim K, Welp LR, Yu Q. 2010.** A modeling investigation of canopy-air oxygen isotopic exchange of water vapor and carbon dioxide in a soybean field. *Journal of Geophysical Research* **115**: 10.1029/2009jg001163.
- Xiao W, Lee X, Wen X, Zhang S. 2012.** Modeling biophysical controls on canopy foliage water  $^{18}\text{O}$  enrichment in wheat and corn. *Global Change Biology* **18**: 1769-1780.
- Yakir D, Sternberg LDL. 2000.** The use of stable isotopes to study ecosystem gas exchange. *Oecologia* **123**: 297-311.
- Yepez EA, Williams DG, Scott RL, Lin G. 2003.** Partitioning overstory and understory evapotranspiration in a semiarid savanna woodland from isotopic composition of water vapor. *Agricultural and Forest Meteorology* **119**: 53-68.
- Yepez EA, Scott RL, Cable WL, Williams DG. 2007.** Intraseasonal variation in water and carbon dioxide flux components in a semiarid riparian woodland. *Ecosystems* **10**: 1100-1115.
- Zhang Y, Shen Y, Sun H, Gates JB. 2011.** Evapotranspiration and its partitioning in an irrigated winter wheat field: A combined isotopic and micrometeorologic approach. *Journal of Hydrology* **408**: 203-211.



## 1.7. Supporting information

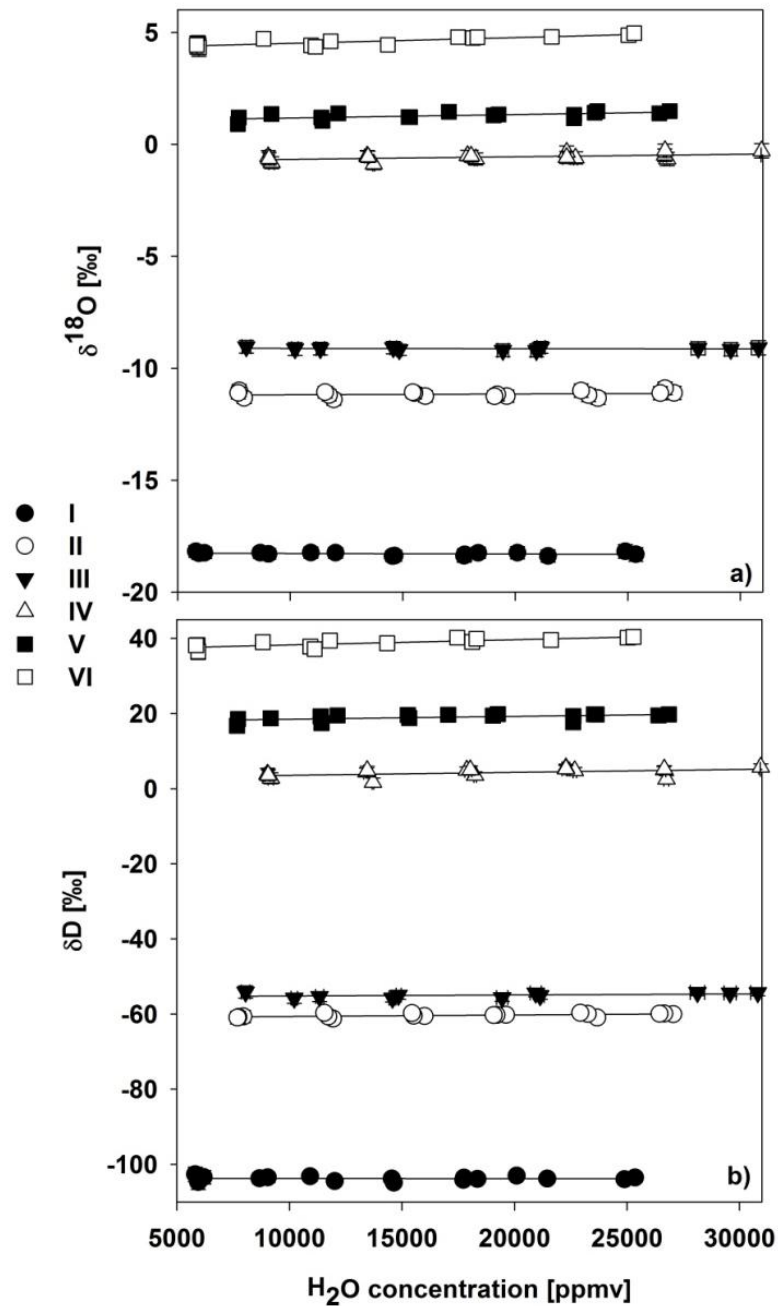


**Figure S1:** Concentration dependencies of the Cavity Ring-Down Spectrometer at six different oxygen (a) and deuterium (b) isotopic signatures. Each sample with distinct signature (I-VI; see Table S1) was measured from 5000 to 30000 ppmv H<sub>2</sub>O concentration.

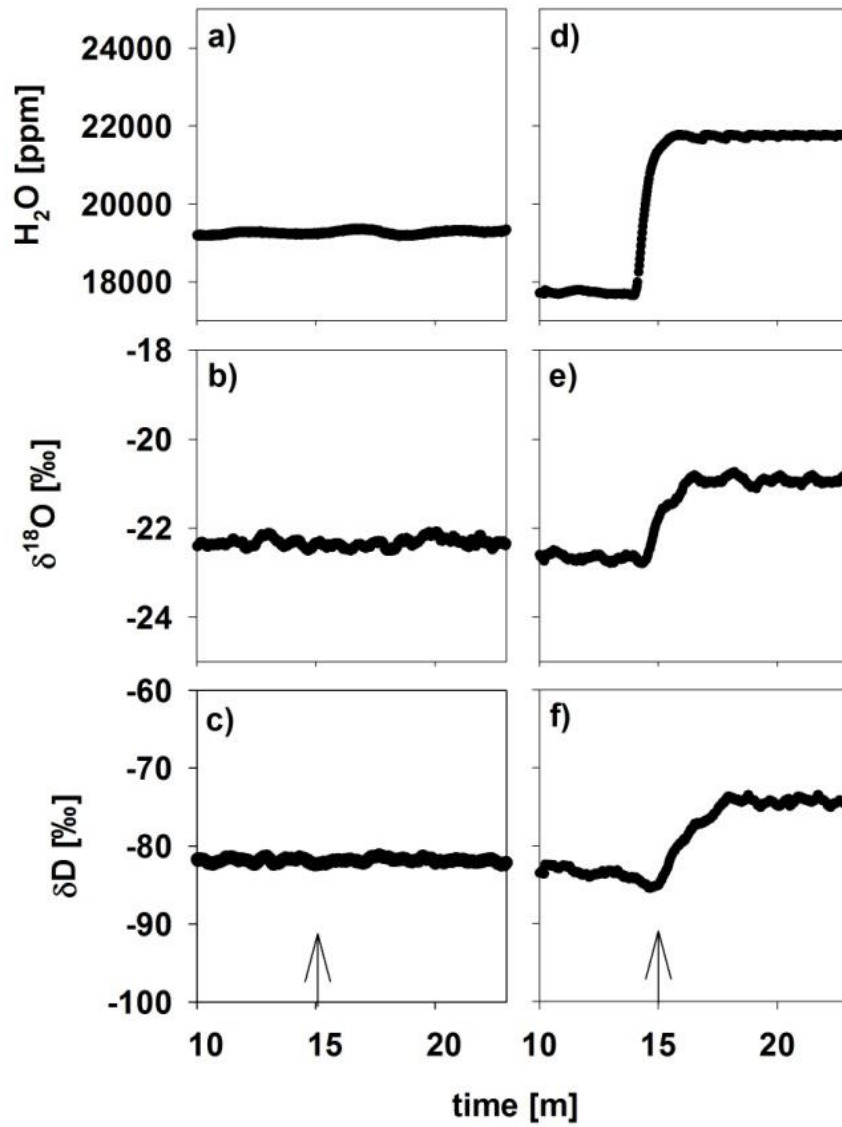


**Figure S2:**  $H_2O$  (ppm),  $\delta^{18}O$  and  $\delta D$  (‰) observed with the Cavity Ring-Down Spectrometer of ambient air and blank branch chamber (a-c) and of ambient air and branch chamber with branch enclosed (d-f). Arrows denote switch from ambient air going into the branch chamber to air coming out of the branch chamber.

**Table S1:** Equations, R<sup>2</sup> and p values for the Concentration dependencies of the Cavity Ring-Down Spetrometer at six different oxygen and deuterium isotopic signatures as shown in Fig. S1.

<i>standards</i>	$\delta^{18}O(\text{‰})$	<b>R<sup>2</sup></b>	<b>p</b>
I (4.3)	0.000026* <i>H2O</i> +4.3	0.72	<0.001
II (1.0)	0.000015* <i>H2O</i> +1.02	0.39	0.007
III (-0.8)	0.000011* <i>H2O</i> -0.78	0.3	0.02
IV(-9.1)	0.0000011* <i>H2O</i> -9.1	0.02	n.s.
V (-11.2)	0.0000036* <i>H2O</i> -11.2	0.03	n.s.
VI (-18.2)	0.0000027* <i>H2O</i> -18.2	0.07	n.s.
<i>standards</i>	$\delta D(\text{‰})$	<b>R<sup>2</sup></b>	<b>p</b>
I (36.9)	0.00014* <i>H2O</i> +36.9	0.63	<0.001
II (17.7)	0.0000759* <i>H2O</i> +17.7	0.29	0.03
III (2.8)	0.0000775* <i>H2O</i> +2.8	0.28	0.02
IV(-55.4)	0.00000257* <i>H2O</i> -55.4	0.17	n.s.
V (-61.0)	0.0000039* <i>H2O</i> -61.0	0.29	0.02
VI (-103.7)	0.00000546* <i>H2O</i> -103.7	0.001	n.s.

## 2. STUDY II: PARTITIONING EVAPOTRANSPIRATION – TESTING THE CRAIG AND GORDON MODEL WITH FIELD MEASUREMENTS OF OXYGEN ISOTOPE RATIOS OF EVAPORATIVE FLUXES

Maren Dubbert<sup>1,\*</sup>; Matthias Cuntz<sup>2</sup>; Arndt Piayda<sup>2</sup>; Cristina Maguás<sup>3</sup>; and Christiane Werner<sup>1</sup>

<sup>1</sup>Department of Agroecosystem Research, University of Bayreuth, Universitätsstraße 30, 95447 Bayreuth, Germany

<sup>2</sup>UFZ – Computational Hydrosystems, Helmholtz Centre for Environmental Research, Permoserstraße 15, 04318 Leipzig, Germany

<sup>3</sup>Centro da Biologia Ambiental, Faculdade de Ciencias, University of Lisbon, Campo Grande, 1749-016 Lisbon, Portugal

\*Corresponding author: Maren Dubbert ([maren.dubbert@uni-bayreuth.de](mailto:maren.dubbert@uni-bayreuth.de))



## 2.1. Abstract

Stable oxygen isotopes of water provide a valuable tracer for water movements within ecosystems and are used to estimate the contribution of transpiration to total ecosystem evapotranspiration ( $ft$ ). We tested the Craig and Gordon equation against continuous field measurements of isotopic composition of evaporation and assessed the impact for partitioning evapotranspiration. Therefore, evaporation ( $E$ ) and its isotopic signature ( $\delta^{18}O_E$ ) on bare soil plots, as well as evapotranspiration ( $ET$ ) and its corresponding isotopic composition of ( $\delta^{18}O_{ET}$ ) of an herbaceous layer was measured with a cavity ring-down spectrometer connected to a soil chamber on a field site in central Portugal. We quantified the variation in  $\delta^{18}O_E$  arising from uncertainties in the determination of environmental input variables to the Craig and Gordon equation: the isotope signature ( $\delta^{18}O_e$ ) and the temperature at the evaporating site ( $T_e$ ), and the kinetic fractionation factor ( $\alpha_k$ ). We could hence quantify  $ft$  based on measured  $\delta^{18}O_{ET}$ , modeled  $\delta^{18}O_E$  from observed soil water isotopic composition at the evaporating site ( $\delta^{18}O_e$ ), and modeled  $\delta^{18}O$  of transpiration ( $\delta^{18}O_T$ ) from observed total soil water isotopic composition.

Our results demonstrate that predicting  $\delta^{18}O_E$  using the Craig and Gordon equation leads to good agreement with measured  $\delta^{18}O_E$  given that the temperature and  $^{18}O$  isotope profiles of the soil are thoroughly characterized. However, modeled  $\delta^{18}O_E$  is highly sensitive to changes in  $T_e$  and  $\delta^{18}O_e$  as well as  $\alpha_k$ . This markedly affected the partition results of transpiration and evaporation from the total  $ET$  flux: The fraction of transpiration ( $ft$ ) varied strongly using different formulations for  $\alpha_k$  and assuming steady or non-steady state transpiration. These findings provide a first comparison of laser-based and modeled isotopic compositions of evaporation based on the Craig and Gordon equation under field conditions. This is of special interest for studies using stable isotopes to separate soil evaporation and plant transpiration fluxes and highlights the need for a thorough characterization of the micrometeorological and isotopic constitution of the upper soil layer to locate the evaporating front with a resolution of a few cm soil depths. We also call on a better characterization of the kinetic fractionation factor of soil evaporation.

## 2.2. Abbreviations

$\alpha_k/\alpha^+$	kinetic fractionation factor/equilibrium fractionation factor
$\delta^{18}\text{O}$	oxygen stable isotope signature (‰)
$\Theta$	volumetric water content
$R$	Isotope ratio of [ $^{18}\text{O}$ ]/[ $^{16}\text{O}$ ]
$E$	soil evaporation
$T$	plant transpiration
$ET$	evapotranspiration
$ft$	$T/ET$
$w$	$\text{H}_2\text{O}$ concentration
$h$	relative humidity
$nk$	exponent relating $\alpha_{k, \text{diff}} = (D_v/D_v^i)$ to $\alpha_k$
$D_v^i$	diffusivity of $\text{H}_2^{18}\text{O}$ in air
$D_v$	diffusivity of $\text{H}_2\text{O}$ in air
$ns/na$	constants used in the definition of the $nk$ exponent related to soil and atmosphere controlled diffusivity (1 and 0.5, respectively)
$g_t$	total leaf conductance to water vapor ( $\text{mol m}^{-2} \text{s}^{-1}$ )
$V$	water volume ( $\text{mol m}^{-2}$ )
$T$	Temperature
$s$	soil
$e$	evaporating surface
$v$	ambient water vapor
$m$	liquid mesophyll water
$r$	residual
$sat$	saturation
$surf$	surface
$lw$	leaf water

### 2.3. Introduction

Oxygen isotope signatures are valuable tracers for water movements within the ecosystem because of the distinct isotopic compositions of water in the soil and vegetation (Yakir and Sternberg, 2000). Evaporation from the soil modifies the isotopic composition of source water and was first described by Craig and Gordon (1965). Evaporated water vapor is strongly depleted in relation to the evaporating water source based on isotope fractionation associated with equilibrium isotope effects at the vapor-liquid interface (equilibrium fractionation,  $\alpha^+$ ) and diffusion-controlled isotope effects (kinetic fractionation,  $\alpha_k$ ). The evaporation model proposed by Craig and Gordon is widely used in ecological and modeling studies to determine the oxygen isotopic composition of soil evaporation and plant leaf water enrichment. It has been used to achieve better understanding of the dynamics of hydrological processes (Barbour, 2007; Braud et al., 2005a, b; Cuntz et al., 2007; Haverd and Cuntz, 2010), and to partition ecosystem water fluxes into their components: soil evaporation and plant transpiration (e.g. Haverd et al., 2011; Williams et al., 2004; Yepez et al., 2005, 2007).

Evaporation from the soil occurs at the vapor-liquid interface (the evaporating front) below which liquid transport and above which vapor transport is dominant (Braud et al., 2005a). It has been shown for unsaturated soils that this front is related to a strong enrichment in soil water isotopic composition relative to the rest of the soil column and an exponential depletion in isotopic signature within few cm of the underlying soil due to evaporative enrichment of the remaining liquid water (Zimmermann et al., 1967). A precise determination of the evaporating front is therefore very important for a correct estimation of  $\delta^{18}O_E$  but its precise determination remains a challenge in most field studies due to the requirement of large sample sizes (see Lai et al., 2006; Wang et al., 2010; Williams et al., 2004; Yepez et al., 2005, 2007).

While soil evaporation is seldom in the steady state, plant transpiration reaches steady state at certain times of the day. During steady state transpiration the  $\delta^{18}O$  of the transpiration flux is equal to the isotope signature of xylem/source water (Dawson, 1993). The large differences between evaporative non-steady state  $\delta^{18}O$  (depleted compared to source water) and transpirational steady state  $\delta^{18}O$  (equal to source water) then provide the basis using stable isotopes to separate soil evaporation and plant transpiration fluxes (e.g. Lai et al., 2006; Wang et al., 2010; Williams et al., 2004; Yepez et al., 2007).

However, it has to be taken into account that steady state conditions are not always found due to the transient changes in atmospheric conditions (Yakir and Sternberg, 2000). Thus, non-steady state transpiration is depleted in  $\delta^{18}\text{O}$  relative to xylem/source water during parts of the day (Cuntz et al., 2007; Dongmann et al., 1974; Farquhar and Cernusak, 2005).

Recent developments in laser spectroscopy enable the measurement of  $\delta^{18}\text{O}$  of atmospheric water vapor ( $\delta^{18}\text{O}_v$ ), and evapotranspiration ( $\delta^{18}\text{O}_{ET}$ ) and its components with a high temporal resolution in the field (Werner et al., 2012). In the past, however, precise determinations of  $\delta^{18}\text{O}_{ET}$ ,  $\delta^{18}\text{O}_E$  and  $\delta^{18}\text{O}_T$  have been a challenge since measurements of water vapor were difficult to obtain using cold-trapping methods (e.g. Helliker et al., 2002; Williams et al., 2004; Yopez et al., 2005). Several studies have conducted experiments on isotopic evaporation (Cappa et al., 2003; Craig et al., 1963; Merlivat, 1978; Rozanski and Chmura, 2006; Stewart, 1975), but only few studies (i.e. Braud et al. 2009a,b; Kim and Lee, 2011) used continuous measurements of  $\delta^{18}\text{O}$  of evaporation or ambient water vapor. Field studies comparing modeled with directly measured isotope signatures of evaporation are even scarcer (but see Haverd and Cuntz, 2010 and for controlled conditions Rothfuss et al., 2010 and 2012). To close this research gap we measured the isotopic composition of evaporation ( $\delta^{18}\text{O}_E$ ) obtained with a cavity ring-down spectrometer connected to a soil chamber on experimental plots in a herbaceous community of an open oak woodland in central Portugal. We tested the Craig and Gordon equation against directly measured  $\delta^{18}\text{O}_E$ . Specifically, we quantified the variation in  $\delta^{18}\text{O}_E$  arising from uncertainties in the determination of important environmental input variables to the Craig and Gordon equation: the isotope signature at the evaporating site ( $\delta^{18}\text{O}_e$ ), the temperature at the evaporating site ( $T_e$ ), and the kinetic fractionation factor ( $\alpha_k$ ). Finally, we measured the isotopic composition ( $\delta^{18}\text{O}_{ET}$ ) and fluxes of evapotranspiration of an herbaceous understory layer and quantified the contribution of transpiration to evapotranspiration ( $f_t$ ) based on measured  $\delta^{18}\text{O}_{ET}$  and modeled  $\delta^{18}\text{O}_E$  and  $\delta^{18}\text{O}_T$  on vegetation plots.

## 2.4. The Craig and Gordon equation

Craig and Gordon (1965) developed an equation describing the isotopic composition of evaporation from an open water body:



$$R_E = \frac{1}{\alpha_k \alpha^+ (1-h)} (R_e - \alpha^+ h R_v) \quad (1)$$

where  $R_E$  is the isotope ratio ( $^{18}\text{O}/^{16}\text{O}$ ) of evaporated vapor,  $R_e$  is the isotope ratio at the evaporating sites and  $R_v$  is the isotope ratio of ambient water vapor,  $\alpha_k$  is the kinetic fractionation factor,  $\alpha^+$  is the water vapor equilibrium fractionation factor (Majoube, 1971;  $\alpha_k$  and  $\alpha^+ > 1$ ), and  $h$  is the relative humidity normalized to the temperature at the evaporating sites ( $T_e$ ). Most of the environmental input ( $T_e$ ,  $h$ , and  $R_v$ ,  $R_e$ ) need to be determined and a thorough estimation with respect to spatial (e.g. conditions at different soil depths) and temporal variation remains challenging.

The evaporation of water in air is characterized by a fractionation effect that derives from two fractionating processes: equilibrium fractionation and kinetic fractionation. Equilibrium isotope effects ( $\alpha^+$ ) occur because the lighter isotopologue ( $\text{H}_2^{16}\text{O}$ ) evaporates more easily compared to the heavier isotopologue ( $\text{H}_2^{18}\text{O}$ ). This is a rather well characterized, temperature dependent process (Majoube, 1971). In contrast, a determination of the kinetic fractionation ( $\alpha_k$ ) and an agreement on the correct formulation remains controversial (Braud et al., 2005a,b; Braud et al., 2009 a,b; Cappa et al., 2003; Horita et al., 2008; Luz et al., 2009; Rothfuss et al., 2012). Kinetic fractionation occurs because the lighter isotopologue diffuses faster compared to the heavier isotopologue. It involves molecular diffusion through the soil and resistance to water vapor transport in a laminar boundary layer as well as turbulent conditions above the boundary layer. Previous studies determined experimentally the molecular diffusion coefficient ( $D_v/D_v^i$ ). Cappa et al. (2003) recommended a value of  $D_v/D_v^i = 1.032$  according to the kinetic theory of gases. On the other hand Merlivat (1978) and more recently Luz et al. (2009) determined a value of  $D_v/D_v^i = 1.0285$  that deviate from the kinetic theory. Additionally to pure molecular diffusion, studies determined an exponent  $nk$  to  $\alpha_k$ , allowing for the nature of the transport conditions:  $nk$  evolves from 1 when molecular diffusion is the dominant process to 0.5 when turbulent transport becomes most important. When only molecular diffusion plays a role, as in dry soils,  $\alpha_k = D_v/D_v^i$  (Barnes and Allison, 1983). There are various expressions in the literature for the exponent  $nk$  according to the hypotheses made on the influence of molecular and turbulent resistance (for a summary see Braud et al., 2005a). The exponent  $nk$  proposed by Stewart (1976) and Mathieu

and Bariac (1996) is empirically derived and relates the soil water content  $\theta$  to the contribution of turbulent resistance to total transport resistances in an unsaturated soil:

$$\alpha_k = \left( \frac{D_v}{D_v^i} \right)^{nk} \quad (2).$$

The exponent  $nk$  reads as follows:

$$nk = \frac{(\theta_{surf} - \theta_r)n_a + (\theta_{sat} - \theta_{surf})n_s}{(\theta_{sat} - \theta_r)} \quad (3),$$

with  $\theta_{surf}$ ,  $\theta_{sat}$  and  $\theta_r$  as the volumetric soil water content at the soil surface, saturated and residual volumetric soil water content. Residual water content was  $0.01 \text{ m}^3 \text{ m}^{-3}$  on all plots whereas saturated water content differed between the specific plot types:  $0.24 \text{ m}^3 \text{ m}^{-3}$  for vegetation plots,  $0.2 \text{ m}^3 \text{ m}^{-3}$  for root plots, and  $0.18 \text{ m}^3 \text{ m}^{-3}$  for soil plots.

**Table 1:** Description of the three approaches used in this study to calculate  $\delta^{18}\text{O}_E$  varying the soil depth used to derive the isotopic signature and temperature at the evaporating site ( $\delta^{18}\text{O}_e$  and  $T_e$ ) and the kinetic fractionation factor ( $\alpha_k$ ).

	$\delta^{18}\text{O}_e/T_e$	formulation for $\alpha_k$	$nk$	Reference for $\alpha_k$
<b>I</b>	evaporating front	Turbulent and molecular resistance $\alpha_k = \left( \frac{D_v}{D_v^i} \right)^{nk}$	$nk = \frac{(\theta_{surf} - \theta_r)n_a + (\theta_{sat} - \theta_{surf})n_s}{(\theta_{sat} - \theta_r)}$	Mathieu and Bariac (1996)
<b>II</b>	evaporating front	Molecular resistance only $\alpha_k = \left( \frac{D_v}{D_v^i} \right)$	$nk = n_s = 1$	Barnes and Allison (1983)
<b>III</b>	mean 0-10 cm	Turbulent and molecular resistance $\alpha_k = \left( \frac{D_v}{D_v^i} \right)^{nk}$	$nk = \frac{(\theta_{surf} - \theta_r)n_a + (\theta_{sat} - \theta_{surf})n_s}{(\theta_{sat} - \theta_r)}$	Mathieu and Bariac (1996)

Notations:  $D_v$  ( $\text{m}^2 \text{ s}^{-1}$ ) is the vapour diffusivity of ordinary water in the air;  $D_v^i$  ( $\text{m}^2 \text{ s}^{-1}$ ) is the vapour diffusivity of isotope  $i$  in the air;  $\theta_l$  ( $\text{m}^3 \text{ m}^{-3}$ ) is the volumetric liquid water content of the soil;  $\theta_r$  ( $\text{m}^3 \text{ m}^{-3}$ ) is the residual volumetric water content;  $\theta_{sat}$  ( $\text{m}^3 \text{ m}^{-3}$ ) is the saturated volumetric water content. Constants  $n_a$  and  $n_s$  are 0.5 and 1, respectively.

Residual and saturated water contents were derived empirically from observed minima and maxima of

volumetric soil water content throughout the years 2010 and 2011.  $nk$  increases from  $n_a = 0.5$  under saturated soil conditions to  $n_s = 1$  on dry soil, where kinetic fractionation is dominated by molecular diffusion resistances (Mathieu and Bariac, 1996; see Table 1).

## 2.5. Materials and Methods

### 2.5.1. Study site

We tested the Craig and Gordon model in a savannah-type oak-oak (*Quercus suber* L., ~200 individuals per ha) woodland in central Portugal approximately 100 km north-east of Lisbon (N39°8'17.84'' W8°20'3.76''). It is a bi-layered system with an understory layer dominated by native annual plants with a peak growth in spring (April-May), contributing up to 50 % to ecosystem carbon uptake (Unger et al., 2010) and senescing from late May - early June with the onset of summer drought. We established three types of plots sized 40\*80 cm in an open area: bare soil plots with total exclusion of root in-growth by inserting trenching meshes (mesh diameter < 1  $\mu$ m, Plastok, Birkenhead, UK), root plots with exclusion of vegetation layer directly on the plots but allowing neighboring roots to grow in, and understory vegetation plots with undisturbed herbaceous understory vegetation. All plots were established 1 year before measurements to minimize effects of disturbance and germinating seedlings were regularly removed.

### 2.5.2. Environmental variables

Photosynthetic photon flux density (PPFD, LI-190SB, LI-COR, Lincoln, USA), rainfall (ARG100 Rain gauge, Campbell Scientific, Logan, UT, USA), air temperature, and relative humidity (h, CS-215 Temperature and Relative Humidity Probe, Campbell Scientific, Logan, UT, USA) were measured and 30 min averages were stored in a datalogger (CR10x, Campbell Scientific, Logan, UT, USA). Soil temperature (custom built pt-100 elements) and volumetric water content ( $\theta$ , 10hs, Decagon, Washington, USA) in 5, 15, 30 and 60 cm depth were measured in vegetation, root, and soil plots and 60 min averages were stored in a datalogger (CR1000, Campbell Scientific, Logan, UT, USA;  $n = 4$  per for each soil depth and plot type). Temperature at the soil surface was manually measured on each

measurement day in diurnal cycles corresponding with the gas exchange measurements using temperature probes (GMH 2000, Greisinger electronic, Regenstauf, Germany).

#### 2.5.3. *Sampling and measurement of $\delta^{18}O_s$*

Soil samples for water extraction and analysis of  $\delta^{18}O$  were taken on April 8, 12, 18, and 26 and May 2, 2011 on vegetation, root and soil plots using a soil corer. Samples were collected from the soil surface (up to 0.5 cm depth), 2, 5, 10, 15, 20, and 40 cm soil depths ( $n = 4$  per for each soil depth and plot type) and stored in 12 ml glass vials, sealed with parafilm and immediately frozen until water extraction. Water samples were extracted on a custom build vacuum line by cryogenic distillation (design of R. Siegwolf). Samples were heated at approximately 80 °C for 90 min under vacuum of 0.04 to 0.08 mbar. Water traps that were cooled with liquid  $N_2$  were used to collect the water vapor.

Samples were stored in Eppendorf vials at 4°C until analysis. Water  $\delta^{18}O$  analysis was performed by headspace equilibration on an Isoprime IRMS (Elementar, Hanau, Germany) coupled via open split connection to a  $\mu$ gas autosampler (Elementar, Hanau, Germany) and sample preparation system. Equilibration was done for 5 hours at 40°C. For every batch of ~47 samples 3 different laboratory standards were analysed 3 times for  $\delta^{18}O$  calculation versus VSMOW. Laboratory standards were regularly calibrated against VSMOW, SLAP, and GISP water standards (IAEA, Vienna). Analytical precision was  $< 0.1\text{‰}$ .

#### 2.5.4. *CRDS based measurements of $\delta^{18}O_E$ and understory $\delta^{18}O_{ET}$ and their respective fluxes*

Fluxes and isotopic composition of soil evaporation on the root and soil plots as well as of evapotranspiration on vegetation plots ( $n = 3$  per treatment) were measured using a Cavity Ring-Down Spectrometer (CRDS, Picarro, Santa Clara, USA) in combination with soil chambers, custom built, following the design of Pape et al. (2009), in an open gas exchange system. A transparent Plexiglas soil chamber was coated with an isotope inert FEP foil (4PTFE, Stühr, Germany) with a total volume of 60 L. The background air inlet port and the sampling air outlet port were located in 10 and 50 cm height, respectively. The background air was sampled from 1.5 distance and buffered with a 200 L buffer volume. The flow through the chamber was regulated as described in Pape et al. (2009) using a

fan inside the inlet sampling tube and could be adjusted between 0 and 40  $L \min^{-1}$ . The CRDS was calibrated 3 times a day using a standards delivery module and vaporizer (SDM, Picarro, Santa Clara, USA) with two laboratory standards that were regularly calibrated against VSMOW and SLAP. Measurement precision was  $< 0.2\%$ .  $H_2O$  concentrations (ppmv) of the CRDS were calibrated prior to each measurement campaign in the laboratory using a dew point generator (Walz, Effeltrich, Germany). During field campaigns the running precision of the instrument was regularly crosschecked using an equally calibrated infrared gas analyzer (Li840, Licor Biosciences, Lincoln, USA). The precision of the CRDS was below 100 ppmv throughout the measurement period. We measured background and sampling air alternately until stable values were reached. The chamber maintained on the plots until stabilization was reached, which was  $< 10$  min. The observed increase in air temperature above ambient values was ca. 3 °C after 5 min and stable thereafter, which is smaller compared to those found in Pape et al. (2009). A 5 min interval average was finally recorded for the calculation of evaporation ( $E$ ) and evapotranspiration ( $ET$ ) with the gas exchange equations of von Caemmerer & Farquhar (1981).

Isotope signatures of evaporation and evapotranspiration were calculated by mass balance:

$$\delta^{18}O = \frac{w_{out}\delta^{18}O_{out} - w_{in}\delta^{18}O_{in}}{w_{out} - w_{in}} \quad (4)$$

where  $\delta^{18}O_{out}$  and  $\delta^{18}O_{in}$  is the isotope ratio of the chamber and background air and  $w_{out}$  and  $w_{in}$  as the  $H_2O$  concentration of the chamber and background air, respectively. Measurements were obtained on five days during April, corresponding with the soil water isotope sampling.

#### 2.5.5. Estimation of $\delta^{18}O_E$ , $\delta^{18}O_e$ , and $\delta^{18}O_T$ and $ft$

We modeled  $\delta^{18}O_E$  using approaches differing in the three input variables – temperature ( $T_e$ ), isotopic composition at the evaporating sites ( $R_e$ ), and kinetic fractionation factor ( $\alpha_k$ , for a detailed overview see Table 1). In approach I values of  $T_e$  and  $R_e$  measured at the evaporating front and the formulation for  $\alpha_k$  provided by Mathieu and Bariac (1996) were used. Approach II was also calculated with values

of temperature and  $R_e$  measured at the evaporating front but with kinetic fractionation only influenced by molecular diffusion as suggested by Barnes and Allison (1983,  $nk = 1$ ). Approach III again used the formulation of Mathieu and Bariac (1996) for  $\alpha_k$  but used average values of the upper 10 cm of the soil profile for  $R_e$  and  $T_e$  (see Table 1). The evaporating front is characterized by a large enrichment of the soil  $\delta^{18}\text{O}$  signature. Thus,  $R_e$  and  $T_e$  were taken from the depth where the strongest enrichment in  $\delta^{18}\text{O}$  could be detected, which was commonly the soil surface (see Barnes and Allison, 1983; Braud et al., 2005; Harverd and Cuntz, 2010). In the few cases where the strongest isotopic enrichment was found in 2 cm soil depth soil temperature measured at 5 cm depth was taken for  $T_e$  as direct measurements in 2 cm depths were not available on our plots. Comparisons between soil temperature in 2 cm and 5 cm depth on a soil profile adjacent to our plots revealed that temperatures differences between 2 and 5 cm depths were on average less than 1 °C (data not shown).

The isotope signature of evapotranspiration ( $ET$ ) is influenced by soil evaporation ( $E$ ) and plant transpiration ( $T$ ) and can be calculated if the isotope signatures of  $T$  ( $\delta^{18}O_T$ ),  $E$  ( $\delta^{18}O_E$ ), and  $ET$  ( $\delta^{18}O_{ET}$ ) are known. Therefore, we measured fluxes and isotope signatures of  $ET$  and modeled  $\delta^{18}O_E$  and  $\delta^{18}O_T$ .  $\delta^{18}O_E$  on vegetation plots was modeled as for root and soil plots with approach I and II (see above). To calculate  $\delta^{18}O_T$ , in a first step the isotopic composition of leaf water at the evaporating sites ( $\delta^{18}O_e$ ) was calculated. We followed the method of Cuntz et al. (2007) and used the iterative solution of the ordinary differential equation for leaf water at the evaporating sites in non-steady state as in Dongmann et al. (1974). In this case it is assumed that environmental conditions that influence  $\delta^{18}O_e$  change to a new value at time  $t$  and stay fixed over a time period  $dt$ . This “Dongmann-style solution” then reads (Dongmann et al., 1974; Cuntz et al., 2007):

$$R_e(t + dt) = R_c + (R_e(t) - R_c) e^{-\frac{g_t w_i}{\alpha_k \alpha^* V_m} dt} \quad (5)$$

with  $R_e(t+dt)$  as the isotope ratio of leaf water at the evaporating sites at time  $t+dt$ ,  $R_e(t)$  as the isotope ratio of leaf water at the evaporating sites at time  $t$ . A time step of 1 h was used in our calculations, as environmental measurements did not allow a more precise resolution of environmental variables.  $g_t$  is

total conductance ( $\text{mol m}^{-2} \text{s}^{-1}$ ) calculated with canopy temperatures measured inside the canopy with a custom built PT-100 element.  $w_i$  is the humidity in the stomatal cavity, i.e. vapor saturation at leaf temperature ( $\text{mol H}_2\text{O mol air}^{-1}$ ),  $V_m$  the mesophyll water volume ( $\text{mol m}^{-2}$ ), where gravimetric estimates of lamina water volume were used,  $\alpha_k$  and  $\alpha^+$  are the kinetic and equilibrium fractionation factors, respectively.  $\alpha^+$  was calculated as for soil evaporated  $\delta^{18}\text{O}$  (see above) and  $\alpha_k$  was assumed to be 1.0189 corresponding to a laminar boundary layer.  $R_e$  is the Craig and Gordon steady-state isotope ratio at the evaporating sites, i.e. Eq. (1) rearranged for  $R_e$  with  $R_E = R_x$ , and  $R_x$  being the isotope ratio of xylem water. It has to be noted that we were not able to sample xylem water in large sample sizes, due to methodological restrictions related to the size and lacking lignifications of the herbaceous plant species. Therefore we estimated the source/xylem isotopic ratio by assuming root water uptake proportional to root density, which was estimated as root biomass (g) per kg soil along the soil profile. In very dry soil conditions this method could pose some error since plants can shift water uptake into deeper, wetter soil layers. However, typically non woody species, such as the understory vegetation in this study, lack high ability to shift water uptake depths, mainly because they have shallow root systems (Moreno-Gutierrez et al., 2012; Otieno et al., 2011). We could detect understory roots only down to 50 cm and root density declined dramatically below 20 cm with more than 80 % of the root system in the upper 15 cm depth during the whole study period.

Knowing the isotopic signature of leaf water at the evaporating sites, the isotopic signature of plant transpiration can finally be calculated using the Craig and Gordon formulation (see Eq. 1) with the isotopic signature of leaf water at the evaporating sites in the non-steady-state as  $R_e$ .

The contribution of  $T$  to  $ET$ ,  $ft = T/ET$ , was estimated based on measured  $\delta^{18}O_{ET}$  and modeled  $\delta^{18}O_E$  and  $\delta^{18}O_T$ :

$$ft = \frac{\delta^{18}O_{ET} - \delta^{18}O_E}{\delta^{18}O_T - \delta^{18}O_E} \quad (6)$$

## 2.6. Results

### 2.6.1. Environmental conditions

The first half of April 2011 was dry and hot with high solar radiation (max.  $2000 \mu\text{mol m}^{-2} \text{s}^{-1}$ ; Fig. 1a) and air temperatures reaching  $30^\circ\text{C}$  (Fig. 1b) and vapor pressure deficit up to 3 kPa (VPD; Fig. 1d). Temperatures in the upper soil layer reached  $35^\circ\text{C}$  on soil and root plots (Fig. 1e). No rain events occurred in early April resulting in decreasing volumetric soil water content ( $\theta_s$ ) in the upper soil layers from about  $0.1 \text{ m}^3 \text{m}^{-3}$  to  $0.04 \text{ m}^3 \text{m}^{-3}$  on April 18 (Fig. 1f). The second half of the month was characterized by more volatile weather conditions with rainy and sunny periods, a decrease in maximum temperature and VPD, and higher soil water availability.

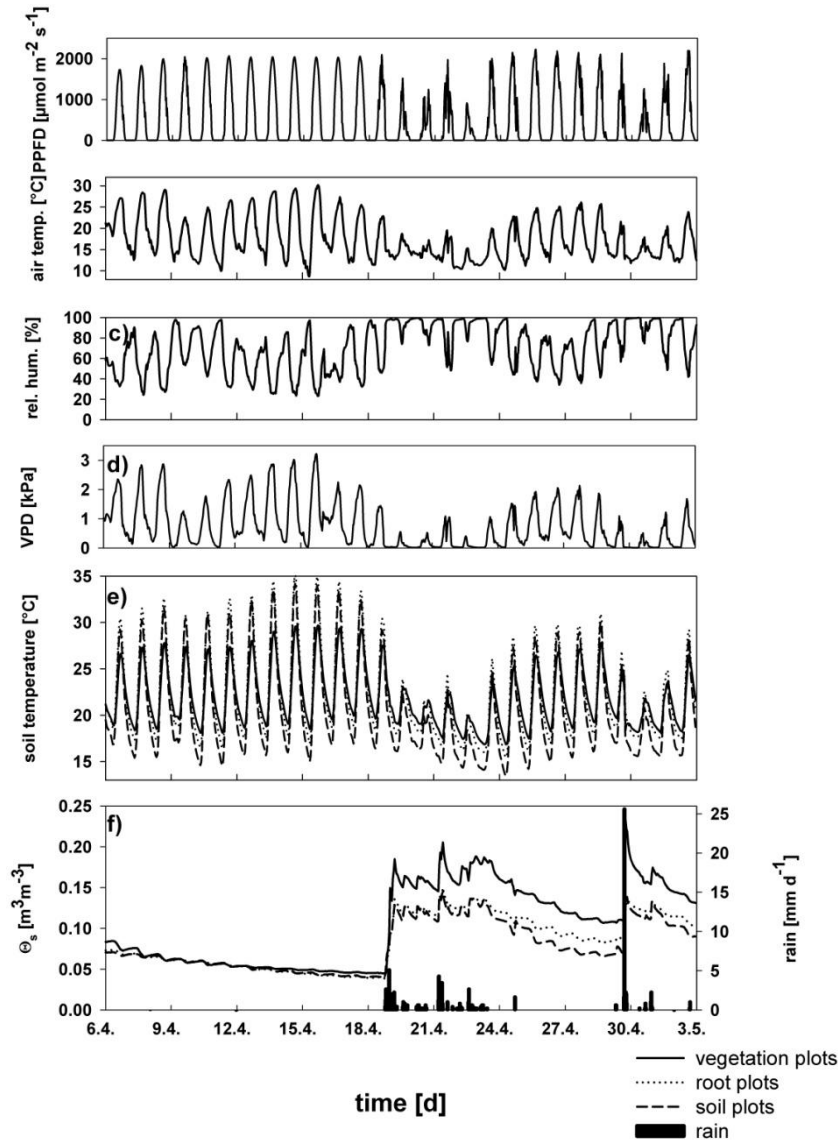


**Figure 1:**

Environmental conditions from April 6 to May 3, 2011. a) Photosynthetic photon flux density (PPFD,  $\mu\text{mol m}^{-2} \text{s}^{-1}$ , black lines), b) air temperature ( $^\circ\text{C}$ , black lines), c) relative humidity (%), d) vapor pressure deficit (VPD, kPa, black lines), e) soil temperature in 5 cm soil depth on vegetation (black lines), roots (black dotted lines) and bare soil plots (black dashed lines), and f) soil volumetric water content in 5 cm soil depth ( $\theta_s$ ,  $\text{m}^3 \text{m}^{-3}$ ) on vegetation (black lines), roots (black dotted lines) and bare soil plots (black dashed lines) as well as rainfall ( $\text{mm d}^{-1}$ , black bars). Black arrows indicate measurement dates (April 8, 12, 18, 26, and May 2, 2011).



### 2.6.2. Profiles of soil temperature, volumetric water content and $\delta^{18}O$

The oxygen isotopic composition in the soil ( $\delta^{18}O_s$ ) differed significantly across the soil depths but was constant between 10 and 40 cm at app. -7‰ (Fig. 2) reflecting rain water isotopic composition during the study period (data not shown). However, we found a strong increase in  $\delta^{18}O_s$  in the top of the soil profile with the most enriched  $\delta^{18}O_s$  values at 0-5 cm soil depth between 4‰ and -3‰. During most of the study period the evaporating front (the depth with the most enriched isotopic signal) was directly at the soil surface. However, with decreasing volumetric soil water content ( $\theta_s$ ) between April 12 and 18, the peak in  $\delta^{18}O$  decreased to around 2 cm soil depth for root and bare soil plots (Fig. 2).

Vegetation cover strongly affected the soil water oxygen isotope profile. The peak in  $\delta^{18}O$  of the soil profile was not as pronounced on vegetation plots compared to soil and root plots (Fig. 2). While the isotope enrichment in  $\delta^{18}O$  in the soil profile varied between ~ -3‰ and 1.5‰ in vegetation plots (Fig. 2a-e) it ranged between 1.5 ‰ and 4 ‰ in root and soil plots (Fig. 2f-o). Furthermore, in the vegetation plots the evaporating front did not move into deeper soil layers with decreasing  $\theta_s$  as in soil and root plots during the study period (Fig. 2).

Volumetric soil water content ( $\theta_s$ ) was rather similar in all soil depths and decreased from nearly 0.1 to 0.04 m<sup>3</sup>m<sup>-3</sup> in the first half of April (Fig. 2). Following rain events in the second half of the month,  $\theta_s$  increased in the upper 10 cm soil (to 0.14 m<sup>3</sup>m<sup>-3</sup>). Soil temperature was also variable between the soil depths. Midday soil temperature was highest in the upper 5 cm of the soil profile (up to 30 °C) and exponentially decreased to minimum values in 60 cm soil depth (around 18 °C). At the soil surface, the midday temperature was between 24 and 26 °C (Fig. 2).

In general, vegetation cover has a strong influence on microclimatic conditions in the soil. Both the maximum soil temperature and the diurnal amplitude of soil and surface temperatures were reduced in plots with vegetation cover (from ~15 °C on bare soil/root plots to ~9 °C on vegetation plots; Fig. 1, 2). During the dry down period in the first half of April, the  $\theta_s$  profile was similar between the three plot types. However, following the rainfall events between April 18 and 24, plots with vegetation cover exhibited higher soil moisture contents in the upper 10 cm than did the other plot types (Fig. 2).

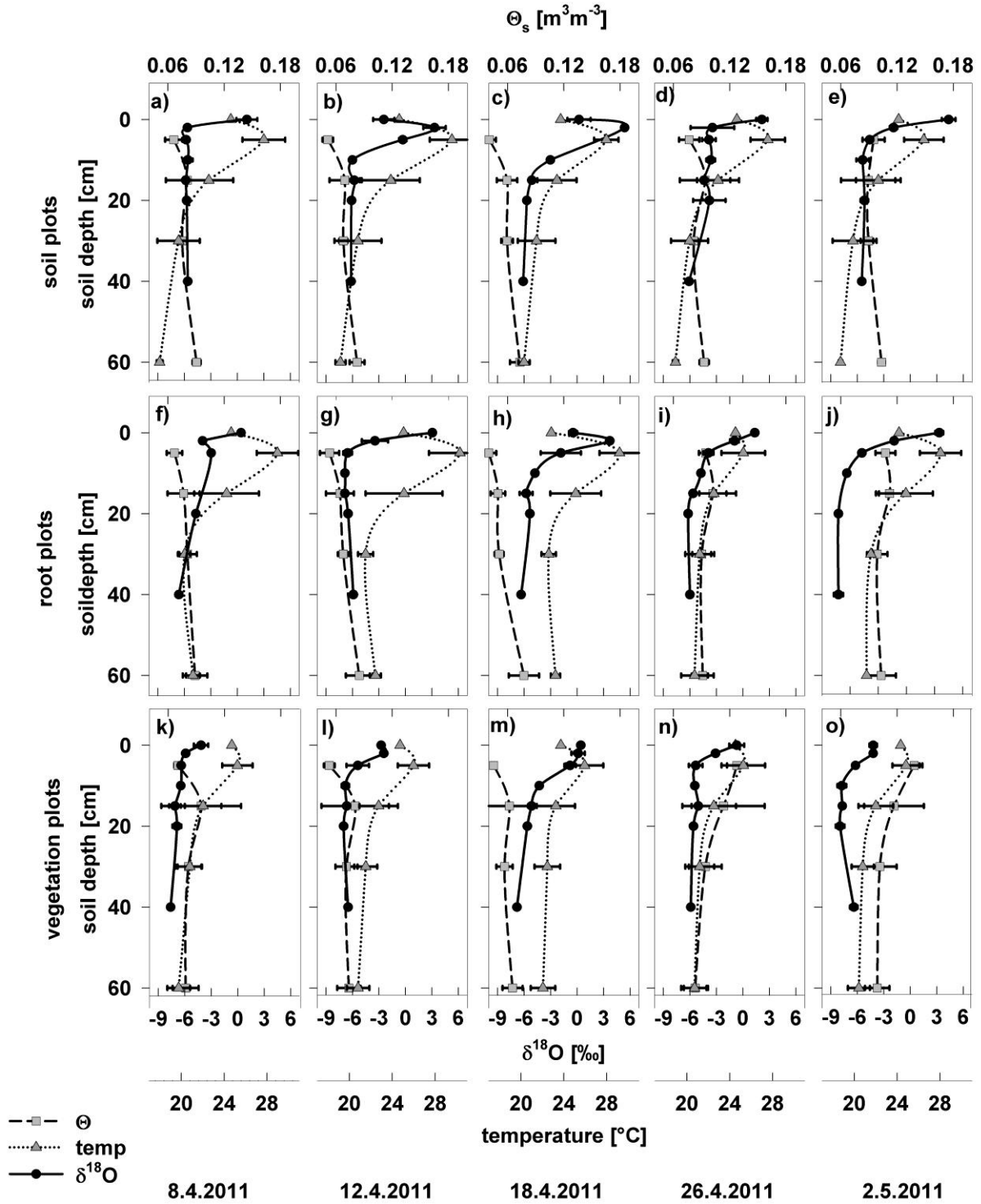


**Figure 2:** Soil profiles of volumetric water content ( $\theta_s$ , dashed black lines and grey squares; mean  $\pm$  SD,  $n=3-4$ ; depths 5, 15, 30, and 60 cm) temperature (dotted black lines and dark grey up triangles; mean  $\pm$  SD,  $n=3-4$ ; depths 0, 5, 15, 30, and 60 cm), and soil  $\delta^{18}\text{O}$  (black solid lines and circles; mean  $\pm$  SD,  $n=3-4$ ; depths 0, 2, 5, 10, 15, 20, and 40 cm) on roots, soil and vegetation plots on 5 days between April 8 and May 2, 2011.

### 2.6.3. Measured and modeled $\delta^{18}O_E$

Measured oxygen isotope signatures of soil evaporation ( $\delta^{18}O_E$ ) ranged from -13.1‰ to -20.1‰ on soil plots (Fig. 3a-e) and from -14.8‰ to -19.9‰ on root plots (Fig. 3f-j) and were thus in all cases strongly depleted in relation to both mean soil  $\delta^{18}O$  (Fig. 2) and rain water  $\delta^{18}O$  which ranged between -6‰ and -8‰. We found strong diurnal courses of  $\delta^{18}O_E$  in both treatments.  $\delta^{18}O_E$  was highest in the morning and evening and decreased by 3.5‰ to 7‰ during the day (Fig. 3b, d, g, i).

We modeled  $\delta^{18}O_E$  based on the Craig and Gordon equation with 3 approaches differing in their input variables all using the fractionation factors of Merlivat (1978; see Table 1). In approach I the isotopic composition and temperature from the evaporating front were used (which is equivalent to the most enriched  $\delta^{18}O$  signal in the soil  $\delta^{18}O$  profile) to calculate  $\alpha^+$  and  $h$  and the formulation of Mathieu and Bariac (1996) for  $\alpha_k$ . Kinetic fractionation  $\alpha_k$  as obtained by this method ranged between 1.021 and 1.022 under relatively wet conditions on May 2 on root and soil plots, respectively, to a maximum of 1.0262 on both root and soil plots under the driest soil conditions on April 18. A different formulation for the kinetic fractionation  $\alpha_k$  was used in approach II with  $nk = 1$  (Barnes and Allison, 1983), thus ignoring the influence of turbulent resistances on diffusion controlled fractionation. Finally, we used mean values of the upper 10 cm for soil temperature and the soil water isotopic composition and the formulation for  $\alpha_k$  of Mathieu and Bariac (1996; approach III).

Approach I nicely reflected measured values (Fig. 3) and remained within the standard deviation of measured  $\delta^{18}O_E$  with few exceptions, i.e. May 2 where measured  $\delta^{18}O_E$  on soil plots was in better agreement with modeled  $\delta^{18}O_E$  using  $nk=1$ , hence approach II. Neglecting the turbulent component in the formulation for the kinetic fractionation  $\alpha_k$  (approach II) led to strong negative offsets from measured  $\delta^{18}O_E$  between 2 to 7‰ (Fig. 3). The magnitude of this offset depended on the soil water content and was stronger in conditions of high soil water content than during lower soil water content (compare the dry April 12 with the wet April 26, Fig. 3b, g, d, and i). Approach III led to a strong negative offset relative to measured  $\delta^{18}O_E$  of up to 15‰ between 14:00 and 19:00 (Fig. 3). Further, using averaged values from the upper 10 cm soil for temperature and soil  $\delta^{18}O$  also strongly overestimated the diurnal amplitude in  $\delta^{18}O_E$ , which reached between 10‰ and 20‰ in approach III.

In contrast, the diurnal amplitude of measured  $\delta^{18}O_E$  was between 5 and 8‰ (Fig. 3).

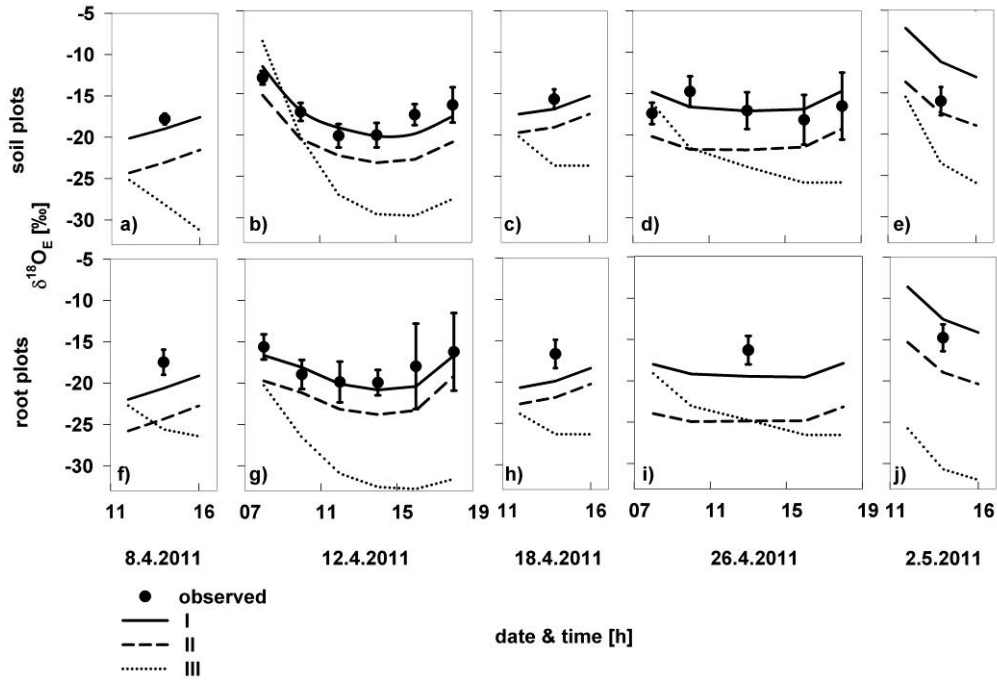


**Figure 3:** Measured  $\delta^{18}O_E$  on root and bare soil plots (black circles) and calculated with the Craig and Gordon equation using approach I (solid black lines), II (long dashed black lines) and III (dotted black lines) according to Table 1. Measured  $\delta^{18}O_E$  are shown as mean values  $\pm$  SD ( $n=3$ ).

Similar results could be observed when calculating  $\delta^{18}O_E$  with parameters taken from an average of the upper 10 cm and  $\alpha_k$  with  $nk=1$  (data not shown), which led to the same slope as in approach III with the same negative offset as between approaches I and II (Fig. 3).

#### 2.6.4. Measured $\delta^{18}O$ of evapotranspiration

Measured  $ET$  in the vegetation plots ranged between  $\sim 0.5 \text{ mmol m}^{-2} \text{ s}^{-1}$  in the morning to  $3.8 \text{ mmol m}^{-2} \text{ s}^{-1}$  during midday. Maximum midday  $ET$  was highest on April 8 and declined until April 18 to  $1.3 \text{ mmol m}^{-2} \text{ s}^{-1}$  (Fig. 4a-c). After the rainfall events between April 18 and 24 maximum midday  $ET$  increased again to around  $2\text{-}3 \text{ mmol m}^{-2} \text{ s}^{-1}$  (Fig. 4d, e). In contrast, soil evaporation, measured on bare soil and root plots never exceeded  $1.9 \text{ mmol m}^{-2} \text{ s}^{-1}$  and was between  $0.4$  and  $0.7$  in first dry half of April and between  $1$  and  $1.9 \text{ mmol m}^{-2} \text{ s}^{-1}$  in the second wetter half of the month (data not shown).

CRDS based measured  $\delta^{18}O_{ET}$  ranged from  $-21.3\text{‰}$  to  $-12.4\text{‰}$  (Fig. 4a-e). In general, measured  $\delta^{18}O_{ET}$

varied strongly within a day with most negative values in the morning (-17.8‰ to -21.3‰).  $\delta^{18}O_{ET}$  increased throughout the day and reached values between -16.6‰ and -12.4‰ in the evening (Fig. 4b and d).

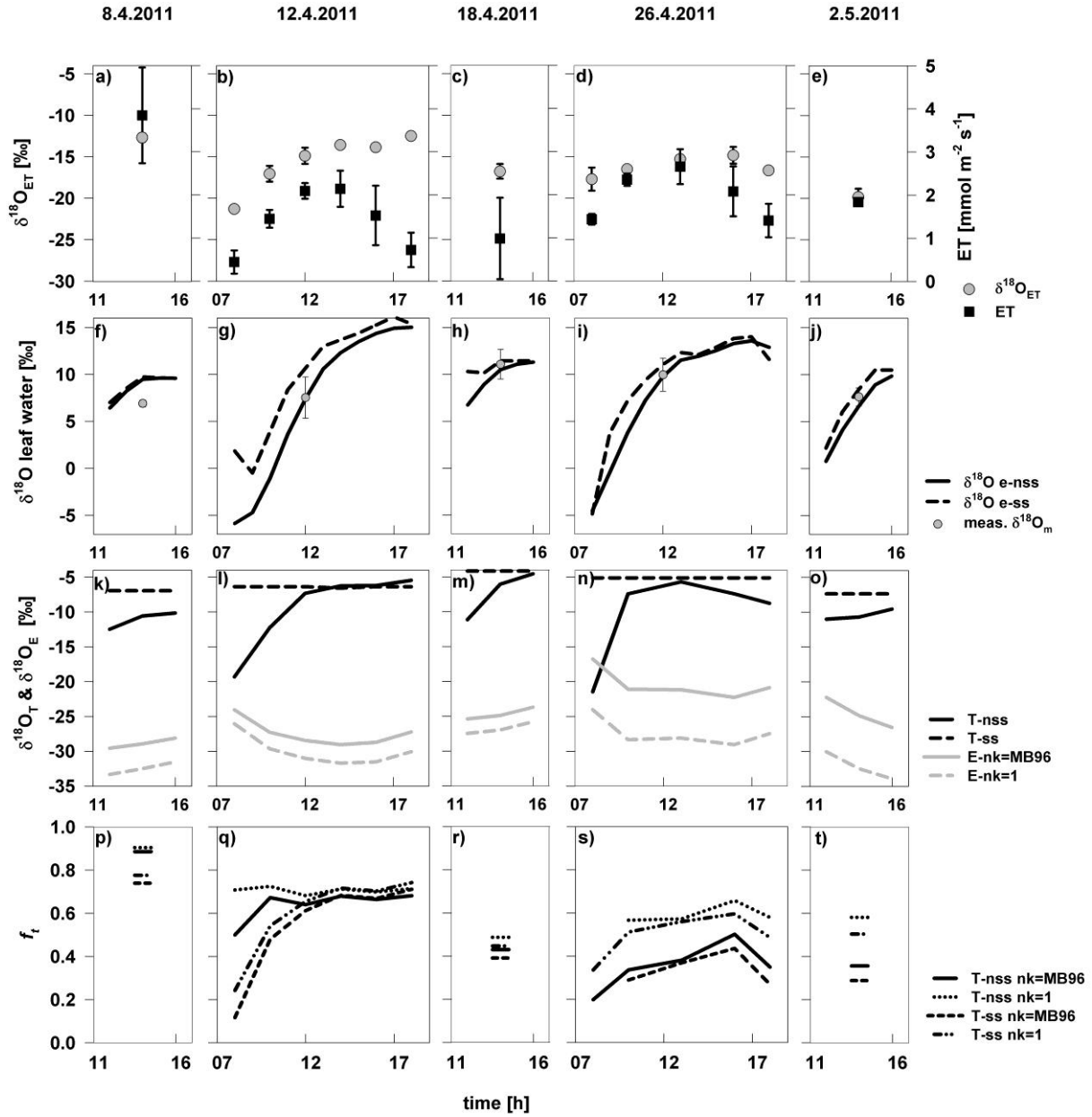


**Figure 4:** a-e) Measured evapotranspiration (ET, black squares) and  $\delta^{18}O_{ET}$  (grey circles, ‰) based on CRDS measurements from April 8 to May 2, 2011 (mean  $\pm$  SD, n = 3). f-j) Modeled isotopic signature of leaf water at the evaporating sites in steady state ( $\delta^{18}O_{e-ss}$ , dashed black lines) and non-steady state ( $\delta^{18}O_{e-nss}$ , solid black lines) and measured  $\delta^{18}O$  of leaf mesophyll water at midday (grey circles, mean values  $\pm$  SD, n=5). k-o) Modeled isotopic composition of leaf transpired water ( $\delta^{18}O_T$ ) in steady-state ( $\delta^{18}O_{T-ss}$ , black dashed lines) and non-steady state ( $\delta^{18}O_{T-nss}$ , black solid lines) and isotopic composition of soil evaporated water  $\delta^{18}O_E$  using different formulations for the kinetic fractionation factor on vegetation plots. p-t) Contribution of plant transpiration to total understory evapotranspiration ( $f_t$ ) using all combinations of  $\delta^{18}O_T$  and  $\delta^{18}O_E$  of k-o). No values for  $f_t$  are displayed if  $f_t < 0$  or  $f_t > 1$ .

#### 2.6.5. Calculating $\delta^{18}O_E$ and $\delta^{18}O_T$ for vegetation plots

The isotopic signature of evapotranspiration ( $ET$ ) consists of and is influenced by soil evaporation ( $E$ ) and plant transpiration ( $T$ ). Knowing these values allows for the prediction of their relative contributions to  $ET$ .

Therefore, we modeled  $\delta^{18}O$  of soil evaporation and understory plant transpiration ( $\delta^{18}O_T$ ) on vegetation plots (Fig. 4k-o). We calculated  $\delta^{18}O_T$  in the non-steady state by modeling the leaf water enrichment at the evaporating sites in non-steady state ( $\delta^{18}O_{e-nss}$ , Fig. 4f-j). Leaf water  $\delta^{18}O_{e-nss}$  was most negative during the early morning (about -5‰) and increased steadily throughout the diurnal course until a plateau was reached around 15:00 (~ 10 to 15‰). In comparison,  $\delta^{18}O$  of leaf water at the evaporating sites assuming steady state transpiration was slightly enriched with the strongest deviation from non-steady state values during the morning (Fig. 4f-j).

Accordingly, transpired  $\delta^{18}O$  in non-steady state was most negative during the morning (~ -20‰) and then increased steadily until steady state was reached in the afternoon. Steady state was reached between 14:00 (April 26, Fig. 4l, i) and 18:00 (April 12, Fig. 4n) where  $\delta^{18}O_T$  matched  $\delta^{18}O$  of source water (~ -6 to -8‰). In comparison, the isotope signature of transpiration assuming steady state ranged around source water values of -6 to -8‰ during the whole day.

$\delta^{18}O$  of soil evaporation ( $\delta^{18}O_E$ ) on vegetation plots was modeled using approach I, which led to the best fit with measured values on root and bare soil plots (see Fig. 3) and approach II for comparison (see Table 1). The calculated isotope signature of soil evaporation on vegetation plots was between -20 and -30‰ and thus depleted by approximately 7‰ relative to  $\delta^{18}O_E$  on soil and roots plots (compare Fig. 3 and 4k-o). This corresponds well with the higher increase of soil  $\delta^{18}O$  at the evaporating front on soil and root plots compared to vegetation plots (Fig. 2). Albeit this strong negative offset  $\delta^{18}O_E$  followed similar diurnal pattern in all three treatments (Fig. 3 and 4k-o). We additionally calculated  $\delta^{18}O_E$  assuming only molecular transport ( $nk = 1$ ). Similar as in root and bare soil plots this led to negative offsets the magnitude of which were dependent on the soil water content (Fig. 1 and 4k-o).

#### 2.6.6. *Calculating the contribution of T to ET*

In order to test the variability in the calculated contribution of  $T$  to  $ET$  ( $ft$ ) that arises due to assumptions on the (non-)steady state of plant transpiration or the nature of transport resistances and the formulation of kinetic fractionation we calculated  $ft$  using  $\delta^{18}O$  of transpiration in the steady state and in the non-steady state and  $\delta^{18}O$  of evaporation by both including and excluding influences of turbulent resistance on kinetic fractionation ( $nk = 1$  and  $nk = \text{Mathieu and Baric, 1996}$ ; Fig. 4p-t).

All four combinations differed strongly in their outcome. Calculating  $ft$  assuming non-steady state transpiration and including turbulent resistance in the estimation of kinetic fractionation led to  $ft$  during the measurement period between 0.8 and 0.2.  $ft$  declined from around 0.8 in the beginning of the study period (April 8 and 12, Fig. 4p, q) to around 0.5 with the onset and after the heavy rain falls between April 18 and 24 (Fig. 4r-t).  $ft$  also varied within a day albeit in smaller magnitude from 0.5-0.7 and 0.2-0.5 on April 12 and 26, respectively (Fig. 4q, s).

The difference between using steady state and non-steady state calculations of transpirational  $\delta^{18}O$  was highest in the morning when steady state transpiration was not yet reached and amounted up to 0.7 (0.8 and 0.1 for  $\delta^{18}O_{T-nss}$  and  $\delta^{18}O_{T-ss}$ , respectively; Fig. 4q and s). Assuming steady state transpiration  $ft$  was far more variable within a day and did not result in values between 0 and 1 on April 26 in the early morning (Fig. 4s).

Moreover, using  $nk = 1$  and  $nk = \text{Mathieu and Baric (1996)}$  showed both similar diurnal fluctuations but differed strongly across the different measurement days. This is caused by the difference between  $\delta^{18}O$  of evaporation calculated by the two formulations of  $nk$ , which gets larger in times of higher soil water content  $\theta_s$  (compare Fig. 4p-r to s-t).

### 2.7. Discussion

#### 2.7.1. $\delta^{18}O_E$ and uncertainties in regard to changes in $\delta^{18}O_e$ , temperature and $\alpha_k$

In general, our results show that modeling the isotopic composition of evaporation ( $\delta^{18}O_E$ ) with the Craig and Gordon equation effectively reproduces the temporal dynamics of  $\delta^{18}O_E$  measured with a laser spectrometer (Fig. 3). However, special care has to be taken concerning the use of key

parameters of the Craig and Gordon equation, namely the spatial resolution of the isotopic composition of the soil profile used to determine the  $\delta^{18}\text{O}$  signal at the evaporating sites ( $\delta^{18}\text{O}_e$ ), the temperature used to normalize  $h$  and to derive  $\alpha^+$ , and the formulation used to estimate the kinetic fractionation factor ( $\alpha_k$ ).

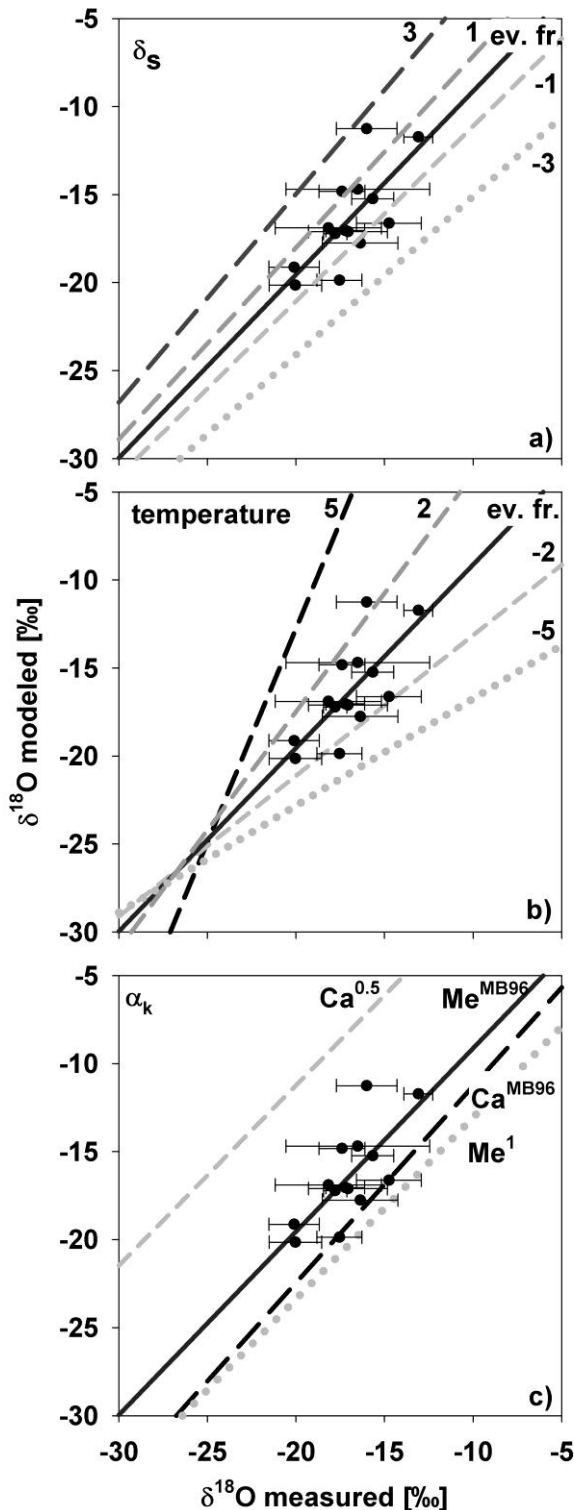


**Figure 5:** Regressions of measured against modeled  $\delta^{18}\text{O}_E$  on soil plots varying a) the oxygen isotope composition of the evaporating surface ( $\delta^{18}\text{O}_e$ ); b) temperature and c) the formulation for  $\alpha_k$ . a)  $\delta^{18}\text{O}_e$  was varied relative to the nominal values at the evaporating front by +1‰ (grey dashed line), +3‰ (dark grey dashed line), -1‰ (light grey dashed line), -3‰ (grey dotted line) and as obtained at the evaporating front (black line). b) temperature (te) was equally varied relative to values obtained at the evaporating front by +2 °C (grey dashed line), +5 °C (black dashed line), -2 °C (light grey dashed line), -5 °C (grey dotted line) and as obtained at the evaporating front (black line). c) In order to test the sensitivity of the modeled  $\delta^{18}\text{O}_E$  in regard to  $\alpha_k$  we obtained  $\delta^{18}\text{O}_E$  by using the formulations for  $\alpha_k$  as follows: diffusivity coefficient of Merlivat et al. (1978) in combination with  $\text{nk}=\text{MB96}$  (black line), in combination with  $\text{nk}=1$  (grey dotted line) and the diffusivity coefficient of Cappa et al. (2003) in combination with  $\text{nk}=\text{MB96}$  (black dashed line) and  $\text{nk}=0.5$  (grey dashed line). Black circles are measured ( $\pm$  SD,  $n = 3$ ) against modeled values with the nominal values of  $\delta^{18}\text{O}_e$  and temperature at the evaporative front and  $\alpha_k = \text{Me78}^{\text{MB96}}$ .



Although soil water  $\delta^{18}\text{O}$  showed little variation below 10 cm soil depth, we have demonstrated that  $\delta^{18}\text{O}_s$  varied considerably in the upper 10 cm of the soil profile. Especially near the evaporating front changes of several ‰ occurred within few mm to cm (Fig. 2; Barnes and Allison, 1983; Braud et al., 2005a), thus imprecise estimations of  $\delta^{18}\text{O}_s$ , hence  $\delta^{18}\text{O}_e$ , will have a huge impact on the estimate of  $\delta^{18}\text{O}_E$  (see Fig. 3). To gain more insight into the required precision for the soil isotope profile for reliable  $\delta^{18}\text{O}_E$  estimations, we calculated  $\delta^{18}\text{O}_E$  varying  $\delta^{18}\text{O}_e$  between +3 and -3‰ from the observed value at the evaporating front (Fig. 5a). A deviation in  $\delta^{18}\text{O}$  of 1‰ relative to  $\delta^{18}\text{O}$  of soil water at the evaporating front leads to rather small offsets relative to measured values of  $\delta^{18}\text{O}_E$  of also about 1‰; however this offset increases non-linearly to 5‰ when  $\delta^{18}\text{O}$  of soil water deviates 3‰ from its observed value (Fig. 5a). A change of 3‰ occurs easily within 1-2 cm of the soil near the evaporating front (Fig. 2). Therefore a deviation of more than 1-2 cm from soil  $\delta^{18}\text{O}$  measured at the evaporating front or averaging over several cm of the soil profile (approach III; Fig. 3) leads to poor agreement with measured  $\delta^{18}\text{O}_E$  (Fig. 5a). This is of special importance in ecosystems with unsaturated surface soil layers. However, precisely estimating the evaporating front remains a challenge in field studies and often isotope data of the soil column is averaged over several cm of the soil column (e.g. Lai et al., 2006; Yepez et al., 2005) or evaporative enrichment at the evaporating front is neglected and isotopic signatures of irrigation water are used instead (e.g. Wang et al., 2010).

Similar to oxygen isotope profiles the temperature also varied considerably in the upper cm of the soil profile (see Fig. 2). Since the soil temperature must be determined at the evaporating front to normalize  $h$  and to derive  $\alpha^+$ , we wanted to quantify the uncertainty in the calculation of  $\delta^{18}\text{O}_E$  arising from soil temperature variations modifying the temperature ( $T_e$ ) between +5 and -5 °C from values obtained at the evaporating front (Fig. 5b). Altering  $T_e$  strongly influenced the comparison of measured versus calculated  $\delta^{18}\text{O}$  of evaporation ( $\delta^{18}\text{O}_E$ ). The typical maximum diurnal temperature measured at the evaporating front was around 24-26 °C with a diurnal temperature amplitude of about 6 °C. A deviation from that temperature by 2 °C in either direction led to an offset in  $\delta^{18}\text{O}_E$  of about 2‰. The variation in temperature also influenced the diurnal amplitude of  $\delta^{18}\text{O}_E$  with higher temperatures leading to small diurnal changes in  $\delta^{18}\text{O}_E$  and lower temperatures leading to stronger alterations in  $\delta^{18}\text{O}_E$  throughout the day (Fig. 5b). Soil temperature was not equal throughout the soil

profile and changes of 2 °C often occurred within the upper 10 cm and soil temperature of the upper 60 cm was about 5 °C lower compared to soil surface temperatures at midday. The air temperature measured at 1.5 m height differed even stronger to soil surface temperature, especially on bare soil plots. Therefore soil temperature measurements need to be done in a very fine scale especially between the soil surface and 10 cm soil depth for a precise estimation of temperature at the evaporating sites.

In previous studies no agreement on the value of the kinetic fractionation factor was found and both published values for the fractionation factor of molecular diffusion are still in use (compare Cappa et al., 2003 and Merlivat, 1978; see also Luz et al., 2009). There is additionally no general solution as how to express the combined influence of different resistances on the apparent kinetic fractionation factor (for a summary see Braud et al., 2005a, b). Stewart et al. (1974) linked the apparent kinetic fractionation factor  $\alpha_k$  with the fractionation of molecular diffusion by an exponential relation:  $\alpha_k = (D_v/D_v^i)^{nk}$  (see Table 1).  $nk$  is then dependent on the nature of the transport and can evolve from  $nk = 0.5$  (turbulent conditions,  $\alpha_k = 1.014$ ) to  $nk = 1$  ( $\alpha_k = 1.0285$ ; pure molecular diffusion; Dongmann et al., 1974). According to Stewart et al. (1974) when the soil is near saturation at the soil surface, transfer processes are atmosphere controlled ( $nk = na = 0.5$ ). With the dry down of the soil surface a vapor diffusion layer evolves and the transfer processes will be increasingly soil controlled ( $nk = ns = 1$ ; Mathieu and Bariac, 1996). Thus  $nk$  values evolve from  $na = 0.5$  up to  $ns = 1$  for soils drying under the influence of a turbulent air flow. Mathieu and Bariac (1996) proposed a formulation for the exponent  $nk$  on the basis of the volumetric soil water content at the soil surface  $\theta_{surf}$  compared to residual  $\theta_{res}$  and saturated  $\theta_{sat}$  that makes the kinetic fractionation factor very plastic with changes in surface volumetric soil water content ( $\theta_{surf}$ , see Table 1). Rothfuss et al. (2012) suggested likewise that under field conditions the kinetic fractionation factor is not constant. However, there is still controversy since kinetic fractionation factors estimated by Rothfuss et al. (2012) as well as Braud et al. (2009a,b) contradict the theory of Mathieu and Bariac (1996) since their obtained kinetic fractionation was near to diffusive conditions (1.0285) under wet soil conditions and near to laminar conditions (1.0189) under dry soil conditions. In our study, the kinetic fractionation factor calculated using the equation by Mathieu and Bariac (1996) ranged from 1.0261 (when the soil was driest at

April 18;  $nk = 0.91$ ) to 1.022 (when soil was wettest at May 2;  $nk = 0.77$ ), suggesting that conditions always ranged between diffusive and laminar. Notably, a retreat of the evaporating front away from the soil surface could only be detected on April 12 (soil plots only) and 18 and the evaporating front never decreased below 2 cm soil depth, which is in agreement with modeling approaches (Braud et al., 2005a, b; Harverd and Cuntz, 2010).

In general it has to be noted that assuming  $\alpha_k$  to vary with the dry down of the soil, which is not common to our knowledge in studies determining the isotopic composition of evaporation for partitioning purposes (e.g. Lai et al., 2006; Yopez et al., 2007), considerably improved the agreement between modeled and measured evaporative  $\delta^{18}\text{O}$  (Fig. 3).  $nk = 1$  leads to a negative offset of about 4‰ in comparison to the better fitting solution of Mathieu and Bariac (1996) on soil and root plots under rather dry soil conditions with soil water contents between 0.04 and 0.1  $\text{m}^3\text{m}^{-3}$  in this study (Fig. 5c). For  $\delta^{18}\text{O}_E$  measured on root plots this offset is not constant but varies around 2-3‰ during times of low soil water content and 5-6‰ after rainfall (data not shown). The different response of the treatment plots on the exclusion of  $nk$  can be explained by the difference in volumetric soil water content over time. Soil plots only slightly differed in  $\theta_{surf}$  before and after rainfall (Fig. 1, 4% increase from April 18 to 26), but the increase in  $\theta_{surf}$  after rainfall was far stronger on root plots (7% increase from April 18 to 26). Consequently, transfer processes were also affected by atmospheric turbulence and molecular diffusion in the soil did not play the sole role. Recently modeling studies address the issue of how to correctly estimate  $\alpha_k$  under changing environmental conditions (Braud et al., 2005a; Harverd and Cuntz, 2010; Harverd et al., 2011; Rothfuss et al., 2012), but no general conclusion could be derived. Despite the overall promising results of modeled  $\delta^{18}\text{O}_E$  obtained using the equation of Mathieu and Bariac (1996) to estimate  $\alpha_k$ , it has to be noted that this formulation did not fit on every single measurement day. On May 2 measured values seemed to be in better agreement with modeled values when assuming diffusive conditions (1.0285) while on root plots on April 26 the agreement was better when assuming laminar conditions (1.0189, data not shown). Further, the values for  $\alpha_k$  derived in this study did not display a very broad range since soil conditions were never near saturation. We would thus strongly urge for more tests regarding the formulation for  $\alpha_k$  under more contrasting soil conditions ranging from saturation to residual soil water content. Finally, it has to be noted that

measured  $\delta^{18}O_E$  might have been influenced by chamber effects. Any gas-exchange chamber needs to be well mixed for a proper estimation of fluxes; however this influences the boundary layer so that chamber conditions might be nearer to turbulent conditions than under natural conditions (at least for small to average wind speeds, see Pape et al., 2009). This influence will be especially large in dense forest ecosystems, which are relatively wind-still, compared to open grasslands as in this study.

Likewise, there is still no agreement on the use of which molecular diffusivity ratio  $D_v/D_v^i$  (see Braud et al., 2005a; Horita et al., 2008; Luz et al., 2009). Both values experimentally determined by Merlivat (1978, 1.0285) and Cappa et al. (2003, 1.032) are still in use in experimental field studies aiming to partition ecosystem water fluxes (Lai et al., 2006; Williams et al., 2004; Yezpez et al., 2007). Recently, Luz et al. (2009) confirmed the value estimated by Merlivat (1978) that deviates from kinetic theory, although the reason for this deviation remains an open question. A test of both values against measured evaporative  $\delta^{18}O$  ( $\delta^{18}O_E$ ) showed that the use of Cappa et al. (2003) produced negative offsets  $\delta^{18}O_E$  of about 2-3‰ compared to measured  $\delta^{18}O_E$  using  $nk$  of Mathieu and Bariac (1996) and even 5‰ using  $nk = 1$  (data not shown). Therefore we additionally assumed pure atmosphere controlled conditions ( $nk = na = 0.5$ ), although this is not realistic in an un-saturated soil as in this study. This led to strong positive offsets of about 8‰ (Fig. 5c). It can thus be concluded that no formulation for  $\alpha_k$  in combination with the diffusivity ratio of Cappa et al. (2003) led to satisfying agreement with measured  $\delta^{18}O_E$ .

### 2.7.2. Modeling $\delta^{18}O_E$ , $\delta^{18}O_e$ and $\delta^{18}O_T$ on vegetation plots

The isotope signature of leaf water at the evaporating sites ( $\delta^{18}O_e$ ) in steady and non-steady state both steadily increased over the diurnal course as was expected (see Cuntz et al., 2007; Farquhar and Cernusak, 2005).  $\delta^{18}O_e$  in the non-steady state is depleted relative to steady state  $\delta^{18}O_e$  by up to 2‰ during large parts of the day especially in the morning hours, which is within the expected range for species with short water turnover times in leaves (Lai et al., 2006; Yezpez et al., 2007).

$\delta^{18}O_e$  in non-steady state was surprisingly similar to measured midday bulk leaf water  $\delta^{18}O$ , which ranged between 7‰ and 11‰ (Fig. 4f-j). Bulk leaf  $\delta^{18}O$  contains a mixed signal of non-fractionated

xylem water and water at the evaporating sites that is highly enriched in  $\delta^{18}\text{O}$  (Cuntz et al., 2007; Gan et al., 2002; Yakir, 1992; Yakir et al., 1994). Therefore measured leaf water should be depleted compared to leaf water at the evaporative sites due to the Péclet effect (Farquhar and Lloyd 1993), which the observations only hint upon. We calculated  $\delta^{18}\text{O}$  of transpiration ( $\delta^{18}O_T$ ) based on non-steady state leaf water enrichment as well as assuming steady state transpiration throughout the day. According to changes in  $\delta^{18}\text{O}$  at the evaporating sites in the non-steady state ( $\delta^{18}O_{e-nss}$ ),  $\delta^{18}O_T$  was rather negative in the morning by -20‰ and increased to source water values throughout the day (Fig. 4k-o), which is in agreement with previous studies (e.g. Yepez et al., 2007).

Modeled  $\delta^{18}\text{O}$  of evaporation ( $\delta^{18}O_E$ ) on vegetation plots was markedly depleted compared to modeled and measured  $\delta^{18}O_E$  on root and soil plots. The amount of this relative depletion corresponded to the difference in evaporative enrichment in soil  $\delta^{18}\text{O}$  at the evaporating front (Fig. 2, compare Fig. 3 and 4k-o), thus the differing microclimatic conditions and profiles of  $\delta^{18}O_s$  on vegetation plots in comparison to soil and root plots had a large influence on  $\delta^{18}O_E$ .

### 2.7.3. Partitioning evapotranspiration

The knowledge of the isotope signatures of evapotranspiration and its components – plant transpiration and soil evaporation – provides the possibility to estimate the relative contribution of T to ET ( $ft$ ; Fig. 4p-t). Previous studies already demonstrated the importance of taking into account the non-steady state of plant transpiration; however the assumption of steady state transpiration can still be found in partitioning studies. Further, it is not common to account for transport resistances other than molecular diffusion ( $nk = 1$ ) let alone possible changes in the kinetic fractionation factor over time due to changes in the nature of transport resistances, i.e. from atmosphere dominated transport in saturated soils to molecular diffusion dominated transport in dry soils. We calculated  $ft$  based on measured  $\delta^{18}O_{ET}$  and modeled  $\delta^{18}\text{O}$  of evaporation and transpiration ( $\delta^{18}O_E$  and  $\delta^{18}O_T$ ) assuming both steady and non-steady state transpiration and including and excluding the effect of turbulent resistance to kinetic fractionation in the calculation of  $\delta^{18}O_E$  to demonstrate the consequences regarding the variability in  $ft$ . All four approaches considerably varied in their outcome.

Measured evapotranspiration ( $ET$ , Fig. 4a-e) was highest in the beginning of the month and declined with the ongoing dry-down period of the soil water content ( $\theta_s$ ). However, with rising  $\theta_s$   $ET$  only slightly increased in the second half of the study period suggesting that  $ET$  was mainly driven by VPD and not  $\theta_s$  during the measurement period (Fig. 1 and 4a-e; see also Cavanaugh et al., 2011). The isotope signature of  $ET$  also slightly decreased throughout the measurement period (Fig. 5a-e). This can either be caused by changing source water isotopic conditions or varying contributions of plant transpiration ( $ft$ ) to total  $ET$ . Source water  $\delta^{18}O$  did not decrease throughout the month and only slightly varied between  $\sim -6$  to  $-8\text{‰}$  with a peak on April 18, suggesting that changes in  $ft$  were the cause of variation during the measurement period.

Previous studies have shown that  $ft$  considerably varies between ecosystems and in time. On an annual basis  $ft$  is mostly within the range of 0.3 to 0.8 (see Cavanaugh et al., 2011; Raz-Yaseef et al., 2012; Williams et al., 2004; Yepez et al., 2003, 2005, 2007; Zhang et al., 2011). Raz-Yaseef et al. (2012) and Cavanaugh et al. (2011) both investigated how the temporal changes in soil moisture distribution due to precipitation influence the  $ET$  partitioning (see also Yepez et al., 2007; Zhang et al., 2011). Both studies concluded that soil evaporation was basically driven by volumetric soil water content ( $\theta_s$ ) in the top soil layer. In contrast, plant transpiration was found to be driven by  $\theta_s$  of the root zone and VPD. If this holds for the investigated understory vegetation in our study, we would expect  $ft$  to be large during the first half of the study period with low top layer  $\theta_s$  but high VPD and to decrease with the onset of the rainfalls in the middle of the month, where VPD was considerably lower but top soil layer  $\theta_s$  increases due to rainfall infiltration (Fig. 1).

Using the exponent  $nk$  of Mathieu and Bariac (1996; see Table 1) to calculate the isotopic composition of evaporation obviously led to the best agreement with our hypothesis on the development of  $ft$  throughout the study period. Calculating  $\delta^{18}O$  of evaporation ( $\delta^{18}O_E$ ) with  $nk$  = Mathieu and Bariac (1996) led to progressive changes in  $ft$  between the periods before and after the rainfalls between April 18 and 25:  $ft$  was initially high (about 0.9) and decreased to 0.4 during midday after the rain events.

A decrease in  $ft$  as observed in this study by assuming non-steady state transpiration and  $nk$  = Mathieu and Bariac (1996) could also be caused by changing vegetation cover (Wang et al., 2010; Yepez et al., 2007). Here the vegetation cover decreased throughout the study period from 87% to 74% vegetation

cover. However, this small decrease in vegetation cover is unlikely to explain such a drastic decrease in  $f_t$  from ~0.9 to 0.4.

When changes in the kinetic fractionation factor during the study period were neglected ( $nk = 1$ )  $f_t$  was more stable ranging between 0.6 and 0.75. However, this approach led to strong offsets of modeled compared to measured  $\delta^{18}O_E$  on both root and soil plots (Fig. 3) and thus we would not recommend to use static values for the kinetic fractionation factor in field studies that deal with broad changes in volumetric soil water content near the soil surface (see also Rothfuss et al., 2012). Different assumptions made on the nature of transport resistances may thus easily lead to strong deviations in  $f_t$  – in this study up to 0.3 (Fig. 4p-t). However, the parameterization of  $nk$  was developed (Mathieu and Bariac, 1996) and tested here on bare soil and root plots. It is still unclear to what extent vegetation cover might change the importance of the different transport resistances to the effective fractionation coefficient  $\alpha_k$ .

Comparisons between modeled transpirational  $\delta^{18}O$  with and without the assumption of non-steady state indicate that the understory vegetation was not at steady state during large parts of the day (Fig. 4k-o). Steady state was reached between approximately 14:00 and 17:00. Accordingly, differences between  $f_t$  based on the assumption of steady versus non-steady state transpiration were rather small during the afternoon. During the rest of the day, especially before 12:00, assuming steady state transpiration led to much stronger diurnal fluctuations and low  $f_t$  before midday. Errors in the estimation of  $f_t$  due to steady state assumptions previously reported in literature are between 9 and 25% (Yepez et al., 2007). Here, we found even larger deviations between  $f_t$  estimated with transpiration in steady versus non-steady state: in the morning deviations between  $f_t$  with the assumption of steady versus non-steady state transpiration were between 0.2 and 0.7 (Fig. 4p-t). Further, it has to be noted that – when assuming steady-state transpiration –  $f_t$  could not be predicted in the early morning of April 26 as it was not within the range of 0-1 (Fig. 4s). After midday, however, agreement between  $f_t$  calculated with and without the assumption of steady state was much better. In conclusion, assuming non-steady state conditions of plant transpiration is important for studies that focus on diurnal measurements as plants did not transpire in steady state over large parts of the day.

## 2.8. Conclusions

In this study we demonstrated that predicting  $\delta^{18}\text{O}$  of evaporation by the Craig and Gordon equation led to good agreement with  $\delta^{18}\text{O}_E$  based on CRDS and gas-exchange measurements under changing environmental conditions in the field. However, special care must be taken concerning key parameters of the Craig and Gordon equation since  $\delta^{18}\text{O}_E$  is sensitive to even small uncertainties in  $\delta^{18}\text{O}$  and temperature at the evaporating sites ( $\delta^{18}\text{O}_e$  and  $T_e$ ) and the kinetic fractionation factor ( $\alpha_k$ ). Our results emphasize the need for thorough characterization of the soil profile isotopic and climatic properties for correct estimations of  $\delta^{18}\text{O}_E$ . We also urge for a better characterization of the formulation of  $\alpha_k$  of soil evaporation and we would not recommend to use static values for the kinetic fractionation factor in field studies that deal with broad changes in volumetric soil water content near the soil surface. Furthermore, we have shown that varying the formulation for kinetic fractionation of soil evaporation or assuming steady state transpiration led to drastic changes in the estimation of  $f_t$  of up to 0.7. To gain a more complete understanding further studies are needed investigating modeled and measured  $\delta^{18}\text{O}_E$  over longer time-scales with even stronger changes in environmental conditions, such as wet springs or autumns compared to summer drought.

## 2.9. Acknowledgements

We thank the Herdade da Machoqueira do Grou and J.S. Pereira for logistical support and allowing the establishment of our field site. We gratefully acknowledge valuable comments of three anonymous referees and help in the field from Alex Mosen and Alexandra Correia. We especially thank Rodrigo Maia and Kathrin Remmert for their help with water extractions and technical assistance in the laboratory and field. Funding for this project was provided by the Deutsche Forschungsgemeinschaft (WATERFLUX Project: # WE 2681; # CU 173/2-1) and the Deutsche Akademische Austausch Dienst.

## 2.10. Literature

Barbour, M.M., 2007. Stable oxygen isotope composition of plant tissue: a review. *Functional Plant Biology*, 34 (2): 83-94.



- Barnes, C.J., Allison, G.B., 1983. The distribution of Deuterium and  $^{18}\text{O}$  in dry soils. *Journal of Hydrology*, 60:141-156.
- Braud, I., Bariac, T., Gaudet, J.-P., and Vauclin, M., 2005a. SiSPAT-Isotope, a coupled heat, water and stable isotope (HDO and (H<sub>2</sub>O)-O-18) transport model for bare soil. Part I. Model description and first verifications. *Journal of Hydrology*, 309: 277-300.
- Braud, I., Bariac, T., Vauclin, M., Boujamlaoui, Z., Gaudet, J.-P., Biron, P., and Richard, P., 2005b. SiSPAT-Isotope, a coupled heat, water and stable isotope (HDO and (H<sub>2</sub>O)-O-18) transport model for bare soil. Part II. Evaluation and sensitivity tests using two laboratory data sets. *Journal of Hydrology*, 309: 301-320.
- Braud, I., Biron, P., Bariac, T., Richard, P., Canale, L., Gaudet, J.P., Vauclin, M., 2009a. Isotopic composition of bare soil evaporated water vapor. Part I: RUBIC IV experimental setup and results. *Journal of Hydrology*, 369(1-2): 1-16.
- Braud, I., Bariac, T., Biron, P., Vauclin, M., 2009b. Isotopic composition of bare soil evaporated water vapor. Part II: Modeling of RUBIC IV experimental results. *Journal of Hydrology*, 369(1-2): 17-29.
- Cappa, C.D., Hendrichs, M.B., DePaolo, D.J., Cohen, R.C., 2003. Isotopic fractionation of water during evaporation. *Journal Geophysical Research*, 108: 4525.
- Cavanaugh, M.L., Kurc, S.A., Scott, R.L., 2011. Evapotranspiration partitioning in semiarid shrubland ecosystems: a two-site evaluation of soil moisture control on transpiration. *Ecohydrology*, 4: 671-681.
- Craig, H., Gordon, L.I., Horbie, Y., 1963. Isotopic exchange effects in evaporation of water. 1. Low-temperature experimental results. *Journal Geophysical Research*, 68: 5079.
- Craig, H. and Gordon, L.I., 1965. Deuterium and oxygen-18 variations in the ocean and the mairitme atmosphere. Paper presented at the Stable Isotopes in Oceanographic Studies and Paleotemperatures, Spoleto, Italy.
- Cuntz, M., Ogee, J., Farquhar, G.D., Peylin, P., and Cernusak, L.A., 2007. Modelling advection and diffusion of water isotopologues in leaves. *Plant, Cell and Environment*, 30 (8): 892-909.
- Dawson, T., 1993. Hydraulic lift and water transport to, through and from roots. *Plant Physiology*, 102: 29.
- Dongmann, G., Nurnberg, H.W., Forstel, H., Wagener, K., 1974. On the enrichment of H<sub>2</sub><sup>18</sup>O in the leaves of transpiring plants. *Radiation and Environmental Biophysics*, 11:41-52.
- Farquhar, G.D, Lloyd, J., 1993. Carbon and oxygen isotope effects in the exchange of carbon dioxide between terrestrial plants and the atmosphere. In: Ehleringer, J.R., Hall, A.E., Farquhar, G.D. (Eds.), *Stable Isotopes and Plant Carbon-Water Relations*. Academic Press, San Diego, pp. 47–70.
- Farquhar, G.D., Cernusak, L.A., 2005. On the isotopic of leaf water in the non-steady state. *Functional Plant Biology*, 32: 293-303.
- Gan, K.S., Wong, S.C., Yong, J.W.H., Farquhar, G.D., 2002.  $^{18}\text{O}$  spatial pattern of vein xylem water, leaf water, and dry matter in cotton leaves. *Plant Physiology*, 130: 100-1021.
- Haverd, V. and Cuntz, M., 2010. Soil-Litter-Iso: A one-dimensional model for coupled transport of heat, water and stable isotopes in soil with a litter layer and root extraction. *Journal of Hydrology*, 388 438-455.
- Haverd, V., Cuntz, M., Griffith, D., Keitel, C., Tados, C., Twining, J., 2011. ; Measured deuterium in water vapour concentration does not improve the constraint on the partitioning of evapotranspiration in a tall forest canopy, as estimated using a soil vegetation atmosphere transfer model. *Agricultural and forest Meteorology*, 151: 645-654.
- Helliker, B.R., Ehleringer, J.R., 2000. Differential O-18 enrichment of leaf cellulose in C-3 versus C-4 grasses. *Functional Plant Biology*, 29: 435-442.

- Horita, J., Rozanski, K., Cohen, S., 2008. Isotope effects in the evaporation of water: a status report of the Craig-Gordon model. *Isotopes in Environmental and Health Studies*, 44: 23-49.
- Kim, K. and Lee, X., 2011. Isotopic enrichment of liquid water during evaporation from water surfaces. *Journal of Hydrology*, 399 364-375.
- Lai, C.T., Ehleringer, J.R., Bond, B.J., and U.K., 2006. Contributions of evaporation, isotopic non-steady state transpiration and atmospheric mixing on the delta O-18 of water vapor in Pacific Northwest coniferous forests. *Plant, Cell and Environment*, 29 (1): 77-94.
- Luz, B., Barkan, E., Yam, R., Shemesh, A., 2009. Fractionation of oxygen and hydrogen isotopes in evaporating water. *Geochimica et Cosmochimica Acta*, 73: 6697-6703.
- Majoube, M., 1971. Oxygen-18 and Deuterium Fractionation between Water and Steam. *Journal of Chemical Physics*, 68 (10): 1423.
- Mathieu, R., Bariac, T., 1996. A numerical model for the simulation of stable isotope profiles in drying soils. *Journal of Geophysical Research*, 101: 12685-12696.
- Merlivat, L., 1978. Molecular Diffusivities of (H<sub>2</sub>O)-O-16 and (H<sub>2</sub>O)-O-18 in Gases. *Journal of Chemical Physics*, 69 (6): 2864-2871.
- Moreno-Gutierrez, C., Dawson, T.E., Nicolas, E., Querejeta, J.I., 2012. Isotopes reveal contrasting water use strategies among coexisting plant species in a Mediterranean ecosystem. *New Phytologist*, 196: 489-496.
- Otieno, D., Mirzaei, H., Hussain, M., Li, Y., Schmidt, M., Wartinger, M., Jung, E., Ribeiro, N., Pereira, J., Tenhunen, J., 2011, Herbaceous layer development during spring does not deplete soil nitrogen in the Portuguese Montado, *Journal of Arid Environments* 75: 231-238
- Pape, L., Ammann, C., Nyfeler-Brunner, A., Spirig, C., Hens, K., and Meixner, F.X., 2009. An automated dynamic chamber system for surface exchange measurement of non-reactive and reactive trace gases of grassland ecosystems. *Biogeosciences*, 6 : 405-429.
- Raz-Yaseef, N., Yakir, D., Schiller, G., Cohen, S., 2012. Dynamics of evapotranspiration partitioning in a semi-arid forest as affected by temporal rainfall pattern. *Agricultural and Forest Meteorology*, 157: 77-85.
- Rothfuss, Y., Biron, P., Braud, I., Canale, L., Durand, J.-L., Gaudet, J.-P., Richard, P., Vauclin, M., and Bariac, T., 2010. Partitioning evapotranspiration fluxes into soil evaporation and plant transpiration using water stable isotopes under controlled conditions. *Hydrological Processes*, 24 3177-3194.
- Rothfuss, Y., Braud, I., LeMoine, N., Biron, P., Durand, J.-L., Vauclin, M., Bariac, T., 2012. Factors controlling the isotopic partitioning between soil evaporation and plant transpiration: Assessment using a multi-objective calibration of SiSPAT-Isotope under controlled conditions. *Journal of Hydrology*, 442:75-88.
- Rozanski, K., Chmura, L., 2006. Isotope effects accompanying evaporation of water from leaky containers. In: *International workshop on the isotope effects in evaporation*, Pisa, Italy, pp. 51-59.
- Stewart, M.K., 1975. Stable isotope fractionation due to evaporation and isotopic exchange of falling waterdrops. Application to atmospheric processes and evaporation of lakes. *Journal of Geophysical Research*, 80: 1133-1146.
- Unger, S., Maguas, C., Pereira, J.S., Aires, L.M., David, T.S., Werner, C., 2010. Disentangling drought-induced variation in ecosystem and soil respiration using stable carbon isotopes. *Oecologia*, 163: 1043-1057.
- Von Caemmerer, S., Farquhar, G.D., 1981. Some relationships between the biochemistry of photosynthesis and the gas-exchange of leaves. *Planta*, 153: 376-387.
- Wang, L.X., Caylor, K.K., Villegas, J.C., Barron-Gafford, G.A., Breshears, D.D., and Huxman, T.E., 2010. Partitioning evapotranspiration across gradients of woody plant cover: Assessment of a

- stable isotope technique. *Geophysical Research Letters*, 37.
- Werner, C., Schnyder, H., Cuntz, M., Keitel, C., Zeeman, M.J., Dawson, T.E., Badeck, F.-W., Brugnoli, E., Ghashghaie, J., Grams, T.E.E., Kayler, Z., Lakatos, M., Lee, X., Maguas, C., Ogee, J., Rascher, K.G., Siegwolf, R., Unger, S., Welker, J., Wingate, L., Gessler, A., 2012. Progress and challenges in using stable isotopes to trace plant carbon and water relations across scales. *Biogeosciences*, 9: 3083-3111.
- Williams, D.G., Cable, W., Hultine, K., Hoedjes, J.C.B., Yepez, E.A., Simonneaux, V., Er-Raki, S., Boulet, G., de Bruin, H.A.R., Chehbouni, A., Hartogensis, O.K., and Timouk, F., 2004. Evapotranspiration components determined by stable isotope, sap flow and eddy-covariance techniques. *Agricultural and Forest Meteorology*, 125 (3-4): 241-258.
- Yakir, D., 1992. Variations in the natural abundance of O-18 and deuterium in plant carbohydrates. *Plant, Cell and Environment*, 15: 1005-1020.
- Yakir, D., Berry, J.A., Giles, L., 1994. Isotopic heterogeneity of water in transpiring leaves – identification of the component that controls the delta-O-18 of atmospheric O-2 and CO2. *Plant, Cell and Environment*, 17: 73-80.
- Yakir, D. and Sternberg, L.D.L., 2000. The use of stable isotopes to study ecosystem gas exchange. *Oecologia*, 123 (3): 297-311.
- Yepez, E.A., Williams, D.G., Scott, R.L., Lin, G., 2003. Partitioning overstory and understory evapotranspiration in a semiarid savanna woodland from isotopic composition of water vapor. *Agricultural and Forest Meteorology*, 119: 53-68.
- Yepez, E.A., Huxman, T.E., Ignace, D.D., English, N.B., Weltzin, J.F., Castellanos, A.E., and Williams, D.G., 2005. Dynamics of transpiration and evaporation following a moisture pulse in semiarid grassland: A chamber-based isotope method for partitioning flux components. *Agricultural and Forest Meteorology*, 132 (3-4): 359-376.
- Yepez, E.A., Scott, R.L., Cable, W.L., and Williams, D.G., 2007. Intraseasonal variation in water and carbon dioxide flux components in a semiarid riparian woodland. *Ecosystems*, 10 (7): 1100-1115.
- Zhang, Y., Shen, Y., Sun, H., Gates, J.B., 2011. Evapotranspiration and its partitioning in an irrigated winter wheat field: A combined isotopic and micrometeorological approach. *Journal of Hydrology*, 40: 203-211.
- Zimmermann, U., Ehhalt, D., Munnich, K.O., 1976. Soil-water movement and evapotranspiration; changes in the isotopic composition of the water. In: *Proc. Symp. Isotopes in Hydrology*, IAEA, Vienna, pp. 567-54.

### 3. STUDY III: INFLUENCE OF WOODY TISSUE AND LEAF CLUMPING ON VERTICALLY RESOLVED LEAF AREA INDEX AND ANGULAR GAP PROBABILITY ESTIMATES

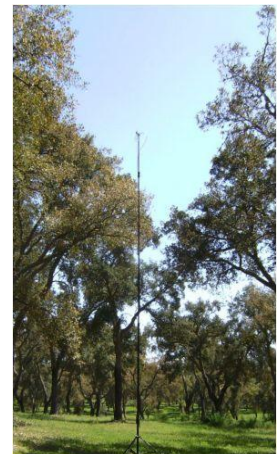
Arndt Piayda<sup>1,✉</sup>; Maren Dubbert<sup>2</sup>; Christiane Werner<sup>2</sup>; Alexandre Vaz Correia<sup>3</sup>; Joao Santos Pereira<sup>3</sup>; and Matthias Cuntz<sup>1</sup>

<sup>1</sup>Department of Computational Hydrosystems, UFZ Helmholtz Centre for Environmental Research, Permoserstr. 15, 04318 Leipzig, Germany

<sup>2</sup>Agroecosystem Research Department, BayCEER Center, University of Bayreuth, Universitätsstr. 30, 95447 Bayreuth, Germany

<sup>3</sup>Department of Forestry, Instituto Superior de Agronomia, Technical University of Lisbon, Tapada da Ajuda, 1349-017 Lisbon, Portugal

✉ corresponding author: Arndt Piayda ([arndt.piayda@ufz.de](mailto:arndt.piayda@ufz.de))



### 3.1. Abstract

Leaf area index  $L$  is a key vegetation parameter that can be used in soil-vegetation-atmosphere exchange modeling. To represent the structure of ecosystems in vertically distributed modeling, vertically resolved  $L$  distributions as well as vertical and angular gap probability  $P_{gap}(\theta)$  distributions are needed, but they are rarely available. On the experimental side, studies often neglect woody plant components when using indirect methods for  $L$  or observations. This can lead to significantly biased results, particularly in semi-arid savannah-type ecosystems with low  $L$  values.

The objective of this study is to compare three non-destructive leaf area index measurement techniques in a sparse savannah-type cork oak canopy in central Portugal in order to derive vertically resolved  $L$  as well as vertically and angularly resolved  $P_{gap}(\theta)$ . We used the established LAI-2000 device as well as fast digital cover photography (DCP), which was vertically and angularly distributed. We applied object-based image analysis to DCP to exclude woody plant components. We compared the results with vertically distributed LAI-2000 measurements and with vertical estimates based on easily measurable crown parameters.

Height and angularly distributed DCP was successfully applied here for the first time. It delivers gap probability and effective leaf area index measurements that are comparable to the established LAI-2000. The height and angularly dependent leaf clumping index  $\Omega$  could be determined with DCP, which led to a 30% higher total leaf area index  $L$  for DCP compared to LAI-2000. The exclusion of woody tissue from DCP yields on average a 6.9% lower leaf area index  $L$ . Including  $\Omega$  and excluding woody tissue, the  $L$  of DCP matched precisely with direct measurements using litter traps. However, the set-up and site-specific adjustment of the image analysis algorithm remains challenging. We propose a special filter for LAI-2000 to enhance data quality when used in open canopies. Finally, if height-dependent observations are not feasible, ground-based observations of crown parameters can be used to derive very reasonable  $L$  height distributions from a single, ground-based  $L$  observation.

### 3.2. Introduction

Leaf area index  $L$  is defined as the one-sided leaf area per unit of ground area (Watson, 1947). It is an important structural parameter of plants, canopies and ecosystems and strongly influences amounts of carbon uptake by photosynthesis (e.g. Bunce, 1989) and transpiration (e.g. Monteith, 1965). It determines the radiative energy absorbed and reflected by the canopy (Monteith, 1959) as well as the maximum capacity of rainfall interception, and thus canopy evaporation (Rutter et al., 1971).

The structural parameter quantifying the amount of light passing through the canopy is the gap probability  $P_{gap}(\theta)$ , which depends on  $L$ , tree density and other stand attributes. It is the probability of a direct beam of radiation passing through the canopy without being intercepted by the foliage (Monsi and Saeki, 1953, 2005). It controls the energy distribution between plant surfaces and the soil surface as well as within the plant (Chen and Black, 1992; Nilson, 1971) and, thus, the ecosystem albedo.

$P_{gap}(\theta)$  and  $L$  are important ecosystem parameters that are needed in soil-vegetation-atmosphere transfer modeling (De Pury and Farquhar, 1997; Sellers and Dorman, 1987; Sinclair et al., 1976) or radiative transfer schemes (Jacquemoud et al., 2000; Haverd et al., 2012). Because recent model development aims for high-resolution multi-layer models (Baldocchi, 1997), the demand for vertically resolved plant or ecosystem parameters such as  $P_{gap}(\theta)$  and  $L$  is increasing. Although vertically distributed observations in tree canopies are challenging (Meir et al., 2000), expensive and often not feasible, several observation approaches have been applied (Beadle et al., 1982; Hutchison et al., 1986; Parker et al., 1989; Strachan and McCaughey, 1996; Wang et al., 1992). Such approaches either required labor-intensive destructive sampling, heavy equipment, and 'above canopy readings' with a tower, or did not take into consideration important factors such as the leaf clumping index  $\Omega$ .

Multiple techniques exist and have been widely used to measure leaf area index  $L$  and gap probability  $P_{gap}(\theta)$ . They can be classified into direct and indirect methods. Direct techniques include destructive sampling or litter traps (Jonckheere et al., 2004) and are not suitable for measuring. In general, they deliver the most precise results but are very labor intensive, and multiple observations during the year are often not feasible. Indirect techniques include the inclined point quadrat method (Warren Wilson, 1960, 1965), the commercially available LAI-2000 plant canopy analyzer (LI-COR, 1992; Cutini

et al., 1998) or digital hemispherical (DHP) and digital cover photography (DCP) (Ryu et al., 2010b; Macfarlane et al., 2007a). DCP offers the advantage of using off-the-shelf digital cameras and providing a minimum of image distortion. Thus, common image analysis software can be used. Indirect techniques deliver  $P_{gap}(\theta)$ ,  $L$  and other structural parameters of the canopy, such as crown cover and porosity (Macfarlane et al., 2007b). They are less labor intensive than direct methods and allow repeat observations throughout the year (Ryu et al., 2012), but they are inferior in accuracy.

Most indirect techniques are based on the observation of and use the gap probability theory by Nilson (1971) to infer  $L$ . Some techniques need additional information about leaf inclination angles  $\alpha$  to convert the projected leaf area observed by the sensors into actual leaf surface (Warren Wilson, 1960). Techniques such as the LAI-2000 instrument (LI-COR, 1992; Miller, 1967) or DCP applied at (Macfarlane et al., 2007b; Pisek et al., 2011; Wit, 1965) circumvent this need. However, DCP applied at angles  $0 < \theta < 90$  comes with a biased mean compared to DHP because a rectangular area is averaged but not a spherical sector. Still, when images represent only a small horizontal view span compared to 360, the bias on mean is small.

Using methods based on the influence of the spatially non-homogeneous distribution of leaves on  $P_{gap}(\theta)$ , expressed as clumping index  $\Omega$ , needs to be considered because the gap probability theory assumes random distributed light intercepting elements (Fassnacht et al., 1994; Nilson, 1971). This greatly influences  $L$  derivation in open, heterogeneous stands such as savannah-type ecosystems. However, estimating the spatial and angular distribution of  $\Omega$  within a plant stand remains challenging (Leblanc et al., 2005; Ryu et al., 2010b).

The contribution of woody tissue (e.g., stems, branches, twigs) to observed gap probability  $P_{gap}(\theta)$ , and thus inferred leaf area index  $L$ , is still an unsolved problem for indirect measurements. It is assumed to introduce substantial biases depending on the ecosystem type  $L$  (Chen et al., 1997a, 1997b; Deblonde et al., 1994; LI-COR, 1992). Commonly, observations during leafless periods are used to estimate wood area index  $W$  and subtract it from  $L$ , which is only feasible in deciduous forests (Deblonde et al., 1994; Ryu et al., 2012) and assumes a random distribution of woody tissue with respect to the position of the leaves. Only a few approaches attempt to quantify this influence (Kucharik et al., 1998) and to our knowledge, it has not yet been included directly in computations.

The aim of the present study is to compare the performance of the established LAI-2000 against the DCP method with respect to leaf clumping effects, methodological biases and the influence of woody tissue. We derive height and angularly dependent gap probability  $P_{gap}(\theta)$  and height dependent leaf area index  $L$  in an open savannah-type woodland. Additionally, we test a ground-based approach to estimate height dependent  $L$  when height distributed measurements are not feasible. We address the following research questions: (1) How do gap probability  $P_{gap}(\theta)$ , leaf area index  $L$  and clumping index  $\Omega$  change with height and view zenith angle? (2) How strong is the influence of non-homogeneity on both methods? (3) How does the image size of DCP influence the accuracy of gap probability  $P_{gap}(\theta)$  and leaf area index  $L$  observations? (4) How strong is the influence of woody tissue on gap probability  $P_{gap}(\theta)$  and leaf area index  $L$ ? (5) How well can we derive height distributed leaf area index  $L$  with only ground-based observations?

### 3.3. Materials and methods

#### 3.3.1. Theory

##### 3.3.1.1. Gap probability theory

Beer's law for absorption of light by particles (Bouguer, 1729; Beer, 1852) is used to relate leaf area index  $L$  to the gap probability  $P_{gap}(\theta)$  of the canopy (Nilson, 1971):

$$P_{gap}(\theta) = \exp\left(\frac{-G(\theta) L \Omega(\theta)}{\cos(\theta)}\right) \quad (1)$$

where  $P_{gap}(\theta)$  is the gap probability of the canopy,  $G(\theta)$  is the leaf projection function,  $L$  [ $\text{m}^2\text{leaf}/\text{m}^2\text{ground}$ ] is the leaf area index (sometimes referred to as  $L_t$ ),  $\Omega(\theta)$  is the clumping index, and  $\theta$  [ $^\circ$ ] is the view zenith angle. In fact,  $L$  refers to foliage area index if it has not been corrected for the influence of wooden tissue on  $P_{gap}(\theta)$ . By dividing through  $\cos(\theta)$  leaf area index is normalized to unity path length independent of the incidence angle.  $G(\theta)$  was introduced in Eq. (1) by Monsi and Saeki (1953) to transform the projection of leaf area perpendicular to the view direction into actual



leaf area index. The shape of  $G(\theta)$  is dependent on the distribution of leaf angles  $f(\alpha)$ . Wilson (1960, 1967) gave the solution as:

$$G(\theta) = \int_0^{\frac{\pi}{2}} \phi(\theta, \alpha) f(\alpha) d\alpha \quad (2)$$

with

$$\phi(\theta, \alpha) = \begin{cases} \cos(\theta) \cos(\alpha) & \text{for } \alpha \leq \theta \\ \cos(\theta) \cos(\alpha) \left[ 1 + \left( \frac{2}{\pi} \right) (\tan(\theta) - \theta) \right] & \text{otherwise} \end{cases} \quad (3)$$

where  $\vartheta = \cos^{-1}(\cos(\theta) \cos(\alpha))$ .  $\alpha$  [ $^\circ$ ] is the angle of the leaf's normal to the zenith.  $\phi(\theta, \alpha)$  results from the scalar product of both, the directional vector of the view direction and the directional vector of the leaf's normal. It is integrated over the azimuth angle assuming the same distribution of leaf inclination over the entire azimuthal range. While Wilson (1967) assumes a uniform distribution of leaf angles  $f(\alpha)$ , Goel and Strebel (1984) proposed a Beta-distribution with two parameters, to represent leaf inclinations of real plants.

The original formulation of Beer's law assumes random distribution of light intercepting elements in the pathway of penetrating beams. Since leaf elements in natural canopies are seldom randomly distributed but clumped into crowns, Nilson (1971) introduced the clumping index  $\Omega(\theta)$  in Eq. (1). It distributes leaf area index from within crowns upon the entire canopy or region of measurement and is unity for randomly distributed leaf elements and decreases with increasing clumping.

### 3.3.1.2. LAI-2000

The internal software of the LAI-2000 as well as the FV2200 windows-software (LI-COR Biosciences, Inc., 2010) for post processing calculates gap probability  $P_{gap}(\theta)$  for each reading from the ratio of above canopy light intensity A and below canopy light intensity B. This is used to calculate the contact frequency  $K(\theta)$  for each view zenith angle  $\theta$  of the instrument following Miller (1967, 1986):

$$K(\theta) = -\ln(P_{gap}(\theta)) \cos(\theta) = G(\theta)L_e \quad (4)$$

$K(\theta)$  arises from the inclined point quadrat method (Wilson, 1959, 1960) and is averaged over all readings for each angle to  $\overline{K(\theta)}$  within each measurement. Since the clumping index  $\Omega(\theta)$  is unknown here, only effective leaf area index  $L_e$  can be described by Eq. (4) underestimating actual leaf area index  $L$ . By the instrument software, the average gap probability  $\overline{P_{gap}(\theta)}$  is reversely calculated via:

$$\overline{P_{gap}(\theta)} = \exp\left(\frac{-\overline{K(\theta)}}{\cos(\theta)}\right) \quad (5)$$

according to Eq. (4). Miller (1967) derived a solution to determine  $L_e$  directly from  $\overline{K(\theta)}$  without knowledge of  $G(\theta)$  under the condition that measurements of  $\overline{K(\theta)}$  exist for different angles  $\theta$  as:

$$L_e \int_0^{\frac{\pi}{2}} G(\theta) \sin(\theta) d\theta = \int_0^{\frac{\pi}{2}} \overline{K(\theta)} \sin(\theta) d\theta \quad (6)$$

and since  $\int_0^{\frac{\pi}{2}} G(\theta) \sin(\theta) d\theta = 0.5 \quad \forall \mu, \nu \in \mathfrak{R}_+ \setminus \{0\}$  of the leaf angle distribution function  $f(\alpha)$ , Eq. (6) reduces to:

$$L_e = 2 \int_0^{\frac{\pi}{2}} \overline{K(\theta)} \sin(\theta) d\theta \quad (7)$$

Recently, Ryu et al. (2010a) reported on the effects of averaging  $K(\theta)$  instead of  $P_{gap}(\theta)$  in Eq. (4) on the estimation of  $L_e$  by the LAI-2000 instrument software which introduces an apparent clumping effect, partially compensating the unknown clumping index  $\Omega(\theta)$  of Eq. (4). Therefore, the correct averaging method (averaging  $P_{gap}$  instead of  $K(\theta)$ ) as well as the standard instrument software averaging is applied throughout this work to compare the influence of apparent clumping of leaves on leaf area index estimation. With the correct averaging method,  $\overline{P_{gap}(\theta)}$  is calculated directly from readings and Eq. (7) leads to effective leaf area index  $L_e$  assuming random distributed leaf elements making Eq. (5) obsolete.

### 3.3.1.3. Digital cover photography

The whole image must be separated in areas of gaps and plant tissue by some algorithm. If only the total number of pixels within gaps is known, the assumption must be made to face random distributed leaf elements resulting in effective leaf area index  $L_e$  (Macfarlane et al., 2007a,b):

$$L_e = \frac{-\ln\left(\frac{\overline{gt}}{A}\right)\cos(\theta)}{G(\theta)} \quad (8)$$

Where  $\overline{gt}$  [pxl] is the number of pixels in all gaps average over all images and  $A$  [pxl] is the total number of pixels in each image file that  $P_{gap} = \overline{gt} / A$ . DCP offers the advantage to determine different gaps in the canopy separately, i.e. between crowns as well as gaps within crowns. Therefore, the clumping of leaf elements into crowns can be considered explicitly when calculating leaf area index  $L$ :

$$L = \frac{-\left(1 - \frac{\overline{gl}}{A}\right)\ln\left(\frac{\overline{gt}-\overline{gl}}{A-\overline{gl}}\right)\cos(\theta)}{G(\theta)} \quad (9)$$

where  $\overline{gl}$  [pxl] is the average number of pixels in the largest gap on the image which is normally, but not always, the gap between adjacent crowns. The expression  $(\overline{gt} - \overline{gl}) / (A - \overline{gl})$  calculates the gap probability within the crown envelopes. Since this gap probability is only valid within crowns, it needs to be scaled to total canopy according to the ratio of the crowns envelope to whole image area by  $1 - \overline{gl} / A$  following Leblanc (2002).  $\overline{gl}$ ,  $\overline{gt}$  and  $A$  should further be understood as angularly dependent in this work, since the DCP method is applied for different angles. Hence, leaf area index  $L$  and effective leaf area index  $L_e$  can be calculated from observations at any  $\theta$  since  $G(\theta)$  is known.

The clumping index  $\Omega(\theta) = L_e / L$  mentioned in section 2.1.1 can be directly estimated via (Leblanc, 2002):

$$\Omega(\theta) = \frac{\ln\left(\frac{\bar{gl}}{\bar{A}}\right)}{\ln\left(\frac{\bar{gl}-\underline{gl}}{\bar{A}-\underline{gl}}\right)} \left( \frac{1}{1 - \frac{\bar{gl}}{\bar{A}}} \right) \quad (10)$$

Additionally, the prior averaging of gap fractions avoids undefined leaf area index  $L$  and clumping index  $\Omega(\theta)$  from images showing solely sky and prevents data loss.

### 3.3.2. Site description

The study was conducted in a Portuguese savannah-type cork-oak forest located ca. 100 km north-east of Lisbon (39°8 0 20.7 00 N, 8°20 0 3.0 00 W, 162 m above mean sea level) which is part of the European integrated carbon observation system ICOS. The only tree species on the site is the evergreen *Quercus suber* (L.) with a tree density of 209 ha<sup>-1</sup>. The understory vegetation consists of annual grasses and herbs that undergo annual die back at the onset of summer drought (Dubbart et al., 2013). The site is managed by local farmers for the purpose of cork and cattle production.

### 3.3.3. Sampling design and measurements

In August 2011 a 100 m × 100 m regular transect grid close to the Eddy-covariance flux tower was established under consideration of a semivariogram analysis of previous, ground-based leaf area index measurement with DCP (Fig.1). On each point of the grid, a large but lightweight tripod of 8.5 m maximum height was set up and equipped with a LAI-2000 plant canopy analyser sensor head (LI-COR Biosciences Inc., Lincoln, NE, USA) operated in remote below mode connected to the control unit on the ground. At 3, 4, 5, 6, 7, 8, and 8.5 m height a sequence of 5 replicates were measured considering all 5 rings of the sensor head (view zenith angle  $\theta = 7^\circ, 23^\circ, 38^\circ, 53^\circ, 68^\circ$ , respectively), each enclosing a view angle span  $\theta_v$  of  $10^\circ$  to  $13^\circ$ . Simultaneously on the nearby Eddy-covariance flux tower, a second plant canopy analyser was operated in remote above mode with an automatic logging interval of 15 s. Both sensor heads were equipped with  $180^\circ$  view caps, calibrated against each other and aligned in the same azimuthal direction. All LAI-2000 measurements were conducted during dusk and dawn to avoid direct sunlight conditions. After the measurement both control units

were connected for data exchange.

During daylight conditions, the tripod was equipped with a Canon PowerShot D10 digital camera (Canon Inc., Tokyo, Japan) mounted on a tiltable rack that can be inclined to zenith view angles  $\theta = 0^\circ, 10^\circ, 23^\circ, 38^\circ, 53^\circ, 68^\circ, 71^\circ$ , and  $90^\circ$  by a bowden cable and is triggered by a custom built remote control. Images facing in one azimuthal direction were taken at each height mentioned before. The camera has a 1/2.3 inch (ca.  $6.16 \times 4.62$  mm) CCD sensor and a focal length of 6.2 mm enclosing a horizontal and vertical view angle span  $\theta_v$  of  $53^\circ$  and  $41^\circ$ , respectively. It was set to the maximum resolution of  $4000 \times 3000$  pixel, fine compression ratio, automatic exposure and no zoom.

On 105 trees the height of the crown top  $ht$  and crown bottom  $hb$  were determined from the ground using a digital hypsometer (Forestor Vertex, Hagl'of Sweden). The crown radius  $rc$  was measured with a measuring tape in  $0^\circ, 90^\circ, 180^\circ$  and  $270^\circ$  azimuthal direction and averaged for each tree.

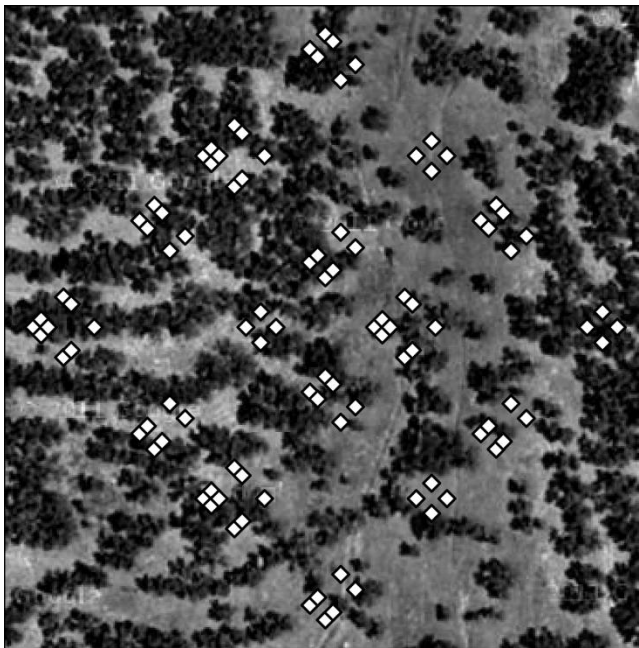


**Figure 1:** Rectangular transect grid (white squares) with 100 observation points of  $100 \times 100$  m extend. Background: aerial photograph of study site in central Portugal with *Q. suber* trees (Google, 2013).

### 3.3.4. Data processing and analysis

#### 3.3.4.1. LAI-2000 and DCP

The readings of the LAI-2000 device were treated with the original and the correct averaging method according to Section 2.1.2 for each height. Standard errors were estimated using bootstrap.

The digital cover images were analysed in original size representing a vertical view angle span  $\theta_v$  of

41 ° and cropped sizes representing  $\theta_v$  spans of 20.5°, 10.25° and 5.625°. The separation in gap, leaf and trunk area in the image was done by object-based image analysis using the eCognition software (Trimble Germany GmbH). The images were segmented using multiresolution segmentation with step- wise increased object sizes (Trimble, 2012). Gaps were classified by thresholds on object averages of brightness  $\overline{\text{bri}}$  , blue difference  $\overline{\text{bd}}$  and blue ratio  $\overline{\text{br}}$  (defined in Appendix B). The differences between neighbouring objects were used to strengthen the discriminatory power on the edges of gap areas (Appendix B). Image objects were classified as wooden tissue by thresholds based on shape features as well as  $rgb$  sum  $\sum \overline{\text{RGB}}$  and green ratio  $\overline{\text{gr}}$  (Appendix B). Objects are only classified as wooden tissue when they did not obscure - or been obscured by - leaves (Kucharik et al., 1998) using the relative amount of gap objects in a certain radius around the object as threshold.

The number of pixels in gaps between crowns  $gl$  and the number of pixels in all gaps  $gt$  were averaged using bootstrap and used according to Section 2.1.3 for each height. The 90° view zenith angle images were used to determine leaf angle distribution  $f(\alpha)$  and leaf projection function  $G(\theta)$  utilizing the open source image processing package Fiji (Schindelin et al., 2012) measuring the angle of leaves whose lamina is aligned perpendicular to the view direction (Ryu et al., 2010b).

#### 3.3.4.2. Auxiliary data

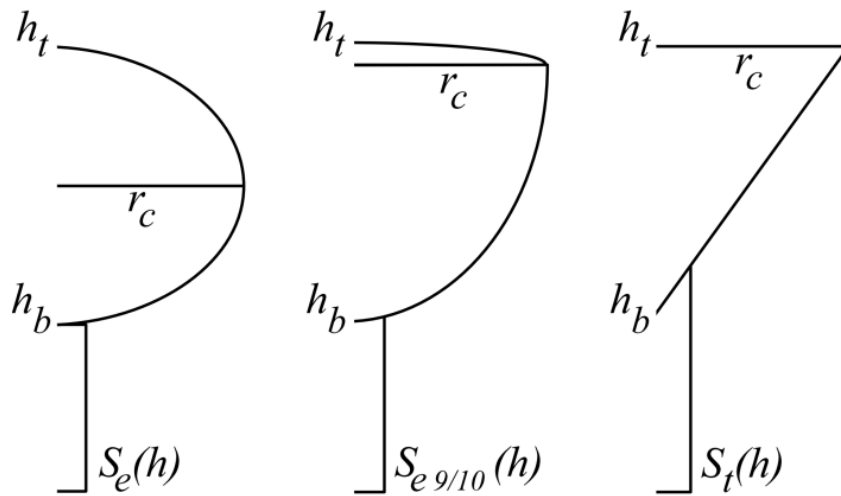


**Figure 2:** Sketches of crown models: ellipsoidal  $S_e(h)$ , asymmetric ellipsoidal  $S_{e9/10}(h)$  and triangular model  $S_t(h)$ .  $h_t$  = crown top height,  $h_b$  = crown bottom height,  $r_c$  = crown radius.

To infer the height distribution of leaf area index  $L$  from purely ground-based observations, each set of crown top height  $ht$ , crown bottom height  $hb$  and crown radius  $rc$  observations were used to set up a crown shape model representation. All representations of a certain crown shape model were averaged using bootstrap, normalized to unity and multiplied by leaf area index  $L$  of 3 m height. This was done for a symmetric ellipsoid crown shape model  $Se(h)$ , asymmetric ellipsoid crown shape model  $Se_{9/10}(h)$  and triangular crown shape model  $St(h)$  illustrated in Fig. 2.  $h$  [m] is height above ground,  $rc$  [m] is the horizontal semiaxis and  $(ht - hb)/2$  [m] is the vertical semiaxis of the crown. The asymmetric crown shape model  $Se_{9/10}(h)$  (ellipse centre at 9/10th of ellipse height) is estimated on the site to be the most representative crown shape. Additionally, the ellipsoidal  $Se(h)$  and triangular  $St(h)$  crown shape model were used to estimate the influence of the model shape on  $L$  height distribution. For each model, the leaf density is assumed to be uniform over the entire height range.

### 3.4. Results and discussion

In this section, an improvement of the LAI-2000 readings treatment is proposed and observed gap fraction distributions  $P_{gap}(\theta)$  of LAI-2000 and DCP are compared. Accordingly, the leaf projection function  $G(\Theta)$  as well as the angular leaf clumping dependency  $\Omega(\Theta)$  are discussed with regard to leaf area index calculations. Then, the observed effective leaf area index  $Le$  and the leaf area index  $L$  are compared for both methods. The influence of view the angle span on DCP uncertainty is shown and the bias on  $L$  due to the influence of woody foliage is quantified. Finally, a purely ground-based approach for estimating  $L$  height distribution is proposed.

#### 3.4.1. LAI-2000 bad readings handling

The LAI-2000 device measures light intensity above and below the canopy to infer gap probability  $P_{gap}(\theta)$ . By default, the instrument software ignores transmittance readings, where at least one of the rings of the below canopy light intensity readings  $B$  returns a higher value than the respective above canopy light intensity reading  $A$  resulting in  $P_{gap}(\theta)$  values  $> 1$ . It is assumed that these values are

caused by operational errors, which is reasonable in canopies with higher leaf area index  $L$  (LI-COR, 1992). However, this introduces a large negative bias when used in open canopies since light attenuation is generally small, A and B reading differences are small and normal measurement variations can lead to  $P_{gap}(\theta) > 1$ . This appears in about 50% of observations made for this work.

Inspecting the distribution of angularly averaged  $P_{gap}(\theta) > 1$ , the majority does not exceed 10% deviation (Fig. 3). Only few, distinct values apart from the main distribution exceed 10% deviation, indicating multiple  $P_{gap}(\theta)$  values larger than unity due to operational errors. This can only be observed when plotting the angularly averaged  $P_{gap}$  instead of gap fractions from all rings individually, since the magnitude of deviation depends on the view angle and multiple deviation distributions superpose each other making an error detection impossible.  $\overline{P_{gap}(\theta)}$  values larger than 10% deviation were excluded from further calculations employing a median absolute difference filter (MAD) based on 2.5 standard deviations. The retained  $P_{gap}(\theta)$  values were set to unity. The amount of bad readings could thus be reduced from 50% to 3% and by setting  $P_{gap}(\theta)$  with deviations below 10% to unity instead of excluding them from calculation, resulting  $L$  is reduced by 26% at 3 m height to 63% at 8.5 m height, respectively.  $P_{gap}(\theta)$  and effective leaf area index  $L_e$  are then very comparable to DCP (Fig. 4, 7a), which is not subject to this source of error. Hence, this bad readings handling is considered to be appropriate to deal with the occurrence of large gaps in the canopy and is used in the further analysis.



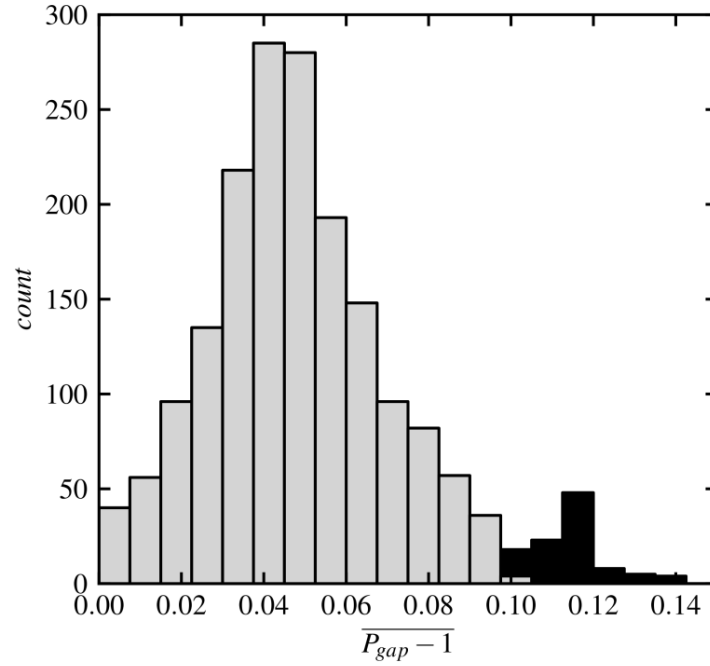


**Figure 3:** Histogram of angular averaged transmittance deviations from unity  $P_{gap} - 1$ . Light grey: values set to 1 and kept for further analysis. Black: considered operational errors and excluded from further analysis with MAD filter based on 2.5 standard deviations.

### 3.4.2. Gap probability distribution

The height and angularly dependent gap probability  $P_{gap}(\theta)$  was measured with the LAI-2000 and DCP, which is further used to calculate leaf area index  $L$ . At 3 m height,  $P_{gap}(\theta)$  is nearly identical at all observed angles  $\theta$  using both methods (Fig. 4), with a maximum difference of 6.5%. For all other heights, the differences do not exceed 10.6% (data not shown for the sake of clarity). In general, differences may be caused by occasionally falling below the minimum distance from the sensors to the leaves defined in Lang (1986); LI-COR (1992, App. F). This is much more likely while measuring within tree crowns than below the canopy. However, both methods follow the same behaviour of increasing  $P_{gap}(\theta)$  with increasing height above ground  $h$  and decreasing  $P_{gap}(\theta)$  with increasing view zenith angle  $\theta$ . DCP shows a more consistent picture for the height and angular dependence. The standard error of LAI-2000 is smaller than that of DCP since each LAI-2000 measurement integrates over a larger azimuthal angle range (see section 3.6). The good agreement of both methods proves the reasonable handling of bad readings of section 3.1. LAI-2000  $P_{gap}(\theta)$  calculated with the standard software, excluding all readings with  $P_{gap}(\theta) > 1$ , leads to up to 29.2% lower gap probabilities, never

reaching values larger than 0.72, even at the highest height.

The outer most rings of the LAI-2000 sensor head are reported to be significant sources of error due to the contamination of scattered light (Kobayashi et al., 2013; Comeau et al., 2006; Stenberg et al., 1994; Comeau et al., 1998; LI-COR, 1992) leading to an artificially higher  $P_{gap}$ . Compared to DCP, which is not subject to contamination, this effect cannot be observed here. In fact, LAI-2000  $P_{gap}(\theta)$  is rather lower than DCP  $P_{gap}(\theta)$ . Hence, to infer effective leaf area index  $L_e$  and leaf area index  $L$  for the LAI-2000 method, all rings are considered in this work.

Beer's law calculates effective leaf area index  $L_e$  and leaf area index  $L$  from  $P_{gap}(\theta)$  observations (Eq. (1)). When the clumping index  $\Omega(\theta)$  is incorporated in the calculation, the influence of a non-homogeneous leaf distribution can be considered (Nilson, 1971) in DCP. Beer's law is plotted in Fig. 4 with the effective leaf area index  $L_e$  neglecting the non-homogeneous leaf distribution and with a fit to the angular dependent clumping index  $\Omega(\theta)$  of Fig. 6 (see section 3.4). Under consideration of angularly dependent leaf clumping, angular dependence of Beer's law is improved, following closer the measured angularly dependent gap probability  $P_{gap}(\theta)$ . Hence, the derivation of  $L$  from  $P_{gap}(\theta)$  is improved, in particular for higher view zenith angles  $\theta$ . This is of great importance for DCP, when observations of leaf angle  $\alpha$  are missing and  $L$  is derived from  $P_{gap}(\theta = 57.3^\circ)$  (see section 3.3). Clumping is taken into consideration for the calculation of  $L$  from  $P_{gap}(\theta)$  in the further analysis as shown in section 3.4.

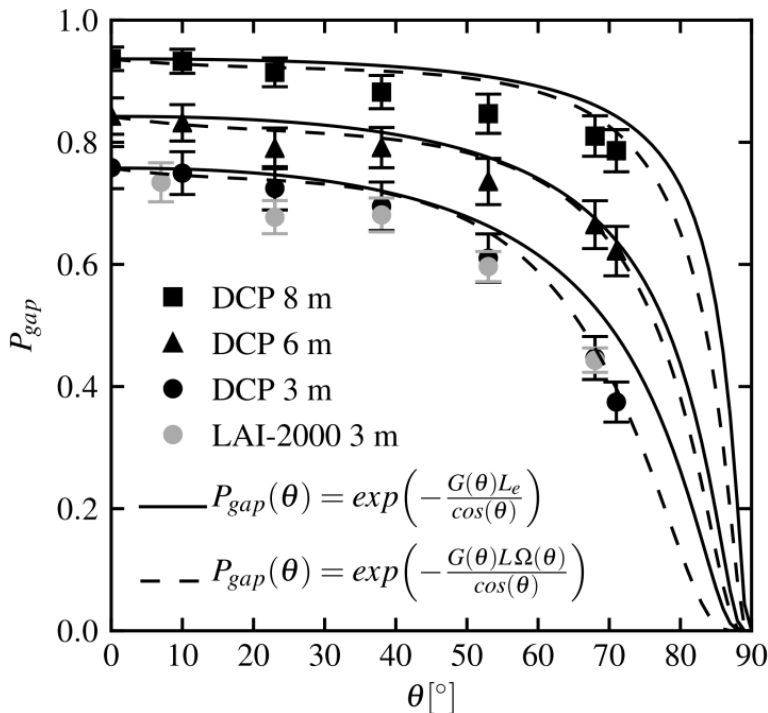


**Figure 4:** Dependency of gap probability  $P_{gap}$  on zenith view angle  $\theta$ . Black symbols: DCP method at 3, 6 and 8 m height. Grey symbols: LAI-2000 method at 3 m height (6 and 8 m heights not shown). Solid lines: Beer's law with effective leaf area index  $L_e$ . Dashed lines: Beer's law with angular dependent leaf clumping  $\Omega(\theta)$  of Fig. 6.

### 3.4.3. Leaf projection function

The calculation of leaf area index  $L$  from gap probability  $P_{gap}(\theta)$  requires information on the leaf projection function  $G(\theta)$  and, therefore, on leaf inclination angle distribution  $f(\alpha)$  (Eq. 1 and 2). To incorporate the empirical distribution of leaf angles into  $G(\theta)$  calculation, a non-parametric kernel smooth (Härdle and Müller, 1997), considered as the best approximation of the empirical distribution, and the two-parameter Beta-distribution of section 2.1.1 is used. The distributions are normalized to unity and plotted over  $\alpha/90^\circ$  in 5a. Both distributions lead to similar leaf projection functions  $G(\theta)$  with comparable, narrow uncertainty bands (Fig. 5b). Hence, the beta distribution is considered appropriate for the *Q. suber* stand approving results from Wang et al. (2007) and is used for the entire treatment due to lower computational expense.

The majority of leaves of the *Q. suber* trees are tilted at angles between  $30^\circ$  to  $75^\circ$  (Fig. 5a). Only a small amount of leafs is horizontally aligned, typical for trees adapted to high incoming radiation. Hence, the derived leaf projection function  $G(\theta)$  shows very little change with view zenith angle and is 0.5 at  $57.3^\circ$  (Fig. 5b) according to theory (Pisek et al., 2011; Wit, 1965). Therefore, the influence on the transformation from gap probability  $P_{gap}(\theta)$  to leaf area index  $L$  is nearly equal for all view zenith angles  $\theta$  here. However, the need for leaf inclination angle information can generally be avoided for a single  $L$  estimation by choosing  $\theta = 57.3^\circ$  for observations of  $P_{gap}$  so that  $G(\theta) = 0.5$  and is independent of  $f(\alpha)$  (Macfarlane et al., 2007b).

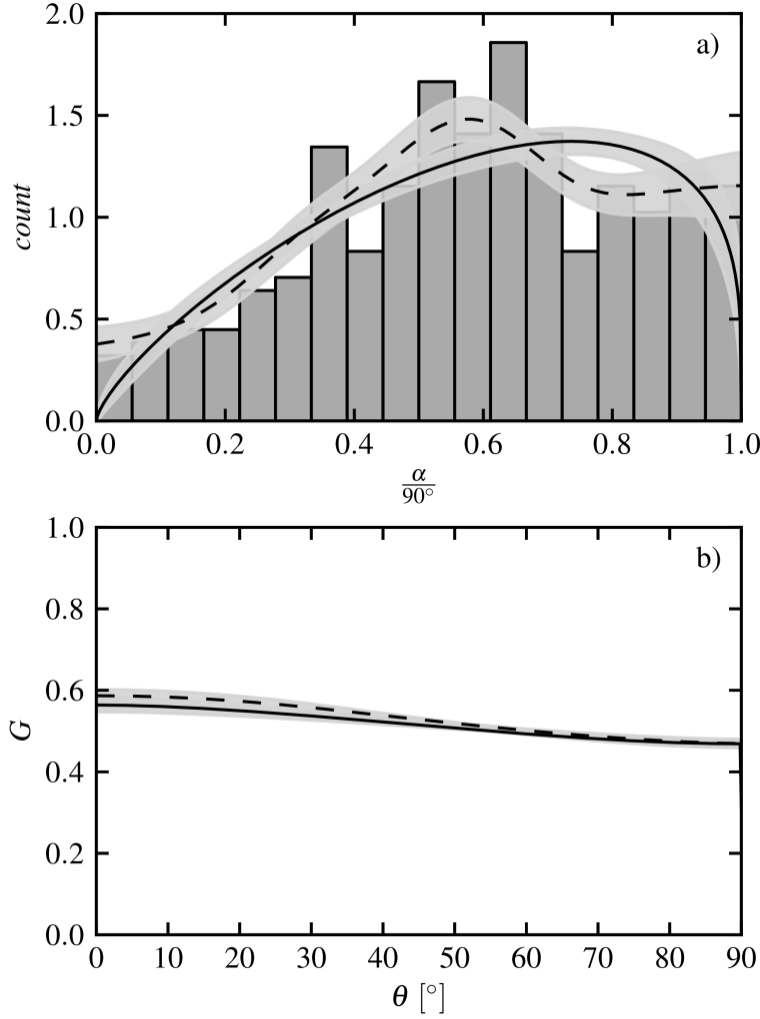


**Figure 5:** a) Empirical leaf inclination angle  $\alpha$  distribution (bars,  $n=281$ ), non-parametric kernel smooth distribution function (dashed line), two-parameter Beta-distribution (solid line). The abscissa displays angle of the leaf normal to zenith: 0 = horizontal aligned leaves, 1 = vertical aligned leaves. b) Leaf projection function  $G(\theta)$  over view zenith angle  $\theta$  derived from kernel smooth (dashed line) and Beta-distribution (solid line). Uncertainty bands present standard error.

#### 3.4.4. Clumping index

The angular dependency of leaf clumping index  $\Omega(\theta)$  is usually determined with the TRAC instrument based on gap size distribution or inversely modelled from independent estimates of leaf area index  $L$  and effective leaf area index  $L_e$  (Ryu et al., 2010b; Leblanc et al., 2005; Leblanc, 2002; Kucharik et al., 1997; Chen and Cihlar, 1995; Chen and Black, 1992). Here, DCP is used to derive height and angularly distributed  $\Omega(\theta)$  for the first time (Fig. 6).

$\Omega(\theta)$  decreases with increasing height above ground according to theory, since the gaps within crowns  $gt - gl$  observed by the sensor decrease and the gaps between crowns  $gl$  increase. Theoretically,  $\Omega(\theta)$  increases monotonically with increasing  $\theta$  and approaches 1 at  $90^\circ$  since the cameras sensing pathway through the canopy approaches infinite length and large gaps are successively decomposed in to smaller ones (Haverd et al., 2012; Ryu et al., 2010b; Norman and Welles, 1983). This is only true for lower heights where the edges of the camera view angle span  $\theta_v$  do not exceed the canopy top height.

At upper heights, a certain amount of clear sky over the canopy top is always visible, even at low angles. Therefore,  $\Omega(\theta) = 1$  is never reached.

However, observed  $\Omega(\theta)$  shows a sigmoid behaviour for all heights here with a decline at the mid view zenith angles around  $40^\circ$ . This behaviour is comparable to TRAC and model findings of Leblanc et al. (2005), Kucharik et al. (1997), and Ryu et al. (2010b) and the values are low as in other savannah-type ecosystems. The reasons for the sigmoid behaviour is still unclear. Ryu et al. (2010b) proposed the heterogeneous ecosystem scale tree distribution pattern causing different clustering of trees at different zenith view angles  $\theta$ . This could be a possible explanation here, since the western part of the experimental site is planted much denser than the eastern part (Fig. 1) and the *Q. suber* trees are planted in loosely series along the contour lines of the site causing a stand-scale clumping effect.

Another possible cause for increasing  $\Omega(\theta)$  at mid view zenith angles can be observation points located directly below or within a tree crown. Observations at the very centre of the crown are impossible since the position is occupied by the trunk. Hence, observations always take place at a certain distance to the horizontal crown centre. When the instrument is tilted and faces towards the crown centre, the path length through the crown increases with increasing  $\theta$  thus leads to monotonically increasing  $\Omega(\theta)$ . If the instrument is tilted and faces away from the crown centre, path length within the crown decreases with  $\theta$  and leads to decreasing  $\Omega(\theta)$  until the next adjacent tree crown interferes the sensor pathway. Even when the observation points are numerous, 50% of all observations below or within crowns are affected by decreasing path length with increasing  $\theta$  and so is the canopy average. This effect should only occur when tree density is low and adjacent trees are interfering the sensing pathway only at very high  $\theta$  such as in savannah-type ecosystems and depend on the crown shape. However, this effect should diminish with increasing height above ground which cannot be observed here. Additionally, the clumping of leaves to shoots within crowns is not considered in DCP so far. It may change with view zenith angle due to changing shoot angles projected to the view zenith angle resulting in different gap size distributions. This may counteract the mid view angle decline of  $\Omega(\theta)$ .

The influence on resulting leaf area index  $L$  remains unclear. The decreased  $\Omega(\theta)$  may lead to an artificial overestimation of  $L$  or account for the shortened pathway at these particular observation positions leading to the correct  $L$ . This is of peculiar importance when  $L$  is inferred from  $P_{gap}(\theta =$

57.3°) since this effect occurs in the mid zenith view angles and needs therefore further investigations e.g. with a radiative transfer model or investigations on the within crown gap size distribution. However, to represent the angular dependency of  $\Omega(\theta)$  in Eq. (1) for further computations in section 3.2, a third degree polynomial fit is used.

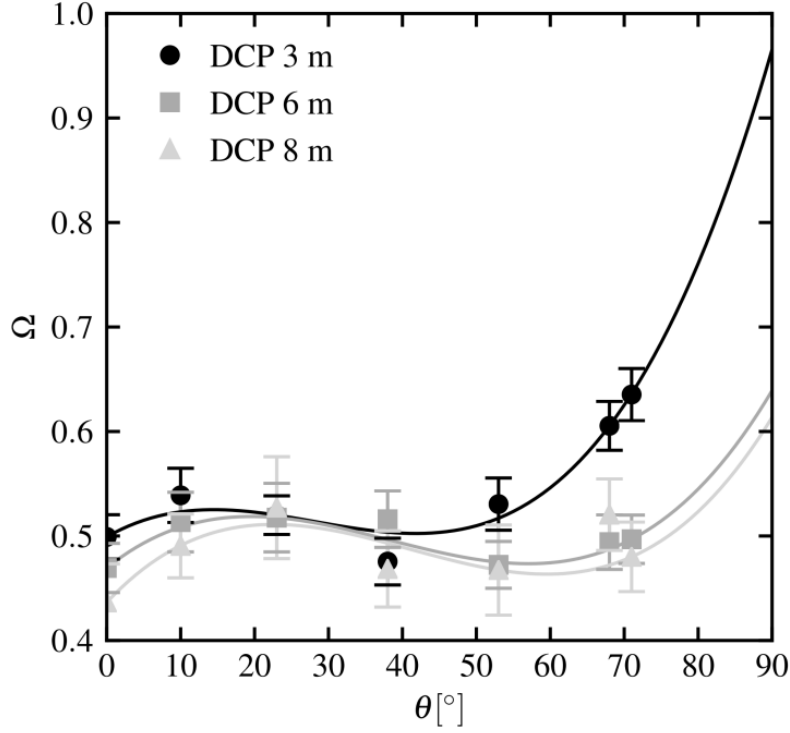


**Figure 6:** Change of clumping index  $\Omega$  with zenith view angle  $\theta$  at 3, 6 and 8 m height. Solid lines: fitted third degree polynomials.

#### 3.4.5. Cumulative leaf area index height distribution

The effective leaf area index  $\sum L_e$  is calculated from  $\overline{P_{gap}(\theta)}$  (with non-homogeneous leaf distribution omitted) for both methods and from  $\theta = 53^\circ$  under consideration of leaf projection function  $G(\theta) = 0.5$  for DCP. The cumulative leaf area index  $\sum L$  distribution (Fig. 7b) of LAI-2000 is calculated by  $\overline{\ln(P_{gap})}$ -averaging of the standard software introducing an apparent leaf clumping index (see section 2.1.2), whereas the cumulative DCP  $\sum L$  distribution is calculated under explicit consideration of leaf clumping (Eq. (9) and section 3.4).

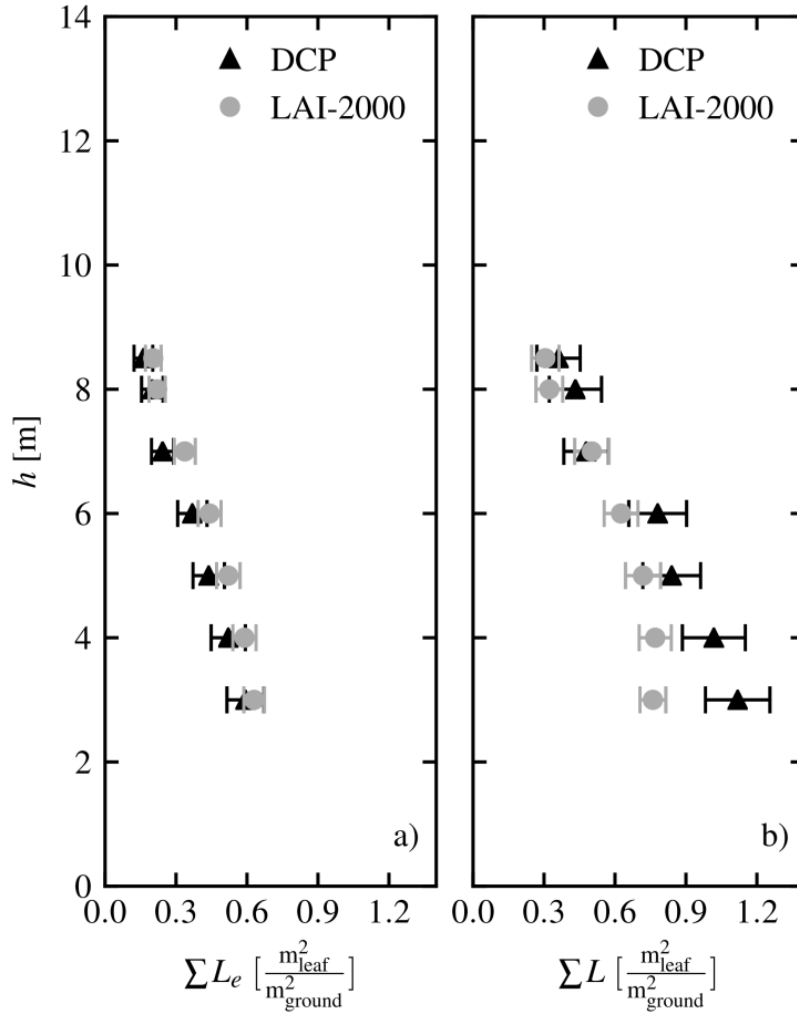


**Figure 7:** a) Height distribution of cumulative effective leaf area index  $\Sigma L_e$  for LAI-2000 and DCP derived from  $P_{gap}$  ( $53^\circ$ ). b) Same for cumulative leaf area index  $\Sigma L$ .

Both methods show very similar cumulative  $\Sigma L_e$  height distributions and comparable uncertainties (Fig. 7a) as a result of well matching  $P_{gap}$  observations (Fig. 4).

However, the distribution of total canopy leaf area index shows considerable differences among both methods. Only the estimate by DCP (Fig. 7b) matches very well with direct litter trap based measurements of the same period with of 1.15 to 1.05 (Costa e Silva et al., unpublished results), and it is comparable to other savannah-type ecosystems (Ryu et al., 2010b; Pereira et al., 2007; Kim et al., 2006). At a height of 3 meters, LAI-2000  $L$  is 32% lower than DCP and underestimates strongly compared to the litter trap measurements. This difference decreases with increasing height above the ground. Ryu et al. (2010a) showed that the apparent clumping of LAI-2000 overestimates  $\Omega(\Theta)$ , leading to lower  $L$ , which can be confirmed in this study. Thus, with an independent estimation of clumping, LAI-2000 cannot be used to estimate  $L$  in this open canopy. Additionally, the decreasing

difference between LAI-2000 and DCP with height above ground indicates a decrease in apparent clumping of LAI-2000 with decreasing canopy cover, proving the model results from Ryu et al. (2010a). This trend changes according to the order of canopy cover, and cannot be correlated to actual clumping.

### 3.4.6. Influence of view angle span on DCP results

The view angle span  $\theta_v$  of the camera determines the amount of angular integration present in each image. Hence, the larger  $\theta_v$ , the smaller is the standard error of mean gap probability  $\sigma_{\overline{P_{gap}}}$  and leaf area index  $\sigma_{\overline{L}}$  as shown in Fig. 8b,d. The standard error for the LAI-2000 device is generally smaller than for DCP since each LAI-2000 measurement integrates over  $180^\circ$  azimuth angle compared to  $53^\circ$  to  $6.625^\circ$  angle (maximum sensor width to smallest image crop) of DCP.

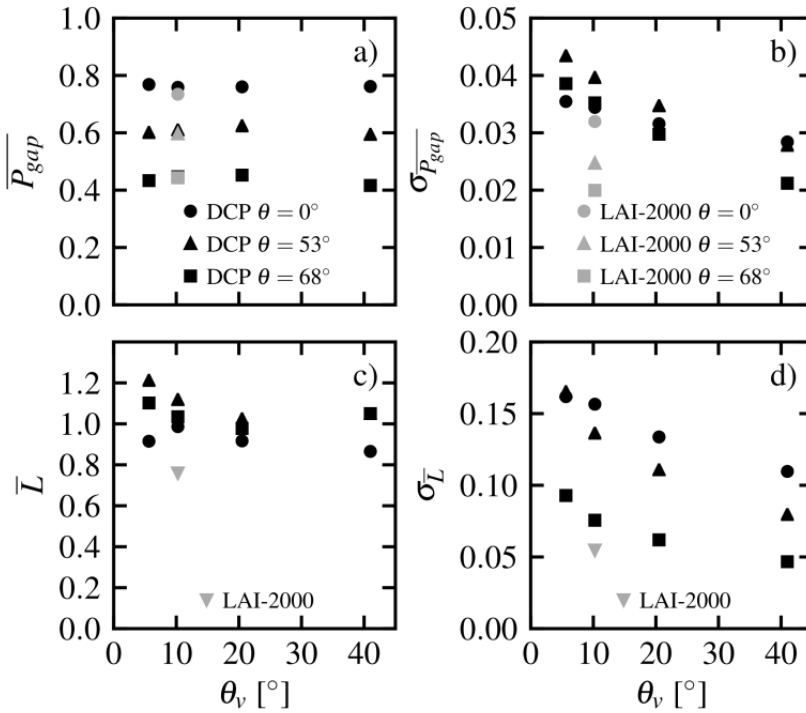


**Figure 8:** a, b) change of mean gap probability  $\overline{P_{gap}}$  and standard error  $\sigma_{\overline{P_{gap}}}$  with view angle span  $\theta_v$ . c, d) change of mean leaf area index  $\overline{L}$  and standard error  $\sigma_{\overline{L}}$  with view angle span  $\theta_v$ . All plots display observations at zenith view angles of  $0^\circ$ ,  $53^\circ$ ,  $68^\circ$  and 3 m height above ground for LAI 2000 and DCP.

However, the mean gap probability  $\overline{P_{gap}}$  itself shows no change according to view angle span  $\theta_v$  (Fig. 8a), illustrating the robustness of DCP to different image sizes. Nevertheless, the larger  $\theta_v$ , the larger is the bias due to taking one leaf projection function  $G(\theta)$  and  $\cos(\theta)$  value for the whole image leading to differences in resulting mean leaf area index  $L$  (Fig. 8c) according to  $\theta_v$ . Here, this bias is



comparably small since  $G(\theta)$  is rather flat (see Fig. 5). When  $G(\theta)$  is strongly bent, e.g. with planophile leaves, the bias will be larger. Hence, the image needs to be cropped to an optimal size minimizing the higher bias coming with large image sizes and the higher uncertainty coming with smaller image sizes. Throughout the rest of this study,  $P_{gap}$  and  $L$  values with  $\theta_v = 10.25^\circ$  are used to be comparable to the LAI-2000 ring span.

Theoretically, observation of DCP gap probability  $P_{gap}(\theta)$  at a certain height should lead to the same leaf area index  $L$ , independent from the chosen view zenith angle  $\theta$ . However, average differences of 10.5% occurred with varying  $\theta$  (Fig. 8c), most likely due to an insufficient estimation of the angular dependency of clumping index  $\Omega(\theta)$  mentioned in section 3.4. According to Eq. (9), errors in  $\Omega(\theta)$  or leaf projection function  $G(\theta)$  linearly propagate to  $L$ . However, uncertainties associated with  $G(\theta)$  are comparably small (Fig. 5) with respect to uncertainties of  $\Omega(\theta)$ .

#### 3.4.7. Exclusion of wooden tissue

By excluding wooden tissue like trunk and branch area in each image (see Sec. 2.4.1), the influence on gap probability  $P_{gap}$  and leaf area index  $L$  is quantified. The relative bias by not excluding the trunks and branches on gap probability  $\varepsilon P_{gap}(\theta)$  is rather small and ranges up to -2.2%. The relative bias on leaf area index  $\varepsilon L$  is stronger ranging from 3.1% to 20.9%. However, for angles and heights used here it is on average 6.9%. An overview of the relative bias depending on view zenith angle is listed in Tab. 1.  $\varepsilon P_{gap}(\theta)$  decreases with decreasing zenith view angle  $\theta$  and decreases with increasing height above ground  $h$  since the amount of trunk area in the sensor view field is decreasing. In contrast, no height dependent behaviour is evident for  $\varepsilon L$ , since wooden tissue either occluded gaps between or within crowns. Hence, the exclusion of wooden tissue raises or diminishes clumping index  $\Omega(\theta)$  with no clear height dependency and superposes the influence of  $\varepsilon P_{gap}(\theta)$  on  $\varepsilon L$ . Throughout the whole treatment,  $P_{gap}(\theta)$  and  $L$  values corrected for the wooden tissue influence are used.

**Table 1:** Relative bias of gap probability  $P_{gap}$  and leaf area index  $L$  when wooden tissue is not excluded.  $h$  = height above ground,  $\varepsilon P_{gap}(\theta)$  = relative bias of gap probability at  $0^\circ$ ,  $53^\circ$  and  $71^\circ$  view zenith angle,  $\varepsilon L$  = relative bias of leaf area index  $L$  derived from  $P_{gap}$  ( $53^\circ$ ).

$h$ [m]	$\varepsilon P_{gap}(0^\circ)$ [%]	$\varepsilon P_{gap}(53^\circ)$ [%]	$\varepsilon P_{gap}(71^\circ)$ [%]	$\varepsilon L$ [%]
8.5	0	-0.3	-0.4	8.5
8	-0.1	-0.4	-0.7	7.2
7	-0.4	-0.6	-0.8	7.6
6	-0.5	-0.6	-0.8	4.7
5	-0.5	-1.2	-1.2	8.0
4	-0.9	-1.0	-2.2	6.2
3	-0.6	-1.1	-2.2	5.8

The wooden tissue bias presented here can be understood as a "best-case" estimation since the classification algorithm is designed to rather failing to detect wooden tissue than wrongly classifying leaves as wooden tissue, to avoid an overestimation of the bias.

The whole image analysis process is fully automated by using an object-based image analysis software to detect number of pixels in all gaps  $gl$  automatically by object attributes. This overcomes time consuming manual treatments as required in previous studies (e.g. Ryu et al., 2010b; Macfarlane et al., 2007b,a) and contributes towards a more standardized and less labour intense processing of DCP images suitable for long term observations. Additionally, the detection based on objects is less sensitive to thresholds, since the mean over the pixels contained in an object is used for classification instead of every single pixel value separately. Furthermore, it offers much more characteristics, e.g. geometry and neighbourhood, to classify images than pixel based approaches. Finally, the influence of wooden tissue on gap probability  $P_{gap}(\theta)$  and leaf area index  $L$  can be quantified even in evergreen canopies where no leafless period occurs and one of the disadvantages of indirect  $L$  estimation methods can be overcome (e.g. Macfarlane et al., 2007b; Coops et al., 2004; Kucharik et al., 1998; Whitford et al., 1995).

However, the set-up of the algorithm and the adjustment of the thresholds, especially for the detection of wooden tissue (see sec. 2.4.1), is site-specific and challenging. It requires expert knowledge in object based image analysis and to our knowledge, currently no open source software is available for this purpose. The presented algorithm is additionally computationally expensive compared to common

image processing software. Further, it is desirable to improve the algorithm with more transferable thresholds allowing a fast application in different ecosystems.

#### 3.4.8. *Auxiliary data derived height distributions*

Estimating vertical leaf area index  $L$  distributions in tall canopies is challenging since height distributed observations within the entire canopy are often not feasible. Therefore, an approach demanding only ground-based observations is tested here. In Fig. 9a, the height distribution of leaf area index  $L$  derived from the observed crown top height  $ht$ , crown bottom height  $hb$ , crown radius  $rc$ , and bottom leaf area index  $L$  at 3 m height is shown for each crown model (see Section 2.4.2). The shape as well as the height of maximum  $L$  varies according to the model chosen. The higher the centre of gravity of the crown model, the higher is maximum  $L$  located in the crown. The integrated, cumulative  $P L$  distributions are plotted in Fig. 9b together with the measured cumulative  $P L$  height distribution of DCP. The ground-based crown model estimates fit very well to the distributions observed ( $R^2_e = 0.96$ ,  $R^2_{e\ 9/10} = 0.95$ ,  $R^2_t = 0.91$ ) even if each crown model assumes a uniform leaf density distribution with height, that is rather unlikely at the site in Portugal. The ellipsoidal and triangular crown model  $Se(h)$  and  $St(h)$  are considered as most extreme assumptions on the natural crown shape. However, they do not significantly exceed the observations uncertainties. The relative error of the model based distribution to the observed distribution is 3% for the ellipsoidal and asymmetric ellipsoidal crown model and 16% for the triangular crown model. Hence, if an appropriate crown model is chosen, it has a minor influence on the resulting distribution compared to other sources of error like the influence of woody tissue or neglecting leaf clumping. The assessment of  $L$  height distributions via ground-based observations of crown parameters and a single, ground-based  $L$  observation is feasible and a great opportunity for application in tall canopies where height dependent gap probability  $Pgap$  observations are challenging.

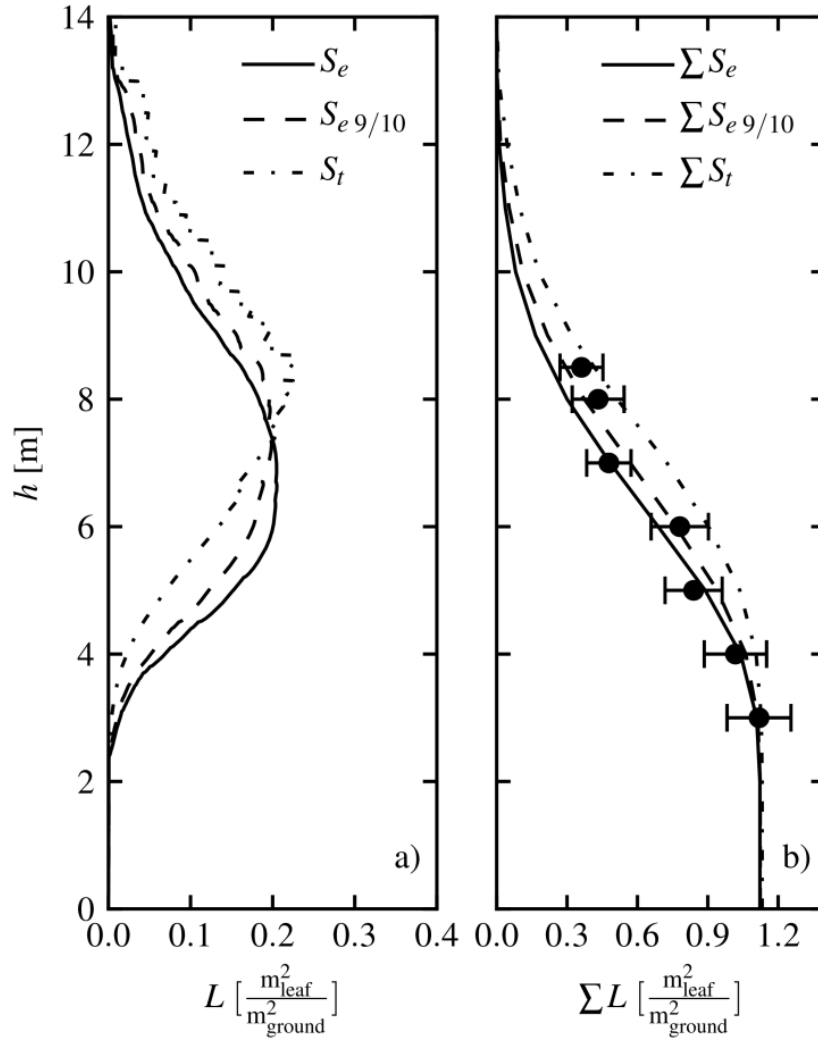


**Figure 9:** a) Height distribution of leaf area index  $L$  estimated with the ellipsoidal ( $S_e$ , solid line), asymmetric ellipsoidal ( $S_e 9/10$ , dashed line) and triangular ( $S_t$ , dotted-dashed line) crown model from crown parameters and leaf area index  $L$  derived from  $Pgap$  ( $53^\circ$ ) at 3 m height. b) Height distribution of cumulative leaf area index  $\sum L$ . Dots: measured cumulative height distribution with DCP. Lines: estimated cumulative height distribution by integration of  $S_e$ ,  $S_e 9/10$  and  $S_t$  from a).

### 3.5. Conclusions

In this study, we employed vertically and angularly distributed gap probability  $Pgap$  observations and derived vertical leaf area index  $L$  and effective leaf area index  $Le$  distributions for LAI-2000 and digital cover photography DCP in an open *Q. suber* forest. Additionally, we estimated vertical  $L$  distributions with ground-based observations of crown parameters and a single ground-based  $L$  observation.

We observed the following results: (1) Height and angularly dependent digital cover photography (DCP) was successfully applied here for the first time. It delivers very similar gap probability  $Pgap(\theta)$

and effective leaf area index  $Le$  as the established LAI-2000. (2) Height and angularly dependent leaf clumping index  $\Omega$  could be successfully determined with DCP and is mandatory for deriving correct leaf area index  $L$  from gap probability  $P_{gap}(\theta)$  at any view zenith angle  $\theta$ . (3) The effect of leaf clumping index  $\Omega$  on total leaf area index  $L$  yield 30% higher  $L$  compared to approximated  $L$  from LAI-2000 observations. This difference decreases with increasing height above ground. (4) The exclusion of wooden tissue from DCP by object-based image analysis yield on average 6.9% lower leaf area index  $L$  values. This is a 'best case' approximation, since the algorithm is designed not to overrate the effect. (5) When clumping index  $\Omega$  is included and woody tissue is excluded from DCP,  $L$  of DCP matched precisely with direct measurements using litter traps. (6) When LAI-2000 is used in open canopies, we recommend treatment of bad readings to avoid strong biases on gap probability  $P_{gap}$ , effective leaf area index  $Le$  and leaf area index  $L$  due to small variations in light intensities. (7) When height dependent observations are not feasible, ground-based observations of crown parameters can be used to derive reasonable leaf area index  $L$  height distributions from a single, ground based  $L$  observation.

For an efficient estimation of leaf area index height profiles of a forest canopy we recommend the following steps:

- Use below canopy digital cover photography DCP at a view zenith angle  $\theta = 57.3^\circ$  since no information on leaf projection function  $G(\theta)$  is needed.
- Exclude wooden tissue from the images with object-based image analysis.
- Infer total leaf area index  $L$  of the canopy explicitly including leaf clumping  $\Omega(\theta)$ .
- Use a digital hypsometer to measure crown top height  $ht$ , crown bottom height  $hb$ , and crown radius  $rc$  from the ground.
- Use the crown parameters and a suitable crown model to extrapolate total leaf area index  $L$  along the height above ground.

### 3.6. Acknowledgements

We thank the owners of Herdade da Machoqueira do Grou for the permission to establish our field site. We thank Sebastian Gimper for technical support and Rene Höfer for software support. We thank

Juliane Mai for help with mathematics. This study was funded by the Deutsche Forschungsgemeinschaft (WATERFLUX Project: # WE 2681/6-1; # CU 173/2-1) and kindly supported by Helmholtz Impulse and Networking Fund through Helmholtz Interdisciplinary Graduate School for Environmental Research (HIGRADE) (Bissinger and Kolditz, 2008).

### 3.7. Appendix A: Nomenclature

$A$ [pxl]	total number of pixels in each image
$f(\alpha)$ [–]	leaf angle distribution function
$G(\theta)$ [–]	leaf projection function
$gl$ [pxl]	number of pixels in gaps between crowns
$gt$ [pxl]	number of pixels in all gaps (gaps between crowns + gaps within crowns envelopes)
$h$ [m]	height above ground
$ht$ [m]	height of the crown top
$hb$ [m]	height of the crown bottom
$K(\theta)$ [–]	contact frequency
$L$ [m <sup>2</sup> /m <sup>2</sup> ]	leaf are index
$\sum L$ [m <sup>2</sup> /m <sup>2</sup> ]	cumulative leaf are index
$\varepsilon L$ [%]	relative bias of leaf are index
$Le$ [m <sup>2</sup> /m <sup>2</sup> ]	effective leaf are index
$\sum Le$ [m <sup>2</sup> /m <sup>2</sup> ]	cumulative effective leaf are index
$P_{gap}(\theta)$ [–]	gap probability
$\varepsilon P_{gap}(\theta)$ [%]	relative bias of gap probability
$rc$ [m]	crown radius
$Se(h)$ [–]	ellipsoidal crown shape model
$Se\ 9/10(h)$ [–]	asymmetric ellipsoidal crown shape model
$S\ t(h)$ [–]	triangular crown model
$\theta$ [°]	view zenith angle
$\alpha$ [°]	angle of the leaf's normal to the zenith

$\theta_v [^\circ]$	view angle span
$W [m^2/m^2]$	wood area index
$\Omega(\theta) [-]$	clumping index

### 3.8. Appendix B: Image object classification criteria

The colour criteria used for the classification of gap objects are brightness  $\overline{bri}$  , blue difference  $\overline{bd}$  :

$$\overline{bd} = \overline{B} - \left( \frac{\overline{G} + \overline{R}}{2} \right) \quad (B.1)$$

and blue ratio  $\overline{br}$  :

$$\overline{br} = \frac{3\overline{B}}{\overline{B} + \overline{G} + \overline{R}} \quad (B.2)$$

They are combined in a threshold criteria as:

$$gap = \begin{cases} (\overline{br} > 0.95) \wedge (\overline{bri} > 127) & \text{or} \\ (\overline{bri} > 230) & \text{or} \\ (\overline{br} > 1.5) & \text{or} \\ (\overline{bd} > 10) \wedge (\overline{bri} > 230) \wedge (0.95 < \overline{br} < 1.8) & \end{cases} \quad (B.3)$$

Within a radius of 50 pixels around each object classified as gap, the average difference to neighbouring gap and unclassified objects of brightness (  $\overline{bri_{difgap}}$  and  $\overline{bri_{difunc}}$  ) and blue ratio (  $\overline{br_{difgap}}$  and  $\overline{br_{difunc}}$  ) are calculated for the refinement of the gap edges. All gap objects missing

following threshold are declared as unclassified:

$$unc = \begin{cases} (\overline{bri_{dif\ unc}} < 100) \wedge (\overline{bri_{dif\ gap}} < -30) \wedge (\overline{bri_{dif\ gap}} > 40) & \text{or} \\ (\overline{bri_{dif\ unc}} < 70) \wedge (\overline{bri_{dif\ gap}} < -0.15) \end{cases} \quad (B.4)$$

This threshold is iteratively applied until no further changes in classification occurs. Image objects were classified as wooden tissue by thresholds based on the shape features area/width, length/width, curvature/length, border length/area, roundness, ellipse ratio, elliptic fit, and rectangular fit (feature description can be found in Trimble (2012)) as well as rgb sum  $\sum RGB$ :

$$\sum \overline{RGB} = \overline{B} + \overline{G} + \overline{R} \quad (B.5)$$

and green ratio  $\overline{gr}$  :

$$\overline{gr} = \frac{3\overline{G}}{\overline{B} + \overline{G} + \overline{R}} \quad (B.6)$$

The thresholds values for the wooden tissue detection are dependent on object size classes, therefore numerous and not shown here.

### 3.9. References

- Baldocchi, D., 1997. Measuring and modelling carbon dioxide and water vapour exchange over a temperate broad-leaved forest during the 1995 summer drought. *Plant, Cell & Environment* 20 (9), 1108–1122.
- Beadle, C., Talbot, H., Jarvis, P., 1982. Canopy structure and leaf area index in a mature scots pine forest. *Forestry* 55 (2), 105–123.
- Beer, A., 1852. Bestimmung der absorption des rothen lichts in farbigen flüssigkeiten. *Annal. Phys. Chem.* 86, 78–88.



- Bissinger, V., Kolditz, O., 2008. Helmholtz interdisciplinary graduate school for environmental research (higrade). *GAIA* 1, 71–73.
- Bouguer, P., 1729. *Essai d'optique sur la gradation de la lumière*. Gauthier-Villars et Cie, Paris.
- Bunce, J. A., 1989. Growth rate, photosynthesis and respiration in relation to leaf area index. *Annals of Botany* 63 (4), 459–463.
- Chen, J., Black, T., 1992. Foliage area and architecture of plant canopies from sunfleck size distributions. *Agricultural and Forest Meteorology* 60 (3-4), 249 – 266.
- Chen, J., Blanken, P., Black, T., Guilbeault, M., Chen, S., 1997a. Radiation regime and canopy architecture in a boreal aspen forest. *Agricultural and Forest Meteorology* 86 (1-2), 107 – 125.
- Chen, J., Cihlar, J., may 1995. Quantifying the effect of canopy architecture on optical measurements of leaf area index using two gap size analysis methods. *Geoscience and Remote Sensing, IEEE Transactions on* 33 (3), 777 –787.
- Chen, J. M., Rich, P. M., Gower, S. T., Norman, J. M., Plummer, S., 1997b. Leaf area index of boreal forests: Theory, techniques, and measurements. *Journal of Geophysical Research: Atmospheres* 102 (D24), 29429–29443.
- Comeau, P., Heineman, J., Newsome, T., 2006. Evaluation of relationships between understory light and aspen basal area in the british columbia central interior. *Forest Ecology and Management* 226 (1-3), 80 – 87.
- Comeau, P. G., Gendron, F., Letchford, T., 1998. A comparison of several methods for estimating light under a paper birch mixedwood stand. *Canadian Journal of Forest Research* 28 (12), 1843–1850.
- Coops, N. C., Smith, M. L., Jacobsen, K. L., Martin, M., Ollinger, S., 2004. Estimation of plant and leaf area index using three techniques in a mature native eucalypt canopy. *Austral Ecology* 29 (3), 332–341.
- Cutini, A., Matteucci, G., Mugnozza, G. S., 1998. Estimation of leaf area index with the li-cor lai 2000 in deciduous forests. *Forest Ecology and Management* 105 (1-3), 55 – 65.
- De Pury, D. G. G., Farquhar, G. D., 1997. Simple scaling of photosynthesis from leaves to canopies without the errors of big-leaf models. *Plant, Cell & Environment* 20 (5), 537–557.
- Deblonde, G., Penner, M., Royer, A., 1994. Measuring leaf area index with the li-cor lai-2000 in pine stands. *Ecology* 75 (5), pp. 1507–1511.
- Dubbert M., Cuntz M., Piayda A., Maguas C., Werner C., 2013. Partitioning evapotranspiration – Testing the Craig and Gordon model with field measurements of oxygen isotope ratios of evaporative fluxes. *Journal of Hydrology*.
- Fassnacht, K. S., Gower, S. T., Norman, J. M., McMurtric, R. E., 1994. A comparison of optical and direct methods for estimating foliage surface area index in forests. *Agricultural and Forest Meteorology* 71 (1-2), 183 – 207.
- Goel, N. S., Strebel, D. E., 1984. Simple beta distribution representation of leaf orientation in vegetation canopies. *Agron. J.* 76 (5), 800–802.
- Hardle, W., Müller, M., 1997. Multivariate and semiparametric kernel regression. *Discussion Papers, Interdisciplinary Research Project 373: Quantification and Simulation of Economic Processes* 1997,26, Berlin.
- Haverd, V., Lovell, J., Cuntz, M., Jupp, D., Newnham, G., Sea, W., 2012. The canopy semi-analytic *Pgap* and radiative transfer (canspart) model: Formulation and application. *Agricultural and Forest Meteorology* 160 (0), 14 – 35.
- Hutchison, B. A., Matt, D. R., McMillen, R. T., Gross, L. J., Tajchman, S. J., Norman, J. M., 1986. The architecture of a deciduous forest canopy in eastern tennessee, u.s.a. *Journal of Ecology* 74 (3), pp. 635–646.
- Jacquemoud, S., Bacour, C., Poilvé, H., Frangi, J.-P., 2000. Comparison of four radiative transfer

- models to simulate plant canopies reflectance: Direct and inverse mode. *Remote Sensing of Environment* 74 (3), 471 – 481.
- Jonckheere, I., Fleck, S., Nackaerts, K., Muys, B., Coppin, P., Weiss, M., Baret, F., 2004. Review of methods for in situ leaf area index determination: Part i. theories, sensors and hemispherical photography. *Agricultural and Forest Meteorology* 121 (1-2), 19 – 35.
- Kim, J., Guo, Q., Baldocchi, D., Leclerc, M., Xu, L., Schmid, H., 2006. Upscaling fluxes from tower to landscape: Overlaying flux footprints on high-resolution (ikonos) images of vegetation cover. *Agricultural and Forest Meteorology* 136 (3- 4), 132 – 146.
- Kobayashi, H., Ryu, Y., Baldocchi, D. D., Welles, J. M., Norman, J. M., 2013. On the correct estimation of gap fraction: How to remove scattered radiation in gap fraction measurements? *Agricultural and Forest Meteorology* 174-175 (0), 170 – 183.
- Kucharik, C. J., Norman, J. M., Gower, S. T., 1998. Measurements of branch area and adjusting leaf area index indirect measurements. *Agricultural and Forest Meteorology* 91 (1-2), 69 – 88.
- Kucharik, C. J., Norman, J. M., Murdock, L. M., Gower, S. T., 1997. Characterizing canopy nonrandomness with a multiband vegetation imager (mvi). *Journal of Geophysical Research: Atmospheres* 102 (D24), 29455–29473.
- Lang, A., Jan. 1986. Leaf-area and average leaf angle from transmission of direct sunlight. *Aust. J. Bot.* 34 (3), 349–355.
- Leblanc, S. G., Dec 2002. Correction to the plant canopy gap-size analysis theory used by the tracing radiation and architecture of canopies instrument. *Appl. Opt.* 41 (36), 7667–7670.
- Leblanc, S. G., Chen, J. M., Fernandes, R., Deering, D. W., Conley, A., 2005. Methodology comparison for canopy structure parameters extraction from digital hemispherical photography in boreal forests. *Agricultural and Forest Meteorology* 129 (3-4), 187 – 207.
- Li-COR, 1992. LAI-2000 Plant Canopy Analyzer. Lincoln, NE, USA.
- Macfarlane, C., Grigg, A., Evangelista, C., 2007a. Estimating forest leaf area using cover and fullframe fisheye photography: Thinking inside the circle. *Agricultural and Forest Meteorology* 146 (1-2), 1–12.
- Macfarlane, C., Hoffman, M., Eamus, D., Kerp, N., Higginson, S., McMurtrie, R., Adams, M., 2007b. Estimation of leaf area index in eucalypt forest using digital photography. *Agricultural and Forest Meteorology* 143 (3-4), 176 – 188.
- Meir, P., Grace, J., Miranda, A. C., 2000. Photographic method to measure the vertical distribution of leaf area density in forests. *Agricultural and Forest Meteorology* 102 (2-3), 105 – 111.
- Miller, J., Jan. 1967. A formula for average foliage density. *Aust. J. Bot.* 15 (1), 141–144. Miller, J. B., 3 1986. The foliage density equation revisited. *The ANZIAM Journal* 27, 387–401.
- Monsi, M., Saeki, T., 1953. "über den lichtfaktor in den pflanzengesellschaften und seine bedeutung für die stoffproduktion. *Japanese Journal of Botany* 14 (1), 22–52.
- Monsi, M., Saeki, T., 2005. On the factor light in plant communities and its importance for matter production. *Annals of Botany* 95 (3), 549–567.
- Monteith, J., 1965. Evaporation and environment. *Symposia of the Society for Experimental Biology* 19.
- Monteith, J. L., 1959. The reflection of short-wave radiation by vegetation. *Quarterly Journal of the Royal Meteorological Society* 85 (366), 386–392.
- Nilson, T., 1971. A theoretical analysis of the frequency of gaps in plant stands. *Agricultural Meteorology* 8 (0), 25 – 38.
- Norman, J. M., Welles, J. M., 1983. Radiative transfer in an array of canopies. *Agron. J.* 75 (3), 481–488. Parker, G. G., O'Neill, J. P., Higman, D., 1989. Vertical profile and canopy organization in a mixed deciduous forest. *Vegetatio* 85 (1-2), 1–11.
- Pereira, J. S., Mateus, J. A., Aires, L. M., Pita, G., Pio, C., David, J. S., Andrade, V., Banza, J., David,

- T. S., Paco, T. A., Rodrigues, A., Sep. 2007. Net ecosystem carbon exchange in three contrasting mediterranean ecosystems - the effect of drought. *Biogeosciences* 4 (5), 791–802.
- Pisek, J., Lang, M., Nilson, T., Korhonen, L., Karu, H., 2011. Comparison of methods for measuring gap size distribution and canopy nonrandomness at j arvselja rami (radiation transfer model intercomparison) test sites. *Agricultural and Forest Meteorology* 151 (3), 365 – 377.
- Rutter, A., Kershaw, K., Robins, P., Morton, A., 1971. A predictive model of rainfall interception in forests, 1. derivation of the model from observations in a plantation of corsican pine. *Agricultural Meteorology* 9 (0), 367 – 384.
- Ryu, Y., Nilson, T., Kobayashi, H., Sonnentag, O., Law, B. E., Baldocchi, D. D., 2010a. On the correct estimation of effective leaf area index: Does it reveal information on clumping effects? *Agricultural and Forest Meteorology* 150 (3), 463 – 472.
- Ryu, Y., Sonnentag, O., Nilson, T., Vargas, R., Kobayashi, H., Wenk, R., Baldocchi, D. D., 2010b. How to quantify tree leaf area index in an open savanna ecosystem: A multi-instrument and multi-model approach. *Agricultural and Forest Meteorology* 150 (1), 63 – 76.
- Ryu, Y., Verfaillie, J., Macfarlane, C., Kobayashi, H., Sonnentag, O., Vargas, R., Ma, S., Baldocchi, D. D., 2012. Continuous observation of tree leaf area index at ecosystem scale using upward-pointing digital cameras. *Remote Sensing of Environment* 126 (0), 116 – 125.
- Schindelin, J., Arganda-Carreras, I., Frise, E., Kaynig, V., Longair, M., Pietzsch, T., Preibisch, S., Rueden, C., Saalfeld, S., Schmid, B., Tinevez, J.-Y., White, D. J., Hartenstein, V., Eliceiri, K., Tomancak, P., Cardona, A., Jul. 2012. Fiji: an open-source platform for biological-image analysis. *Nat Meth* 9 (7), 676–682.
- Sellers, P. J., Dorman, J. L., May 1987. Testing the simple biosphere model (sib) using point micrometeorological and biophysical data. *J. Climate Appl. Meteor.* 26 (5), 622–651.
- Sinclair, T. R., Murphy, C. E., Knoerr, K. R., 1976. Development and evaluation of simplified models for simulating canopy photosynthesis and transpiration. *Journal of Applied Ecology* 13 (3), pp. 813–829.
- Stenberg, P., Linder, S., Smolander, H., Flower-Ellis, J., 1994. Performance of the lai-2000 plant canopy analyzer in estimating leaf area index of some scots pine stands. *Tree Physiology* 14 (7-8-9), 981–995.
- Strachan, I. B., McCaughey, J. H., 1996. Spatial and vertical leaf area index of a deciduous forest resolved using the lai-2000 plant canopy analyzer. *Forest Science* 42 (2), 176–181.
- Trimble (Ed.), 2012. eCognition Developer 8.7.1 Reference Book. Trimble Germany GmbH.
- Wang, W.-M., Li, Z.-L., Su, H.-B., 2007. Comparison of leaf angle distribution functions: Effects on extinction coefficient and fraction of sunlit foliage. *Agricultural and Forest Meteorology* 143 (1-2), 106 – 122.
- Wang, Y. S., Miller, D. R., Welles, J. M., Heisler, G. M., 1992. Spatial variability of canopy foliage in an oak forest estimated with fisheye sensors. *Forest Science* 38 (4), 854–865.
- Watson, D. J., 1947. Comparative physiological studies on the growth of field crops: I. variation in net assimilation rate and leaf area between species and varieties, and within and between years. *Annals of Botany* 11 (1), 41–76.
- Whitford, K., Colquhoun, I., Lang, A., Harper, B., 1995. Measuring leaf area index in a sparse eucalypt forest: a comparison of estimates from direct measurement, hemispherical photography, sunlight transmittance and allometric regression. *Agricultural and Forest Meteorology* 74 (3-4), 237 – 249.
- Wilson, J. W., 1959. Analysis of the spatial distribution of foliage by two-dimensional point quadrats. *New Phytologist* 58 (1), 92–99.
- Wilson, J. W., 1960. Inclined point quadrats. *New Phytologist* 59 (1), 1–7. Wilson, J. W., 1965. Stand structure and light penetration. i. analysis by point quadrats. *Journal of Applied Ecology* 2 (2),

pp. 383–390.

Wilson, J. W., 1967. Stand structure and light penetration. iii. sunlit foliage area. *Journal of Applied Ecology* 4 (1), pp. 159–165. Wit, C. d., 1965. Photosynthesis of leaf canopies. Tech. rep., Wageningen.



#### **4. Study IV: INFLUENCE OF TREE COVER ON HERBACEOUS LAYER DEVELOPMENT AND CARBON AND WATER FLUXES IN A PORTUGUESE CORK-OAK WOODLAND**

Maren Dubbert<sup>1,✉,\*</sup>; Alexander Mosena<sup>2,\*</sup>; Arndt Piayda<sup>3</sup>; Matthias Cuntz<sup>3</sup>; Alexandra C. Correia<sup>4</sup>; Joao Santos Pereira<sup>4</sup>; and Christiane Werner<sup>1</sup>

<sup>1</sup>Agroecosystem Research, BayCeer, University of Bayreuth, Universitätsstraße 30, 95447 Bayreuth, Germany

<sup>2</sup>Experimental and Systems Biology, University of Bielefeld, Universitätsstrasse 25, 33615 Bielefeld

<sup>3</sup>UFZ – Computational Hydrosystems, Helmholtz Centre for Environmental Research, Permoserstraße 15, 04318 Leipzig, Germany

<sup>4</sup>Instituto Superior de Agronomia, Technical University of Lisbon, Tapada da Ajuda, Lisbon, Portugal

\*both authors contributed equally to the work

✉Corresponding author: Maren Dubbert ([maren.dubbert@uni-bayreuth.de](mailto:maren.dubbert@uni-bayreuth.de))



#### **4.1. Abstract**

Facilitation and competition between different vegetation layers may have a large impact on small-scale vegetation development. We propose that this should not only influence overall herbaceous layer yield but also species distribution and understory longevity, and hence the ecosystems carbon uptake capacity especially during spring. We analyzed the effects of trees on microclimate and soil properties (water and nitrate content) as well as the development of an herbaceous community layer regarding species composition, aboveground biomass and net water and carbon fluxes in a cork-oak woodland in Portugal, between April and November 2011.

The presence of trees caused a significant reduction in photosynthetic active radiation of  $35 \text{ mol m}^{-2} \text{ d}^{-1}$  and in soil temperature of  $5^{\circ}\text{C}$  from April to October. At the same time differences in species composition between experimental plots located in open areas and directly below trees could be observed: species composition and abundance of functional groups became increasingly different between locations from mid April onwards. During late spring drought adapted native forbs had significantly higher cover and biomass in the open area while cover and biomass of grasses and nitrogen fixing forbs was highest under the trees. Further, evapotranspiration and net carbon exchange decreased significantly stronger under the tree crowns compared to the open during late spring and the die back of herbaceous plants occurred earlier and faster under trees. This was most likely caused by interspecific competition for water between trees and herbaceous plants, despite the more favorable microclimate conditions under the trees during the onset of summer drought.

## 4.2. Introduction

Mediterranean oak woodlands are savannah type, pastoral agro-forestry ecosystems (called ‘Montado’ in Portugal) which cover large areas of the Mediterranean basin. They are highly diverse and considered a habitat of high conservation value (Perez-Ramos et al., 2008). The ‘Montado’ is a multi-layered ecosystem consisting of a widely spaced tree cover composed of *Quercus. suber* L., *Quercus ilex* or a combination of these, and an understory layer comprised of shrub formations and/or grasslands, fallows or cereal crops (Diaz et al., 1997; Perez-Ramos et al., 2008). In the ‘Montado’ ecosystem, the life cycle of herbaceous plants, which typically consist of annual  $C_3$  plants, is terminated by the beginning of the dry season. Commonly the vegetative cycle starts in autumn after the first rains and lasts until the onset of the drought season (Aires et al., 2008), with the main growth phase in spring between March and late May (Jongen et al. 2011; 2013a; Otieno et al., 2011). However, changes in seasonal rainfall can alter this pattern (Figuerola and Davy, 1991; Miranda et al., 2002). Furthermore, factors such as extent of rainfall and the duration of the summer drought period may influence resource availability and affect plant species composition and productivity (Schwinning and Ehleringer, 2001).

The contribution of the herbaceous layer to ecosystem fluxes and productivity consequently varies intra-annually and can be remarkably high, especially in spring. Paço et al. (2009) showed that in times of high water availability (October-May/June) herbaceous evapotranspiration is equal to and sometimes exceeds tree transpiration (see also Dubbert et al., 2013). Furthermore, the herbaceous layer can make up to more than 50% of total gross primary productivity (*GPP*) during spring and thus play a significant role for ecosystem productivity (Unger et al., 2009, 2010). Herbaceous plants also play an important role in the nitrogen budget enhancing soil nitrogen input and retention in the ecosystem (Otieno et al., 2011) and enhancing growth rate and fruit production of the trees (Pulido, et al., 2010).

The high spatial heterogeneity created by the sparse tree cover, affects microclimate and nutrient availability (Huber-Sannwald and Jackson, 2001; Hussain et al., 2009; Moreno, 2008), creating distinct patches where herbaceous plants grow in the open or under the tree crown. In summer and late spring, the combination of water stress with high radiation can lead to plant photoinhibition (Werner and Correia, 1996; Werner et al., 2001, 2002). Trees can potentially mitigate the photosynthetic



damage in the herbaceous vegetation providing shade and temporarily moistening the top soil layers by hydraulic lift (Cubera and Moreno, 2007). This process is characterized by water movement upwards through the root systems of plants that have access to deeper soil depths (Caldwell et al., 1998) and may temporarily increase the soil water content in the upper soil layers (e.g. Kurz-Besson et al., 2006). Hydraulic lift might have a facilitating effect for herbaceous plants, but that effect might easily be overwhelmed by competition for water with trees (Ludwig et al., 2004). Soil nutrient content has also been found to be positively affected by trees (e.g. Gallardo et al., 2000; Gallardo, 2003). However, trees might also act as competitors for nutrients, water and light for the understory, since competition for resources in agro-forestry systems is a frequent phenomenon (José et al., 2004).

Most studies on tree versus herbaceous interactions in these ecosystems focus on biomass production (Scholes and Archer, 1997) at large spatial scales (landscape level; Casado et al., 2004; Costa et al., 2009; Jose et al., 2004). An issue that has not been adequately covered yet is how changes might occur in the competitive balance between trees and the herbaceous layer over the course of a year. During times when water is generally not a limiting factor, maybe shade effects of trees crowns have no significant impact on the herbaceous layer. With increasing drought intensity though, facilitation may play a more important role, although also the opposite was found in ‘Montado’ systems (Bertness and Callaway, 1994; Maestre et al., 2009; Moreno, 2008). According to previous findings in ‘Montado’ sites with similar annual rainfall than our site (i.e. Moreno, 2008), we hypothesize that the herbaceous layer will overall profit from the reduced light and temperature stress that should occur under the trees. We propose that this should not only influence overall herbaceous layer yield but also species composition and understory longevity, and hence the ecosystems carbon uptake capacity especially during spring. The main aim of this study was to determine possible facilitating and competitive effects of tree cover on herbaceous vegetation (cover and biomass, species composition and water and carbon fluxes) and their impact during distinct periods within the year: the peak growing period (April-May); the transition of wet spring to summer drought (late May-June); peak summer drought (September) and the re-wetting period at the beginning of autumn (October-November).

### 4.3. Materials and Methods

#### 4.3.1. Study site

Measurements were conducted between April 6 and November 22 2011 in an open cork-oak woodland (*Quercus suber* L.) in central Portugal, approximately 100 km north-east of Lisbon (N39°8'17.84'' W8°20'3.76''; Herdade de Machoqueira do Grou). The oak-trees are widely spaced (209 individuals ha<sup>-1</sup>) with a leaf area index of 1.1 and a gap probability of 0.7. The oak-trees are managed for cork production, were planted approximately 50 years ago and have a mean maximum crown height of 10 m and diameter at breast height of 25 cm (Piayda et al., unpublished). It is a bi-layered system containing an annual herbaceous layer dominated by native forbs and grasses, with a biomass peak in spring (April-May) and senescence occurring between late May and early June with the onset of summer drought. In autumn 2009 the site was ploughed, limed and then seeded with a legume-rich seed mixture of native species, a common practice in these agro-silvopastoral systems in Portugal to improve productivity and soil fertility (Crespo, 2006). The seed mixture contained: *Trifolium subterraneum* L., *Trifolium michelianum* L., *Trifolium resupinatum* L., *Trifolium vesiculosum* Savi., *Trifolium incarnatum* L., *Trifolium glanduliferum* Boiss., *Biserrula pelecinus* L., *Ornithopus sativus* Brot., *Ornithopus compressus* L. and *Lolium multiflorum* Lam. In total 20 herbaceous species were observed during the measurement period in 2011 (Table 1).

The soil is a Cambisol, its substrate consists of 81% sand, 14% silt and 5% clay. The site is characterized by a Mediterranean climate, with wet spring conditions and hot, dry summers. Long-term mean annual temperature is approximately 15.9 °C and long-term mean annual precipitation is 680 mm (Instituto de Meteorologia, Lisbon).

We established plots in two different locations: one directly under the oak trees crown projected area and another one in an adjacent open area, approximately 5-7 m distant from canopy cover. A total of 10 permanent herbaceous layer plots of 40 x80 cm were installed with 5 plots in each location. The distance to the cork-oak crown was selected in order to ensure similar soil and environmental

conditions between locations and on the other hand eliminate shading or influence of cork-oak roots, which was verified with soil profiles to 100 cm depth.

**Table 1:** List of herbaceous species growing in the open and tree site in 2011.

<b>N-fixing forbs</b>	<b>Forbs</b>	<b>Grasses</b>
<i>Ornithopus compressus</i> L.	<i>Crepis vesicaria</i> L.	<i>Briza maxiamia</i> L.
<i>Ornithopus sativus</i> Brot.	<i>Geranium spec</i>	<i>Lolium multiflorum</i> Lam.
<i>Trifolium glanduliferum</i> Boiss.	<i>Plantago coronopus</i> L.	<i>Vulpia bromoides</i> Gray
<i>Trifolium michelianum</i> Savi	<i>Rumex acetosella</i> L.	<i>Vulpia geniculata</i> Link
<i>Trifolium incarnatum</i> L.	<i>Silene gallica</i> L.	
<i>Trifolium subterraneum</i> L.	<i>Spergula arvensis</i> L.	
<i>Trifolium resupinatum</i> L.	<i>Tolpis barbata</i> (L.) Gaertn.	
<i>Trifolium vesiculosum</i> Savi	<i>Tuberaria guttata</i> (L.) Fourr.	

#### 4.3.2. Environmental parameters

In the open and the tree plots photosynthetic photon flux density was measured below the oak canopy and above the herbaceous vegetation at approximately 1.5 m height (*PPFD*, LI-190SB, LI-COR, Lincoln, USA). Rainfall (ARG100 Rain gauge, Campbell Scientific, Logan, UT, USA), air temperature and relative humidity were all measured continuously in the open area (CS-215 Temperature and Relative Humidity Probe, Campbell Scientific, Logan, UT, USA) and means were stored in a datalogger every 30 minutes (CR10x, Campbell Scientific, Logan, UT, USA). Vapor pressure deficit (*VPD*, kPA) was calculated from relative humidity and air temperature data.

Soil temperature (custom built Pt-100 elements) and volumetric water content ( $\theta$ , 10hs, Decagon, Washington, USA) in 5, 15, 30 and 60 cm depth were measured on both plots and stored in a datalogger as 60 minutes means (CR1000, Campbell Scientific, Logan, UT, USA). The total daily water reduction of the upper 60 cm of the soil profile (the sum of plant transpiration and soil evaporation as well as runoff and drainage) was calculated from  $\theta$  measurements. Therefore, the reduction in  $\theta$  over 24 h (midnight to midnight) was estimated for each depth separately and then integrated for the whole upper 60 cm of the soil profile.

#### 4.3.3. *Vegetation Cover and aboveground biomass*

Vegetation cover of the permanent plots was analyzed four times during each of three measuring periods: moist spring (April 6 - May 3), the transition of wet spring to summer drought (May 23 - June 16) and the re-wetting period at the beginning of autumn (October 25 - November 22). Cover was estimated as the percentage of species canopy cover in each plot and thereafter pooled into functional groups: grasses and forbs (subdivided into N-fixing forbs and other forbs). Only living plant material was recorded.

To compare species similarity between both locations, Renkonen similarity was calculated. This index was chosen because it is rather robust, as it is not strongly influenced by the number of species and sample size (Krebs, 1998). The Renkonen similarity index was calculated for every measuring day. As a means of abundance, species cover percentage was used in the calculations (Krebs, 1998):

$$P = \sum_i \min(P_{1i}, P_{2i}) \quad 1)$$

where  $P$  is the percentage similarity between sample 1 and 2,  $P_{1i}$  the percentage of species  $i$  in community sample 1, and  $P_{2i}$  the percentage of species  $i$  in community sample 2.

Living aboveground biomass of herbaceous plants was determined destructively on five 40x40 cm plots in the open and under the trees randomly selected near the permanent plots. Harvesting took place in 6 measuring dates: four in spring and two in November. All green fresh aboveground plant biomass was collected, divided by functional groups, dried (60 °C, 48 hours) and weighed.

#### 4.3.4. *Soil nitrate content*

Soil samples for the determination of nitrate content were collected on May 25, September 20 and November 10. Soil was sampled at 0-10, 10-20 and 20-30 cm depth ( $n = 3$  on the open and tree plots each). Nitrate extraction was carried out using Flow Injection Analysis (MLE FIA-II, Dresden, Germany). 30 ml  $\text{CaCl}_2$  (0.01 mol) were added to 15 mg fresh soil, shaken for 1 hour and then filtrated. 15 ml of the solution were injected into the FIA laboratory device and automatically

analyzed.

#### 4.3.5. Gas-exchange measurements

Net CO<sub>2</sub> exchange (*NEE*) and evapotranspiration (*ET*) on vegetation plots were measured using a cavity ring-down spectrometer (CRDS, Picarro, Santa Clara, USA) and a CO<sub>2</sub> infrared gas analyzer (BINOS100; Fisher-Rosemount GmbH & Co., Hasselroth, Germany) in combination with transparent chambers in an open gas exchange system. Chambers were custom built, following the design of Pape et al. (2009, see also Dubbert et al., 2013). A transparent Plexiglas soil chamber was coated with an isotope inert FEP foil (4PTFE, Stuhr, Germany) with a total volume of 60 L. The background air inlet port and the sampling air outlet port were located in 10 and 50 cm height, respectively. The background air was sampled with a tube from 1.5 m distance to the ground and buffered with a 200 L buffer volume. The flow through the chamber was regulated as described in Pape et al. (2009) using a fan inside the inlet sampling tube and could be adjusted between 0 and 40 L min<sup>-1</sup>. We measured background and sampling air alternately until stable values were reached. The chamber was maintained on the plots until stabilization was reached, which was <10 min. The observed increase in air temperature above ambient values was ca. 3 °C after 5 min and stable thereafter, which is smaller compared to those found in Pape et al. (2009). A five minutes interval average for the calculation of *NEE* and *ET* was used. Fluxes of *NEE* and *ET* were calculated with the gas exchange equations of von Caemmerer and Farquhar (1981). Total daytime sums of *NEE* and *ET* and midday averages of  $g_{nw}$  of the herbaceous layer were calculated. The relative contribution of total daytime *ET* to the total water loss from the 60 cm upper soil layer (thereafter termed “relative soil water use”) was estimated by relating the total daily water loss from the upper soil layers to total daytime *ET* of the herbaceous layer. Gas-exchange measurements were carried out between April and the end of November, corresponding to the measurement intervals of vegetation cover.

#### 4.3.6. *Statistical analysis*

All results are presented as mean values ( $\pm$  SD,  $n=3-5$ ). T-tests were conducted to test for significant differences in nitrate content between study plots within each soil depths and seasons. Mann-Whitney U-tests were carried out to examine location specific differences in vegetation cover and aboveground biomass separately for distinct functional groups for all measuring dates. The same test was used to examine location specific differences in evapotranspiration and net carbon exchange for each sampling date in spring, summer and autumn separately.

Non-linear correlations were used to relate the location differences in total *NEE* during daylight in spring with the location differences in *PPFD*, relative water use. For all calculations of between location differences only those dates were used, where measurements on open and tree plots were conducted on consecutive days with comparable environmental conditions. Linear regressions were used to relate *NEE* in spring on both plots with *PPFD* and  $\theta$ . Statistical analyses were carried out with the software Statistica (Statistica 6.0, StatSoft, Inc., Tulsa, USA).

### 4.4. Results

#### 4.4.1. *Development of microclimatic conditions and soil nitrate content*

Over the course of the study period, air temperature followed the typical Mediterranean climate pattern with mean temperatures around 10 °C at the beginning of the year but rising above 25 °C in August and September (Fig. 1a). Consequently, vapor pressure deficit (*VPD*) was low during winter and high during summer and strongly variable with values ranging from 0.6 to 3 kPa (Fig. 1a). During summer, soil temperatures exceeded air temperature by up to 10 °C. Moreover, daily mean soil temperature was generally 5 °C higher on the open plots compared to the tree plots between April and October (Fig. 1b).

With a total amount of 816 mm rainfall 2011 was rather high compared to the long term average (680 mm). Major rainfall occurred during spring and winter with barely any rain during the summer

months. After the last rainfalls occurred between late May and early June and  $\theta$  dropped below  $0.05 \text{ m}^3 \text{ m}^{-3}$  on both study areas (Fig. 1c).

During the winter months (January-March and November-December), mean daily integrated *PPFD* was  $13 \text{ mol m}^{-2} \text{ d}^{-1}$  on both plots. On the open plots, *PPFD* increased until mid-June to a peak of  $64.4 \text{ mol m}^{-2} \text{ d}^{-1}$  and then declined towards the end of the year (Fig. 1d), while it remained rather stable under the trees with a mean value of about  $14 \text{ mol m}^{-2} \text{ d}^{-1}$ , never exceeding  $22 \text{ mol m}^{-2} \text{ d}^{-1}$  (Fig. 1d).

Soil nitrate content ranged between  $0.13$  and  $3.1 \text{ mg kg}^{-1}$  (Table 2). Generally, soil nitrate content declined rapidly with depth (with the exception of November), and especially in May soil nitrate content was considerably higher on the open plots compared to the tree plots (Table 2).

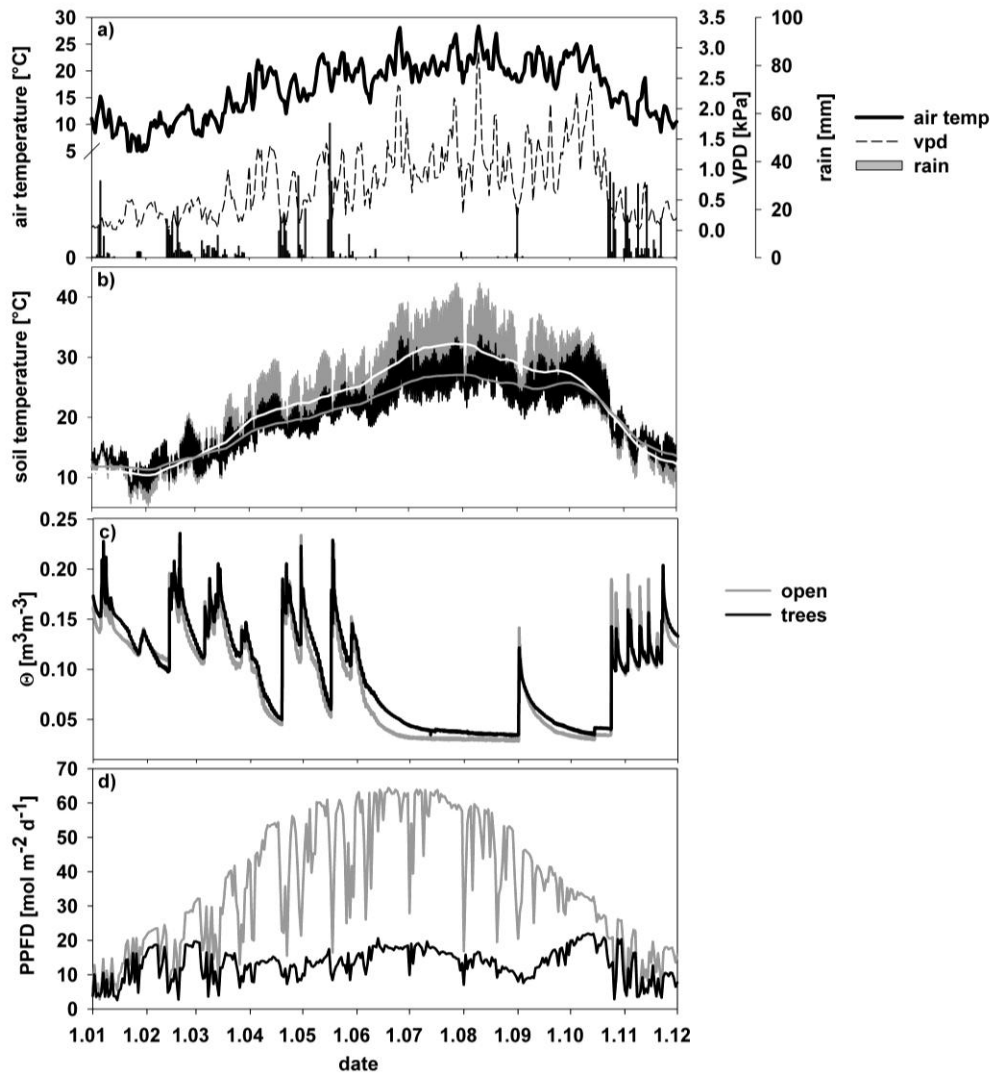


**Figure 1:** Environmental conditions during 2011; a) daily mean air temperature (black line), vapor pressure deficit (VPD; black long dashed line) and daily rainfall (black bars) observed in the open area; b) soil temperature in the open and tree plots (grey and black lines, respectively). The lighter grey lines indicate daily means; c) soil volumetric water content ( $\Theta$ ) in 5 cm soil depth in the open and tree plots (grey and black lines, resp.) and d) daily sums of photosynthetic photon flux density (PPFD) in the open (grey line) and tree plots (black line).

**Table 2:** Nitrate content in different soil depths in May, September and November 2011 (mean values  $\pm$  SD; n = 3). \* denote statistic significant differences between the open and the tree site ( $p < 0.05$ ).

Month	Soil depth (cm)	Nitrate content (mg kg <sup>-1</sup> ) in the soil		Sign.
		Open plots	Tree plots	
May	0-10	1.33 $\pm$ 0.99	0.27 $\pm$ 0.11	*
	10-20	0.53 $\pm$ 0.29	0.16 $\pm$ 0.04	*
	20-30	0.47 $\pm$ 0.46	0.13 $\pm$ 0.08	n.s.
September	0-10	3.1 $\pm$ 0.42	2.48 $\pm$ 0.02	n.s.
	10-20	1.05 $\pm$ 0.08	0.97 $\pm$ 0.02	n.s.
	20-30	1.12 $\pm$ 0.03	1.26 $\pm$ 0.23	*
November	0-10	0.77 $\pm$ 0.06	0.43 $\pm$ 0.06	*
	10-20	0.68 $\pm$ 0.27	0.43 $\pm$ 0.06	n.s.
	20-30	0.67 $\pm$ 0.08	0.33 $\pm$ 0.02	*

#### 4.4.2. Herbaceous layer species distribution and aboveground biomass

plant cover reached a maximum of 90 and 88% in late May (Fig.2) and a total aboveground biomass was  $69 \pm 4$  and  $72 \pm 21$  g m<sup>-2</sup> in the beginning of April on the open and tree plots, respectively (Table 3). On the first sampling date in April species composition was relatively similar between open and tree plots (Renkonen similarity of 65%, Fig. 3a-b) and no significant plot specific differences could be found regarding the percentage cover and biomass of each functional group (U-tests;  $p > 0.05$ ). Although total green aboveground biomass and cover did not significantly differ until the end of May between locations (U-tests,  $p > 0.05$ ; Fig. 2 and Table 3), species composition, cover and biomass of each functional group developed differently between locations from April 24 until June 14 (Fig. 3, Table 3). This is underlined by the Renkonen similarity, decreasing rapidly from early April to late May to 30% (Fig. 3a-b).

Between early April and late May grass cover and biomass slightly increased on the tree plots reaching 42% and 44 g m<sup>-1</sup>, respectively. While always present on the tree plots, grasses completely vanished from the open plots during late spring. During the same time forbs, such as *Tuberaria guttata*, roughly doubled their cover and aboveground biomass reaching 55% and 51 g m<sup>-2</sup>, respectively (Fig. 3c).



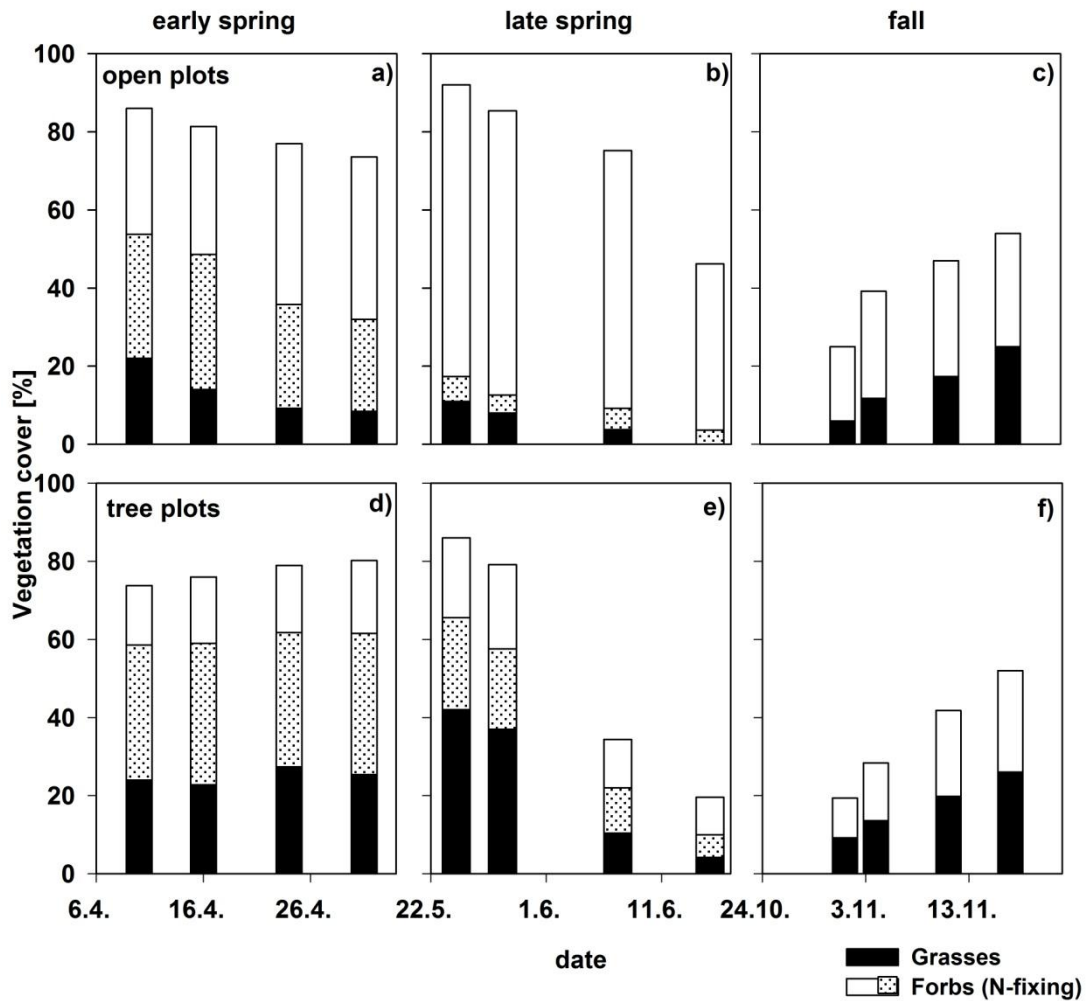


**Figure 2:** a-h) Relative vegetation cover in % of living biomass of distinct functional groups of the herbaceous layer (Grasses, N-fixing and other forbs) in early spring, late spring and fall 2011 on the open (a-e) and tree plots (f-h; mean values; n = 5).

In addition, the herbaceous understory began to die off 2 weeks earlier on the tree plots compared to the plots in the open (Fig. 2b and f). The retarded wilting rate on the open plots was mostly caused by the persistence of two species, *T. guttata* and *T. barbata* (Fig. 3c), which played only a minor role on the tree plots (highest cover value of 12% in the second half of May, Fig. 3d). Among forbs, nitrogen fixers, especially *Trifolium* species, became more abundant on the tree plots compared to those in the open, contributing by 36% to total cover (Fig. 2 and 3f).

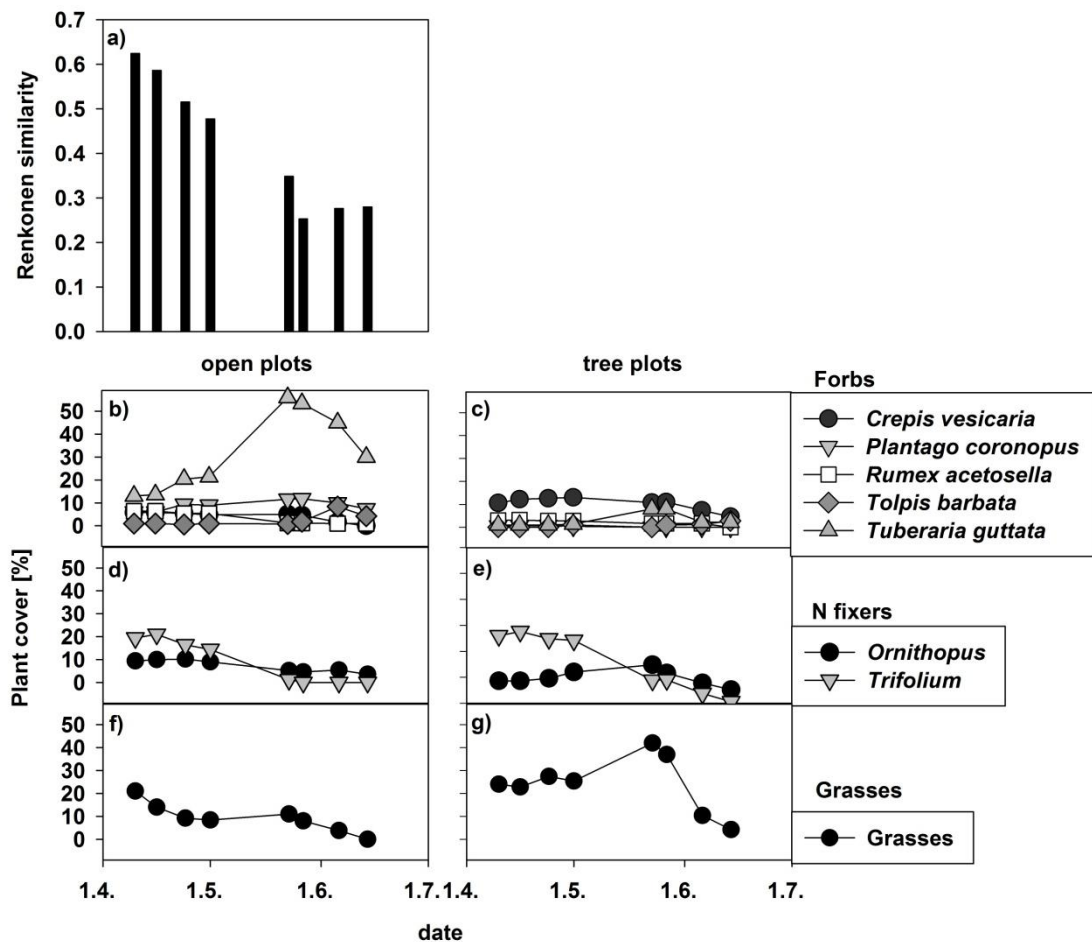


**Figure 3:** a) Renkonen index showing the relative (0-1) similarity between the open and the tree site from April to June. b-g) Relative vegetation cover in % of each species of the three functional groups of the herbaceous layer (Grasses, N-fixing and other forbs) on the open (left) and the tree site (right) from April to June (mean values; n = 5).

In contrast to spring, plant species composition was relatively homogeneous and no significant differences between locations could be found during germination and initial growth in autumn. After the first rain events in autumn plants started to germinate and quickly reached a total cover of roughly 50% within one month. During the germination phase single plants were initially so small that species identity could not be determined allowing only a general classification of grasses and forbs. Thus we did not distinguish any further between N-fixing and other forbs in autumn.

**Table 3:** Living aboveground biomass [ $\text{g m}^{-2}$ ] of distinct functional groups of the herbaceous layer (Grasses, N-fixing and other forbs) in spring and fall 2011 on the open and tree site (mean values  $\pm$  SD;  $n=5$ ).

date	open site				tree site			
	grasses	forbs		total	grasses	forbs		total
		other forbs	N-fixing forbs			other forbs	N-fixing forbs	
<b>8.4.2011</b>	$20 \pm 12$	$26 \pm 7$	$23 \pm 10$	$69 \pm 4$	$32 \pm 15$	$11 \pm 10$	$29 \pm 12$	$72 \pm 21$
<b>24.4.2011</b>	$18 \pm 3$	$30 \pm 5$	$22 \pm 5$	$70 \pm 9$	$32 \pm 8$	$10 \pm 6$	$29 \pm 10$	$71 \pm 11$
<b>27.5.2011</b>	$11 \pm 5$	$51 \pm 4$	$5 \pm 2$	$67 \pm 7$	$44 \pm 35$	$10 \pm 8$	$18 \pm 10$	$72 \pm 23$
<b>14.6.2011</b>	0	$30 \pm 20$	$3 \pm 3$	$33 \pm 12$	$6 \pm 5$	$4 \pm 3$	$7 \pm 2$	$17 \pm 9$
<b>1.11.2011</b>	$6 \pm 2$		$8 \pm 2$	$14 \pm 2$	$8 \pm 2$		$7 \pm 2$	$15 \pm 4$
<b>14.11.2011</b>	$23 \pm 7$		$20 \pm 2$	$43 \pm 7$	$23 \pm 7$		$18 \pm 2$	$41 \pm 7$

#### 4.4.3. Herbaceous layer evapotranspiration, water loss in the soil and total conductance

Total evapotranspiration ( $ET$ ) of the herbaceous layer during daytime, calculated for the open and tree plots, was generally highest during spring (Fig. 4 a, b, e, and f) and lowest during summer drought (Fig. 4 c, g), when herbaceous vegetation had vanished and soil  $\theta$  was low.  $ET$  did not differ significantly between the open and tree plots during summer and autumn (Fig. 4 c, d, g, and h; U-tests,  $p>0.05$ ) and was  $0.13 \pm 0.02 \text{ mm d}^{-1}$  during summer and  $0.4 \pm 0.03 \text{ mm d}^{-1}$  in autumn. In contrast, herbaceous layer  $ET$  was significantly lower on the tree plots compared to the open plots during spring (U-test,  $p<0.05$ ), and especially in the transition period between spring and summer (late May - mid June; Fig. 4 a, b, e, and f). Herbaceous layer  $ET$  amounted up to  $2 \text{ mm d}^{-1}$  on the open and up to  $1.7 \text{ mm d}^{-1}$  on the tree plots; on average  $ET$  was  $0.53 \pm 0.16 \text{ mm d}^{-1}$  higher on the open plots between late May and mid June (Fig. 4 b, f). In contrast to summer and autumn where  $ET$  was relatively stable,  $ET$  was highly variable in spring on both locations.  $ET$  correlated well with  $VPD$  (in case of soil  $\theta > 0.09 \text{ m}^3 \text{ m}^{-3}$ ) and soil  $\theta$  (in case of  $VPD > 0.8 \text{ kPa}$ ; data not shown). Typically, rain events occurred roughly every 7-10 days during spring, followed by dry-down periods (Fig. 1 a, c), leading to rapid changes in  $VPD$  and  $\theta$  and hence  $ET$ .

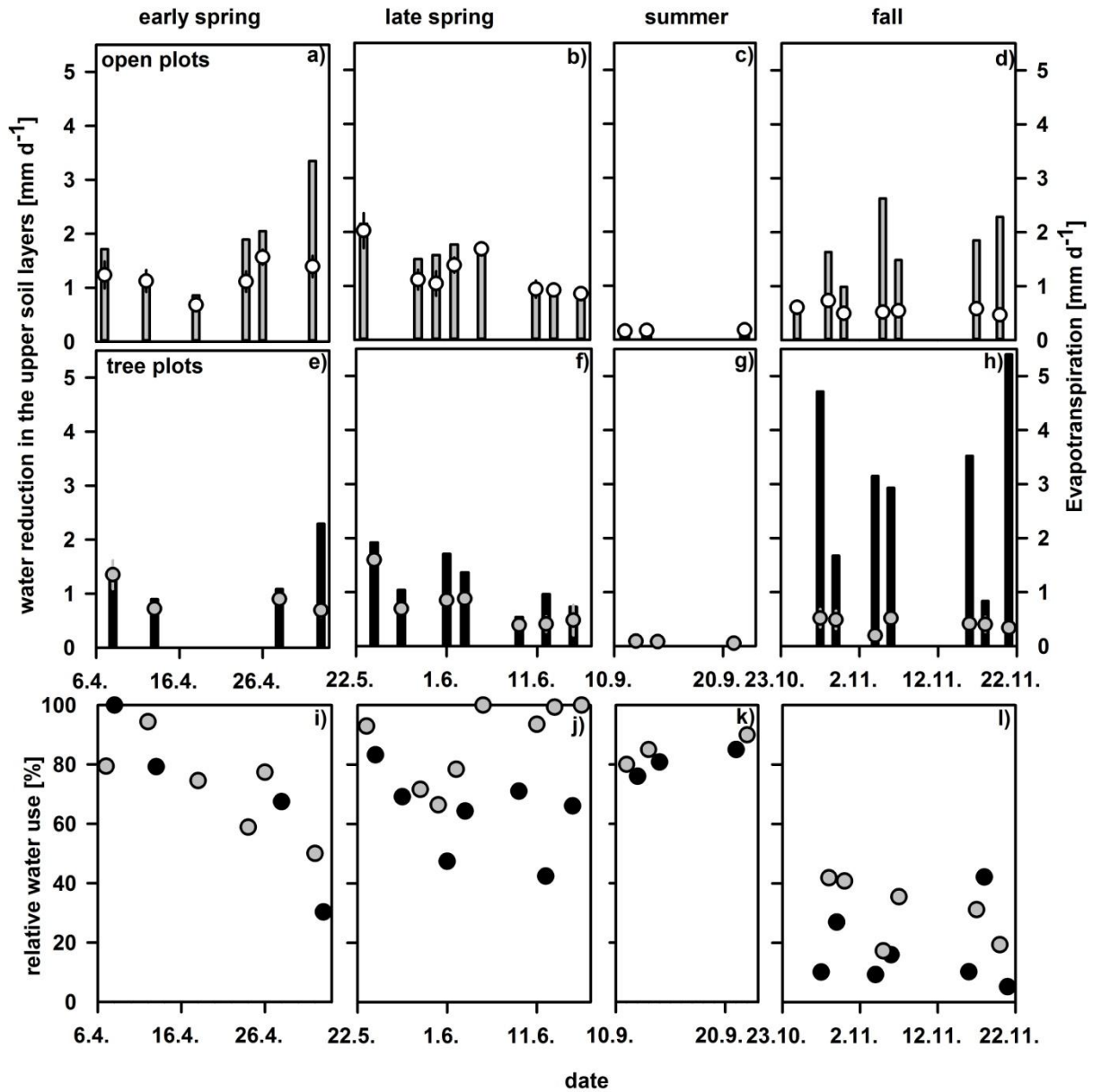


**Figure 4:** a-h) Total daily water reduction in the upper 60 cm of the soil in the open and the tree plots (grey and black bars, respectively) as well as total herbaceous evapotranspiration (*ET*) during daylight on the open (a-d) and tree plots (e-h; white and black circles, respectively). Results are presented as mean values ( $\pm$  SD in case of *ET*;  $n=3-4$ ) and i-l) relative water use of the herbaceous layer [%] on the open (grey circles) and tree plots (black circles), between April 4 and November 22, 2011: early spring (a, e, i), late spring (b, f, j), summer (c, g, k), and fall (d, h, l).

The total daily water loss within the upper soil layers (where herbaceous roots were detected from 0 to roughly 60 cm soil depth) was highest during times of high rainfall in autumn (up to 5 mm d<sup>-1</sup>) and lowest during summer drought ( $0.15 \pm 0.02$  mm d<sup>-1</sup>; Fig. 4). During springtime water loss in the soil profile mainly followed rainfall patterns with high soil water loss immediately after rainfall reaching 2

and  $2.2 \text{ mm d}^{-1}$  in the tree and open plots, respectively. Mean spring water loss from the upper soil layers was similar in both plots with  $1.400 \pm 0.2 \text{ mm d}^{-1}$ .

By relating the total daily water loss from the upper soil layers to total daily *ET* of the herbaceous layer we calculated the relative contribution of *ET* to the total water loss from the upper soil where herbaceous roots have access (thereafter termed “relative soil water use”, Fig. 4i-l). In general, relative soil water use was high during dry periods (spring and summer, Fig. 4i-k) and low during wet periods (autumn, Fig. 4l). During early spring (April 6 to May 23) relative soil water use did not differ much between the study locations. However, starting from the onset of summer in late May until mid June it was clearly visible that the relative soil water use was considerably higher on open plots, reaching 100%. In comparison the relative soil water use on the tree plots was only 60% on average during this period.

#### 4.4.4. Net $\text{CO}_2$ exchange of the herbaceous layer

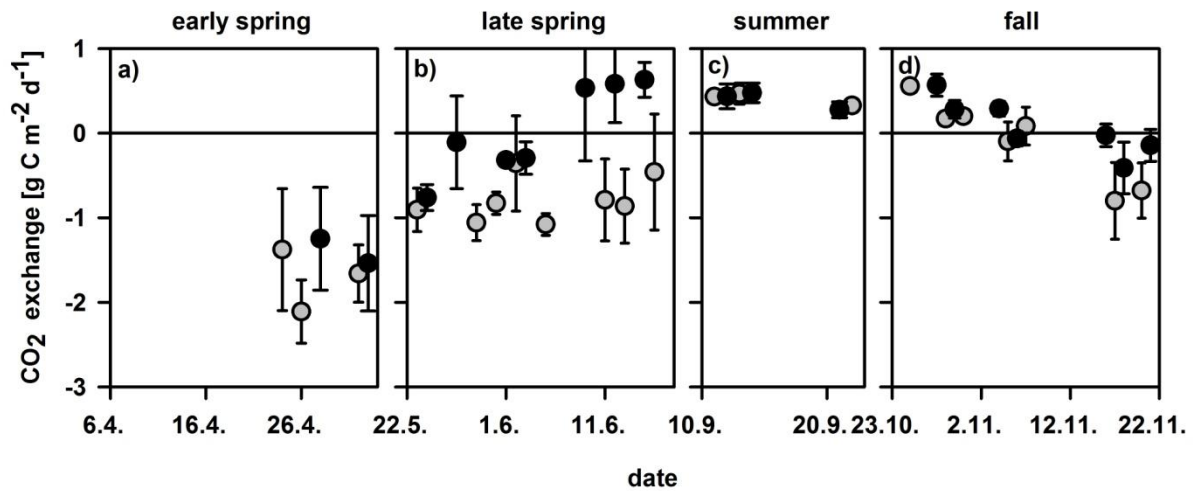


**Figure 5:** a-d) Total net  $\text{CO}_2$  exchange during daylight on the open and tree site (grey and black cycles) during the four measurement campaigns between April 24 and November 22, 2011: early spring (a), late spring (b), summer (c), and fall (d). Results are mean values  $\pm$  SD ( $n=3$ ).

Total net herbaceous  $\text{CO}_2$  exchange during daytime (*NEE*; comprising plant and soil net  $\text{CO}_2$  exchange) was calculated for the open and tree plots ranging between  $-2.1 \pm 0.38$  and  $0.56 \pm 0.08 \text{ g C m}^{-2} \text{ d}^{-1}$  (negative and positive values indicate net  $\text{CO}_2$  uptake and release, respectively; Fig. 5a-d). Generally, herbaceous net  $\text{CO}_2$  uptake was highest during the growth peak in April and declined

during the spring to summer transition with the dying of the herbaceous vegetation and dry down of the soil (Fig. 5a-d). In the absence of living herbaceous vegetation we found net respiration of maximum  $0.56 \pm 0.08 \text{ g C m}^{-2} \text{ d}^{-1}$  in September and October before the germination of the herbaceous vegetation. After the first rainfall at the end of October herbaceous fluxes turned from net respiration to net carbon uptake within 2 weeks only (Fig. 5d). Thereafter, net carbon uptake ranged between  $-0.02 \pm 0.13$  and  $-0.8 \pm 0.45 \text{ g C m}^{-2} \text{ d}^{-1}$  and remained considerably smaller than spring time values. While *NEE* was similar on both plots during summer and autumn (Mann-Whitney-U tests, n.s.), we found lower net  $\text{CO}_2$  uptake on tree plots during spring, which became more and more pronounced with the transition to summer drought ( $p < 0.05$  between June 1 and 16). The shift from a net carbon sink to a net carbon source was considerably earlier on tree plots (beginning of June) when we still observed net  $\text{CO}_2$  uptake of on average  $-0.66 \pm 0.18 \text{ g C m}^{-2} \text{ d}^{-1}$  on open plots.

Strong differences in *PPFD* between open and tree plots could be detected between April and October and led to the assumption that the differences between locations in herbaceous  $\text{CO}_2$  uptake in late spring might be related with a shading effect of the tree canopy. However, no correlations between *PPFD* and *NEE* in spring time (April-June) within each plot type could be detected (Fig. 6a) and also no correlation between the differences between locations in *PPFD* and in *NEE* was found (Fig. 6d). In contrast, location specific differences were found in spring regarding the relationship of *NEE* and soil water content ( $\theta$ ). Under the trees *NEE* seemed to be strongly influenced by  $\theta$  in spring, while this was not the case for the open area (Fig. 6b). Moreover, the difference in relative soil water use between open and tree plots was highly correlated to open versus tree plot differences in *NEE* (Fig. 6e).

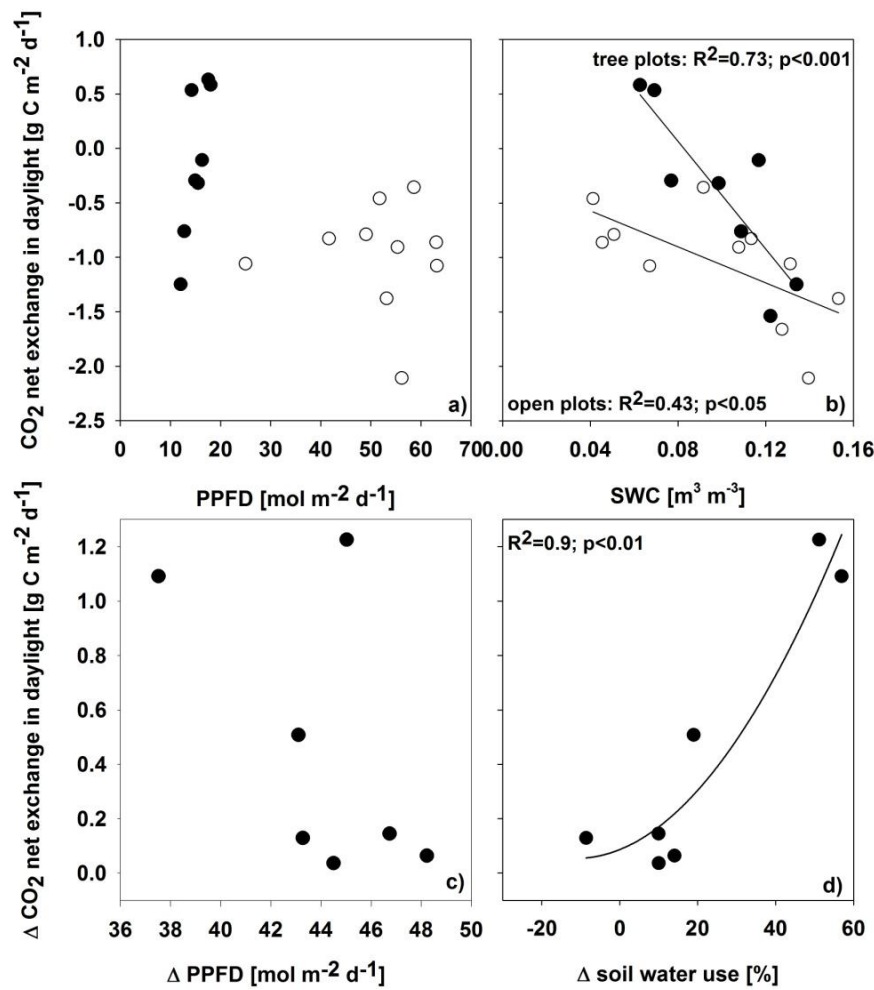


**Figure 6:** a-b) Open and tree site (white and black circles, respectively) net  $\text{CO}_2$  exchange during daylight ( $NEE$ ) in spring (April-June) versus open and tree site photosynthetic photon flux density (a, PPFD), and soil water content in 5 cm depth (b). c-d) Difference between open and tree site in spring ( $\Delta_{\text{open}} - \text{tree site}$ ; April-June) net  $\text{CO}_2$  exchange during daylight ( $NEE$ ) versus difference between open and tree site photosynthetic photon flux density (c, PPFD), and water use (d). Sites specific differences could only be calculated for measurements on consecutive days. Black lines depict linear regressions between  $NEE$  and  $SWC$  (b) and non-linear regressions between  $\Delta NEE$  and  $\Delta \text{soil water use}$  (d).

#### 4.5. Discussion

Interactions between different ecosystem plant layers are always a sum of facilitation and competition effects (Campbell et al., 1991). Previous studies have demonstrated that the nature of the influence of trees on herbaceous vegetation is highly variable between ecosystems and often depends on general ecosystem characteristics such as physical soil properties, annual amount of rainfall and radiation (Hussain et al., 2009; Moreno, 2008). For Mediterranean oak woodlands with annual precipitation regimes similar to our field site, previous studies often report beneficial effects of tree presence on herbaceous biomass production (Cubera and Moreno, 2007; Joffre and Rambal, 1993). However, most of these studies focus on herbaceous productivity and crop yield rather than the influence of trees regarding species composition, water and carbon fluxes and competitive balance within a year or even season. In the following, we will discuss 1) the influence of tree cover on herbaceous layer cover and

biomass development, species composition and functional group abundance in distinct seasons and 2) address how competition for water between trees and herbaceous vegetation affects herbaceous layer longevity and its contribution to ecosystem carbon gain during spring.

#### *4.5.1. Influence of tree cover on herbaceous layer productivity and the development of distinct functional groups*

Biomass development is mainly influenced by microclimatic conditions, soil water and nutrient availability (Pereira et al., 2006). For Mediterranean evergreen oak-savannahs, it has been shown that the positive effects of tree cover on microclimatic conditions, such as reduced light stress and temperature, may counterbalance negative effects of trees through competition for soil water or nutrients (Moreno, 2008; Scholes and Archer, 1997), which is in accordance with the stress gradient hypothesis that postulates increasing importance of facilitation with increasing abiotic stress (Bertness and Callaway, 1994). However, recent studies demonstrated that this cannot be generalized for arid or semi-arid regions (Maestre et al., 2005; 2006; Rolo and Moreno, 2011). For example, Moreno (2008) showed that the positive effect of trees on microclimatic conditions has a strong effect in sub-humid oak savannahs, while this may be counterbalanced by competition for water in semi-arid savannahs.

Here a facilitating effect of tree cover herbaceous total green aboveground biomass and total green herbaceous ground cover could not be detected (70 and 72 g m<sup>-2</sup> and 88 and 90 % cover in the open and tree plots, respectively, Fig. 2, Table 3). Further, net CO<sub>2</sub> exchange was not significantly different between open and tree plots during most of the study period (Fig. 5). It is likely that tree cover did not have a significant influence on aboveground biomass production during most parts of the vegetation period, because its influence on microclimate and soil properties became significant only late within the main vegetative growth phase of the herbaceous plants, i.e. between April and May when peak biomass and cover, and during summer where herbaceous plants were dormant (see also Hussain et al., 2009; Ma et al., 2007; Aires et al., 2008).

Scholes and Archer (1997) report, that the difference in species composition beneath and beyond the tree cover is stronger in low rainfall sites and weaker in high rainfall sites. Considering overall annual rainfall amount and species composition in early April, this is in agreement with our results, which is



underlined by the high Renkonen-similarity ratio of 66% at the beginning of April. However, the timing of precipitation and drought periods can further lead to strong intra-annual differences in location specific biomass and cover development (Schwinning and Ehleringer, 2001; Miranda et al., 2002; Jongen et al., 2011). Accordingly, an increasing deviation in % cover of different functional groups could be observed starting from mid April. This development corresponded well to the growing plot differences in microclimatic conditions and a first 3 week dry-down period, which resulted in soil moisture contents below  $0.05 \text{ m}^3\text{m}^{-3}$  (Fig. 1c). Plants adapted to high radiation, temperature and aridity (native forbs such as *T. guttata* and *T. barbata*; Ellenberg, 1996) increased in abundance (i.e. % ground cover) in the open plots, profiting from the strong decline in total cover of species probably less tolerant towards drought and high light conditions such as grasses, i.e. *Briza maxima*, *Lolium multiflorum* and the *Vulpia* species, or introduced legumes such as *Ornithopus* or *Trifolium* (Jongen et al., 2013a, b). In the open area the decline in grass and N-fixer cover and biomass was only compensated by the increase of native forbs at the end of May, leading to slightly lower total plant cover at the open area compared to below tree plots between mid April to beginning of May. Likewise, grasses increased their total cover and aboveground biomass on tree plots during the same time, profiting from the shading effect of the trees. The higher cover and biomass of legumes under trees during late spring/drought onset may be related with their supposed competitive advantage due to their ability to fix nitrogen (Snapp and Silim, 2002), since the availability of nitrate in the soil under the trees was extremely low during May (Table 2; see also Jongen et al., 2013b; Otieno et al., 2011). Finally, it has to be noted, that although tree vs. open plot differences regarding cover and biomass were not significant at the first sampling point in April, a higher abundance of native forbs on open plots and of nitrogen fixing forbs on tree plots was already prevalent from the previous year. Therefore, increased long term deviation of the herbaceous vegetation under trees and in the open can thus be expected although the regular process of sowing at this site (every 3-5 years) disrupts this development. Indeed, a shift in species composition and abundance from spring 2010 (first growth period after sowing) to spring 2011 could be observed (data not shown), indicating that 1) the seed mixture had a distinctive effect on species composition of the herbaceous layer and 2) this effect declines swiftly even within one year. Specifically the abundance of *Trifolium* species, which were

included in the seed mixture, declined from 2010 to 2011 throughout the entire study site and the abundance of naturally occurring grasses (below the trees) and of native forbs (*Tuberaria* and *Tolpis*, in the open area) increased at the same time (M. Jongen, personal communication).

#### 4.5.2. *Competition for water during late spring between herbaceous layer and trees*

A shift from competition to facilitation following increasing environmental stress over the course of one growing season has been observed by Kikvidze et al. (2006). Here, we found neither a clear net facilitation nor competition effect under favorable conditions until late May. However, when environmental stress increased, i.e. soil water contents dropped to  $0.05 \text{ m}^3 \text{ m}^{-3}$ , and the “stress gradient hypothesis” would predict an increased facilitation effect by the trees (Bertness and Callaway, 1994), in fact the opposite was observed: in the understory of trees the herbaceous layer turned from being a  $\text{CO}_2$  sink to a  $\text{CO}_2$  source two weeks earlier compared to the open area, accompanied by a drastic decrease in aboveground living biomass and green cover. During these two weeks net  $\text{CO}_2$  uptake on open plots still amounted ca.  $-0.66 \pm 0.18 \text{ g C m}^{-2} \text{ d}^{-1}$  (fig. 5), indicating that tree cover strongly reduced the herbaceous carbon gain. This might even influence the ecosystem carbon sink strength, since Unger et al. (2009) found that herbaceous plants can make up to over 50% of total ecosystem *GPP* during spring time, thus playing a significant role for ecosystem productivity (Aires et al., 2008; Jongen et al., 2011; Pereira et al., 2007). It has to be noted however, that net  $\text{CO}_2$  fluxes were measured here, so that a decline in *NEE* might be both related to lower herbaceous plant uptake and higher respiration rates of soil microorganisms or roots.

In contrast to previous findings (Hussain et al., 2009), light was not a limiting factor for  $\text{CO}_2$  uptake on either of the locations in our study (Fig. 6a). Additionally, no correlations were observed between the differences in net  $\text{CO}_2$  exchange and light intensity (Fig. 6c). Unfortunately, air temperature and relative humidity were not continuously recorded on each of the plots separately, however point measurements of air temperature did not reveal significant differences between the plots (data not shown), although differences in soil temperature could be detected (Fig. 1). Thus, the early senescence observed under the trees cannot simply be related to microclimatic conditions in our study.

Instead, early senescence corresponding with lower carbon and water fluxes under the trees provides a

strong indication for enhanced belowground competition with trees for water (Scholes and Archer, 1997; Cubera and Moreno, 2007; Moreno et al., 2007). This was not visible from soil water content measurements alone, being similar on both locations and in summer even slightly higher under the trees (Fig. 1). However, during spring a strong difference of the relative soil water use of the herbaceous layer was detected on the tree compared to the open plots (Fig. 4i-l). This can be attributed either to higher drainage/runoff rates or a second sink, i.e. trees taking up water from these depths (0-60 cm). Higher drainage or runoff rates are unlikely, since only very small amounts of rainfall occurred during that time and soil water content was rather low (Fig. 1), suggesting that competition with oak trees for water from the top soil layers negatively affected carbon gain and thus longevity at the end of the herbaceous growth period (Fig. 6b,d). The observed shift of species composition towards grasses and N-fixing forbs under the trees, which are less adapted to drought and high temperatures, might have further accelerated this development. Trees surely tap into ground water or deep soil layers for water supply at this site (Kurz-Besson et al., 2006), and several studies report a niche differentiation regarding the depth of water uptake between trees and herbaceous layer in these ecosystem types (Moreno, 2008; Moreno et al., 2007). By contrast, Rolo and Moreno (2011) found strong competition for water between evergreen oaks and shallow rooted *Cistus ladanifer*, indicating that spatial niche differentiation regarding water and resource uptake between different plant layers is not a general mechanism. Moreover, by using water from the upper soil layers trees can also meet their nutrient need for nitrogen (Table 2). Moreno et al. (2007) speculated that trees do not rely on the upper 30 cm of the soil to take up nutrients. Our results on the other hand suggest that with increasing soil depth nitrate content decreased markedly (see also Otieno et al., 2011). It has to be noted, that measured nitrate content represents just a portion of total N-content and hence interpretation of plant N-availability must be treated with care. Jongen et al. (2013b) found that sometimes ammonium-N was more abundant at the same study site: i.e. 1) during rainy periods, due to higher mobility of nitrate-N and 2) during the main growth period of the herbaceous layer and the oak trees, which can be explained by preferential uptake of nitrate-N by the vegetation (Austin et al., 2006; Marschner, 2012; Jongen et al., 2013b). However, the exponential decrease in nitrate content along the soil profile observed here is very similar to the spatial pattern of total N-content observed by Otieno et al. (2011)

during spring in a comparative cork-oak stand in Portugal. Therefore, we assume that these upper 30 cm of the soil profile might be important for the nitrogen uptake of the overstory trees especially in the growing season, between early May and end of June in 2011. This indicates that the herbaceous plants were exposed to a strong competition for water and possibly nitrogen induced by the overstory trees, leading to lower carbon gain and early senescence.

#### **4.6. Conclusions**

During large parts of the year no significant influence of tree cover regarding maximum total aboveground biomass or cover of the understory could be found. Only by the end of the herbaceous vegetation growing period (during the last 6 weeks before senescence) there was a significant impact of tree cover on herbaceous plants development and net CO<sub>2</sub> and water fluxes. This led 1) to a deviation between open and tree plots regarding the abundance of distinct functional groups and 2) to an earlier and faster senescence of the herbaceous layer under the trees, due to a strong competition for water and possibly nutrients that strongly affected the overall carbon gain of the herbaceous layer during spring.

Our results indicate that the nature of the influence of tree cover on the herbaceous layer changes swiftly within weeks. Thus, our results clearly emphasize the complexity of the interactions between trees and the herbaceous layer occurring at different spatial and temporal resolution.

#### **4.7. Acknowledgements**

We thank the owners and employees of Herdade da Machoqueira do Grou for logistical support and allowing the establishment of our field site. We gratefully acknowledge help in the field from Fabio Gonsalvez, Jan Sauer and Katrin Remmert. We especially thank Marjan Jongen for help with species identification and discussions on the results, Katie Rascher, Tom Steinlein and an anonymous reviewer for valuable comments on the manuscript and Babsi Teichner for technical assistance in the lab. Funding for this project was provided by the Deutsche Forschungsgemeinschaft (WATERFLUX Project: # WE 2681-61; # CU 173/2-1) and the Deutsche Akademische Austausch Dienst.

#### 4.8. Literature

- Aires, L., Pio C., Pereira, J., 2008. Carbon dioxide exchange above a Mediterranean C3/C4 grassland during two climatologically contrasting years. *Global Change Biology*, 14: 539–555.
- Austin, A.T., Sala, O.E., Jackson, R.B., 2006. Inhibition of nitrification alters carbon turnover in the Patagonian steppe. *Ecosystems*, 9: 1257-1265.
- Bertness, M.D., Callaway, R., 1994. Positive interactions in communities. *TREE*, 9: 191- 193.
- Braun-Blanquet, J., 1964. *Pflanzensoziologie: Grundzüge der Vegetationskunde*. Third ed. Springer, Vienna.
- Caldwell, M., Dawson, T., Richards, J., 1998. Hydraulic Lift: Consequences of Water Efflux from the Roots of Plants. *Oecologia*, 113: 151-161.
- Campbell, B.D., Grime, J.P., Mackey, J.M.L., Jalili, A., 1991. The quest for a mechanistic understanding of resource competition in plant-communities- the role of experiments. *Functional Ecology*, 5: 241-253.
- Casado, M., Castro I., Ramírez-Sanz L., Costa-Tenorio M., de Miguel J., Francisco D., 2004. Herbaceous Plant Richness and Vegetation Cover in Mediterranean Grasslands and Shrublands. *Plant Ecology*, 170: 83-91.
- Costa, A., Pereira, H., Madeira, M., 2009. Landscape dynamics in endangered cork-oak woodlands in Southwestern Portugal (1958-2005). *Agroforestry Systems*, 77: 83-96.
- Crespo, D.G., 2006. The role of pasture improvement in the rehabilitation of the “montado/dehesa” system and in developing its traditional products. In: Ribeiro, J.M.C.R., Horta, A.E.M., Mosconi, C., Rosati, A. (eds.), *Animal Products from the Mediterranean Area*, Wageningen Academical Publishing, Wageningen.
- Cubera E., Moreno G., 2007. Effect of single *Quercus ilex* trees upon spatial and seasonal changes in soil water content in Dehesas of central western Spain. *Annals for Forest Science*, 64: 355 – 364.
- Diaz M., Campos P., Pulido F., 1997. The Spanish dehesas: a diversity of land uses and wildlife. In: Pain D and Pienkowski M (Eds). *Farming and birds in Europe: the common agricultural policy and its implications for bird conservation*. London, UK: Academic Press.
- Dubbert M., Cuntz M., Piayda A., Maguas C., Werner C., 2013. Partitioning evapotranspiration – Testing the Craig and Gordon model with field measurements of oxygen isotope ratios of evaporative fluxes. *Journal of Hydrology*.
- Ellenberg, H., 1996. *Vegetation Mitteleuropas mit den Alpen*. 5. Auflage, Stuttgart, Ulmer Verlag.
- Figuerola, M., Davy A., 1991. Response of Mediterranean grassland species to changing rainfall. *Journal of Ecology*, 79: 925–941.
- Gallardo A., Rodríguez-Saucedo J.J., Covelo F., Fernández-Alés R., 2000 Soil nitrogen heterogeneity in a Dehesa ecosystem. *Plant and Soil*, 222: 71-82.
- Gallardo, A., 2003. Effect of tree canopy on the spatial distribution of soil nutrients in a Mediterranean dehesa. *Pedobiologia*, 47: 117-125.
- Huber-Sannwald, E., Jackson, R.B., 2001. Heterogeneous soil-resource distribution and plant responses – from individual-plant growth to ecosystem functioning. *Progress in Botany*, 62: 451-476.
- Hussain M., Otieno D., Mirzae H., Li Y., Schmidt M., Siebke L., Foken T., Ribeiro N., Pereira J., Tenhunen J., 2009. CO<sub>2</sub> exchange and biomass development of the herbaceous vegetation in the Portuguese montado ecosystem during spring. *Agriculture, Ecosystems and Environment*, 132: 143-152.
- Joffre, R., Rambal, S., 1993. How Tree Cover Influences the Water Balance of Mediterranean Rangelands. *Ecology*, 74: 570-582.

- Jongen, M., Pereira, J., Igreja Aires, L., Pioc, C., 2011. The effects of drought and timing of precipitation on the inter-annual variation in ecosystem-atmosphere exchange in a Mediterranean grassland. *Agricultural and Forest Meteorology*, 151: 595–606.
- Jongen, M., Lecomte, X., Unger, S., Pinto-Marijuan, M., Pereira, J.S., 2013a. The impact of changes in the timing of precipitation on the herbaceous understorey of Mediterranean evergreen oak woodlands. *Agricultural and Forest Meteorology*, 171:163-173.
- Jongen, M., Lecomte, X., Unger, S., Fangueiro, D., Pereira, J.S., 2013b. Precipitation variability does not affect soil respiration and nitrogen dynamics in the understorey of a Mediterranean oak woodland. *Plant and Soil*.
- José S., Gillespie A., Pallardy, S., 2004. Interspecific interactions in temperate agroforestry: New visitas in Agroforestry. *Agroforestry Systems* 61, Number 1.
- Kikvidze, Z., Khetsuriani, L., Kikodze, D., Callaway, R., 2006. Seasonal shifts in competition and facilitation in subalpine plant communities of the central Caucasus. *Journal of Vegetation Science*, 17: 77–82.
- Krebs, C., 1998. *Ecological Methodology*. Second ed. Addison-Welsey Longman.
- Kurz-Besson C., Otieno D., Lobo-do-Vale R., Siegwolf R., Schmidt M., David T., Soares David J., Tenhunen J., Pereira J. S., Chaves M., 2006. Hydraulic lift in cork-oak trees in a savannah-type Mediterranean ecosystem and its contribution to the local water balance. *Plant and Soil*, 282: 361-378.
- Ludwig, F., Dawson, T., Prins, H., Berendse, F., De Kroon, H., 2004. Below-ground competition between trees and grasses may overwhelm the facilitative effects of hydraulic lift. *Ecology Letters*, 7: 623–631.
- Ma, S., Baldocchi, D.D., Xu, L., Hehn, T., 2007. Inter-annual variability in carbon dioxide exchange of an oak/grass savannah and open grassland in California. *Agricultural and Forest Meteorology*, 147: 157–171.
- Maestre, F., Valladares, F., Reynolds, J., 2005. Is the change of plant-plant interaction with abiotic stress predictable? A meta analysis of field results in arid environments. *Journal of Ecology*, 93: 748-137.
- Maestre, F., Valladares, F., Reynolds, J., 2006. The stress-gradient hypothesis does not fit all relationships between plant-plant interactions and abiotic stress: further insights from arid environments. *Journal of Ecology*, 94: 17-22.
- Maestre, F., Callaway, R.M., Valladares, F., Lortie, C.J., 2009. Refining the stress-gradient hypothesis for competition and facilitation in plant communities. *Journal of Ecology*, 97: 199-205.
- Marschner, P., 2012. *Marschner's mineral nutrition of higher plants*. Academic, London.
- Miranda, P., Coelho F., Tomé A., Valente M., Carvalho, A., Pires, C., Pires, H., Pires, V., Ramalho, C., 2002. 20th century Portuguese Climate and Climate Scenarios, in Santos, F.D., K. Forbes, and R. Moita (eds), *Climate Change in Portugal: Scenarios, Impacts and Adaptation Measures (SIAM Project)*: 454 pp.
- Moreno, G., Obrador, J.J., Cubera, E., Dupraz, C., 2005. Fine root distribution in Dehesas of Central-Western Spain. *Plant and Soil*, 277: 153-162.
- Moreno G., Obrador, J., García, E., Cubera, E., Montero, M., Pulido, F., Dupraz, C., 2007. Driving competitive and facilitative interactions in oak dehesas through management practices. *Agroforestry Systems*, 70: 25-40.
- Moreno, G., 2008. Response of understorey forage to multiple tree effects in Iberian dehesas. *Agriculture, Ecosystems and Environment*, 123: 239-244.
- Otieno, D., Mirzaei, H., Hussain, M., Li, Y., Schmidt, M., Waringer, M., Jung, E., Ribeiro, N., Pereira, J., Tenhunen, J., 2011. Herbaceous layer development during spring does not deplete soil nitrogen in the Portuguese Montado. *Journal of Arid Environments*, 75: 231-238.

- Paço, T.A., David, T.S., Henriques, M.O., Pereira, J.S., Valente, F., Banza, J., Pereira, F.L., Pinto, C., David, J.S., 2009. Evapotranspiration from a Mediterranean evergreen oak savannah: The role of trees and pasture. *Journal of Hydrology*, 369: 98-106.
- Pape, L., Ammann, C., Nyfeler-Brunner, A., Spirig, C., Hens, K., and Meixner, F.X., 2009. An automated dynamic chamber system for surface exchange measurement of non-reactive and reactive trace gases of grassland ecosystems. *Biogeosciences*, 6: 405-429.
- Pereira, J.S., Chaves, M.-M., Caldeira, M.-C., Correia, A.V., 2006. Water availability and production. In: Morison, J.I.L., Morecroft, M.D. (eds), *Plant growth and climate change*. Blackwell Publishing Ltd., Oxford.
- Pereira, J.S., Mateus, J.A., Aires, L.M., Pit, G., Pio, C., David, J.S., Andrade, V., Banz, J., David, T.S., Paço, T.A., Rodrigues, A., 2007. Net ecosystem carbon exchange in three contrasting Mediterranean ecosystems – the effect of drought. *Biogeosciences*, 4: 791-02.
- Perez-Ramos, I., Zavala, M., Maranon T., Diaz-Villa, M., Valladares, F., 2008. Dynamics of understorey herbaceous plant diversity following shrub clearing of cork-oak forests: A five-year study. *Forest Ecology and Management*, 255: 3242-3253.
- Pulido, F., Garcia, E., Obrador, J., Moreno, G., 2010. Multiple pathways for tree regeneration in anthropogenic savannas: incorporating biotic and abiotic drivers into management schemes. *Journal of Applied Ecology*.
- Rolo, V., Moreno, G., 2011. Shrub species affect distinctively the functioning of scattered *Quercus ilex* trees in Mediterranean open woodlands. *Forest Ecology and Management*, 261: 1750-1759.
- Scholes, R.J., Archer, S.R., 1997. Tree-grass interactions in savannas. *Annual Review of Ecology and Systematics*, 28: 517-544.
- Schwinning S., Ehleringer J., 2001. Water use trade-offs and optimal adaptations to pulse-driven arid ecosystems. *Journal of Ecology*, 89: 464–48.
- Snapp, S.S., Silim, S.N., 2002. Farmer preferences and legume intensification for low nutrient environments. *Plant and Soil*, 245: 181-192.
- Unger S., Máguas C., Pereira J.S., Aires L.M., David T.S. & Werner C., 2009. Partitioning carbon fluxes in a Mediterranean oak forest to disentangle changes in ecosystem sink strength during drought. *Agricultural and Forest Meteorology*, 149: 949–961.
- Unger, S., Maguas, C., Pereira, J.S., Aires, L.M., David, T.S., Werner, C., 2010. Disentangling drought-induced variation in ecosystem and soil respiration using stable carbon isotopes. *Oecologia*, 163: 1043-1057.
- Von Caemmerer, S., Farquhar, G.D., 1981. Some relationships between the biochemistry of photosynthesis and the gas-exchange of leaves. *Planta*, 153: 376-387.
- Werner C., Correia O., 1996. Photoinhibition in cork-oak leaves under stress: Influence of the bark-stripping on the chlorophyll fluorescence emission in *Quercus suber* L. *Trees – Structure and Function*, 10: 288-292.
- Werner C., Ryel R., Correia O., Beyschlag W., 2001. Effects of photoinhibition on whole-plant carbon gain assessed with a photosynthesis model. *Plant, Cell and Environment*, 24: 27-40.
- Werner, C., Correia, O., Beyschlag, W., 2002. Characteristic patterns of chronic and dynamic photoinhibition of different functional groups in a Mediterranean ecosystem. *Functional Plant Biology*, 29: 999-1011.



## **5. STUDY V: STABLE OXYGEN ISOTOPE AND FLUX PARTITIONING DEMONSTRATES UNDERSTORY OF AN OAK SAVANNA CONTRIBUTES UP TO HALF OF ECOSYSTEM CARBON AND WATER EXCHANGE**

Maren Dubbert<sup>1,✉</sup>; Arndt Piayda<sup>2</sup>; Matthias Cuntz<sup>2</sup>; Alexandra C. Correia<sup>3</sup>;  
Filipe Costa e Silva<sup>3</sup>; Joao S. Pereira<sup>3</sup>; and Christiane Werner<sup>1</sup>

<sup>1</sup>Agroecosystem Research, University of Bayreuth, BayCEER, Universitätsstraße 30, 95447 Bayreuth, Germany

<sup>2</sup>UFZ – Computational Hydrosystems, Helmholtz Centre for Environmental Research, Permoserstraße 15, 04318 Leipzig, Germany

<sup>3</sup>Instituto Superior de Agronomia, Technical University of Lisbon, Tapada da Ajuda, Lisbon, Portugal;

✉ Corresponding author: Maren Dubbert ([maren.dubbert@uni-bayreuth.de](mailto:maren.dubbert@uni-bayreuth.de))





## 5.1. Abstract

Semi-arid ecosystems contribute about 40% to global net primary production (*GPP*) even though water is a major factor limiting carbon uptake. Evapotranspiration (*ET*) accounts for up to 95% of the water loss and in addition, vegetation can also mitigate drought effects by altering soil water distribution. Hence, partitioning of carbon and water fluxes between the soil and vegetation components is crucial to gain mechanistic understanding of vegetation effects on carbon and water cycling. However, the possible impact of herbaceous vegetation in savanna type ecosystems is often overlooked. Therefore, we aimed at quantifying understory vegetation effects on the water balance and productivity of a Mediterranean oak savanna. *ET* and net ecosystem  $\text{CO}_2$  exchange (*NEE*) were partitioned based on flux and stable oxygen isotope measurements and also rain infiltration was estimated.

The understory vegetation contributed importantly to total ecosystem *ET* and *GPP* with a maximum of 43% and 51%, respectively. It reached water-use efficiencies (*WUE*; ratio of carbon gain by water loss) similar to cork-oak trees. The understory vegetation inhibited soil evaporation (*E*) and, although *E* was large during wet periods, it did not diminish *WUE* during water-limited times. The understory strongly increased soil water infiltration, specifically following major rain events. At the same time, the understory itself was vulnerable to drought, which led to an earlier senescence of the understory growing under trees as compared to open areas, due to competition for water.

Thus, beneficial understory effects are dominant and contribute to the resilience of this ecosystem. At the same time the vulnerability of the understory to drought suggests that future climate change scenarios for the Mediterranean basin threaten understory development. This in turn will very likely diminish beneficial understory effects like infiltration and ground water recharge and therefore ecosystem resilience to drought.

## 5.2. Introduction

Semi-arid ecosystems contribute about 40% to global net primary productivity (Wang *et al.*, 2012) and in these ecosystems water and carbon dioxide cycles are tightly coupled via ecosystem water use efficiency (David *et al.*, 2004; Pereira *et al.*, 2006). Global climate change is expected to intensify drought and alter precipitation patterns in dry-land regions (IPCC 2007). Moreover, evapotranspiration (*ET*) accounts for up to 95% of the water loss from the ecosystem (Huxman *et al.*, 2005). *ET* has two distinct components: plant transpiration (*T*) and unproductive loss of water during soil evaporation (*E*). Due to their open bi-layered structure, savanna-type ecosystems are particularly suitable to study the effect of water scarcity and the coupling between hydrological and biogeochemical processes of different plant layers (woody vs. herbaceous species) and the soil. They cover large areas world-wide and in Europe they are the predominant land cover type on the southern Iberian Peninsula, covering about 1.5 Mio ha (Bugalho *et al.*, 2011). They consist of a sparse tree cover (e.g. cork-oak, *Quercus suber* L. and holm oak, *Q. ilex*) and an herbaceous understory layer. They are exploited as often low-impact agro-forestry ecosystems with high biodiversity, specifically of the herbaceous layer, and considered a habitat of high conservation value (Moreno *et al.*, 2005; Perez-Ramos *et al.*, 2008). Hence, their sustainability is vitally important for both agronomical and biodiversity aspects, but is currently being threatened by unbalanced management practices (Bugalho *et al.*, 2011). Moreover, while trees have access to deeper soil layers and/or groundwater, shallow rooted herbaceous plants are vulnerable to drought and die back at the onset of summer drought (Paço *et al.*, 2009). Still, the herbaceous understory vegetation has a strong impact on ecosystem productivity: it can make up to more than 50% of total gross primary productivity (*GPP*) during spring (Unger *et al.*, 2009, 2010). While the impact of herbaceous plants and soil on carbon cycling in oak savannas is relatively well characterized, less is known concerning their role in the ecosystem water cycle. In general, introducing dense herbaceous layers to maximize the productive and minimize the unproductive water loss by reducing open soil patches (Wang *et al.*, 2010; Raz-Yaseef *et al.*, 2012) has been considered a major goal in dry-lands (Wang and D'Odorico, 2008). However, the presence of (herbaceous) vegetation has various other impacts on soil water relations than sheer reduction of soil evaporation. Rainfall might be intercepted while at the same time hydraulic redistribution might be altered depending on rooting

depths and structure (Tromble, 1988; Dawson, 1993; Schwinning & Ehleringer, 2001; Devitt & Smith, 2002; Bhark & Small, 2003; Huxman *et al.*, 2005; Scott *et al.*, 2014). Moreover, transpiration of active vegetation can have a huge impact on ecosystem water losses which are modulated by water availability, plant functional type, and stomatal regulation, as well as leaf area index (*LAI*). Paço *et al.* (2009) gave first insights that at least in times of high water availability (October-May/June) understory evapotranspiration can be equal to and sometimes exceeds tree transpiration. Soil evaporation and herbaceous transpiration, however, have seldom been analyzed separately in savanna ecosystems so far. Thus the functional understanding of soil evaporation dynamics and vegetation-soil feedbacks within the water cycle remain a major challenge in semi-arid regions.

Consequently, in dry-land ecosystems partitioning *ET* and analyzing vegetation effects on soil water distribution is not only important to better understand the ecosystem water budget (Haverd *et al.*, 2011; Raz-Yaseef *et al.*, 2012) but also for predictions of carbon cycling, i.e. ecosystem productivity (Scott *et al.*, 2006; IPCC, 2007; Yopez *et al.*, 2007). Oxygen isotope signatures ( $\delta^{18}O$ ) have been used to partition ecosystem *ET* because of the distinct isotopic compositions of water transpired by leaves relative to soil evaporated vapor (Yakir and Sternberg, 2000). In the past however, precise determinations of isotopic compositions of evapotranspiration ( $\delta^{18}O_{ET}$ ), evaporation ( $\delta^{18}O_E$ ) and transpiration ( $\delta^{18}O_T$ ) have been challenging since measurements of water vapor were difficult to obtain using conventional cold-trapping methods (e.g. Helliker *et al.*, 2002; Williams *et al.*, 2004). Recent developments in laser spectroscopy now enable measurements of  $\delta^{18}O$  of ambient water vapor ( $\delta^{18}O_a$ ),  $\delta^{18}O_{ET}$  and its components with high temporal resolution in the field (Werner *et al.*, 2012) and bear a novel opportunity to separate evaporative and transpirational fluxes with higher temporal resolution (Dubbart *et al.*, 2013; Wang *et al.*, 2013).

The main goal of this study was to analyze the contribution of the herbaceous layer to ecosystem water cycle and productivity, which was assessed by combining eddy co-variance and chamber based flux-measurement techniques with a novel laser spectrometer. We hypothesize that the herbaceous understory layer, although vulnerable to drought, plays an important role in the water and carbon cycle and soil water redistribution. We focused on disentangling the inter-seasonal impact of understory vegetation effects on: i) the ecosystem water and carbon fluxes, ii) soil evaporation and iii) the

influence of vegetation on rain infiltration. To explicitly account for the heterogeneity created by the patchy tree cover (Moreno *et al.*, 2007) two experimental sites were installed (under the tree crown and in an adjacent open area) containing understory vegetation and bare soil plots.

### 5.3. Materials and Methods

Isotopic compositions are reported here as ratios  $R$  between the concentrations of rare and common isotopes ( $^{18}O/^{16}O$ ) or expressed as  $\delta$ -notation, i.e. relative to Vienna Standard Mean Ocean Water (V-SMOW; Gonfiantini, 1978):  $\delta^{18}O [‰] = ((R_{sample} - R_{V-SMOW})/R_{V-SMOW}) * 1000$ .

#### 5.3.1. Study site and experimental design

Measurements were conducted in an open cork-oak woodland (*Quercus suber* L.) in central Portugal, approximately 100 km north-east of Lisbon (N39°8'17.84'' W8°20'3.76''; Herdade de Machoqueira do Grou). The trees are widely spaced (209 individuals ha<sup>-1</sup>) with a leaf area index of 1.05 and a gap probability of 0.7 (Piayda *et al.*, under review). The oak trees are managed for cork production and were planted approximately 50 years ago.

**Table 1:** List of herbaceous species growing in the open and tree plots in 2011.

N-fixing forbs	Forbs	Grasses
<i>Ornithopus compressus</i> L.	<i>Crepis vesicaria</i> L.	<i>Briza maxiamia</i> L.
<i>Ornithopus sativus</i> Brot.	<i>Geranium spec</i>	<i>Lolium multiflorum</i> Lam.
<i>Trifolium glanduliferum</i> Boiss.	<i>Plantago coronopus</i> L.	<i>Vulpia bromoides</i> Gray
<i>Trifolium michelianum</i> Savi	<i>Rumex acetosella</i> L.	<i>Vulpia geniculata</i> Link
<i>Trifolium incarnatum</i> L.	<i>Silene gallica</i> L.	
<i>Trifolium subterraneum</i> L.	<i>Spergula arvensis</i> L.	
<i>Trifolium resupinatum</i> L.	<i>Tolpis barbata</i> (L.) Gaertn.	
<i>Trifolium vesiculosum</i> Savi	<i>Tuberaria guttata</i> (L.) Fourr.	

The herbaceous layer is dominated by native annual forbs and grasses (see Table 1 for detailed species composition). The site is characterized by Mediterranean climate, with 30 year long-term mean annual temperature of approximately 15.9 °C and annual precipitation of 680 mm (Instituto de Meteorologia, Lisbon). We established two sites: one directly under the oak crown projected area and another one in an adjacent open area, 5-7 m distant from any canopy cover. Two types of plots (sized 40\*80 cm)

were installed in each site: bare soil plots with total exclusion of above-ground biomass and root ingrowth by inserting trenching meshes (trenching depth = 60 cm; mesh diameter < 1  $\mu$ m, Plastok, Birkenhead, UK), and understory plots with undisturbed herbaceous vegetation (four plots per site and treatment). Both plot types were replicated 4 times at each site and equipped with soil sensors (16 plots, see below), however gas exchange understory chamber measurements (see below) were only replicated 3 times, due to time limitations (12 plots total). All plots were established 1 year before measurements to minimize effects of disturbance.

To assess the impact of the understory to ecosystem carbon and water cycling a combination of continuous (i.e. eddy co-variance, environmental sensors, soil profiles) and non-continuous (i.e. chamber and laser based gas-exchange and isotopic and understory biomass observations) measurements were conducted. At the understory level *ET* partitioning could be done on 26 days at the open and 22 days at the tree site and *NEE* partitioning on 23 days at the open and 20 days at the tree site. Measurements were distributed over four measurement campaigns in spring (7.April – 3.May), late spring (23.May – 16.June), summer (11. – 23.September) and fall (23.October – 22.November). During winter no measurements were obtained due to strong temperature limitation and consequently very low net water and carbon fluxes. At the ecosystem level partitioning could be achieved for days when our understory field site was within the footprint of the eddy co-variance system and eddy co-variance data was of sufficient quality (i.e. no gap-filled data), which resulted in nine days equally distributed between spring, summer drought and fall. Separation of *ET* and *NEE* fluxes was done on diurnal courses repeatedly between 7 a.m. and 7 p.m. (Fig. S1) at 5-6 time points, which were used to calculate day-time sums of *ET*, *E*, *T* of the understory and the oaks and *NEE*, *R<sub>eco</sub>* and *GPP* of understory and oaks. Infiltration of precipitation into the soil on bare soil and vegetated soil patches was estimated for two periods: spring (7. April –16. June) and fall (23.October – 22. November).

### 5.3.2. Environmental variables and herbaceous biomass

Photosynthetic photon flux density was measured at both sites at approximately 1.5 m height (PPFD, LI-190SB, LI-COR, Lincoln, USA). Rainfall (ARG100 Rain gauge, Campbell Scientific, Logan, UT,

USA), air temperature, and relative humidity (rH, CS-215 Temperature and Relative Humidity Probe, Campbell Scientific, Logan, UT, USA) were measured and 30 min averages were stored in the datalogger (CR10x, Campbell Scientific, Logan, UT, USA). Soil temperature (custom built pt-100 elements) in 5, 15, 30, and 60 cm depth was measured in vegetation and bare soil plots at both sites and 60 min averages were stored in a datalogger (CR1000, Campbell Scientific, Logan, UT, USA; 4 sensors per depth and treatment). Temperature at the soil surface was manually measured on each measurement day in diurnal cycles corresponding with the gas exchange measurements using temperature probes (GMH 2000, Greisinger electronic, Regenstauf, Germany). Volumetric soil water content ( $\theta_v$ , 10hs, Decagon, Washington, USA) in 5, 15, 30, and 60 cm depth was measured in vegetation and bare soil plots at both sites and 60 min averages were stored in the datalogger (CR1000, Campbell Scientific, Logan, UT, USA; 4 sensors per depth and treatment). The total water infiltration following each rain event ( $>2 \text{ mm d}^{-1}$ ) into the upper 60 cm of the soil profile was calculated from  $\theta$  measurements. Therefore, the maximum increase in  $\theta$  ( $\text{m}^3 \text{ m}^{-3}$ ) following a rain event was estimated for each depth separately. The 10hs sensors integrate over 10 cm soil profile, thus the estimated infiltration (=increase in  $\theta$ ) was representative for the sensors in 5, 15, 30 and 60 cm for 0-10, 10-20, 25-35 and 55-65 cm, respectively. The increase of  $\theta$ /infiltration in the intermittent depths that were not measured was linearly integrated. Finally, total infiltration into the upper 60 cm of the soil profile was estimated as a sum of all depths and converted to  $\text{mm d}^{-1}$ .

Aboveground biomass of living herbaceous plants was determined destructively on five 40\*40 cm plots per site randomly selected near the permanent plots. Harvesting took place at six measuring dates: four in spring and two in November. All aboveground parts of living plants were collected, dried (60 °C, 48 hours) and weighed.

### 5.3.3. *Eddy-covariance measurements*

An ecosystem eddy-covariance flux tower was set up, equipped with a Gill R3A-50 ultrasonic anemometer (Gill Instruments Ltd., Lymington, UK). The tower was equipped with a LI-7000 closed path  $\text{CO}_2$  /  $\text{H}_2\text{O}$  analyzer (LI-COR, Lincoln, USA). The measurement height was about 23.5 m above

ground and the tower was in 100 m distance of the experimental field site.

Data were continuously acquired on a field laptop with the eddy covariance data acquisition and processing software package EddyMeas (Meteotools, Jena, DE, Kolle, 2007) and are post-processed using EddySoft according to an extended FLUXNET procedure. Heat and water fluxes are corrected for the energy balance closure gap according to Mauder *et al.* (2013). The flux gap-filling was made according to Reichstein *et al.* (2005). Gaps were only filled up to a maximum gap length of 6 days (Piayda *et al.*, 2014).

#### 5.3.4. Cavity Ring-Down Spectrometer based measurements of $\delta^{18}O_E$ and understory $\delta^{18}O_{ET}$ , and gas-exchange flux measurements

Water and carbon dioxide fluxes and isotopic composition of water fluxes were measured using a Cavity Ring-Down Spectrometer (CRDS, Picarro, Santa Clara, USA) and a CO<sub>2</sub> infrared gas analyzer (BINOS100; Fisher-Rosemount GmbH & Co., Hasselroth, Germany) in combination with custom built soil chambers. We used 2 chambers that were switched between plots for measurements, following the design of Pape *et al.* (2009), in an open gas exchange system (n=3 plots per treatment and experimental site; 12 plots in total). The transparent plexiglas soil chamber had a total volume of 60 L. The flow through the chamber was regulated as described in Pape *et al.* (2009) using a fan inside the inlet sampling tube and could be adjusted between 0 and 40 L min<sup>-1</sup>.

All measurements were conducted in diurnal courses with a duration time of roughly 1.5 to 2 hours per measurement point and 5-6 measurement points between 7 a.m. and 7 p.m. (Fig. S1). To conduct each measurement point the two chambers were rotated randomly on 6 plots of one experimental site. To calculate net CO<sub>2</sub> exchange (*NEE*) and evapotranspiration (*ET*) as well as its isotopic composition, background air going into the chamber (at 1.5 m height) and sampling air (coming out of the chamber) were alternately measured. After stable values were reached the final five minutes interval average was used for the calculation of *NEE* and *ET*. Including the time needed to reach stable values, the total duration of the chamber for one measurement point on each plot was between 10 and 15 min. Fluxes of *NEE*, *ET* as well as total conductance (*g<sub>t</sub>*) were calculated with the gas exchange equations of von Caemmerer & Farquhar (1981).

Oxygen isotope compositions of soil evaporation (bare soil plots) as well as evapotranspiration of the understory (vegetation plots) were estimated using a mass balance approach (Dubbett *et al.*, 2013; 2014a):

$$\begin{aligned}\delta_E &= \frac{u_{out} w_{out} \delta_{out} - u_{in} w_{in} \delta_{in}}{u_{out} w_{out} - u_{in} w_{in}} \\ &= \frac{w_{out} \delta_{out} - w_{in} \delta_{in}}{w_{out} - w_{in}} - \frac{w_{in} w_{out} (\delta_{out} - \delta_{in})}{w_{out} - w_{in}}\end{aligned}\quad (1),$$

where  $u$  is flow rate [ $\text{mol}(\text{air}) \text{ s}^{-1}$ ],  $w$  is mole fraction [ $\text{mol}(\text{H}_2\text{O}) \text{ mol}(\text{air})^{-1}$ ] and  $\delta$  is isotope ratio of the incoming (*in*) and outgoing (*out*) air stream of the chamber. Flow rates are measured with humid air so that conservation of dry air gives  $u_{in}(1-w_{in}) = u_{out}(1-w_{out})$ , which leads to the second line of Eq. (1). The second term in Eq. (1) corrects for the increased air flow in the chamber due to addition of water by transpiration. In addition to isotopic signatures of soil evaporation and understory evapotranspiration, the oxygen isotope signatures of ambient water vapor (in 9 m height) were measured with the CRDS.

### 5.3.5. Sampling and measurement of $\delta^{18}\text{O}$ of soil water and precipitation

Soil samples for water extraction and  $\delta^{18}\text{O}$  analysis were taken on vegetation and bare soil plots using a soil corer on 17 and 15 days at the open and tree site respectively (see Table S1 for details). Samples were collected from the soil surface (0-0.5 cm depth), 2, 5, 10, 15, 20, and 40 cm soil depths ( $n=4$  per depth and treatment). Soil water samples were extracted on a custom build vacuum line by cryogenic distillation. Precipitation samples were collected roughly each week. Water  $\delta^{18}\text{O}$  analysis was performed by headspace equilibration on an Isoprime IRMS (Elementar, Hanau, Germany) coupled via open split connection to a  $\mu\text{gas}$  autosampler (Elementar, Hanau, Germany). Equilibration with 5% He and 95%  $\text{CO}_2$  gas was done for 24 hours at 20 °C. For every batch of 44 samples 3 different laboratory standards were analyzed. Laboratory standards were regularly calibrated against VSMOW, SLAP, and GISP water standards (IAEA, Vienna). Analytical precision was  $< 0.1\text{‰}$ .



### 5.3.6. Calculation of $\delta^{18}O$ of soil evaporation

Oxygen isotope signatures of soil evaporation were calculated using the Craig and Gordon equation (1965):

$$R_E = \frac{1}{\alpha_k \alpha^+ (1 - h)} (R_e - \alpha^+ h R_a) \quad (2),$$

where  $R_E$  is the isotope ratio ( $^{18}O/^{16}O$ ) of evaporated water vapor and  $R_e$  is the isotope ratio of bulk soil water at the evaporating sites. The evaporating site is the vapor-liquid interface below which liquid transport and above which vapor transport is dominant (Braud *et al.*, 2005). It has been shown for unsaturated soils that this site is related to a strong enrichment in soil water isotopic composition relative to the rest of the soil column and an exponential depletion in isotopic signature within few cm of the underlying soil due to evaporative enrichment of the remaining liquid water (Haverd and Cuntz, 2010; Dubbert *et al.*, 2013). Thus, for  $R_e$  and temperature at the evaporating sites ( $T_e$ ), temperature (see 2.2.) and oxygen isotope signatures of bulk soil water (see 2.5) were measured along the soil profile and those values along the soil profile were used where the strongest enrichment in bulk soil  $\delta^{18}O$  could be detected (residual soil water volumetric content was only 1% and therefore neglected). Bulk soil  $\delta^{18}O$  was estimated with higher resolution along the soil profile than temperature (compare section 2.2 and 2.5), so in case the highest enrichment in bulk soil  $\delta^{18}O$  was found in a depth where temperature was not measured, linear interpolations of the adjacent values were used. In cases, where bulk soil  $\delta^{18}O$  was not analyzed for specific dates where gas-exchange data was available and partitioning was conducted, values from adjacent sampling dates were taken.  $R_a$  is the isotope ratio of ambient water vapor,  $\alpha_k$  is the kinetic fractionation factor,  $\alpha^+$  is the water vapor equilibrium fractionation factor ( $\alpha_k$  and  $\alpha^+ > 1$ ; Majoube, 1972; Merlivat, 1978; for the formulation of  $\alpha_k = \alpha_{diff}^{nk}$  see Mathieu and Bariac, 1996), and  $h$  is the relative humidity normalized to  $T_e$ .

Although direct estimates of  $E$  and  $\delta^{18}O_E$  were available for bare soil plots, vegetation depresses  $E$  and also influences  $\delta^{18}O_E$  for example due to different isotopic signatures of soil water and also temperature at bare soil and vegetated soil patches (see table S1 and Dubbert *et al.*, 2013). Therefore, bare soil plots only served to validate the Craig and Gordon equation, because on bare soil plots  $E$

contributes entirely to the evaporative flux and could be tested against modeling results. Validation was done site specifically, using measured and modeled  $\delta^{18}O_E$  of 26 and 22 diurnal cycles obtained between 7 April and 22 November 2011 at the open and tree site, respectively. Finally, the Craig and Gordon equation was used to calculate  $\delta^{18}O_E$  of vegetation plots.

### 5.3.7. Modeling $\delta^{18}O$ of plant leaf water at the evaporating sites and transpiration

To calculate  $\delta^{18}O_T$ , in a first step the isotopic composition of leaf water at the evaporating sites ( $\delta^{18}O_e$ ) was calculated. We used the iterative solution of the ordinary differential equation for leaf water at the evaporating sites in non-steady state as in Dongmann *et al.* (1974; see also Cuntz *et al.* 2007):

$$R_e(t + dt) = R_c + (R_e(t) - R_c)e^{-\frac{g_t w_i}{\alpha_k \alpha^+ V_m} dt} \quad (3),$$

where  $R_e(t+dt)$  and  $(t)$  are the isotope ratios of leaf water at the evaporating sites at time  $t$  and after a time step at time  $t+dt$ ,  $g_t$  is the total conductance ( $\text{mol m}^{-2} \text{s}^{-1}$ ),  $w_i$  is the mol fraction in the stomatal cavity, and  $V_m$  the mesophyll water volume ( $\text{mol m}^{-2}$ ).  $R_c$  is the Craig and Gordon steady-state isotope ratio at the evaporating sites, i.e. Eq. (1) rearranged for  $R_e$  with  $R_E = R_x$ , and  $R_x$  being the isotope ratio of xylem/source water. We were not able to sample xylem water in large sample sizes, due to methodological restrictions related to the size and lacking lignifications of the herbaceous plant species. Therefore the source/xylem isotopic ratio was estimated by assuming root water uptake proportional to root density, which was estimated as root biomass (g) per kg soil along the soil profile. In very dry soil conditions this method could pose some error since plants can shift water uptake into deeper, wetter soil layers. However, non woody species, such as the understory vegetation in this study, have shallow root systems and therefore lack high ability to shift water uptake depths (Otieno *et al.*, 2011). For further details see Dubbert *et al.* (2013). Knowing the isotopic signature of leaf water at the evaporating sites, the isotopic signature of plant transpiration can finally be calculated using the Craig and Gordon formulation (Eq. 2) with the isotopic signature of leaf water at the evaporating sites in the non-steady-state as  $R_e$ .

### 5.3.8. Water and carbon partitioning

The contribution of  $T$  to  $ET$  at the herbaceous understory scale,  $ft = T/ET$ , can be estimated based on measured understory  $\delta^{18}O_{ET}$  and modeled soil  $\delta^{18}O_E$  and herbaceous  $\delta^{18}O_T$  (Moreira *et al.*, 1997; Yakir & Sternberg, 2000):

$$ft = \frac{\delta^{18}O_{ET} - \delta^{18}O_E}{\delta^{18}O_T - \delta^{18}O_E} \quad (4).$$

This approach is based on the assumption that the isotopic signature of evapotranspiration is a mixing ratio of not more than the two sources (evaporation and transpiration) and that no water vapor is lost other than by the mixing of the two sources with the atmospheric pool (i.e. no condensation).

At the understory level, strong heterogeneity between understory vegetation growing under the tree crown and in open areas was found regarding species development and net fluxes of  $CO_2$  and water. It is important to account for this heterogeneity when we want to separate understory flux components from net ecosystem carbon or water fluxes. Therefore, an average flux of understory transpiration, soil evaporation and  $NEE$  was calculated as:

$$F = P_{gap} F_{open} + (1 - P_{gap}) F_{tree} \quad (5),$$

where  $F$  denotes the water or carbon flux per  $m^2$  ground area, the subscripts *open* and *tree* denote the open and the tree site, respectively.  $P_{gap}$  is the canopy gap fraction modeled from the daily course of sun inclination angle and the view zenith angle distribution of  $P_{gap}$  (Piayda *et al.*, unpublished).

At the whole ecosystem level,  $ET$  was separated into transpiration of cork-oak trees ( $T_o$ ) by subtracting estimates of understory evapotranspiration measured with the CRDS.

The partitioning of the net  $CO_2$  fluxes ( $NEE$ ) into gross primary production ( $GPP$ ) and ecosystem respiration ( $R_{eco}$ ) followed Lasslop *et al.* (2010).  $GPP$  of the understory was estimated by subtracting  $R_{eco}$  from chamber based estimates of understory  $NEE$ , arguing that  $R_{eco}$  is mainly comprised of heterotrophic soil respiration and root respiration during daytime. This assumption was validated by a comparison of  $R_{eco}$  of the ecosystem tower with  $R_{eco}$  of a nearby understory tower, measuring a very comparable understory community. The  $R_{eco}$  estimates of both towers were in the same range and correlate very well (data not shown).

Water use efficiency (*WUE*) at ecosystem and understory level was calculated. Since changes in *WUE* due to water limitations are often obscured by changes in *VPD* the inherent water use efficiency (*iWUE*; Beer *et al.*, 2009) was calculated as:

$$iWUE = \frac{-NEE \cdot VPD}{ET} \quad (6).$$

At plant level inherent water use efficiency was calculated as follows:

$$iWUE = \frac{-GPP \cdot VPD}{T} \quad (7).$$

### 5.3.9. Statistical Analysis

If not indicated otherwise, all results are presented as mean values with standard error (n=3-4). In the case of diurnal cycles, all values of one treatment were integrated into a mean value that was conducted within one measurement point of roughly 1.5 h. In the case daytime sums are presented, these were estimated for each plot replicate and then averaged.

Mann-Whitney U-tests were used to examine significant site-specific differences at each measurement day regarding PPFD, soil moisture, soil temperature, understory evapotranspiration and net carbon exchange (and their components), conductance and oxygen isotope compositions within the ecosystem. Spearman Rank order correlations were used relating ecosystem *ET* and *NEE* components and environmental factors. Non-linear regressions were performed to relate rainfall amount with infiltration difference between vegetation and bare soil plots and relating volumetric soil water content with difference in *iWUE* on understory level and *iWUE* of understory plants. Statistical analyses were carried out with Statistica (Statistica 6.0, StatSoft, Inc., Tulsa, USA).

## 5.4. Results

### 5.4.1. Environmental conditions and net ecosystem carbon and water fluxes

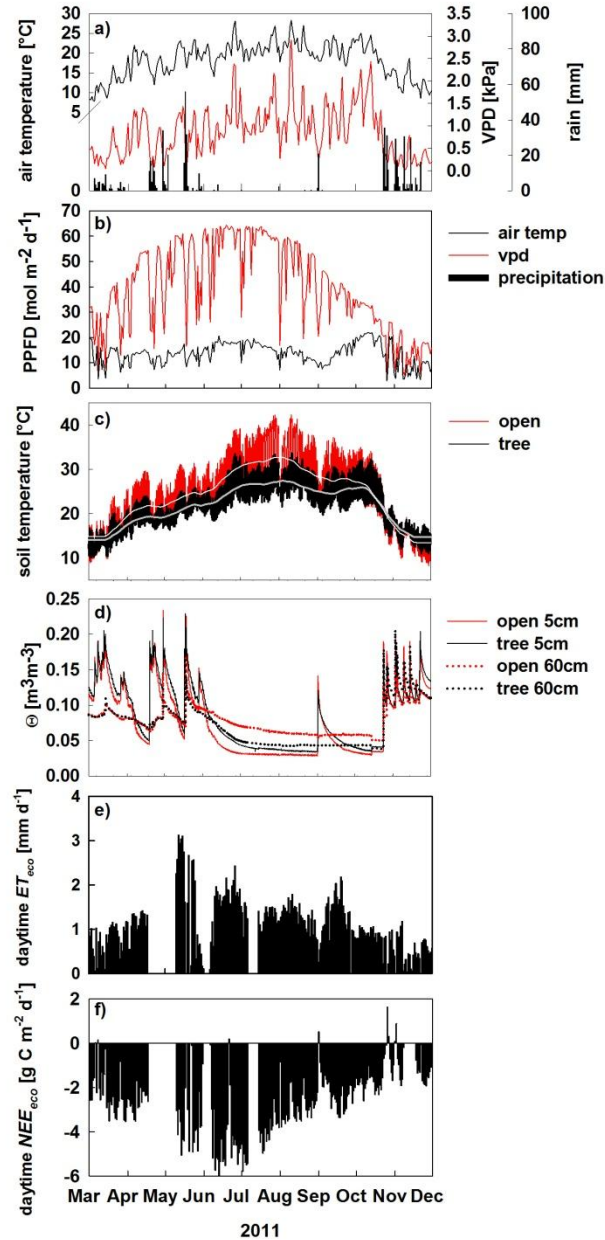


**Figure 1:** Environmental conditions from March to December 2011; a) daily averages of air temperature (grey line), vapor pressure deficit (VPD; grey long dashed line) and rainfall (black bars); b-de) daily sums of environmental conditions at the open (grey) and tree site (black) of: photosynthetic photon flux density (PPFD), soil temperature in 5 cm soil depth (lighter lines denote running averages), soil volumetric water content ( $\Theta$ ) in 5 and 60 cm soil depth. e) daytime integrated net ecosystem fluxes of: net  $\text{CO}_2$  exchange ( $NEE$ ,  $\text{g C m}^{-2} \text{d}^{-1}$ ) and evapotranspiration ( $ET$ ,  $\text{mm d}^{-1}$ , black bars) from March to December 2011.

Over the course of the study period, air temperature and PPFD followed the typical Mediterranean climate pattern (Fig. 1). With a total annual rainfall of 800 mm, 2011 was rather wet compared to the long term 30 years mean of 680 mm. Despite high winter precipitation, we observed a first drought period between April 1 and April 18 with soil water content ( $\theta$ ) dropping below  $0.05 \text{ m}^3 \text{ m}^{-3}$  (Fig. 1d). Between April and October microclimate conditions differed considerably in the open and under the tree crown: light intensity and soil temperature were reduced by the tree shadow by up to  $45 \text{ mol m}^{-2} \text{ d}^{-1}$  (Fig. 1b) and up to  $7 \text{ }^\circ\text{C}$  (Fig. 1c), respectively. Further,  $\theta$  in 60 cm soil depth was  $0.03 \text{ m}^3 \text{ m}^{-3}$  lower at the tree site during the summer drought compared to the open site (June – October, Fig. 1d).

Daytime ecosystem evapotranspiration *ET* reached maximum values in May and declined constantly thereafter (Fig. 1e). Likewise, net ecosystem  $\text{CO}_2$  exchange (*NEE*) exhibit strong seasonal changes reaching maximum uptake rates in June (Fig. 1f). Notably, the ecosystem was a net carbon sink between March and December 2011 (Fig. 1f), although daytime *NEE* declined during summer drought by about 40 %. There were only few days, where *NEE* showed a net  $\text{CO}_2$  release during daytime which correspond either to heavy rain events on dry soils resulting in increased soil respiration (“Birch effect”, see Unger *et al.*, 2012) or low photosynthetic uptake on very cloudy days between September and November (Fig. 1d, f).

#### 5.4.2. Vegetation effects on rainfall infiltration

To investigate the effect of understory vegetation on rain infiltration, maximum infiltration per rain event was calculated for the open and tree sites for bare soil and the understory vegetation layer (Fig. 2). The relative infiltration averaged over all rain events ( $>2 \text{ mm d}^{-1}$ ) was much higher on understory than on bare soil patches, 0.75 compared to 0.41. This could be observed for both sites and the tree canopy did not have significant further effects on infiltration (Fig. 2). Moreover, a significant relationship could be found between the amount of precipitation and the difference in infiltration between bare soil and understory plots (open site:  $R^2=0.88$ ;  $p<0.001$ ; tree site:  $R^2=0.63$ ;  $p<0.001$ ): the stronger the rain event, the bigger was the difference in infiltration between bare soil and understory plots (Fig. 2 insets).

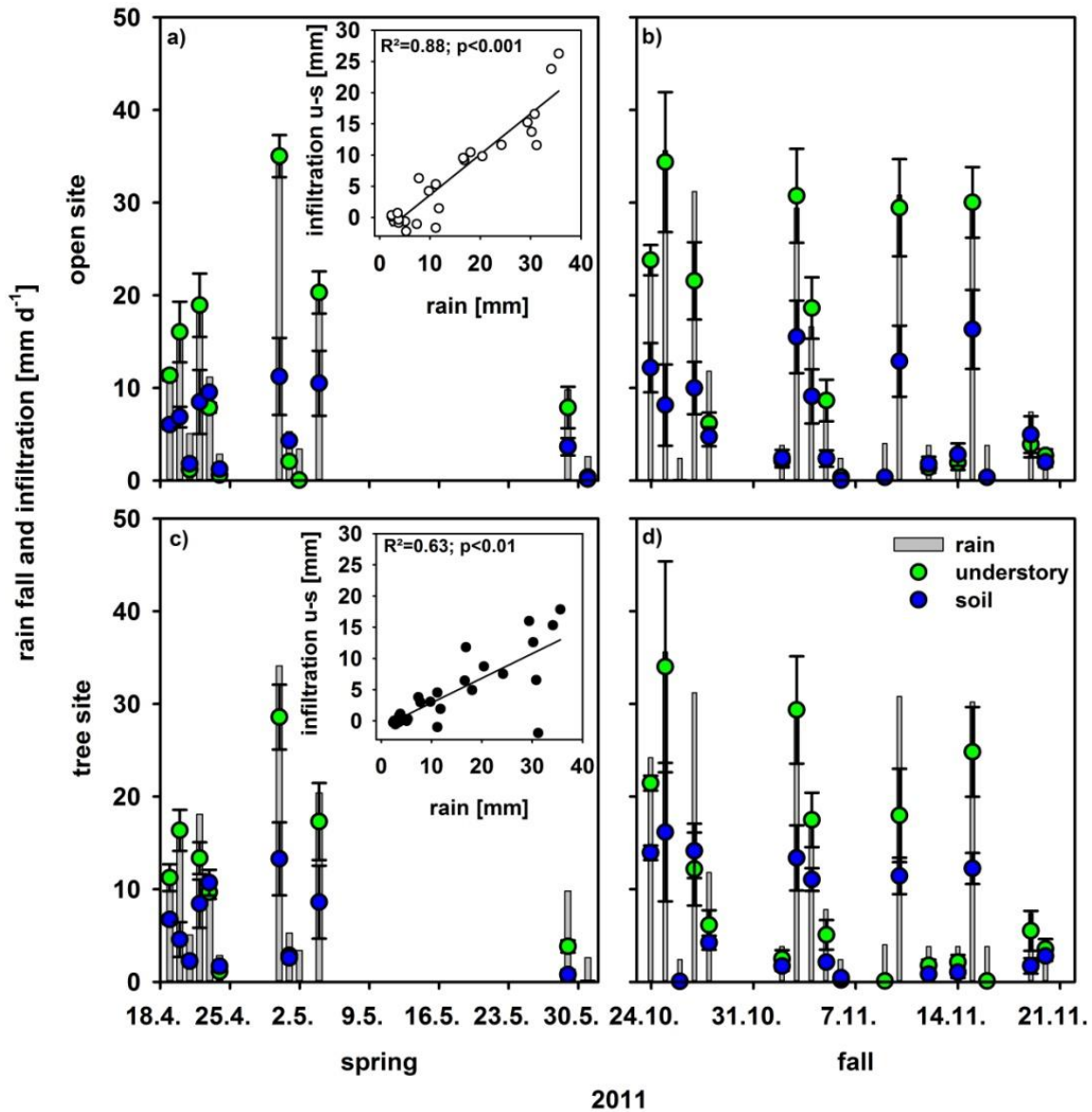


**Figure 2:** Rainfall and infiltration into the soil following rain events > 2 mm at a, b) the open and c, d) tree site on understory plots (green circles), bare soil plots (blue circles, all in mm d<sup>-1</sup>; n=4, mean values ± SE) and rainfall (grey bars). Insets present differences in infiltration between understory and bare soil versus rain amount at the open and tree site. Regression line, coefficient of regression and p-value are given.

#### 5.4.3. Seasonal development of $\delta^{18}O$ within the ecosystem

Besides the influence on rain infiltration, understory vegetation also contributes to ecosystem water loss via transpiration and for a functional understanding of the development of net ecosystem evapotranspiration (*ET*) we separated between plant transpiration and soil evaporation. At the understory level the dense structure of the herbaceous layer prevented a flux based partitioning

approach and stable oxygen isotopes ( $\delta^{18}O$ ) were used to partition  $ET$ . This requires the knowledge of  $\delta^{18}O$  of water sources within the ecosystem as input parameters for modeling  $\delta^{18}O_E$  and  $\delta^{18}O_T$  (Eq. 2).

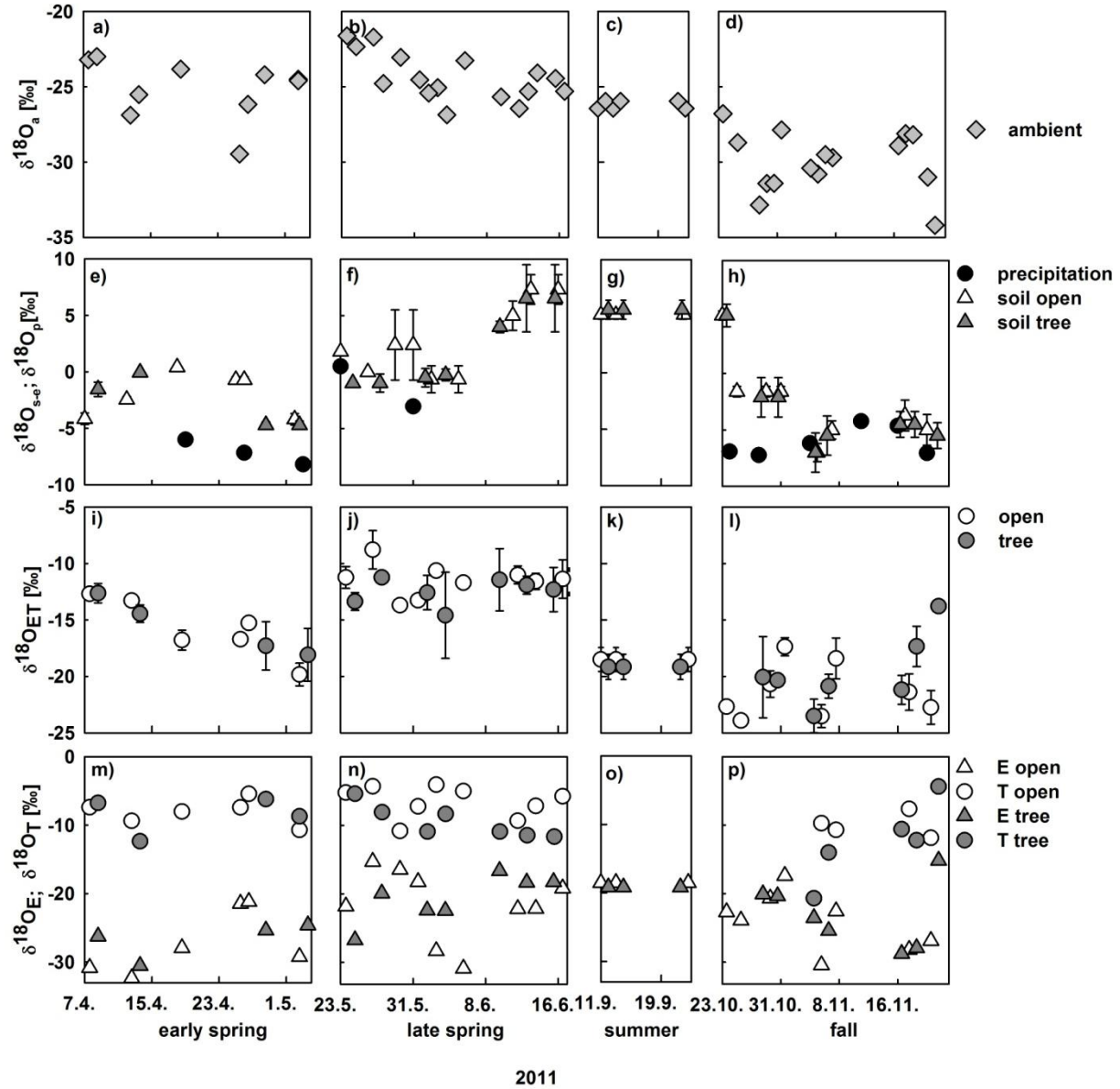


**Figure 3:** Development of midday oxygen isotope signatures within the ecosystem from April to November 2011; a-d) atmospheric  $\delta^{18}O$  at 9 m height (grey diamonds); e-h)  $\delta^{18}O$  of rainfall (black circles) and  $\delta^{18}O$  of soil water at the evaporating site on vegetation plots at the open (white triangles) and tree site (grey triangles, mean values  $\pm$  SD,  $n=3$ ); i-l) measured  $\delta^{18}O$  of evapotranspiration on the open (white circles) and tree site (grey circles, mean values  $\pm$  SD,  $n=3$ ); m-p) modeled  $\delta^{18}O$  of evaporated vapor from vegetation plots on the open (white triangles) and the tree site (grey triangles) and modeled  $\delta^{18}O$  of herbaceous leaf transpired vapor at the open (white circles) and the tree site (grey circles).

Oxygen isotope signatures of ambient vapor ( $\delta^{18}O_a$ ) and precipitation ( $\delta^{18}O_p$ ) both changed substantially between spring and fall (Fig. 3):  $\delta^{18}O_a$  strongly decreased from ca. -25‰ to -30‰ from spring to fall (Fig. 3a-d), which can be explained by seasonal changes in the predominant wind



direction to north-north-east, delivering more continental, i.e.  $^{18}\text{O}$  depleted, air masses during fall.  $\delta^{18}\text{O}_p$  was much higher between -8.2‰ and -0.5‰. In general, oxygen isotope signatures of soil water followed trends in  $\delta^{18}\text{O}_p$ . We show the oxygen isotope signatures of soil water from the depth at which highest isotopic enrichment was found, i.e. the isotopic signature of the evaporating front in the soil profile where evaporation occurs ( $\delta^{18}\text{O}_{s-e}$ ) instead of bulk soil  $\delta^{18}\text{O}$  signatures, because  $\delta^{18}\text{O}_{s-e}$  is an important input for the Craig and Gordon equation.  $\delta^{18}\text{O}_{s-e}$  was heavily enriched during the summer months compared to precipitation due to much stronger evaporative enrichment during summer and spring as compared to fall (Fig. 3; for detailed information on the development of bulk soil  $\delta^{18}\text{O}$  along the soil profile see Table S1).

Observed midday  $\delta^{18}\text{O}$  of understory evapotranspiration varied considerably between -8.8‰ and -23.5‰. Notably, variations in  $\delta^{18}\text{O}_{ET}$  were strong between seasons and also within a season (Fig. 3i-l). Variations in  $\delta^{18}\text{O}_{ET}$  can be either explained by i) variation in the relative contribution of component fluxes  $E$  and  $T$ , with their differing isotopic signatures or ii) by change in oxygen isotopic signatures of the component fluxes  $E$  and  $T$ . Without the knowledge of the component isotopic signatures this cannot be disentangled. Consequently, these were modeled, based on the isotopic input parameters (see section 2.6. and 2.7.).

Before the isotope signature of soil evaporation was modeled at vegetated soil patches (Fig. 3m-p), the Craig and Gordon equation was tested against direct estimates of  $\delta^{18}\text{O}_E$  obtained at bare soil plots, where  $E$  contributes fully to  $ET$ : calculated  $\delta^{18}\text{O}_E$  is in very good agreement with CRDS based measurements of  $\delta^{18}\text{O}_E$  for soil conditions ranging between residual to nearly saturated soil water content (Fig. 4a). The agreement between measured and modeled  $\delta^{18}\text{O}_E$  was best during midday. However, including morning and afternoon records decreased the coefficient of determination but did not significantly alter the regressions slope and offset (Fig. 4).

Modeled midday  $\delta^{18}\text{O}_E$  estimated on vegetation plots ranged from -15.1‰ to -31.2‰ and the inter-seasonal development of  $\delta^{18}\text{O}_E$  was similar to the development of  $\delta^{18}\text{O}_{s-e}$  (Fig. 3m-p).

$\delta^{18}\text{O}_T$  was modeled in two steps, first calculating  $\delta^{18}\text{O}$  of leaf water at the evaporating sites in the non steady state (see section 2.7. and Fig. 4c). Modeled  $\delta^{18}\text{O}$  of leaf water at the evaporating sites was well correlated with measured bulk leaf water  $\delta^{18}\text{O}$ , with a negative offset of measured leaf water of 2.3‰

(Fig. 4d), owing to the Péclet effect (Farquhar & Lloyd, 1993) as bulk leaf  $\delta^{18}\text{O}$  contains a mixed signal of non-fractionated xylem water and water at the evaporating sites that is highly enriched in  $\delta^{18}\text{O}$  (Yakir, 1992). Midday  $\delta^{18}O_T$  ranged between -3.9‰ and -20.1‰ and followed no clear inter-seasonal pattern. Clearly, the strong decrease in  $\delta^{18}O_{ET}$  from -12.7‰ to -19.8‰ during April was caused by a strong decrease in  $T$  (Fig. 3i, m), while the slight overall increase of  $\delta^{18}O_{ET}$  in fall can be mainly explained by decreased  $\delta^{18}O_E$  and increased  $\delta^{18}O_T$  (Fig. 3l, p).

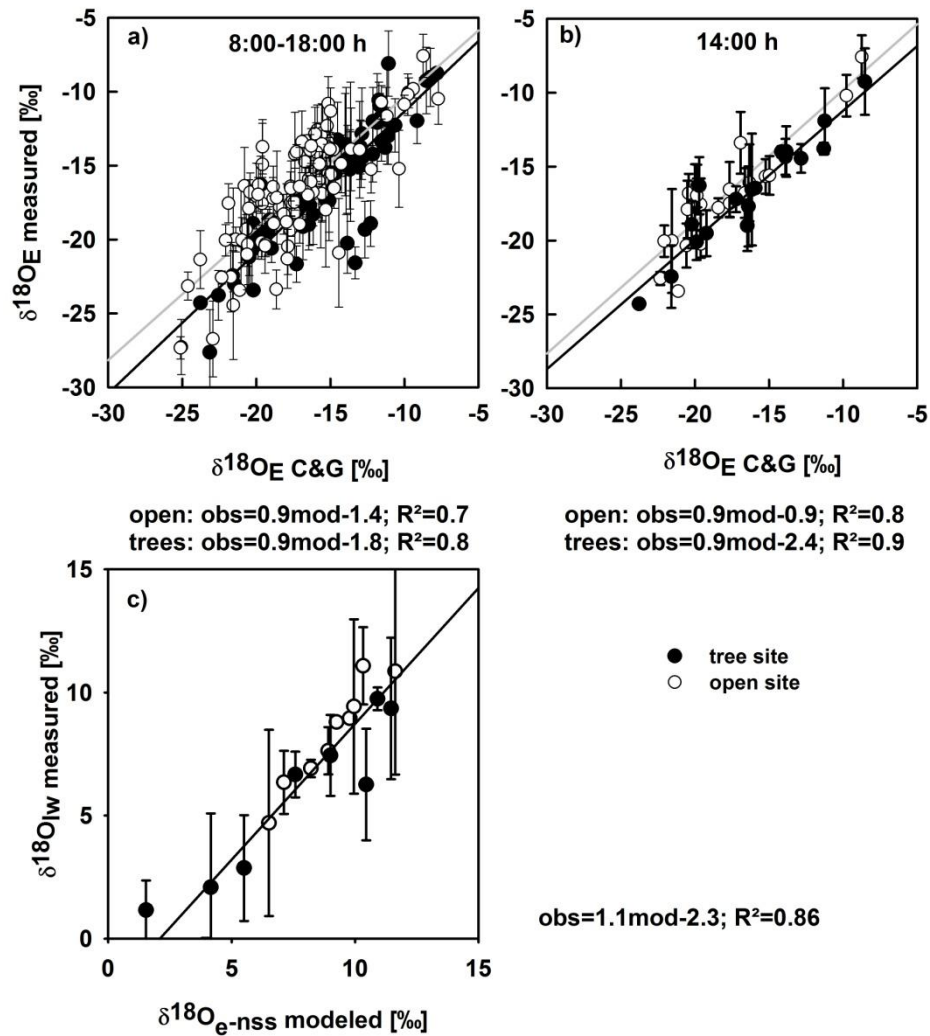


**Figure 4:** a) Oxygen isotope signatures of soil evaporation on bare soil plots calculated with the Craig and Gordon equation versus measured values for the open (white circles) and tree sites (black circles) of all measurements (mean values  $\pm$  SE;  $n=3$ ); the grey and black line denote regression lines for the open and tree sites, respectively. b) Modeled against measured values during midday only (14:00 h). c) Modeled  $\delta^{18}\text{O}$  of leaf water at the evaporating sites in the non steady state versus measured oxygen isotope signatures of bulk leaf water for the open (white circles) and tree site (black circles) for all available data points of measured leaf water  $\delta^{18}\text{O}$  throughout the study period. Regression equations (observed vs. modeled), correlation coefficients are given below the plots. p-values were less than 0.001 for all regressions.

#### 5.4.4. Seasonal development of herbaceous $ET$ and $NEE$ components

Understory  $ET$  partitioning was based on diurnal observations of understory  $ET$ ,  $\delta^{18}O_{ET}$  and derived  $\delta^{18}O_T$  and  $\delta^{18}O_E$ , which were used to calculate day-time sums of  $ET$ ,  $E$ , and  $T$  of the understory (Figure S1). Notably, daytime integrated understory transpiration and soil evaporation displayed strong short-term variability (Fig. 5a, b and e, f). Within April  $T$  varied between 0.28 and 0.99 mm d<sup>-1</sup> at both sites and  $E$  between 0.07 and 1.04 mm d<sup>-1</sup> at both sites, respectively and both fluxes were in the same range during spring. Likewise, the relative contribution of  $T$  to  $ET$  varied between 34 and 93% between April and June. Understory  $ET$  was significantly lower at the tree site compared to the open site during the first half of the growing season (U-test,  $p < 0.05$ ), especially in the transition period between spring and summer (late May to mid June). This was mainly caused by lower understory transpiration due to a significant lower conductance (Fig. 5a-h, Table 2). On an annual basis, herbaceous  $T$  played a dominant role during the main growing season from April to the onset of summer drought, while soil  $E$  was equally high during spring and fall ( $0.4 \pm 0.1$  mm d<sup>-1</sup>), only ceasing during the summer drought period. Thus, the relative small increase of net understory  $ET$  in response to increased soil  $\theta$  in fall was caused by very low  $T$  ( $0.12 \pm 0.03$  mm d<sup>-1</sup>) of the newly established understory vegetation.

**Table 2:** Living aboveground biomass (g m<sup>-2</sup>) of the herbaceous layer in spring and fall 2011 on the open and tree site (mean values  $\pm$  SD; n=5).

date	open site	tree site
<b>8.4.2011</b>	69 $\pm$ 4	72 $\pm$ 21
<b>24.4.2011</b>	70 $\pm$ 9	71 $\pm$ 11
<b>27.5.2011</b>	67 $\pm$ 7	72 $\pm$ 23
<b>14.6.2011</b>	33 $\pm$ 12	17 $\pm$ 9
<b>1.11.2011</b>	14 $\pm$ 2	15 $\pm$ 4
<b>14.11.2011</b>	43 $\pm$ 7	41 $\pm$ 7

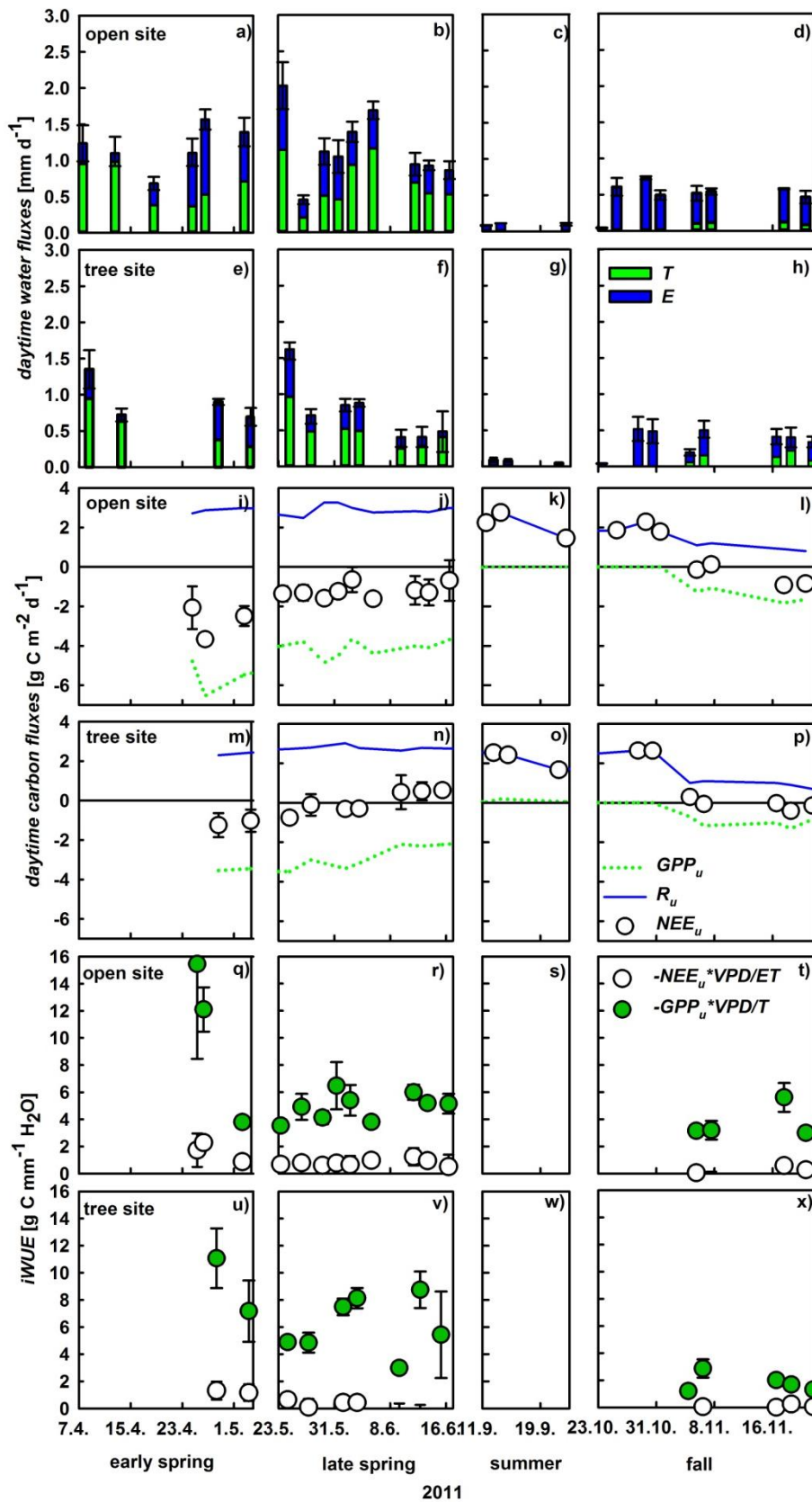
In contrast to ecosystem  $NEE$ ,  $NEE$  of the understory ( $NEE_u$ ) turns to a net carbon source at the onset of summer with net respiration rates of up to 2.8 g C m<sup>-2</sup> d<sup>-1</sup> (Fig. 5i-p). Understory respiration was relatively stable over the measurement period only declining slightly during fall, due to decreasing temperatures. Hence, variability in  $NEE_u$  was mainly triggered by changes in gross primary production of the understory ( $GPP_u$ ) which peaked in late April at -6.5 g C m<sup>-2</sup> d<sup>-1</sup> corresponding to the observed

peak in understory aboveground biomass ( $70 \pm 9$  and  $71 \pm 11 \text{ g m}^{-2}$  at the open and tree site, Table 3). Die-back of the understory vegetation in late spring and accordingly a decline in  $GPP_u$  was responsible for the net release of carbon from the understory during summer, while the germination in late October led to a swift increase of  $GPP_u$  up to  $1.8 \text{ g C m}^{-2} \text{ d}^{-1}$ . Notably, significant site-specific differences were found in  $GPP_u$  and  $NEE_u$  from late May onward (U-test,  $p < 0.05$ ). The die-back of the understory vegetation occurred 2 weeks earlier at the tree site, hence the reduction in  $GPP_u$  was stronger under the trees with 50% compared to 20% reduction from late April to mid June at the open site (Fig. 5i-p).

**Table 3:** Daytime mean conductance ( $\text{mmol m}^{-2} \text{ s}^{-1}$ ) of the herbaceous layer during spring, late spring and fall (mean values  $\pm$  SE) at the open and tree site. Site specific differences are indicated at  $p < 0.05$  (Mann-Whitney U-test).

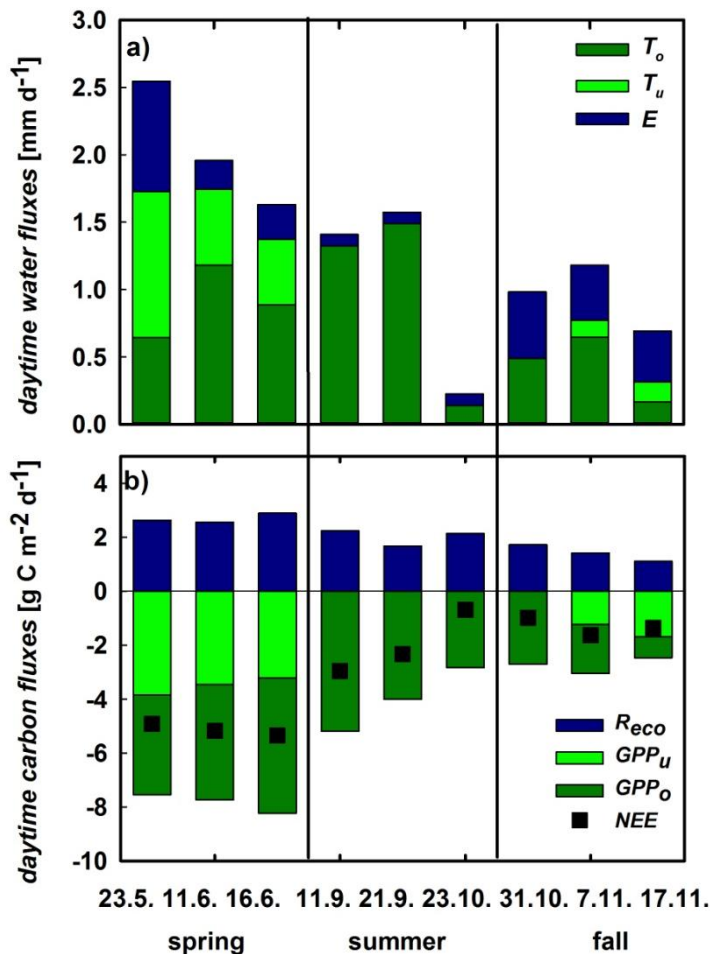
season	open site	tree site	p-level
spring	$111.6 \pm 35$	$85.7 \pm 41$	<i>n.s.</i>
late spring	$102.7 \pm 47$	$65.5 \pm 48$	0.02
fall	$130.2 \pm 101$	$103.8 \pm 93$	<i>n.s.</i>

Inherent water-use efficiency ( $iWUE$ ) was calculated for the whole understory (including respiratory fluxes and soil evaporation) as well as the vegetation level (gross primary productivity and transpiration only; Fig. 5q-x). Understory  $iWUE$  did not show a pronounced inter-seasonal development and was  $2.2 \pm 1.2$  at the open and  $2.5 \pm 1.2 \text{ g C mm}^{-1} \text{ H}_2\text{O}$  at the tree site. Plant level  $iWUE$  was always higher than understory  $iWUE$ , however the difference became very pronounced following rain events and a linear relationship could be detected between volumetric soil water content and difference in  $iWUE$  on understory vs. plant level ( $R^2=0.3$ ;  $p=0.01$ ).



#### 5.4.5. Contribution of understory vegetation and soil to the ecosystem carbon and water fluxes

The contribution of the understory vegetation to whole ecosystem  $ET$  was highest during its growth peak in spring. In contrast, soil  $E$  was the dominant flux of ecosystem  $ET$  in fall reaching 55% of total  $ET$ . Herbaceous  $T$  and soil  $E$  alike decreased towards the beginning of the summer drought period from 43 and 32% in May to 30 and 16% in June, respectively (Fig. 6a), both being negligible for ecosystem  $ET$  during summer. Likewise, herbaceous  $GPP$  displayed the highest contribution to ecosystem  $GPP$  during spring but declining from 51% to 36% towards the onset of summer drought in June. After its germination in fall, understory contribution to  $GPP_{eco}$  increased to 50% within two weeks (Fig. 6b). Despite the long drought period, cork-oak  $GPP$  as well as  $T$  were relatively stable during spring and summer ( $-4.4 \pm 0.65$  g C m<sup>-2</sup> d<sup>-1</sup> and  $1.12 \pm 0.14$  mm d<sup>-1</sup>, respectively) and declining only drastically towards the end of summer and remaining low during autumn ( $-1.8 \pm 0.96$  g C m<sup>-2</sup> d<sup>-1</sup> and  $0.2 \pm 0.16$  mm d<sup>-1</sup>; Fig. 6a, b). Since  $R_{eco}$  was relatively stable throughout the year (at  $2.1 \pm 0.6$  g C



m<sup>-2</sup> d<sup>-1</sup> on average; Fig. 6b), changes in ecosystem  $NEE$ , especially between spring and summer, can mostly be attributed to understory vegetation dynamics.

**Figure 6:** a) Daytime integrated ecosystem evapotranspiration ( $ET$ , sum of the stacked bars) and its components cork-oak transpiration ( $T_o$ , dark green), herbaceous transpiration ( $T_u$ , green) and soil evaporation ( $E$ , blue, all mm d<sup>-1</sup>). b) Daytime integrated  $GPP$  of cork oaks ( $GPP_o$ , dark green) and understory ( $GPP_u$ , green), ecosystem respiration ( $R_{eco}$ ; blue), and net ecosystem CO<sub>2</sub> exchange ( $NEE$ , black squares, all in g C m<sup>-2</sup> d<sup>-1</sup>).

Inherent water-use efficiency was calculated at ecosystem ( $-NEE*VPD/ET$ ) and plant level ( $-GPP*VPD/T$ ; Fig.7). In general, cork-oak  $iWUE$  was within the range of ecosystem  $iWUE$ , which increased to  $3.8 \text{ g C mm}^{-1} \text{ H}_2\text{O}$  with the onset of summer drought but then steadily declined towards fall. Notably, understory  $iWUE$  was similar to cork-oak and also ecosystem  $iWUE$  in spring but much higher in fall (Fig. 7).

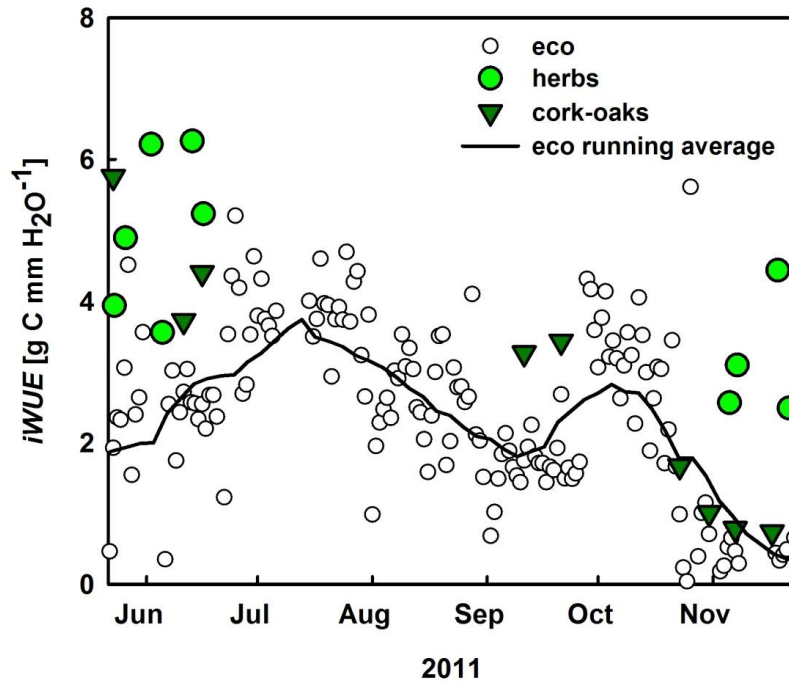


**Figure 7:** Inherent water-use efficiency ( $iWUE$ ,  $GPP*VPD/(E)T$ ) of the ecosystem (white circles), the black line represents the running average, cork oaks (dark green) and understory vegetation (green circles).

## 5.5. Discussion

In semi-arid ecosystems, such as Mediterranean evergreen oak woodlands with sparse tree cover, water is the major factor limiting ecosystem productivity. Future climate change scenarios propose even increased drought and altered precipitation pattern in the Mediterranean (IPCC 2007; Costa *et al.*, 2012; Jongen *et al.*, 2013). Under these conditions, an efficient use of the limited water supply is crucial (Wang *et al.*, 2012) and advancements of observational methods and modeling approaches are vitally important to better understand vegetation-soil-water feedbacks. We hypothesized that in savanna type ecosystems the herbaceous understory layer, despite its ephemeral life form, plays an important role in the water and carbon balances and for ecosystem resilience towards drought. In the following, this shall be discussed with respect to the contribution of the understory to total ecosystem



$ET$  and productivity, as well as influence on unproductive soil water loss, i.e. evaporation ( $E$ ) and soil water distribution.

The recent developments in laser spectroscopy enabled us to measure  $\delta^{18}O$  of ambient vapor ( $\delta^{18}O_a$ ), of understory evapotranspiration ( $\delta^{18}O_{ET}$ ) and its components with a high temporal resolution. The direct observations of  $\delta^{18}O_E$  on bare soil plots allowed a detailed validation of the Craig and Gordon (1965) model for the first time over a whole growing season regarding short time-scales, i.e. differences on a diurnal basis, as well as under extreme conditions (saturated or dry soils; Dubbert *et al.*, 2013; Wang *et al.*, 2013). We could show that calculated  $\delta^{18}O_E$  is in very good agreement with measurements of  $\delta^{18}O_E$  even during early morning and afternoon, where environmental conditions change swiftly. However, a thorough validation of the models estimating  $\delta^{18}O$  soil evaporation (Dubbert *et al.*, 2013) and plant transpiration ( $T$ , Dubbert *et al.*, 2014a) are pivotal. For example, assuming  $T$  to be in isotopic steady-state leads to offsets of up to 70% in the estimation of the fraction of  $T$  on total understory evapotranspiration in this ecosystem (Dubbert *et al.*, 2013), exceeding previous uncertainty estimates of around 25% (Yepez *et al.*, 2007). This also indicates that the impact of not considering the effect of non-steady-state transpiration on  $ET$  partitioning probably differs between plant functional types and ecosystems (see Dubbert *et al.*, 2014a). Similarly, the Craig and Gordon equation is very sensitive to uncertainties in estimates of temperature and oxygen isotope signatures of soil water at the evaporating front ( $T_e$  and  $R_e$ ; see Braud *et al.*, 2005; Dubbert *et al.*, 2013; Rothfuss *et al.*, 2012); hence taking averages of parts of the soil profile, as done by previous studies (Lai *et al.*, 2006; Yepez *et al.*, 2005; Wang *et al.*, 2010), likely leads to large uncertainties not only in the estimate of  $\delta^{18}O_E$  but also in the partitioning ( $T/ET$ ).

The coupling of the laser spectrometer to gas-exchange chambers for this isotope based  $ET$  partitioning approach further offered the opportunity to separate between herbaceous transpiration and soil evaporation for the first time over a whole growing season with a temporal resolution exceeding by far that of previous studies, who mostly were able to estimate  $T/ET$  for 1 up to 6 days over the growing season (see for comparison Williams *et al.*, 2004; Yepez *et al.*, 2007; Wang *et al.*, 2013; Hu *et al.*, 2014). This has strong potential to enhance our functional understanding of soil evaporation dynamics and vegetation-soil feedbacks within the water cycle, specifically for grassland ecosystems



where  $ET$  can hardly be separated by classical flux based approaches (but see the modeling approach of Hu *et al.*, 2009).

One main observation of this study was the distinct responses of understory  $T$  and soil  $E$  to changes in environmental conditions. The small contribution of  $T$  shortly after a rain pulse is due to the swift increase in soil  $E$  (Scott *et al.*, 2006, Raz-Yaseef *et al.*, 2012). In contrast, plant  $T$  strongly decreased upon rain events and only very gradually increased thereafter. During drought,  $E$  also declined much faster, while plants maintained a relatively stable transpiration rate even under rather dry soil conditions. Raz-Yaseef *et al.* (2012) explained such findings with the regulation of  $T$  and  $E$  by different soil layer  $\theta_s$ . However, a correlation between  $T$  and  $\theta_s$  of all obtained depths (5, 15, 30 and 60cm) could not be detected even when  $\theta_s$  was low. While  $E$  was significantly correlated with top soil  $\theta_s$  ( $R^2=0.55$ ,  $p<0.001$ ), a correlation with VPD could only be observed when  $\theta_s$  was strongly limiting  $E$ . By contrast, understory  $T$  was correlated with VPD instead ( $R^2=0.57$ ,  $p<0.001$ ), highlighting that considering  $E$  and understory  $T$  separately is crucial for understanding changes in net  $ET$ . Moreover, soil evaporation at both sites was correlated with understory biomass development: the higher aboveground biomass the smaller the soil fluxes (see also Barr *et al.*, 2004). Vegetation cover, depending mostly on  $LAI$ , can largely reduce unproductive soil evaporation (Hu *et al.*, 2009; Wang *et al.*, 2010; Raz-Yaseef *et al.*, 2012). We found up to 40% reduction of  $E$  on understory vegetation plots compared to bare soil plots (bare soil  $E$  rates are not shown). Reducing bare soil evaporation has therefore been addressed as a critical issue in many dry-lands (Wang *et al.*, 2012). Averaged for the periods where understory vegetation was present, soil  $E$  contributed a similar amount to ecosystem  $ET$  than understory  $T$  (27% and 29%, respectively), which was largely neglected in previous studies (Paço *et al.*, 2009; Jasechko *et al.*, 2013). However, soil  $E$  contributed significantly only when water was not limiting plant photosynthesis and growth. By contrast, during times of low water availability, inherent water use efficiency increased, which was at least in parts due to strongly decreased soil evaporation rates (Fig. 5 and 6, Pereira *et al.*, 2007).

Furthermore, comparisons of inherent water use efficiency reflecting water limitation effects (Vickers *et al.*, 2012; Eamus *et al.*, 2013) at ecosystem versus plant scale were conducted. In semi-arid regions  $iWUE$  often increases in times of moderate drought stress of the vegetation, reflecting the ability of

plants to adjust their photosynthetic capacity and/or stomatal control in times of lower water availability (Scott *et al.*, 2006; Yepez *et al.*, 2007; Jongen *et al.*, 2011; Vickers *et al.*, 2012; Eamus *et al.*, 2013), which can be seen at the ecosystem level during early summer (June-July). The decrease in ecosystem and tree *iWUE* over the later course of summer might be explained, on the other hand, by temperature and light stress (Pereira *et al.*, 2006). Trees did not down-regulate their transpiration very strongly until late August (D’Odorico; Fig. 6), probably due to their supposed access to deep soil water layers and/or groundwater, but the photosynthetic apparatus might still have been limited by the higher average (leaf) temperatures in summer compared to spring (Werner & Correia, 1996; Werner *et al.*, 2006), thus leading to a decrease in *iWUE* (Pereira *et al.*, 2007). Comparing ecosystem with plant level *iWUE*, a large impact of either soil evaporation or ecosystem respiration on ecosystem water use efficiency should be reflected in lower ecosystem scale *iWUE* ( $-NEE*VPD/ET$ ) compared to *iWUE* of cork-oaks and the understory ( $-GPP*VPD/T$ ). While *iWUE* of the cork-oaks was mostly within range of ecosystem *iWUE*, *iWUE* of the understory plants was higher than ecosystem *iWUE* in both spring and fall. In early spring and fall these smaller values on ecosystem scale were caused by both high soil evaporation and  $R_{eco}$  rates. During late spring however, soil evaporation was small and the lower ecosystem *iWUE* compared to plant *iWUE* was mainly caused by high  $R_{eco}$  rates. This confirms that during times of water limitation ecosystem *iWUE* is not negatively affected by soil *E*. Notably, even the strong differences between ecosystem and plant *iWUE* at the understory scale, immediately following rain events, were caused by a strong increase in plant *iWUE* due to decreased  $T_u$  immediately after rainfall and not by a decrease in  $iWUE_{eco}$ . Moreover, the impact of the understory vegetation on ecosystem productivity was as large as its contribution to the water cycle (see also Unger *et al.*, 2009, 2010), leading to similar or even higher *iWUE* of the understory and cork-oaks and, hence, a significant contribution of the understory layer to the ecosystem sink strength in spring and fall.

In addition to this contribution to ecosystem productivity and the reduction of soil evaporation, a third beneficial effect of understory vegetation on ecosystem functioning was identified: understory vegetation impact on soil water infiltration (Tromble, 1988; Dawson, 1993; Schwinning & Ehleringer, 2001; Devitt & Smith, 2002; Bhark & Small, 2003; Huxman *et al.*, 2005; Kurz-Besson *et al.*, 2006;

Scott *et al.*, 2014). A positive feedback of vegetation biomass on rain water infiltration is often found in arid ecosystems with open canopies, where it alters spatial distribution and enhances rain use efficiency of the vegetation (Bromley *et al.*, 1997; Coutron & Kokou, 1997; Rietkerk *et al.*, 2002; D'Odorico *et al.*, 2006; Chen *et al.*, 2013). On the other hand, vegetation canopies intercept rainfall, and a substantial proportion of this rainfall interception can be lost due to evaporation from plant surfaces (Tromble, 1988). Here, we observed contrasting effects on rainfall infiltration of the two different vegetation types: the cork-oak canopy had no significant influence on infiltration, while the understory vegetation cover significantly increased infiltration compared to bare soil plots. Bhark & Small (2003) report that this beneficial influence is enhanced in ecosystems with strong natural surface run-off on bare soils with reduced hydraulic conductivity due to a sealed soil layer during the dry period (Chen *et al.*, 2013), which is the case at our study site. Notably, a significant relationship between rain fall intensity and differences in infiltration between bare soil and understory patches could be observed (Bhark & Small, 2003). Likewise, Thompson *et al.* (2010) found an increasing effect of vegetation biomass on infiltration with decreasing soil water availability. Therefore, the presence of a fully developed herbaceous layer should be even more important with increased drought. Moreover, herbaceous understory vegetation has been shown to facilitate tree growth and fruit production by increasing soil N (Pulido *et al.*, 2010; Rolo & Moreno, 2011). It can be expected that repeated ploughing, liming and sowing of a legume rich seed mixture, a common practice in agro-silvo-pastoral systems in Portugal also done in a three to five year interval at our site, significantly increases the contribution of N-fixing species intensifying this effect (Crespo, 2006).

However, the understory vegetation itself is highly vulnerable to drought, which is underlined by the significantly earlier die back of the understory vegetation under the trees compared to open areas at the onset of summer drought, when environmental stress increased. This earlier senescence below the tree canopy predominantly affected N-fixers and grasses and suggests competition with oak trees for water from the top soil layers as also herbaceous vegetation transpiration and conductance were significantly reduced by 40% and 45%, respectively (see also Moreno, 2008; Dubbert *et al.*, 2014b). This drought induced competition even influenced total ecosystem sink strength in spring, as it reduced the overall understory productivity on average by 22% on the tree compared to the open sites during the last 3

weeks of the herbaceous vegetation period.

In conclusion, beneficial understory vegetation effects were dominant, as herbaceous biomass strongly increased rain infiltration, diminished soil  $E$  and significantly added to the ecosystem carbon sink strength. However, the observed vulnerability of the understory vegetation to drought and competition for water with trees suggests, that increased drought and altered precipitation pattern as predicted in future climate change scenarios for the Mediterranean basin not only threaten understory development. They also very likely decrease rain infiltration and ground water recharge by decreasing understory vegetation cover and increasing amount of heavy precipitation events with high run-off from sealed bare soils. This in turn can severely diminish cork-oak productivity and hence the resilience of the ecosystem towards drought (Scott *et al.*, 2014).

## 5.6. Acknowledgements

We would like to thank the Herdade da Machoqueira do Grou for logistical support and allowing the establishment of our field site. We gratefully acknowledge help in the field from Stephan Unger, Alexander Mosena, Fabio Gonsalvez, Jan Sauer, and Katrin Remmert. We especially thank Rodrigo Maia, Elke Furlkröger, Verena Lauströer, and Babsi Teichner for technical assistance in the laboratory. Funding for this project was provided by the Deutsche Forschungsgemeinschaft (WATERFLUX Project: # WE 2681/6-1; # CU 173/2-1) and the Deutsche Akademische Austausch Dienst.

## 5.7. Literature

- Barr, A.G., Black, T., Hogg, E., Kljun, N., Morgenstern, K., Nesic, Z. (2004). Inter-annual variability in the leaf area index of a boreal aspen-hazelnut forest in relation to net ecosystem production. *Agricultural and Forest Meteorology* 126, 237 - 255
- Beer, C., Ciais, P., Reichstein, M., Baldocchi, D., Law, B.E., Papale, D., *et al.* (2009). Temporal and among-site variability of inherent water use efficiency at the ecosystem level. *Global biogeochemical cycles* 23.
- Bhark, E.W., Small, E.E. (2003). Association between plant canopies and spatial patterns of infiltration in shrubland and grassland of the Chihuahuan Desert, New Mexico., *Ecosystems* 6, 185-196.
- Braud, I., Bariac, T., Gaudet, J.-P., Vauclin, M. (2005). SiSPAT-Isotope, a coupled heat, water and stable isotope (HDO and (H<sub>2</sub>O)-O-18) transport model for bare soil. Part I. Model description

- and first verifications. *Journal of Hydrology* 309, 277-300.
- Bromley, J., Brouwer, J., Barker, A.P., Gaze, S.R., Valentin, C. (1997). The role of surface water redistribution in an area of patterned vegetation in a semi-arid environment, south-west Niger. *Journal of Hydrology* 198, 1-29.
- Bugalho, M.N., Caldeira, M.C., Pereira, J.S., Aronson, J., Pausas, J.G. (2011). Mediterranean cork oak savannas require human use to sustain biodiversity and ecosystem services. *Frontiers in Ecology and Environments* 9, 278-286.
- Chen, L., Sela, S., Svoray, T., Assouline, S. (2013). The role of soil-surface sealing, microtopography, and vegetation patches in rainfall-runoff processes in semiarid areas. *Water resources research* 49, 5585-5599.
- Couteron, P., Kokou, K. (1997). Woody vegetation spatial patterns in a semi-arid savanna of Burkina-Faso, West Africa. *Plant Ecology* 132, 211-227.
- Costa, A.C., Santos, J.A., Pinto, J.G. (2012). Climate change scenarios for precipitation extremes in Portugal. *Theoretical and Applied Climatology* 108, 217-234.
- Craig, H., Gordon, L.I. (1965). Deuterium and oxygen-18 variations in the ocean and the mairitme atmosphere. Paper presented at the Stable Isotopes in Oceanographic Studies and Paleotemperatures, Spoleto, Italy.
- Crespo, D.G., 2006. The role of pasture improvement in the rehabilitation of the “montado/dehesa” sytem and in developing its traditional products. In: Ribeiro, J.M.C.R., Horta, A.E.M., Mosconi, C., Rosati, A. (eds.), *Animal Products from the Mediterranean Area*, Wageningen Academical Publishing, Wageningen.
- Cuntz, M., Ogee, J., Farquhar, G.D., Peylin, P., Cernusak, L.A. (2007). Modelling advection and diffusion of water isotopologues in leaves. *Plant, Cell and Environment* 30, 892-909.
- David, T.S., Ferreira, M., Cohen, S., Pereira, J.S., David, J.S. (2004). Constraints on transpiration from an evergreen oak tree in southern Portugal. *Agricultural and Forest Meteorology* 122, 193-205.
- Dawson, T. (1993). Hydraulic lift and water transport to, through and from roots. *Plant Physiology* 102, 29.
- Devitt, D.A., Smith, S.D. (2002). Root channel macropores enhance downward movement of water in a Mojave Desert ecosystem. *Journal of arid environments* 50, 99-108.
- Dongmann, G., Nurnberg, H.W., Forstel, H., Wagener, K. (1974). On the enrichment of H<sub>2</sub><sup>18</sup>O in the leaves of transpiring plants. *Radiation and Environmental Biophysics* 11, 41-52.
- D’Odorico, P., Porporato, A. (2006). Soil moisture dynamics in water-limited ecosystems. *Dryland ecohydrology*, 31-46.
- Dubbert, M., Cuntz, M., Piayda, A., Maguas, C., Werner, C. (2013). Partitioning evapotranspiration – Testing the Craig and Gordon model with field measurements of oxygen isotope ratios of evaporative fluxes. *Journal of Hydrology* 496, 142-153.
- Dubbert, M., Cuntz, M., Piayda, A., Werner, C. (2014a). Oxygen isotope signatures of transpired water vapor – the role of non-steady-state transpiration under natural conditions. *New Phytologist* 203, 1242-1252.
- Dubbert, M., Mosena, A., Piayda, A., Cuntz, M., Correia, A., Pereira, J.S., Werner, C. (2014b). Influence of tree cover on herbaceous layer development and carbon and water fluxes in a Portuguese cork oak woodland. *Acta Oecologica* 59, 35-45.
- Eamus, D., Cleverly, J., Boulain, N., Grant, N., Faux, R., Villalobos-Vega, R. (2013). Carbon and water fluxes in an arid-zone Acacia savanna woodland: An analyses of seasonal patterns and responses to rainfall events. *Agricultural and Forest Meteorology* 182, 225-238.
- Farquhar, G.D., Lloyd, J. (1993). Carbon and oxygen isotope effects in the exchange of carbon dioxide between terrestrial plants and the atmosphere, in: *Stable Isotopes and Plant Carbon-Water Relations*, eds. J.R. Ehleringer, A.E. Hall, G.D. Farquhar (Academic Press, San Diego).

- Haverd, V., Cuntz, M. (2010). Soil-Litter-Iso: A one-dimensional model for coupled transport of heat, water and stable isotopes in soil with a litter layer and root extraction. *Journal of Hydrology* 388, 438-455.
- Haverd, V., Cuntz, M., Griffith, D., Keitel, C., Tadros, C., Twining, J. (2011). Measured deuterium in water vapour concentration does not improve the constraint on the partitioning of evapotranspiration in a tall forest canopy, as estimated using a soil vegetation atmosphere transfer model. *Agricultural and Forest Meteorology* 151, 645-654.
- Helliker, B.R., Ehleringer, J.R. (2002). Differential O-18 enrichment of leaf cellulose in C-3 versus C-4 grasses. *Functional Plant Biology* 29, 435-442.
- Hu, Z., Yu, G., Zhou, Y., Sun, X., Li, Y., Shi, P., *et al.* (2009). Partitioning of evapotranspiration and its controls in four grassland ecosystems: Application of a two-source model. *Agricultural and Forest Meteorology* 149, 1410-1420.
- Hu, Z., Wen, X.F., Sun, X.M., Li, L.H., Yu, G.R., Lee, X.H. *et al.* (2014). Partitioning of evapotranspiration through oxygen isotopic measurements of water pools and fluxes in a temperate grassland. *Journal of geophysical research – Biogeosciences* 119, 358-371.
- Huxman, T.E., Wilcox, B.P., Breshears, D.D., Scott, R.L., Snyder, K.A., Small, E.E., *et al.* (2005). Ecohydrological implications of woody plant encroachment. *Ecology* 86, 308-319.
- IPCC (2007). Climate change 2007: synthesis report. In: Contribution of Working Groups I, II and III to the Fourth Assessment Report of the Intergovernmental Panel on Climate change (eds. Core Writing Team, Pachauri RK, Reisinger A), 104pp. IPCC, Geneva, Switzerland.
- Jasechko, S., Sharp, Z.D., Gibson, J.J., Birks, S.J., Yi, Y., Fawcett, P.J. (2013). Terrestrial water fluxes are dominated by transpiration. *Nature* 496.
- Jongen, M., Pereira, J.S., Aires, L., Piac, C. (2011). The effects of drought and timing of precipitation on the inter-annual variation in ecosystem-atmosphere exchange in a Mediterranean grassland. *Agricultural and Forest Meteorology* 151, 595–606.
- Jongen, M., Lecomte, X., Unger, S., Pinto-Marijuan, M., Pereira, J.S. (2013). The impact of changes in the timing of precipitation on the herbaceous understorey of Mediterranean evergreen oak woodlands. *Agricultural and Forest Meteorology* 171,163-173.
- Kolle, O., Rebman, C. (2007). EddySoft Documentation of a Software Package to Acquire and Process Eddy Covariance Data. Max-Planck-Institut für Biogeochemie.
- Kurz-Besson, C., Otieno, D., Lobo-do-Vale, R., Siegwolf, R., Schmidt, M., David, T., Soares David, J., Tenhunen, J., Pereira, J.S., Chaves, M. (2006). Hydraulic lift in cork-oak trees in a savannah-type Mediterranean ecosystem and its contribution to the local water balance. *Plant and Soil* 282, 361-378.
- Lai, C.T., Ehleringer, J.R., Bond, B.J., and U., K. (2006). Contributions of evaporation, isotopic non-steady state transpiration and atmospheric mixing on the delta O-18 of water vapor in Pacific Northwest coniferous forests. *Plant, Cell and Environment* 29, 77-94
- Lasslop, G., Reichstein, M., Papale, D., Richardson, A.D., Arneth, A., Barr, A., *et al.* (2010). Separation of net ecosystem exchange into assimilation and respiration using a light response curve approach: critical issues and global evaluation. *Biogeosciences* 16, 187-208.
- Majoube, M. (1971). Oxygen-18 and Deuterium Fractionation between Water and Steam. *Journal of Chemical Physics* 68, 1423.
- Mathieu, R., Bariac, T. (1996). A numerical model for the simulation of stable isotope profiles in drying soils. *Journal of Geophysical Research* 101, 12685-12696.
- Mauder, M., Cuntz, M., Drüe, C., Graf, A., Rebmann, C., Schmid, H.P., *et al.* (2013). A strategy for quality and uncertainty assessment of long-term eddy-covariance measurements. *Agricultural and Forest Meteorology* 169, 122 – 135.
- Merlivat, L. (1978). Molecular Diffusivities of (H<sub>2</sub>O)-O-16 and (H<sub>2</sub>O)-O-18 in Gases.

- Journal of Chemical Physics* 69, 2864-2871.
- Moreira, M.Z., Martinelli, L.A., Victoria, R.L., Barbosa, E.M., Bonates, L.C.M., Nepstads, D.C. (1997). Contribution of transpiration to forest ambient vapour based on isotopic measurements. *Global Change Biology* 3, 439-450.
- Moreno, G., Obrador, J.J., Cubera, E., Dupraz, C. (2005). Fine root distribution in Dehesas of Central-Western Spain. *Plant and Soil* 277, 153-162.
- Moreno, G., Obrador, J., García, E., Cubera, E., Montero, M., Pulido, F., Dupraz, C. (2007). Driving competitive and facilitative interactions in oak dehesas through management practices. *Agroforestry Systems* 70, 25-40.
- Moreno, G. (2008). Response of understorey forage to multiple tree effects in Iberian dehesas. *Agriculture, Ecosystems and Environment* 123, 239-244.
- Otieno, D., Mirzaei, H., Hussain, M., Li, Y.L., Schmidt, M.W.T. Waringer, M., *et al.* (2011). Herbaceous layer development during spring does not deplete soil nitrogen in the Portuguese Montado. *Journal of Arid Environments* 75, 231-238.
- Paço, T.A., David, T.S., Henriques, M.O., Periera, J.S., Valente, F., Banza, J., *et al.* (2009). Evapotranspiration from a Mediterranean evergreen oak savannah: The role of trees and pasture. *Journal of Hydrology* 369, 98-106.
- Pape, L., Ammann, C., Nyfeler-Brunner, A., Spirig, C., Hens, K., Meixner, F.X. (2009). An automated dynamic chamber system for surface exchange measurement of non-reactive and reactive trace gases of grassland ecosystems. *Biogeosciences* 6, 405-429.
- Pereira, J.S., Chaves, M.-M., Caldeira, M.-C., Correia, A.V. (2006). Water availability and production, in: Plant growth and climate change (eds. J.I.L. Morison, M.D. Morecroft). Blackwell Publishing Ltd., Oxford.
- Pereira, J.S., Mateus, J.A., Aires, L.M., Pita, G., Pio, C., David, J.S., *et al.* (2007). Net ecosystem carbon exchange in three contrasting Mediterranean ecosystems – the effect of drought. *Biogeosciences* 4, 791-02.
- Perez-Ramos, I., Zavala, M., Maranon, T., Diaz-Villa, M., Valladares, F. (2008). Dynamics of understorey herbaceous plant diversity following shrub clearing of cork oak forests: A five-year study. *Forest Ecology and Management* 255, 3242-3253.
- Piayda, A., Dubbert, M., Rebmann, C., Kolle, O., Costa e Silva, F., Correia, A., Pereira, J.S., Werner, C., Cuntz, M. (2014). Drought impact on carbon and water cycling in a Mediterranean Quercus suber L. woodland during the extreme drought event in 2012. *Biogeosciences Discussions*.
- Pulido, F., Garcia, E., Obrador, J., Moreno, G. (2010). Multiple pathways for tree regeneration in anthropogenic savannas: incorporating biotic and abiotic drivers into management schemes. *Journal of Applied Ecology*.
- Raz-Yaseef, N., Yakir, D., Schiller, G., Cohen, S. (2012). Dynamics of evapotranspiration partitioning in a semi-arid forest as affected by temporal rainfall patterns. *Agricultural and Forest Meteorology* 157, 77-85.
- Reichstein, M., Falge, E., Baldocchi, D., Papale, D., Aubinet, M., Berbigier, P., *et al.* (2005). On the separation of net ecosystem exchange into assimilation and ecosystem respiration: review and improved algorithm. *Global Change Biology* 11, 1424-1439.
- Rietkerk, M., Boerlijst, M.C., van Langevelde, F., HilleRisLambers, R., van de Koppel, J., Kumar, L., Prins, H.H.T., de Roos, A.M. (2002). Self-organization of vegetation in arid ecosystems. *American Naturalist* 160, 524-530.
- Rolo, V., Moreno, G. (2011). Shrub species affect distinctively the functioning of scattered Quercus ilex trees in Mediterranean open woodlands. *Forest Ecology and Management* 261, 1750-1759.
- Rothfuss, Y., Braud, I., LeMoine, N., Biron, P., Durand, J.-L., Vauclin, M., Bariac, T. (2012). Factors controlling the isotopic partitioning between soil evaporation and plant transpiration:



- Assessment using a multi-objective calibration of SiSPAT-Isotope under controlled conditions. *Journal of Hydrology* 442:75-88.
- Saco, P.M., Willgoose, G.R., Hancock, G.R. (2007). Eco-geomorphology of banded vegetation patterns in arid and semi-arid regions. *Hydrology and Earth System Sciences* 11, 1717-1730.
- Scott, R., Huxman, T., Cable, W., Emmerich, W. (2006). Partitioning of evapotranspiration and its relation to carbon dioxide exchange in a Chihuahuan Desert shrubland. *Hydrological processes* 20, 3227-3243.
- Scott, R.L., Huxman, T.E., Barron-Gafford, G.A., Jenerette, G.D., Young, J.M., Hammerlynck, E.P. (2014). When vegetation change alters ecosystem water availability. *Global Change Biology*, online first.
- Schwinning, S., Ehleringer, J. (2001). Water use trade-offs and optimal adaptations to pulse-driven arid ecosystems. *Journal of Ecology* 89, 464-48.
- Thompson, S.E., Harman, C.J., Heine, P., Katul, G.G. (2010). Vegetation-infiltration relationships across climatic and soil type gradients. *Journal of Geophysical Research* 115, 1-12.
- Tromble, J.M. (1988). Water interception by 2 arid land shrubs. *Journal of Arid Environments* 15: 65-70.
- Unger, S., Máguas, C., Pereira, J.S., Aires, L.M., David, T.S., Werner, C. (2009). Partitioning carbon fluxes in a Mediterranean oak forest to disentangle changes in ecosystem sink strength during drought. *Agricultural and Forest Meteorology* 149, 949-961.
- Unger, S., Maguas, C., Pereira, J.S., Aires, L.M., David, T.S., Werner, C. (2010). Disentangling drought-induced variation in ecosystem and soil respiration using stable carbon isotopes. *Oecologia* 163, 1043-1057.
- Unger, S., Maguas, C., Pereira, J.S., David, T.S., Werner, C. (2012). Interpreting post-drought rewetting effects on soil and ecosystem carbon dynamics in a Mediterranean oak savannah. *Agricultural and Forest Meteorology* 154, 9-18.
- Vickers, H., Gillespie, M., Gravina, A. (2012). Assessing the development of rehabilitated grasslands on post-mined landforms in north-west Queensland, Australia. *Agriculture, Ecosystems and Environment* 163, 72-84.
- Von Caemmerer, S., Farquhar, G.D. (1981). Some relationships between the biochemistry of photosynthesis and the gas-exchange of leaves. *Planta* 153, 376-387.
- Wang, L., D'Odorico, P. (2008). The limits of water pumps. *Science*, 321, 36-37.
- Wang, L., Caylor, K.K., Villegas, J.C., Barron-Gafford, G.A., Breshears, D.D., Huxman, T.E. (2010). Partitioning evapotranspiration across gradients of woody plant cover: Assessment of a stable isotope technique. *Geophysical Research Letters* 37.
- Wang, L., D'Odorico, P., Evans, J.P., Eldrige, D.J., McCabe, M.F., Caylor, K.K., *et al.* (2012). Dryland ecohydrology and climate change: critical issues and technical advances. *Hydrological Earth System Science* 16, 2585-2603.
- Wang, L., Niu, S., Good, S.P., Soderberg, K., McCabe, M., Sherry, R.A., *et al.* (2013). The effect of warming in grassland evapotranspiration partitioning using laser-based isotope monitoring techniques. *Geochimica et Cosmochimica Acta*.
- Werner, C., Correia, O. (1996). Photoinhibition in cork-oak leaves under stress: Influence of the bark-stripping on the chlorophyll fluorescence emission in *Quercus suber* L. *Trees* 10, 288-292.
- Werner, C., Unger, S., Pereira, J.S., Maia, R., Kurz-Besson, C., David, T.S., *et al.* (2006). Importance of short-term dynamics in carbon isotope ratios of ecosystem respiration ( $\delta^{13}\text{C}_\text{R}$ ) in a Mediterranean oak woodland and linkage to environmental factors. *New Phytologist* 172, 330-346.



- Werner, C., Schnyder, H., Cuntz, M., Keitel, C., Zeemran, M.J., Dawson, T.E., *et al.* (2012). Progress and challenges in using stable isotopes to trace plant carbon and water relations across scales. *Biogeosciences* 9, 3083-3111.
- Williams, D.G., Cable, W., Hultine, K., Hoedjes, J.C.B., Yepez, E.A., Simonneaux, V., *et al.* (2004). Evapotranspiration components determined by stable isotope, sap flow and eddy covariance techniques. *Agricultural and Forest Meteorology*, 125, 241-258.
- Yakir, D. (1992). Variations in the natural abundance of O-18 and deuterium in plant carbohydrates. *Plant, Cell and Environment* 15, 1005-1020
- Yakir, D., Sternberg, L.D.L. (2000). The use of stable isotopes to study ecosystem gas exchange. *Oecologia* 123, 297-311.
- Yepez, E.A., Huxman, T.E., Ignace, D.D., English, N.B., Weltzin, J.F., Castellanos, A.E., Williams, D.G. (2005). Dynamics of transpiration and evaporation following a moisture pulse in semiarid grassland: A chamber-based isotope method for partitioning flux components. *Agricultural and Forest Meteorology* 132, 359-376.
- Yepez, E.A., Scott, R.L., Cable, W.L., Williams, D.G. (2007). Intraseasonal variation in water and carbon dioxide flux components in a semiarid riparian woodland. *Ecosystems* 10, 1100-1115.

## 5.8. Supporting information

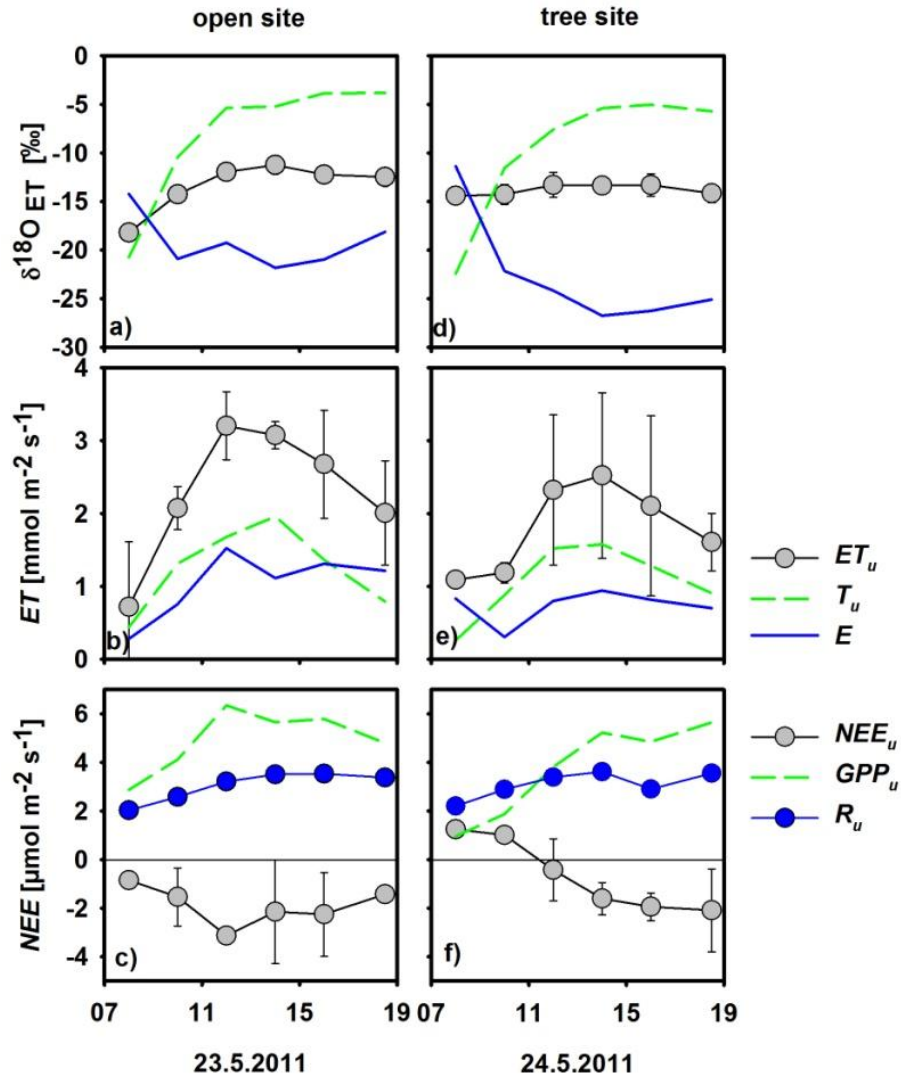


**Figure S1:** Typical diurnal courses of understory  $ET$ ,  $\delta^{18}O_{ET}$ ,  $NEE$  and its components on 23. and 24. May 2011. a,d) of oxygen isotope signatures of measured  $ET$  (grey circles,  $n=3 \pm SD$ ) and modeled  $E$  and  $T$  (blue line and green dashed line) at the open (a) and tree site (d); b, e) of fluxes of measured  $ET$  (grey circles,  $n=3 \pm SD$ ) and modeled  $E$  and  $T$  (blue line and green dashed line) on the open (b) and tree site (e). c, f) Fluxes of measured net understory  $CO_2$  exchange ( $NEE_u$ ; grey circles,  $n=3 \pm SD$ ) and understory respiration ( $R_u$ ; blue circles,  $n=3 \pm SD$ ) and estimated understory plant  $CO_2$  uptake ( $GPP_u$ ; green dashed line) at the open (c) and tree site (f).

**Table S1:** Oxygen isotope signatures of soil water [‰] in 0.5, 2, 5, 10, 15, 20 and 40 cm depth on bare soil and vegetation plots at the open and tree site between 7.4. and 21.11.2011.

Sampling date	Depth (cm)	Open site				Tree site			
		Bare soil (MW±SE)		Vegetation (MW±SE)		Bare soil (MW±SE)		Vegetation (MW±SE)	
7./8.4.2011	0.5	-1.9	2.3	-1.5	2.5	1.1	1.2	-4.2	0.8
	2	-3.8	2.7	-3.3	1.1	-5.6	0.1	-5.9	0.1
	5	-3.5	1.3	-4.5	0.4	-5.8	0.1	-6.4	0.1
	10	-5.2	0.4	-5.3	0.7	-5.6	0.6	-6.5	0.1
	15	-5.4	0.0	-5.5	0.8	-5.8	0.1	-7.1	0.7
	20	-3.0	3.6	-5.3	1.0	-5.7	0.4	-6.9	0.5
	40	-5.5	0.4	-5.6	0.6	-5.6	0.4	-7.6	0.2
12/13.4.2011	0.5	-2.5	1.2	-2.8	0.4	3.5	0.8	-0.2	0.4
	2	3.3	1.3	-2.5	0.4	3.6	0.1	-0.1	0.2
	5	-0.3	0.4	-5.4	1.3	-1.7	1.6	-3.3	2.2
	10	-6.0	0.1	-6.8	0.4	-5.6	0.0	-6.7	0.0
	15	-5.8	0.4	-6.7	0.1	-5.9	0.1	-6.6	0.5
	20	-6.1	0.1	-7.0	0.3	-6.0	0.1	-7.0	0.2
	40	-6.2	0.1	-6.5	0.0	-6.4	0.3	-7.0	0.2
18.4.2011	0.5	0.2	1.3	0.4	0.0	n.a.	n.a.	n.a.	n.a.
	2	5.4	0.3	0.1	0.8	n.a.	n.a.	n.a.	n.a.
	5	n.a.	n.a.	-0.8	0.6	n.a.	n.a.	n.a.	n.a.
	10	-3.0	0.2	-4.3	1.5	n.a.	n.a.	n.a.	n.a.
	15	-5.1	0.0	-5.2	0.4	n.a.	n.a.	n.a.	n.a.
	20	-5.7	0.2	-5.6	0.0	n.a.	n.a.	n.a.	n.a.
	40	-6.1	0.4	-6.8	0.3	n.a.	n.a.	n.a.	n.a.
25.4.2011	0.5	2.2	0.6	-0.7	0.8	n.a.	n.a.	n.a.	n.a.
	2	-3.5	2.5	-3.1	0.1	n.a.	n.a.	n.a.	n.a.
	5	-3.9	0.8	-5.4	0.8	n.a.	n.a.	n.a.	n.a.
	10	-3.7	0.5	-5.5	0.2	n.a.	n.a.	n.a.	n.a.
	15	-4.4	0.1	-5.1	0.1	n.a.	n.a.	n.a.	n.a.
	20	-3.8	1.8	-5.6	0.3	n.a.	n.a.	n.a.	n.a.
	40	-6.1	0.0	-5.9	0.0	n.a.	n.a.	n.a.	n.a.
2./3.5.2011	0.5	4.4	0.8	-4.2	0.4	-1.7	0.2	-4.7	0.0
	2	-1.9	0.4	-4.2	0.5	-4.0	0.3	-5.7	0.3
	5	-4.6	0.3	-6.2	0.1	-5.4	0.3	-6.1	0.4
	10	-5.4	0.7	-7.8	0.5	-5.0	1.2	-5.3	0.1
	15	n.a.	n.a.	-7.7	0.1	-4.4	0.0	-5.2	0.5
	20	-5.2	0.4	-8.0	0.5	-4.8	0.0	-4.9	0.4
	40	-5.5	0.1	-6.4	0.4	-5.0	0.1	-5.7	0.1

Study V: Stable oxygen isotope and flux partitioning demonstrates understory of an oak savanna contributes up to half of ecosystem carbon and water exchange

23./24.5.2011	0.5	1.9	1.5	1.8	2.1	1.8	0.3	-1.0	1.2
	2	-3.9	1.4	-1.7	0.1	0.0	1.8	-1.1	1.0
	5	-2.1	1.8	-3.2	0.5	-1.1	0.6	-3.7	0.9
	10	-4.6	2.5	-5.3	0.8	-4.6	1.7	-3.9	1.1
	15	-3.0	0.5	-4.1	0.1	-5.4	1.5	-4.1	0.1
	20	-4.1	1.5	-4.9	0.2	-3.3	0.9	-3.0	0.1
	40	-5.6	1.8	-3.9	1.2	-4.4	0.2	-4.6	0.2
25./27.5.2011	0.5	1.2	0.6	0.1	0.2	0.8	1.2	-0.5	1.9
	2	-4.8	4.7	-1.8	1.9	-1.3	0.2	-3.2	2.4
	5	-5.6	2.2	-2.0	1.0	-3.3	1.7	-3.8	1.1
	10	-7.5	2.1	-2.8	0.5	-4.9	0.1	-5.9	1.3
	15	-5.2	0.7	-3.9	0.8	-6.6	1.3	-5.6	1.5
	20	-4.4	0.6	-3.9	0.1	-4.7	2.1	-5.2	1.2
	40	-4.9	1.7	-4.2	0.7	-5.3	0.4	-5.8	0.8
31.5.2011	0.5	4.7	0.8	2.4	1.2	n.a.	n.a.	n.a.	n.a.
	2	-2.3	3.4	-0.1	0.7	n.a.	n.a.	n.a.	n.a.
	5	-3.5	1.6	-7.6	4.6	n.a.	n.a.	n.a.	n.a.
	10	-4.6	0.3	-5.6	3.1	n.a.	n.a.	n.a.	n.a.
	15	-4.5	1.1	-4.1	1.5	n.a.	n.a.	n.a.	n.a.
	20	-4.6	2.1	-7.4	3.1	n.a.	n.a.	n.a.	n.a.
	40	-4.7	1.6	-5.7	0.3	n.a.	n.a.	n.a.	n.a.
1./2.6.2011	0.5	-0.3	4.6	-0.6	6.6	-1.4	2.9	-0.2	0.8
	2	-3.1	2.5	-1.9	0.7	-3.2	1.7	-1.7	3.5
	5	-4.2	1.6	-4.0	3.2	-1.1	0.9	-4.1	0.1
	10	-4.6	1.1	-5.6	1.1	-4.4	1.8	-4.9	0.5
	15	-5.5	2.0	-2.5	0.2	-3.8	2.1	-5.1	2.2
	20	-4.0	1.8	-3.6	1.2	-3.9	2.2	-6.0	0.5
	40	-3.7	0.6	-3.0	0.4	-3.7	3.1	-3.4	2.0
9./11.6.2011	0.5	n.a.	n.a.	4.9	1.3	n.a.	n.a.	4.1	0.5
	2	7.4	1.2	-1.8	0.6	8.0	2.0	-1.2	2.0
	5	-0.6	0.7	-4.6	1.4	1.4	1.5	-2.7	1.0
	10	-2.1	0.9	-4.1	0.4	-5.2	4.1	-5.9	1.2
	15	-1.2	1.5	-6.2	0.9	-2.6	0.3	-3.9	1.3
	20	-1.9	0.5	-5.0	2.0	-2.7	3.0	-3.9	1.0
	40	-4.6	0.8	-5.5	0.2	-3.7	0.5	-4.5	1.9
14.6.2011	0.5	n.a.	n.a.	7.0	0.8	-2.2	1.5	3.2	1.2
	2	-2.2	1.0	7.3	1.3	5.2	1.4	6.5	1.2
	5	5.8	0.9	1.6	0.5	5.1	0.8	-6.5	1.0
	10	-1.5	2.1	-1.5	0.3	-3.1	4.5	-1.5	0.1

Study V: Stable oxygen isotope and flux partitioning demonstrates understory of an oak savanna contributes up to half of ecosystem carbon and water exchange

	15	-1.6	0.1	-1.4	0.1	-2.6	3.4	-4.8	1.3
	20	-5.0	3.1	-1.6	1.3	-3.2	0.8	-4.2	3.0
	40	-2.3	1.2	-6.7	2.5	-0.8	0.8	-2.6	2.9
14.9.2011	0.5	n.a.	n.a.	n.a.	n.a.	n.a.	n.a.	-0.6	2.6
	2	n.a.	n.a.	n.a.	n.a.	n.a.	n.a.	5.4	1.5
	5	n.a.	n.a.	5.1	1.9	n.a.	n.a.	5.6	1.2
	10	n.a.	n.a.	2.6	2.0	n.a.	n.a.	-0.5	1.6
	15	n.a.	n.a.	-0.2	0.3	n.a.	n.a.	-1.2	0.8
	20	n.a.	n.a.	-2.9	0.4	n.a.	n.a.	1.5	1.0
	40	n.a.	n.a.	-1.9	0.8	n.a.	n.a.	-0.6	2.6
28./29.10.2011	0.5	-0.7	2.2	-1.6	0.4	1.6	1.7	-2.1	0.3
	2	-3.9	0.2	-2.8	2.0	-1.7	0.2	-2.9	0.3
	5	-4.0	0.2	-2.9	0.5	-2.5	0.7	-4.5	0.3
	10	-5.3	0.7	-5.0	0.5	-3.5	2.9	-5.6	1.7
	15	-4.2	0.4	-2.7	0.3	-2.0	0.4	-2.7	1.2
	20	-5.7	0.2	-4.2	0.5	-5.1	0.3	-2.1	1.6
	40	-4.4	0.8	-6.1	1.3	-4.2	0.3	-2.9	0.2
4./5.11.2011	0.5	n.a.	n.a.	-6.9	0.8	n.a.	n.a.	-6.9	1.8
	2	n.a.	n.a.	-5.8	1.5	n.a.	n.a.	-4.5	2.0
	5	n.a.	n.a.	-4.2	0.1	n.a.	n.a.	-3.4	1.3
	10	n.a.	n.a.	-3.7	0.8	n.a.	n.a.	-4.4	1.0
	15	n.a.	n.a.	-3.8	1.5	n.a.	n.a.	-7.2	1.3
	20	n.a.	n.a.	-4.1	0.3	n.a.	n.a.	-4.7	0.2
	40	n.a.	n.a.	-5.7	0.4	n.a.	n.a.	-5.1	0.6
6./7.11.2011	0.5	-1.0	0.9	-4.9	0.9	0.5	1.9	-5.5	1.7
	2	-3.8	1.9	-4.8	0.7	-2.8	0.2	-4.2	0.3
	5	-4.1	1.8	-3.4	0.9	-3.2	0.4	-5.4	0.4
	10	-3.1	1.5	-3.5	1.7	-4.4	1.8	n.a.	n.a.
	15	-3.7	1.2	-3.1	3.0	-3.1	0.4	-3.3	0.6
	20	-3.7	0.5	-3.3	1.3	-5.4	0.3	-3.1	1.0
	40	-3.7	0.8	-3.2	0.7	-4.3	0.6	-3.3	0.6
16./17.11.2011	0.5	-0.4	0.5	-3.7	0.9	-1.6	1.3	-4.5	0.8
	2	-5.9	1.1	-4.9	0.9	-1.7	2.6	-4.6	0.5
	5	-4.9	2.1	-2.9	1.3	-3.2	1.5	-3.9	0.5
	10	-3.5		-3.0	1.1	-2.7	1.5	-4.0	2.3
	15	-4.4	1.9	-2.6	5.5	-3.0	0.6	-3.6	0.5
	20	-3.4	0.4	-3.2	1.4	-3.9	0.5	-3.3	1.1
	40	-3.7	0.6	-3.9	0.4	-3.6	0.9	-2.4	0.9
20./21.11.2011	0.5	n.a.	n.a.	-4.8	1.4	n.a.	n.a.	-5.7	1.2

Study V: Stable oxygen isotope and flux partitioning demonstrates understory of an oak savanna contributes up to half of ecosystem carbon and water exchange

---

	2	n.a.	n.a.	-3.3	0.2	n.a.	n.a.	-5.1	0.4
	5	n.a.	n.a.	-5.1	0.6	n.a.	n.a.	-5.6	0.3
	10	n.a.	n.a.	n.a.	n.a.	n.a.	n.a.	n.a.	n.a.
	15	n.a.	n.a.	-3.7	0.5	n.a.	n.a.	-2.8	0.6
	20	n.a.	n.a.	-2.9	1.0	n.a.	n.a.	-3.2	1.0
	40	n.a.	n.a.	-2.9	0.8	n.a.	n.a.	-3.6	0.3



## **6. Study VI: EFFECTS OF AN EXTREME DRY WINTER ON *Q. SUBER* WOODLAND: NET ECOSYSTEM EXCHANGE AND TREE PHENOLOGY ADJUSTMENTS**

Filipe Costa e Silva<sup>1,2,✉</sup>; Alexandra C. Correia<sup>1</sup>; Maren Dubbert<sup>3</sup>; Arndt Piayda<sup>4</sup>;  
Christiane Werner<sup>3</sup>; Matthias Cuntz<sup>4</sup>; Jorge S. David<sup>2</sup>; and Joao S. Pereira<sup>1,2</sup>

<sup>1</sup>In+, Instituto Superior Técnico. Universidade de Lisboa. Av. Rovisco Pais 1, 1049-001 Lisboa (Portugal)

<sup>2</sup>CEF, Instituto Superior de Agronomia. Universidade de Lisboa. Tapada da Ajuda, 1349-017 Lisboa (Portugal)

<sup>3</sup>Agroecosystem Research, BayCeer, University of Bayreuth. Universitätsstraße 30, 95447 Bayreuth (Germany)

<sup>4</sup>Department of Computational Hydrosystems, UFZ Helmholtz Centre for Environmental Research. Permoserstraße 15, 04318 Leipzig (Germany)

✉Corresponding author: Filipe Costa e Silva ([filipecs@isa.utl.pt](mailto:filipecs@isa.utl.pt))





## 6.1. Abstract

In seasonally dry climates, such as the Mediterranean, lack of rainfall in the normally wet winter season may originate severe droughts and a great variability in annual precipitation. Droughts, in turn, are a main source of inter-annual variation in carbon sequestration when winter rainfall diminishes. This may alter the seasonal pattern of photosynthetic uptake, which is determined by leaf phenology and gas exchange limitations.

The current study is based on the monitoring of an extremely dry winter in an evergreen cork oak woodland under the Mediterranean climate of central Portugal. Results are centred on net ecosystem exchange (*NEE*), phenology and tree growth measurements during two contrasting years: 2011, a wet year with a standard summer drought pattern and 2012, with an extreme dry winter (only 10 mm of total rainfall) that exacerbated the following summer drought effects. The main aims of this study were to assess: 1) effects of winter drought in annual and seasonal *NEE*; 2) interactions between cork oak phenological events and *NEE*.

The dry year 2012 was marked by a 45% increase in *NEE* (-388 vs. -214 gC m<sup>-2</sup> year<sup>-1</sup>), a 63% reduction in annual tree diameter growth but only a 9% reduction in leaf area index compared to the wet year 2011. A significant reduction of 15% in yearly carbon sequestration was associated with leaf phenological events of canopy renewal. On the contrary to male flower production fruit setting was severely depressed by water stress showing a reduction of 54% during the dry year.

Our results suggest that leaf growth and leaf area maintenance are ecophysiological traits preserved under drought winter and are a sink priority for photoassimilates contrarily to tree diameter growth. Thus, carbon sequestration reductions under low water availabilities in cork oak woodland should be ascribed to stomatal regulation or photosynthetic limitations and in a much less extent to leaf area reductions.

## 6.2. Introduction

Cork oak (*Quercus suber* L.) open woodlands cover an area of about 2-2.5 million ha in the western Mediterranean (Aronson et al., 2009). These are man-made ecosystems exploited with low-impact agro-forestry, with high biodiversity and conservation value (Bugalho et al., 2011). In Portugal these woodlands cover 0.74 million ha and represent 23% of all forested area. Cork oak has a significant economic value. It provides 0.7% of the gross domestic product and supplies 54% of the worldwide cork production (Evangelista, 2010). Cork is a natural product consisting of continuous annual layers of suberized tissue produced by phellogen, a secondary meristem wrapping the inner bark. Cork wine bottle stoppers is the main product and to obtain commercial grade cork stripping is done traditionally every 9 years. Cork removal can only be safely done when the phellogen cells are actively dividing, in late-spring and early-summer, to prevent injuries to the tree (Costa et al., 2003).

Cork oak is well adapted to the adverse semiarid Mediterranean climate and its ecophysiology has been well studied in the last decades (e.g. Otieno et al., 2007; Pereira et al., 2009; Vaz et al., 2010). Adverse conditions result mainly from scarce water resources during a long dry summer season, usually coupled with high temperatures and high radiation. In a seasonal climate such as the Mediterranean, a drought is said to occur when precipitation shortages, often coupled to high evaporative demand, reduce moisture availability for an extended period during the normally wet season (Pereira et al., 2006).

Successful adaptations to cope with water stress range from an efficient root and water transport system (David et al., 2007; Kurz-Besson et al., 2006) to a tight stomatal regulation at the leaf level, restricting water loss while limiting the rate of CO<sub>2</sub> assimilation (Otieno et al., 2007; Pinto et al., 2012; Vaz et al., 2010). Nevertheless, and despite being considered drought resilient, a succession of dry years or severe stress events may lead the trees to surpass breakdown thresholds and result in episodes of tree mortality (Pereira et al., 2009). In addition, the Mediterranean region is among the most responsive regions to climate change, for where all recent climate projections forecast more frequent extreme events (Reichstein et al., 2013), such as heat waves and severe droughts (e.g. Giorgi and Lionello, 2008).

Many Mediterranean-oak ecosystems have already been studied through eddy-covariance monitoring

for carbon sequestration assessment, including both deciduous oaks woodlands – e.g. *Q. cerris* or *Q. douglasii* (Baldocchi et al., 2010; Ma et al., 2007) – and *Q. ilex* evergreen oak woodlands with high (e.g. Allard et al. 2008) or low tree densities (e.g. Baldocchi et al., 2010; Pereira et al., 2007).

Phenological patterns in Mediterranean regions are strongly influenced by a marked climatic seasonality and species evolved to synchronise maximum vegetative activity to the most favourable periods of the year (Misson et al., 2011; Pinto et al., 2011; Richardson et al., 2010). Timing of budburst and growing season length can directly impact on annual net ecosystem carbon uptake (Baldocchi, 2008; Richardson et al., 2010) and leaf age on canopy carbon uptake (Niinemets et al., 2005). However, an earlier spring onset can be associated with either enhanced or decreased productivity later in the growing season (e.g. depending on interactions with water availability), and thus early-season gains being offset by sustained late-season reductions in physiological activity (Richardson et al., 2010). Furthermore, even if early leaf development is generally advantageous in terms of carbon uptake, there are trade-offs between increasing growing season length versus increases in the probability of early-spring frost damages (Saxe et al., 2001). Therefore, the evaluation of interactions between climate change effects, phenological events and net ecosystem exchange requires a species-specific ecosystem scale analysis.

The current study is based on the monitoring of an extremely dry winter (only 10 mm of total rainfall) in a certified cork oak woodland. Results are centred on ecosystem carbon fluxes (micrometeorological method, eddy-covariance technique), phenology and tree growth measurements during two contrasting years: 2011, a wet year with a standard summer drought pattern and 2012, with an extreme dry winter that exacerbated the following summer drought effects. Main aims of this study were to assess 1) the effects of extreme dry winter in annual and seasonal net carbon ecosystem exchange (*NEE*), and 2) the interactions between cork oak phenological events and *NEE*.

## 6.3. Material and Methods

### 6.3.1. Site description

In 2009 an experimental site was established at Herdade da Machoqueira located in Central Portugal (39°08'18.29' N, 8°19'57.68' W). Vegetation consists of a *ca.* 50-yr-old cork oak (*Quercus suber*) open woodland with an understory of shrub species (e.g. *Cistus* sp., *Ulex* sp.) and native grassland. The climate is Mediterranean, with wet and mild winters and dry and hot summers. Average annual precipitation is 680±210 mm and mean annual temperature is 15.9 °C (period 1955–2007, Inst. Meteorologia Lisbon). The soil is a cambisol (FAO), with 81% sand, 5% clay and 14% silt, with roots mainly in the upper horizons (*ca.* 0–40-cm depth) and some sinker roots taking water from deeper soil horizons and subsoil. Other general site characteristics are described in Table 1 for the studied period.

**Table 1:** General soil, climate and vegetation characteristics in 2011 and 2012. Values are means ± se.

Characteristic	2011	2012	Units
Soil			
Organic matter	3.2±0.2		%
C/N	19.3±1.4		
Carbon stock (up to 60 cm)	62.2		T C.ha <sup>-1</sup>
Climate			
Mean temperature	16.1	15.2	°C
Total precipitation	800	469	Mm
Total PAR	13033	13606	mol m <sup>-2</sup> .year <sup>-1</sup>
Vegetation			
Tree density	177		trees ha <sup>-1</sup>
Tree crown cover	50		%
Tree height	7.9		M
Tree DBH	24.7		C m
Maximum LAI	1.15	1.05	m <sup>2</sup> .m <sup>-2</sup>
Total tree C stock	33.7		t C.ha <sup>-1</sup>
Shrubs above-ground C stock	0.34±0.10	0.51±0.18	t C.ha <sup>-1</sup>
Grasses above-ground C stock	0.32±0.05	0.10±0.02	t C.ha <sup>-1</sup>

### 6.3.2. Environmental parameters

Meteorological data on rainfall (ARG100; Environmental Measurements Ltd., Gateshead, UK), solar radiation (BF2; Delta-T Devices Ltd., Cambridge, UK), air humidity and temperature (CS215; Campbell Scientific, Inc., Logan, UT, US) were collected continuously in 30-min time intervals

(CR10X; Campbell Scientific). Soil volumetric water content was measured up to 40-cm depth (2, 10, 20, 30, 40 cm) with dielectric soil moisture sensors in four different places (EC5; Decagon Devices, Inc. Pullman, WA, US). These measurements were automatically collected as 30-min averages. Reference evapotranspiration was determined according to the FAO Penman-Monteith method (Allen et al., 1998).

### 6.3.3. *Phenological and ecophysiological measurements*

Litter fall was collected by 16 baskets of 1 m<sup>2</sup> placed in two transects across the site and sampled every 15 days throughout 2011 and 2012, with separation of leaves, branches, male flowers (catkins) and acorns. Additionally, litter fall was collected in six trees with four baskets each placed at half distance of canopy radius. In these same trees, budburst time and individual leaf dimension were registered in a sampled branch per tree (selected in the south of the canopy) to determine the start and duration of the leaf growth period. Tree leaf area index (*LAI*) was calculated using leaf biomass from litter fall (transects) and species specific leaf area (*SLA*) following Limousin et al. (2009). Maximum *LAI* (*LAI*<sub>max</sub>) was assumed to be coincident with the end of new leaf growth in that year and was determined by the sum of the area of all leaves shed belonging to the leaf cohort of that year. In each date *LAI* was determined by subtracting to *LAI*<sub>max</sub> the area of all leaves shed until that date. Between budburst and complete leaf expansion *LAI* increase was determined assuming a linear leaf growth.

Tree height, tree diameter and tree biomass per hectare was estimated by measuring all tree diameters and heights in a representative plot of 40-m radius. Tree above-ground biomass components (leaves, trunks and branches) were estimated subsequently using species-specific allometric equations (Paulo and Tomé, 2006).

Tree-stem diameter growth was measured with dendrometer bands ( $\pm 0.1$  mm) installed in 12

trees at breast height and registered every 15 days throughout 2011 and 2012. Leaf xylem water potential was measured at predawn ( $\Psi_{pd}$ ) and midday ( $\Psi_{md}$ ) with a Scholander-type pressure chamber (PMS Instruments, Corvallis, OR, US) in six trees. Measurements were done in early summer, day of year (doy) 166 and 171, and in the peak of the summer drought, doy 251 and 256 for both 2011 and 2012, respectively.

#### 6.3.4. *Soil analysis*

Soil samples were taken randomly from 3 10-cm depth soil profiles, together with undisturbed soil samples for soil bulk density calculations. Soil organic carbon concentration was determined by the dry combustion method according to the International Organization for Standardization 10694, using a CNS elemental analyser (Leco CNS-2000, MI, US). Nitrogen concentration was determined by Kjeldahl digestion analysis (Digestion System 40; Kjeltex Auto 1030 Analyser, DEcator, SE). Soil organic carbon content was determined using the method referred in IPCC (2003).

#### 6.3.5. *Ecosystem flux measurements*

The fluxes of CO<sub>2</sub>, water vapour and sensible heat were continuously measured using an eddy-covariance system installed at the top of a 22 m high tower. The system consisted of a 3-D sonic anemometer (R3; Gill Instruments Ltd., Lymington, UK) and a closed-path infrared gas analyser (LI-7000; LI-COR Inc., Lincoln, NE, US) measuring, respectively, the three components of wind velocity and temperature, and the concentration of water vapour and CO<sub>2</sub>. Data were continuously acquired on a field laptop with EddyMeas (Meteotools, Jena, DE; Kolle and Rebmann, 2007).

Eddy flux data was treated using the eddy-covariance data acquisition and processing software package EddySoft and self-written Python scripts. Fluxes were determined on a half-hourly basis by block-averaging the 20 Hz data. Time lags between CO<sub>2</sub> or H<sub>2</sub>O signals and vertical wind velocity were determined through cross correlation analysis following Aubinet et al. (2000). Whenever this cross correlation failed, the dependency on relative humidity was used to determine the lag for the

H<sub>2</sub>O signal (Ibrom et al., 2007). High frequency losses were compensated with the use of inductances derived from co-spectrum analysis (Eugster and Senn, 1995). The sectorial planar fit method was used for the coordinate rotation of wind vectors (Rebmann et al., 2012; Wilczak et al., 2001). Moisture and cross wind correction were applied after Schotanus et al. (1983). The storage term of CO<sub>2</sub> was calculated according to Hollinger et al. (1994) and added to the turbulent CO<sub>2</sub> flux.

For quality control, flags were determined for every half-hourly flux value including the following tests: 20 Hz data was scanned for exceeded physical limits, change rates and variances; a stationarity test was applied to the high frequency data based upon a 50% deviation criterion (Foken and Wichura, 1996); on a half-hourly basis the integral turbulence characteristics were calculated following Thomas et al. (2002) with a 30% deviation criterion; a spike detection routine was used based on the absolute median deviation principle (Papale et al., 2006). All quality control tests were summed up in a simplified flag system (Mauder and Foken, 2011). Total data gaps during the whole study period, due to missing and rejected data, were about 42%. Gap filling and flux-partitioning methods proposed by Reichstein et al. (2005) were used to fill data gaps and to separate the net ecosystem exchange (*NEE*) into gross primary production (*GPP*) and ecosystem respiration (*R<sub>eco</sub>*).

#### 6.3.6. *Data and statistical analysis*

Radiation-use efficiency (*RUE*) was calculated on a seasonal basis, as the slope of the linear regression between daily-integrated gross carbon assimilation (i.e., *GPP*) and the daily-integrated incident photosynthetically active radiation (*PAR*), expressed in g C MJ<sup>-1</sup>. Statistical differences between these seasonal slopes for 2011 and 2012, were performed by the comparison of regression coefficients following Sachs (1992). Radiation use efficiencies were calculated using only non-gapfilled data. Seasonal data comparisons were done considering, e.g., winter corresponding to January + February + March (e.g. 3-months sums of *NEE*).

To examine differences between variables (e.g. litter fall components, leaf water potential) we used one-way ANOVA. When ANOVA assumptions were not met, namely normal distribution of the data and homogeneity of variances, non-parametric Kruskal-Wallis test was carried out. Analysis were

performed using STATISTICA (Version 7, StatSoft, Inc. 2004).

## 6.4. Results

### 6.4.1. *Meteorology and soil water availability*

Water availability is the main constraint to plant productivity in most Mediterranean ecosystems and the years 2011 and 2012 were quite contrasting. The year 2011 was relatively wet with annual rainfall (800 mm) 18% higher than normal (680 mm, 50 year average). Conversely, 2012 was dry: with an annual rainfall (469 mm) 31% lower than the long-term average (Table 1). In particular, 2012 had an extreme low winter rainfall of only 10 mm (Fig. 1a), and winter/spring rainfall was 76% lower than in 2011, where in April and May a total of 217 mm of rain was recorded, about twice the long-term average for the same period. Although 2012 was a dry year, its annual average temperature was lower than that of 2011 (15.2 vs. 16.1 °C, respectively, Table 1). April 2011 showed an unusually high average temperature (17 °C) compared to 2012 (11 °C), both years contrasting with the 50-year April average of 13.5 °C. Furthermore, the 2011 summer drought extended through October with high temperatures until the onset of autumn rains in November whereas in 2012 autumn rains started 30 days earlier.

Due to a higher quantity of sunny days in the first three months of 2012 total *PAR* was 57% higher than in the same period of 2011 (Fig. 1b). Despite the significant lower total rainfall in 2012, the average of maximum vapour pressure deficit ( $VPD_{\max}$ ) was only slightly higher in the summer months of 2012 compared to 2011 (28 vs. 25 hPa, respectively) (Fig. 1c).



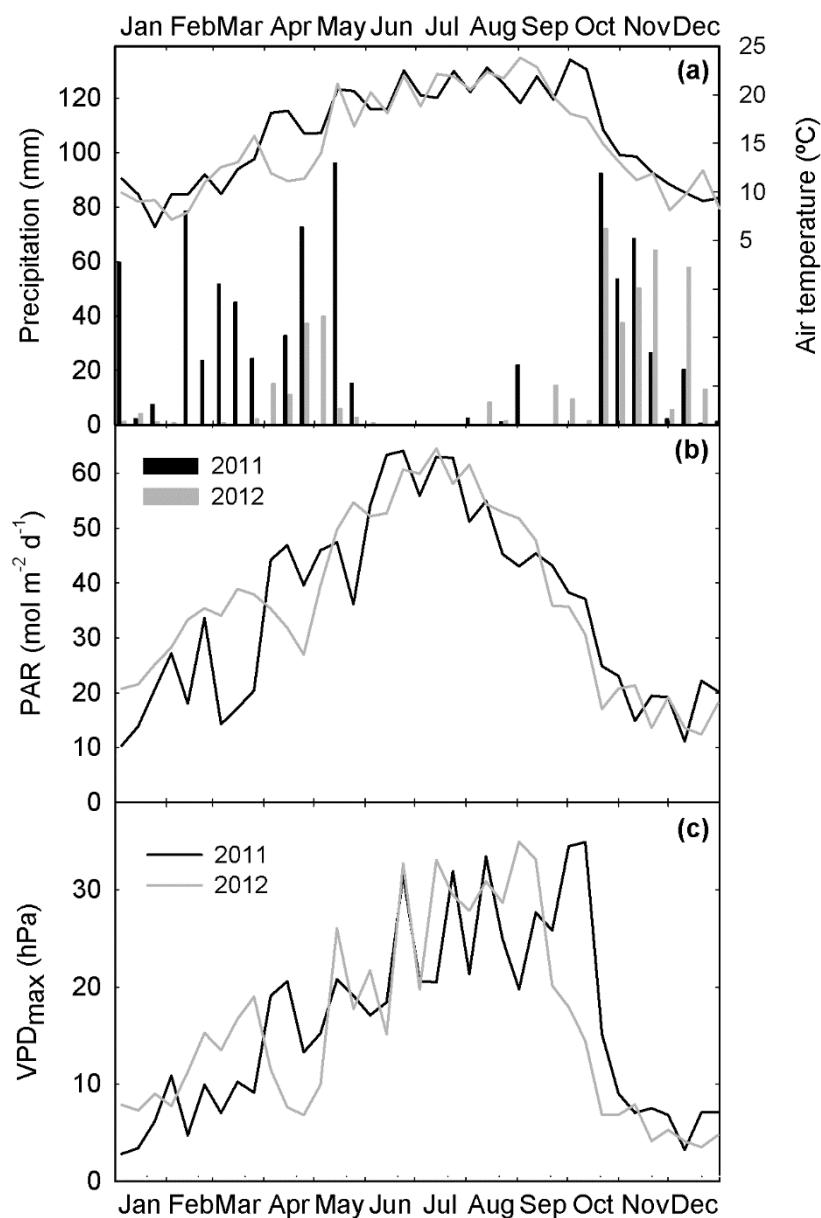


**Figure 1:** Meteorological data during 2011 and 2012. (a) 10-day average air temperatures ( °C) and 10-day sum of precipitation (mm). (b) 10 day average of total incident photosynthetically active radiation (PAR, mol m<sup>-2</sup> d<sup>-1</sup>). (c) 10-day average of maximum vapour pressure deficit (VPD<sub>max</sub>, hPa).

Relative soil water content (SWC) followed closely precipitation events and both at 2 and 40-cm depth, SWC in 2012 was noticeably lower than in 2011 (Fig. 2). Decreases in SWC during 2012, compared to 2011, were progressively larger as time progressed: reductions of 29, 51 and 72% at 40-cm depth in winter (21 vs.15% SWC), spring (21 vs.10% SWC) and summer (14 vs. 4% SWC), respectively. Upon soil rewetting with the autumn rains SWC increased similarly in both years.

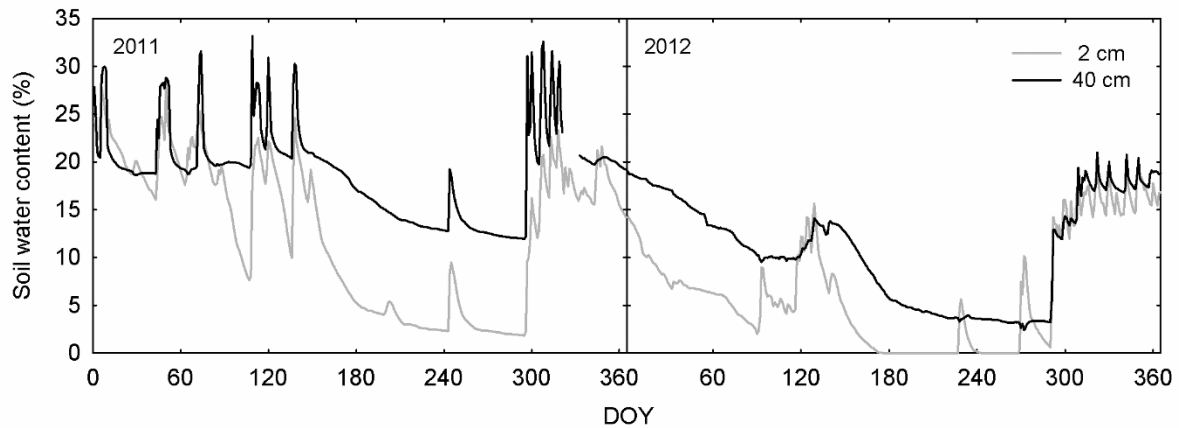


**Figure 2:** Daily mean values of soil water content (%) at 2 and 40 cm depth.

#### 6.4.2. Ecosystem carbon fluxes

Total annual carbon fluxes clearly showed the effect of the extreme dry winter of 2012 on carbon sequestration reduction: net ecosystem exchange (*NEE*) increased from -388 in 2011 to -214 g C m<sup>-2</sup> year<sup>-1</sup> in 2012 (Fig. 3c). However, there were noticeable seasonal differences in *NEE* between years.

Even though 2012 started with three very dry months, *NEE* in this 90-day period was significantly more negative (higher carbon sequestration) than in the same period of 2011 (-111 vs. -56 g C m<sup>-2</sup>, respectively) (Fig. 3c). Following this period, in the early spring of 2011 there was a noticeable increase in *NEE* daily values, going from an average of -28 in March to -15 g C m<sup>-2</sup> in April in spite of the more favorable climatic growing conditions of air temperature and *PAR* in the latter. Similarly, although later in the spring, an even more striking increase in *NEE* occurred in 2012 from April to May (-18 to -1 g C m<sup>-2</sup>, respectively) (Fig. 3b). Interestingly, on an annual basis, the ecosystem is a source of carbon to the atmosphere occasionally, during these short spring periods and in the end of the year after the onset of autumn rains (Fig. 3a and b).

After these low carbon sequestration spring periods, *NEE* gradually decreased until the end of the spring, reaching minima of -5.4 and -4.3 g C m<sup>-2</sup> day<sup>-1</sup> around day 158 in 2011 and 2012, respectively. Nevertheless, when comparing *NEE* sums from April to June in both years, there was a 56% reduction of carbon sequestration in the dry 2012 compared to 2011 (-70 to -161 g C m<sup>-2</sup>). Additionally, while in 2011 high values of carbon sequestration are maintained until day 190 to only subsequently decrease

gradually until the end of summer, in the dry 2012 the decrease in carbon sequestration occurs abruptly after day 160. In fact, from July to September 2012 a 66% decrease in carbon sequestration contrasts with the same period of 2011 (*NEE* of -61 and -178 g C m<sup>-2</sup>, respectively).

In early September 2011 (ca. day 240) an isolated 22 mm rain event caused an ecosystem CO<sub>2</sub> efflux to the atmosphere mostly due to a soil respiration pulse as a consequence of soil rehydration. With the onset of autumn rains the ecosystem turned into a permanent source of carbon to the atmosphere throughout autumn/early winter.

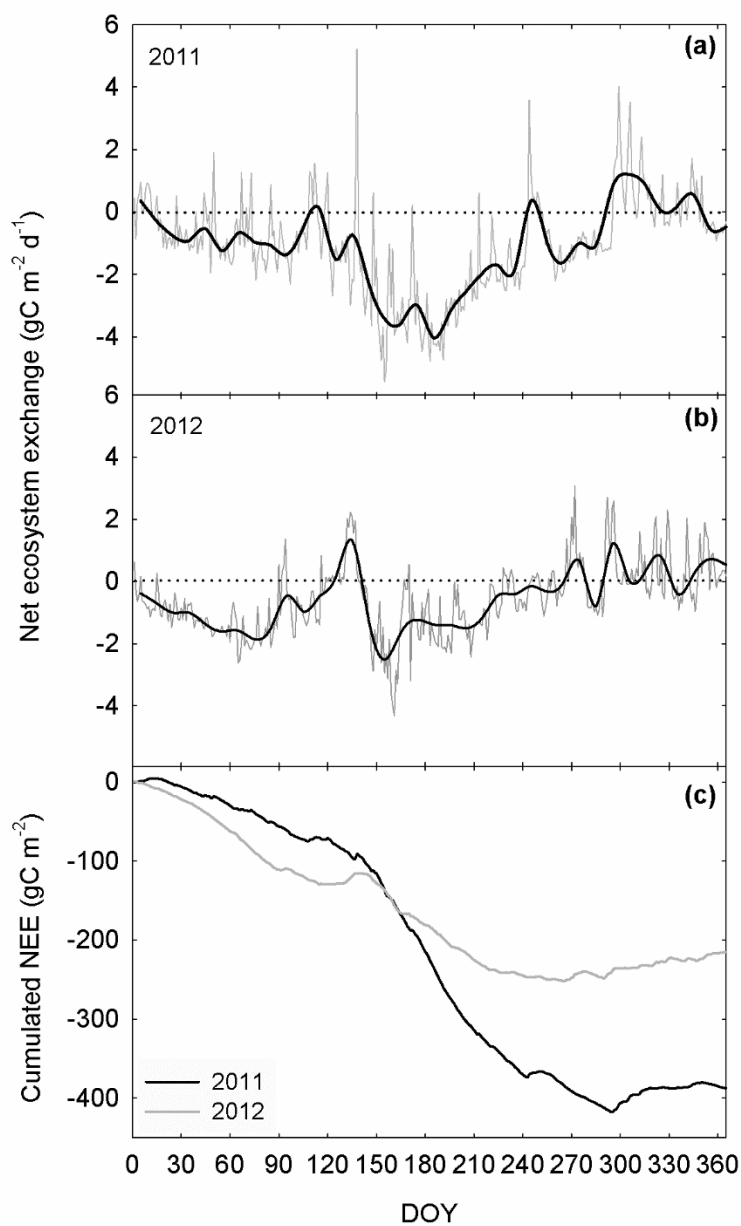


**Figure 3:** Daily values of net ecosystem exchange (NEE, g C m<sup>-2</sup> day<sup>-1</sup>) during 2011 (a) and 2012 (b). Negative values represent carbon sequestration in the ecosystem while positive values represent carbon emissions to the atmosphere. The black line indicates a 10-day running average.

#### 6.4.3. *Radiation use efficiency*

The seasonal variation and interannual differences in *RUE* can be perceived in Fig. 4. The winter 2011 showed a somewhat higher but non-significant *RUE* than in 2012 (0.31 vs. 0.25 g C MJ<sup>-1</sup>, respectively) (Fig. 4a). Although photosynthetic activity is limited in winter by low temperatures and radiation leading to low *GPP*, a higher *RUE* in winter 2011 can have been due to lower direct radiation and greater proportion of diffuse radiation due to more cloudy days in this year. In fact, we have observed that *RUE* nearly doubles when incident sunlight is diffuse, compared to when it is mostly direct (see also Knohl and Baldocchi, 2008). In the spring, even though *GPP* values increased after winter (122% in 2011 and 76% in 2012), correlations with *PAR* were low and not significantly different (Fig. 4b). This low correlation is the result of leaf shedding and canopy renewal (i.e. low tree leaf area index) which led to higher variation in *GPP* for high *PAR* intensities. Differences in *RUE* became highlighted in summer both among seasons and between years (Fig. 4c). Whereas in 2011 *RUE* is highest in summer it shows the lowest seasonal values in 2012 (0.42 vs. 0.21 g C MJ<sup>-1</sup>, respectively,  $P < 0.004$ ,  $df = 154$ ) in accordance to *GPP* response to drought stress (see tree leaf water potentials, Table 2). When comparing the reduction of *GPP* from the peak of the growing season (early summer) to the peak of drought stress (late summer), carbon assimilation was much less affected in 2011 than in 2012 (on average -38% vs. -70%, respectively). Upon recovery of water availability in autumn, *RUE* (0.33 g C MJ<sup>-1</sup>) and average *GPP* (2 g C m<sup>-2</sup> d<sup>-1</sup>) were similar in both years, indicating no long lasting effects of the 2012 summer drought stress (Fig. 4d).

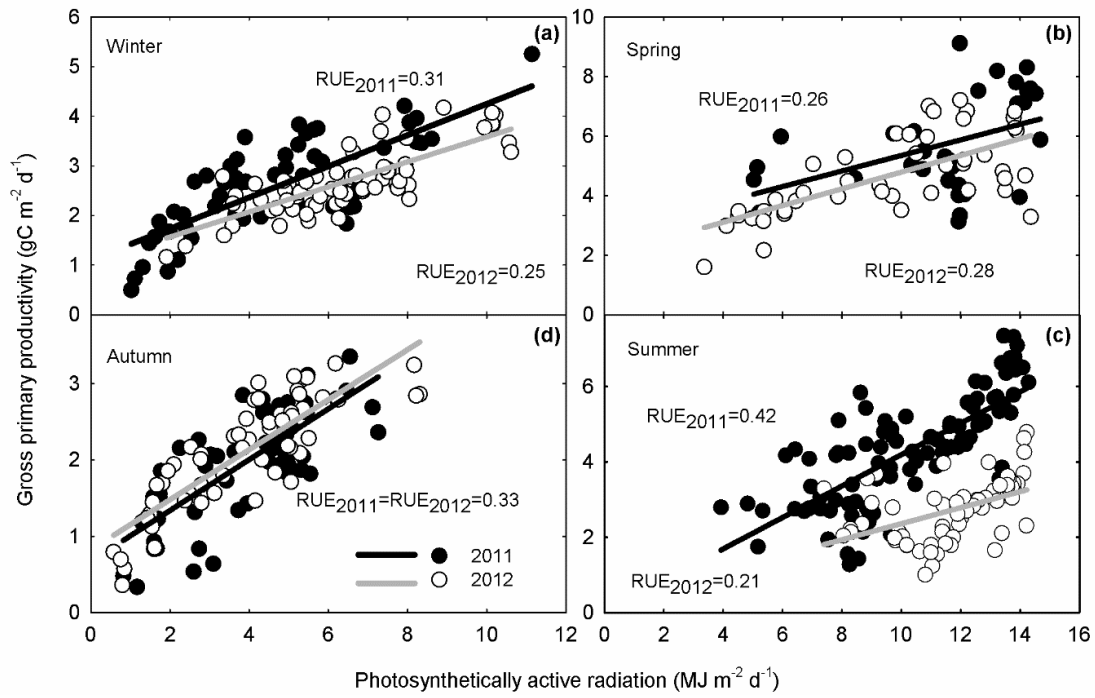


**Figure 4:** Linear regressions between gross primary productivity (GPP) and daily-integrated incident photosynthetically active radiation (PAR) over the seasons in 2011 and 2012. Radiation use efficiency (RUE) expressed in  $\text{g C MJ}^{-1}$ . (a) Winter, 2011:  $y = 0.31x + 1.11$ ,  $r^2 = 0.57$ ,  $n=56$ ; 2012:  $y = 0.25x + 1.06$ ,  $r^2 = 0.62$ ,  $n=71$ . (b) Spring, 2011:  $y = 0.26x + 2.74$ ,  $r^2 = 0.20$ ,  $n=32$ ; 2012:  $y = 0.28x + 2.0$ ,  $r^2 = 0.46$ ,  $n=44$ . (c) Summer, 2011:  $y = 0.42x + 0.02$ ,  $r^2 = 0.58$ ,  $n=96$ ; 2012:  $y = 0.21x + 0.24$ ,  $r^2 = 0.22$ ,  $n=62$ . (d) Autumn, 2011:  $y = 0.33x + 0.67$ ,  $r^2 = 0.55$ ,  $n=61$ ; 2012:  $y = 0.33x + 0.83$ ,  $r^2 = 0.71$ ,  $n=57$ .

#### 6.4.4. Tree leaf water potentials

Tree leaf water potential measured in early summer of both years indicated no signs of water deficits as shown by the high  $\Psi_{pd}$  values and low  $\Psi_{md}$  (Table 2). However, by late summer 2012 a clear water stress had developed with  $\Psi_{pd}$  reaching  $-2.2$  MPa, and its small difference to  $\Psi_{md}$  suggests a high stomatal closure. Conversely, in 2011, the higher water availability in summer is apparent from the higher  $\Psi_{pd}$  and low  $\Psi_{md}$ , maintaining the stomatal conductance in accordance to the exhibited higher productivities.

**Table 2:** Predawn ( $\Psi_{pd}$ ) and midday ( $\Psi_{md}$ ) tree leaf water potential (MPa, n=6) measured during 2011 and 2012 in the early summer and summer end. Values are means  $\pm$  se. Different letters represent statistical significance at  $P < 0.05$ , no letters means no differences.

Leaf water potential (MPa)	Early summer		Late summer	
	$\Psi_{pd}$	$\Psi_{md}$	$\Psi_{pd}$	$\Psi_{md}$
2011	-0.9 $\pm$ 0.1 a	-1.7 $\pm$ 0.1	-1.3 $\pm$ 0.1 a	-2.2 $\pm$ 0.1
2012	-0.4 $\pm$ 0.02 b	-1.6 $\pm$ 0.2	-2.2 $\pm$ 0.2 b	-2.4 $\pm$ 0.2

#### 6.4.5. Tree litter fall and phenological development

Leaves and branches were the main components of litter fall, representing on average 72 and 18 % of total litter fall in both years. However, the mean quantity of shed leaves and branches decreased about 20 % in 2012 compared to 2011 (Table 3). Fruits and catkins showed opposite trends in 2012: fruits decreased by 54 % whereas catkins increased 28 % although showing a higher variability among trees. Budburst in 2011 started in mid-April (doy 111), ca. 30 days earlier than in 2012 (Fig. 5). Catkins also developed earlier in 2011 than in 2012, concomitantly with leaf expansion period, although completing their development earlier and being all shed by doy 137 and 158, respectively. Due to the later budburst in 2012 the completion of leaf expansion was also delayed until early summer (ca. doy 187). Similarly, fruit fall started and ended later in 2012 than in 2011.

**Table 3:** Total annual litter fall and litter fall components during 2011 and 2012 in  $\text{g m}^{-2} \text{ year}^{-1}$ . Values are means  $\pm$  se (n=6). Different letters represent statistical significance at  $P < 0.05$ , no letters means no differences.

Litter component	2011	2012
Leaves	190 $\pm$ 10 (a)	151 $\pm$ 13 (b)
Branches	47 $\pm$ 9	38 $\pm$ 9
Fruits	8 $\pm$ 2 (a)	4 $\pm$ 1 (b)
Flowers (catkins)	13 $\pm$ 4	17 $\pm$ 7
Other	3 $\pm$ 1	2 $\pm$ 0.6
Total litter fall	261 $\pm$ 18 (a)	211 $\pm$ 23 (b)

Leaf fall occurred mainly between doy 95 and 187 in 2011 and 2012 (69 and 77 % of total leaves shed, respectively). In both years the first period of leaf fall is the most intense with highest shedding rates. However, different patterns of leaf shedding can be evidenced between years. Leaf fall started

earlier in 2011 than in 2012 (ca. doy 95 vs 132, respectively) although with a noteworthy higher intensity of leaf shedding in 2012 ( $2.3$  vs.  $3.8 \text{ g m}^{-2} \text{ day}^{-1}$ , respectively).

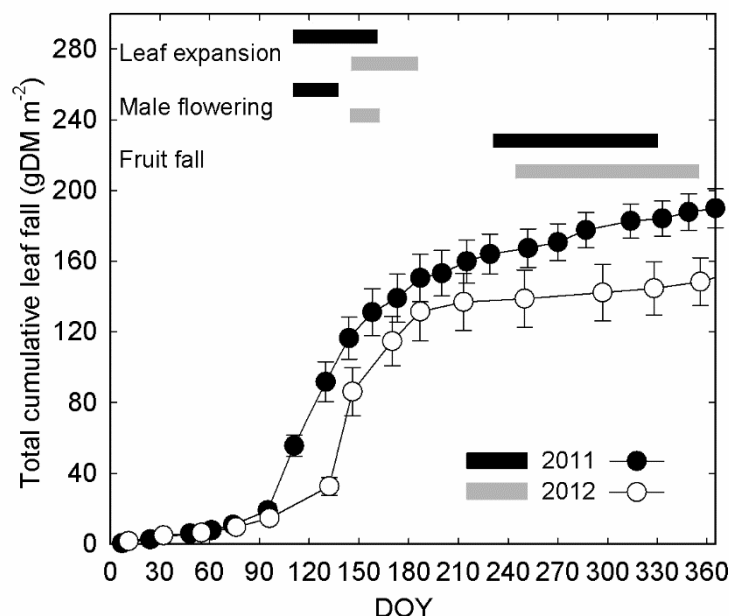


**Figure 5:** Total cumulative leaf fall during 2011 and 2012 in  $\text{g DM m}^{-2}$  and time interval of different phenological stages. Values are means  $\pm$  se ( $n=6$ ).

#### 6.4.6. Leaf area index

Tree leaf area index (*LAI*) is in straight relation with leaf fall and new leaf growth during the spring (Fig. 6). The lower intensity of leaf fall during the spring of 2011 led to a smoother transition of old to new leaves in the canopy which is reflected in a higher minimum *LAI* in 2011 on doy 111 when compared to the minimum *LAI* in 2012 on doy 146 ( $0.56$  vs.  $0.2 \text{ m}^2 \text{ m}^{-2}$ , respectively). In addition, this period of canopy renewal and concomitantly low *LAI* is in accordance to the high *NEE* – low carbon sequestration – and low *PAR* and *GPP* observed correlation in both years (Fig. 2 and Fig. 4b). Furthermore, due to the earlier canopy renewal in 2011,  $LAI_{\text{max}}$  was also reached earlier than in 2012 (ca. doy 158 vs. 187, respectively) which extended the growing season in a favorable period of water availability. Due to the different leaf fall intensities between years the relative contribution of older leaves (matured in the previous spring) to each year *LAI* is also diverse. Therefore, in the early summer of 2011 old leaves contributed with 15.5 % to  $LAI_{\text{max}}$  whereas in 2012 its contribution was restricted to 2.5 %. Nevertheless, in both years by doy 270 all old leaves were shed. Despite greater

leaf fall during 2011 than in 2012,  $LAI_{max}$  was 9.5% higher with 1.15 and 1.05  $m^2 m^{-2}$ , respectively.

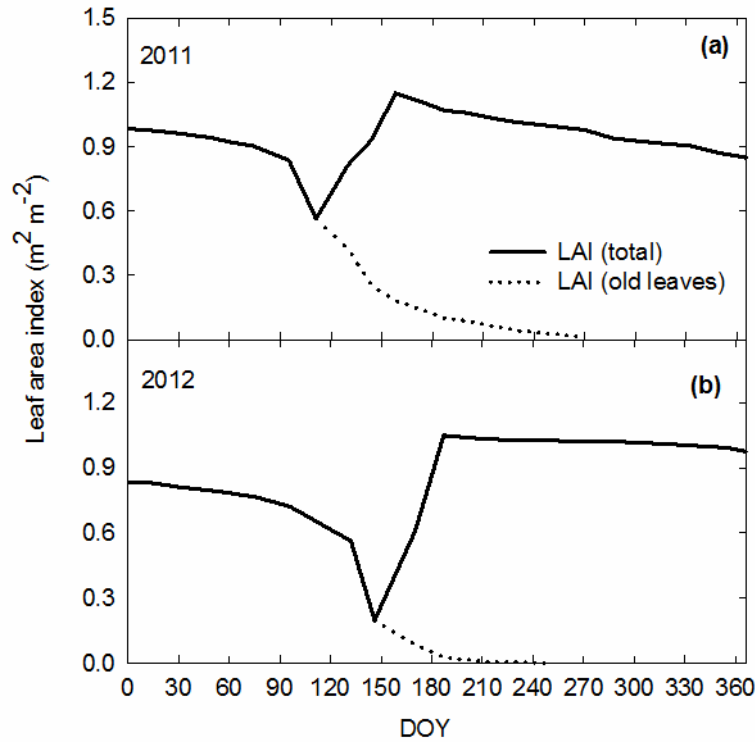


**Figure 6:** Tree leaf area index ( $LAI$ ) during 2011 (a) and 2012 (b). The dash line represents  $LAI$  of old leaves matured in the previous spring.

#### 6.4.7. Tree diameter increment

Tree diameter increment started earlier in 2011 than in 2012 (doy 61 vs. 76, respectively) and with sustained higher daily increments throughout the growing season (Fig. 7). In fact, maximum diameter growth rates in 2011 were double of those in 2012 (ca. 2 vs. 1  $mm month^{-1}$ , respectively). Furthermore, the duration of the growth period extended in 2011 till the end of the summer (doy 270) whereas in 2012 tree diameter increment was inhibited by drought conditions in the middle of the summer even with a decrease in trunk diameter in the period doy 228 to 250. Worth mentioning is the halt observed in tree diameter increment between doy 127 and 156 in the spring of 2012 whereas in 2011 there were continuous growth increments. In addition, a great diameter increment in 2011 was recorded after the first autumn rains in contrast to 2012. Overall, total annual diameter increment in 2012 decreased 63% compared to 2011 (8.8 vs. 3.3  $mm$ , respectively).



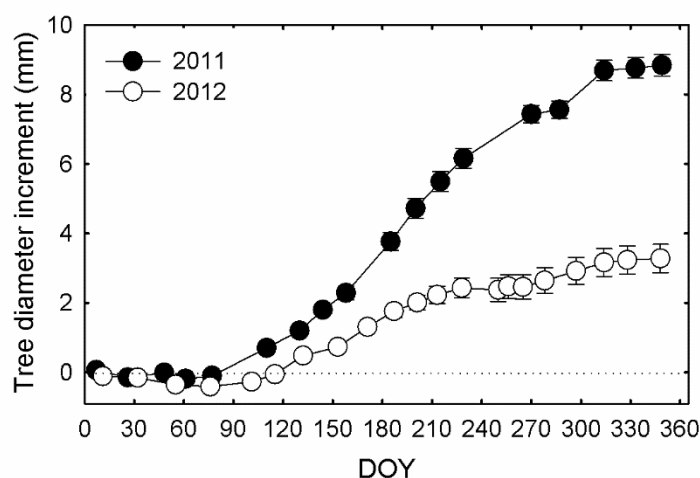


**Figure 7:** Tree diameter increment (mm) during 2011 and 2012. Values are means  $\pm$  se (n=9).

## 6.5. Discussion

In seasonally dry climates with a great variability in precipitation, droughts are a main source of interannual variation in carbon sequestration as they strongly reduce gross primary productivity as well as net ecosystem exchange (*NEE*). At the same time, leaf phenology can be expected to exert an important control on temporal dynamics of tree crown productivity and *NEE*, not only in deciduous forests but also in evergreen species with short leaf life-spans, where the senescence and development of a new canopy each spring control, to a large extent, the patterns of photosynthetic uptake in the most favourable season. Thus, a drought winter can have different effects on plant physiology throughout the following seasons depending both on its intensity and imposed limitations on important leaf phenophase progressions, which will ultimately exacerbate the summer drought effects.

### 6.5.1. Ecosystem carbon fluxes and seasonal patterns

The values for our cork oak ecosystem carbon balance – with an average *NEE* of  $-301 \text{ gC m}^{-2} \text{ year}^{-1}$  – compare well with flux measures of carbon sequestration in related Mediterranean oak ecosystems. For example, a *Quercus ilex* forest in southern France showed an average *NEE* of  $-254 \text{ gC m}^{-2} \text{ year}^{-1}$  (Allard et al., 2008) and a closed canopy mature *Quercus cerris* forest in Central Italy  $-288 \text{ gC m}^{-2} \text{ year}^{-1}$  (Baldocchi et al., 2010). However, when comparing with savannah-like, open woodlands with

more similar tree densities (e.g.  $< 150$  trees  $\text{ha}^{-1}$ ), this cork oak woodland showed higher productivities: a deciduous-oak savannah under a Mediterranean climate in California, presented  $-98 \text{ gC m}^{-2} \text{ year}^{-1}$  and a *Q. ilex* open woodland in southern Portugal  $-87 \text{ gC m}^{-2} \text{ year}^{-1}$  (Baldocchi et al., 2010).

In this Mediterranean climate with marked seasonality the cork oak ecosystem showed a productivity peak in June and July. There was a time-lag between soil water availability and carbon sequestration, reflected in a prolonged productivity throughout summer which only significantly declined after an extreme dry winter as happened in 2012. As a result, a marked difference is observed in comparison to other Mediterranean, such as *Q. ilex* ecosystems, where more than 80% of the yearly *NEE* occurs between March and June and in summer becomes a source of carbon to the atmosphere (e.g. Allard et al., 2008; Pereira et al., 2007). Whereas in our site, regardless of the year, March to June only accounted for 48% of the yearly *NEE* with a further significant carbon sequestration in the summer months (44 and 26% in 2011 and 2012, respectively).

Although changes in spring phenology exert a major influence on the carbon balance of temperate and boreal deciduous forests (e.g. Baldocchi et al., 2001, 2008; Richardson et al., 2010) its effect in evergreen Mediterranean oaks is less evident since phenological changes are not clearly associated with a carbon source-sink transition. For example, Richardson et al. (2010) showed that productivity of evergreen needleleaf forests is less sensitive to phenology variability than deciduous broadleaf forests. However, among evergreen Mediterranean oak species *Q. suber* leaf habits are singular in that leaf life-span is generally short – ca. 12 (Oliveira et al., 1994; Pereira et al., 1987) to 15 months (Escudero and Mediavilla, 2003) – and leaf fall is highly concentrated in a short period of time (Caritat et al., 1996, 2006; Oliveira et al., 1994). These specific traits had a marked influence in the spring carbon balance of the studied cork oak woodland. Thus, in both years a clear carbon sequestration depression is associated to the whole leaf canopy renewal where the ecosystem becomes a temporary carbon source (Fig. 3). This reduction in carbon sequestration in April 2011 and May 2012 represents on average a 15% reduction of yearly *NEE*. Two orders of reasons explain this fact: first, the noticeable transitory decrease in leaf area due to intense leaf fall which led to an average reduction of 49% in *LAI* (Fig. 6) and, second, a decoupling between tree canopy carbon uptake and respiration in

this period. In fact, on average,  $R_{eco}$  increased more than  $GPP$  in this canopy renewal phase (51 vs. 29%, respectively, data not shown) relatively to the month prior to budburst. This decoupling is expected both from carbohydrate and nitrogen translocation during leaf senescence associated with reduced photosynthetic capacity (Escudero and Mediavilla, 2003; Niinemets et al., 2005) and from a negative carbon balance in emerging new leafs with incipient photosynthesis and high growth respiration costs (Dikson, 1989).

*Quercus suber* growth may be limited in winter both by low temperatures (Aranda et al., 2005) and low incident radiation. In 2012 – where carbon sequestration in winter was 45% of yearly total (Fig. 3c) – a great decrease in  $NEE$  was observed by comparison to 2011 in response to a 57% higher incident  $PAR$ , although air temperatures were similar in both years for this period (Fig. 1). Thus, and since precipitation was practically inexistent (10 mm), tree productivity in winter seems to be highly dependent on available incident radiation. This clearly puts into perspective the advantage of evergreenness in environments with relatively mild winters where air temperatures do not strongly limit carbon uptake. Leaf persistence allows a significant ecosystem productivity to be achieved outside of the most favourable growing period – spring to early summer – through an adjustment of growth to environmental resources availability (e.g. Baldocchi et al., 2010). This feature is particularly relevant under the highly variable Mediterranean climate and considering the actual susceptibility of the Mediterranean region to winter/spring climatic changes, namely in temperature and precipitation (e.g. Giorgi and Lionello, 2008).

#### 6.5.2. *Extreme dry winter effects on carbon fluxes*

The effect of a severe dry winter and a consequent low soil water refilling in 2012 led to a 45% decrease in annual carbon uptake in relation to 2011, from  $-388$  to  $-214$  g C m<sup>-2</sup> year<sup>-1</sup>, respectively. This increase in  $NEE$  for the cork oak woodland is similar to that reported for a *Q. ilex* forest (51%, Allard et al., 2008) but lower than the 64% increase found in a *Q. ilex* open woodland (Pereira et al., 2007) during years of severe drought. However, in this *Q. ilex* open woodland with a low tree crown cover (ca. 30%) a large proportion of  $NEE$  was attributable to the carbon assimilated by its annual

vegetation component, which was strongly affected by the shortage of rain in winter (Pereira et al., 2007).

The drought effects in 2012 carbon sequestration differed among seasons and even the yearly reduction was somewhat masked by the opposite winter trend of increased carbon sequestration. Throughout the spring of 2012 and before any noticeable tree water stress – assessed by tree  $\Psi_{pd}$  – there was an already significant 56% decrease in carbon sequestration in comparison to 2011. Even considering the reduction of 9% in tree leaf area index in 2012 (Fig. 7), the reduction in spring carbon sequestration ought to be caused mainly by the extreme drought effects on the understorey herbaceous layer which was severely reduced in 70% biomass in relation to 2011 (Table 1). This is supported both by the very low surface soil water content in spring (Fig. 2) that affect in first instance the understorey vegetation, and by the relevant contribution of this vegetation layer to the ecosystem productivity (Correia et al., 2014; Dubbert et al., 2014; Pereira et al., 2007; Unger et al., 2009).

Nevertheless, it was in summer that the ecosystem showed to be more affected by the low water availability with a reduction of 66% in carbon sequestration in relation to summer 2011. The summer drought stress in 2012 reflected in lower tree leaf water potentials (Table 2) and lower radiation use efficiency (Fig. 4). Similar decreases in ecosystem light use efficiency under water stress were reported for Mediterranean oak woodlands (Pereira et al., 2007) and discussed elsewhere (e.g. Sinclair and Muchow, 1999). Even though *Q. suber* is considered a drought resilient tree well adapted to the adverse semiarid summer conditions (e.g. Pereira et al., 2009), a standard photosynthesis decrease occurs as the result of stomatal closure to regulate transpiration losses (e.g. Besson et al., 2014; Vaz et al., 2010) and photoinhibition (Werner and Correia, 1996). Even under the less-limited water supply conditions in 2011, stomata closure seems to have been still controlling transpiration losses, although later in the summer. This results from the evolutionary safety function of stomata to prevent leaf water potential to fall below a cavitation threshold (Buckley and Mott, 2002) that would lead to catastrophic damages in the root-leaf hydraulic pathway (Tyree and Sperry, 1988), i.e. losses in water transport capability. In both years the minimum leaf water potentials measured in the peak of summer water stress ( $\Psi_{md}$ , Table 2) were above the -2.9 MPa water potential threshold, which causes a 50% loss in hydraulic conductivity (50PLC) due to embolism in *Q. suber* shoots (Pinto et al., 2012). Thus, by

forfeiting summer carbon uptake due to the deep root system and an efficient stomatal control, cork oak trees succeeded in maintaining the minimum leaf water potential above the 50PLC embolism threshold, throughout the experimental period. This also explains why leaf area index was relatively stable during the two years of observation. Vilagrosa et al. (2003) report that leaf dieback only occurs when stomata regulation is no longer effective, allowing PLC to rise and leaf water potential to drop (typically to around -5 MPa). Nevertheless, in the summer drought stress period of 2012 the observed safety margins above the 50PLC threshold were narrower and photosynthetic limitations higher, reflecting the general observed carbon sequestration reduction.

#### 6.5.3. *Extreme dry winter effects in tree growth and phenology*

Annual stem diameter growth decreased 63% in 2012 compared to 2011 (Fig. 7). However, this prominent reduction can be somewhat overestimated due to the natural small decrease in cork diameter increments during the 9-year cork growth cycle (ca. 15% per year, Costa et al., 2003). Nevertheless, even after correcting our increments for a “normalised” growth, there is still a very significant reduction (51%) in stem diameter increment. Furthermore, we also have observed a significant 44% increase in annual stem diameter increment in 2013 – a wet year with 819 mm annual precipitation (data not shown). The seasonal reductions in tree diameter growth follow the same pattern as *NEE* in spring and summer. Thus, diameter growth reductions in 2012 relatively to 2011 were much higher in summer (76%) than in spring (48%). However, if summer growth impairment can be directly linked to the observed low soil water availabilities and photosynthetic limitations (as discussed above), in spring the absence of tree water stress (low  $\Psi_{pd}$ , Table 2) call for a further understanding. It has been shown that spring growth flush in evergreen trees depend both on currently fixed and stored carbohydrates from the previous seasons (Cerasoli et al., 2004, Dickson, 1989) and that those are closely involved in early xylem differentiation in *Q. suber* trees (Aguado et al., 2012). In our case we can dismiss the hypothesis of stored carbon differences between both years in early spring since previous growing conditions were similar or even more favourable during the winter 2012 (Fig. 3). More probably the decrease in stem diameter growth during spring 2012 can be ascribed to three

orders of interconnected effects: 1) a shorter favourable growing season length due to a later budburst (ca. 30 days); 2) higher intensities of leaf fall and a consequent – although temporary – much lower *LAI* and 3) a potential lower canopy nitrogen content (see below).

It has been reported that for Mediterranean oak species air temperature is the main environmental driver for budburst timing (e.g. Morin et al., 2010; Pinto et al., 2011; Sanz-Perez et al., 2009). Although thermal times and base temperatures could not be estimated from our data, the fact that the month of March preceding budburst date in 2011 exhibited an average air temperature 6 °C higher than in March 2012 (Fig. 1) supports that air temperature increase was the main cause for the 30-day earlier budburst in 2011. The extent of this advance agrees with results from Sanz-Perez et al. (2009) where budburst occurred 6–10 days earlier per degree spring temperature increase. The immediate consequence of an earlier budburst is the lengthening of the growing season allowing trees to reach maximum photosynthetic capability earlier in the most favourable stages of the growth season, i.e. late spring and early summer. It has been generally reported that longer growing seasons lead to higher net ecosystem carbon uptakes (e.g. Richardson et al., 2010) in the order of a further 3.7 gC m<sup>-2</sup> per day in evergreen broadleaved forests and Mediterranean oak-grass savannah (Baldocchi, 2008).

Relative to 2011 a higher intensity of leaf shedding was observed in 2012 in the early spring. As a result, the minimum *LAI* in 2012 was 65% lower than in 2011 (Fig. 6). This was reflected both in a steeper *NEE* increase (Fig. 3) and in a concomitant stem diameter growth stop in the same period (day 127 to 156, Fig. 7) in opposition to 2011 where stem diameter growth rates were sustained. This strongly suggests that stored and current carbon uptake were insufficient in spring 2012 for meeting growth sink demands and that new leaf expansion was a priority sink in opposition to diameter stem growth, in accordance to its much greater reduction when compared to *LAI* (48 vs. 9%, respectively). Thus, assuring tree canopy renewal and maintaining a relatively stable *LAI* seems to be an ecological trait preserved even under extreme low winter precipitation and reflects *Q. suber* resilience to drought. Maintaining a threshold *LAI* in these Mediterranean type climates may allow cork oak ecosystems to optimize productivity under a water-availability uncertainty, relying in morphological traits (e.g. depth rooting) and physiological responses (e.g. stomatal regulation) to face unpredictable seasonally water stresses. However, the magnitude and timings of drought events can have significant different *LAI*

costs as was shown for an extreme spring drought in a *Q. ilex* forest occurring in parallel with leaf phenological development, leading to critical impacts impairing ca. 50% of leaf unfolding (Misson et al., 2011).

Finally, we can speculate that during spring 2012 there was a lower canopy nitrogen content with a consequent lower carbon uptake capacity. This is plausible given the high intensity of leaf fall during the spring of 2012 indicating that sink organs were accelerating senescence rate in old leaves to satisfy their nitrogen demand. This was perhaps the result from low rates of nitrogen uptake in roots since low shallow soil water availability in spring (Fig. 2) may have led to low soil nutrient availability for surface roots (Ryell et al., 2010) in a soil with an a priori low nitrogen content (Table 1). This hypothesis is supported by Ono et al. (1996) showing that nitrogen deficiency in new organs changes with sink development and nitrogen uptake rates, and that the rate of leaf senescence is well correlated to nitrogen deficiency.

In contrast to male flower production fruit setting was highly depressed by water stress showing a reduction of 54% during the dry year of 2012 (Table 3). There is evidence that summer drought impairs fruit development through the abortion of immature acorns in Mediterranean oaks (e.g. Montserrat-Marti et al., 2009; Perez-Ramos et al., 2010). Female flower maturation and the following acorn growth occur from early summer up to early autumn (Misson et al., 2011; Oliveira et al., 1994) which makes these phenophases highly dependent on soil water availabilities and photoassimilates produced throughout summer. On the contrary, male flowers are produced in early spring – in synchrony with leaf expansion (Fig. 5) – although being considered to have low carbon costs and low sink priority compared to fruits and even to vegetative growth (Ho, 1992). This would explain a regular male flowering much less dependent on drought effects as it was observed in spring 2012. A similar result was reported by Misson et al. (2011) for *Q. ilex* under an extreme spring drought. Furthermore, in accordance to our results Penuelas et al. (2004) and Montserrat-Marti et al. (2009) showed that most of species – including *Quercus* species – delayed flowering and fruit maturation during dry years.

#### 6.5.4. Conclusion

In summary, cork oak woodland net ecosystem exchange and phenology adjustments were studied here for the first time. Among evergreen Mediterranean oak species *Q. suber* leaf habits are singular in so far as leaf life-span is short and leaf fall is highly concentrated in a short spring period. The whole leaf canopy renewal is associated with an average 15% reduction of yearly carbon sequestration. Both, soil water availability and the extension of the favourable growing season in spring and early summer – as controlled by budburst date and leaf expansion period – were equally determinant for the great reduction in annual carbon sequestration in the dry year of 2012. Furthermore, our results suggest that new leaf growth in spring and maintenance of a relatively stable leaf area index are ecophysiological traits preserved even following an extreme dry winter. On the contrary, tree diameter growth is not a priority sink for photoassimilates. Thus, cork oak woodland reductions in carbon sequestration under low water availabilities are mainly due to stomatal or photosynthetic limitations and to a much lesser extent to leaf area reductions. The present work adds relevant contributions to answer questions such as: how does the ecosystem carbon sequestration seasonality interacts with a changing phenology due to global change?

#### 6.6. Acknowledgements

The authors acknowledge the financial support of FCT (Fundação para a Ciência e Tecnologia), through the postdoctoral fellowships to F. Costa e Silva (SFRH/BPD/46839/2008) and A. Correia (SFRH/BD/39058/2007). The authors wish to thank António Gonçalves Ferreira for providing field site facilities at Machoqueira do Grou and Grupo Amorim for continuous support in the eddy-flux tower maintenance.

#### 6.7. References

- Aguado, P.L., Dolores Curt, M., Pereira, H. and Fernandez, J., 2012. Allocation of C-14 assimilated in late spring to tissue and biochemical stem components of cork oak (*Quercus suber* L.) over the seasons. *Tree Physiology*, 32(3): 313-325.
- Allard, V., Ourcival, J.M., Rambal, S., Joffre, R. and Rocheteau, A., 2008. Seasonal and annual variation of carbon exchange in an evergreen Mediterranean forest in southern France. *Global*



- Change Biology, 14(4): 714-725.
- Allen, R.G., Pereira, L.S., Raes, D. and Smith, M., 1998. Crop evapotranspiration: Guidelines for computing crop requirements. Irrigation and Drainage Paper No. 56. FAO, Italy, 300 pp.
- Aranda, I., Castro, L., Alia, R., Pardos, J.A. and Gil, L., 2005. Low temperature during winter elicits differential responses among populations of the Mediterranean evergreen cork oak (*Quercus suber*). *Tree Physiology*, 25(8): 1085-1090.
- Aronson, J., Pereira, J.S. and Pausas, J., 2009. Cork oak woodlands on the edge: ecology, biogeography, and restoration of an ancient Mediterranean ecosystem. Island Press, Washington, DC.
- Aubinet, M. et al., 2000. Estimates of the annual net carbon and water exchange of forests: The EUROFLUX methodology. *Advances in Ecological Research*, Vol 30, 30: 113-175.
- Baldocchi, D., 2008. Breathing of the terrestrial biosphere: lessons learned from a global network of carbon dioxide flux measurement systems. *Australian Journal of Botany*, 56(1): 1-26.
- Baldocchi, D. et al., 2001. FLUXNET: A new tool to study the temporal and spatial variability of ecosystem-scale carbon dioxide, water vapor, and energy flux densities. *Bulletin of the American Meteorological Society*, 82(11): 2415-2434.
- Baldocchi, D. et al., 2010. On the differential advantages of evergreenness and deciduousness in mediterranean oak woodlands: a flux perspective. *Ecological Applications*, 20(6): 1583-1597.
- Besson, C.K. et al., 2014. Cork oak physiological responses to manipulated water availability in a Mediterranean woodland. *Agricultural and Forest Meteorology*, 184: 230-242.
- Buckley, T.N. and Mott, K.A., 2002. Stomatal water relations and the control of hydraulic supply and demand. *Progress in Botany* 63, 63: 309-325.
- Bugalho, M.N., Caldeira, M.C., Pereira, J.S., Aronson, J. and Pausas, J.G., 2011. Mediterranean cork oak savannas require human use to sustain biodiversity and ecosystem services. *Frontiers in Ecology and the Environment*, 9(5): 278-286.
- Caritat, A., Bertoni, G., Molinas, M., Oliva, M. and DominguezPlanella, A., 1996. Litterfall and mineral return in two cork-oak forests in northeast Spain. *Annales Des Sciences Forestieres*, 53(6): 1049-1058.
- Caritat, A., Garcia-Berthou, E., Lapena, R. and Vilar, L., 2006. Litter production in a *Quercus suber* forest of Montseny (NE Spain) and its relationship to meteorological conditions. *Annals of Forest Science*, 63(7): 791-800.
- Cerasoli, S. et al., 2004. Carbon and nitrogen winter storage and remobilisation during seasonal flush growth in two-year-old cork oak (*Quercus suber* L.) saplings. *Annals of Forest Science*, 61(7): 721-729.
- Correia, A.C. et al., 2014. Carbon sink strength of a Mediterranean cork oak understorey: how do semi-deciduous and evergreen shrubs face summer drought? *Journal of Vegetation Science*, 25(2): 411-426.
- Costa, A., Pereira, H. and Oliveira, A., 2003. Variability of radial growth in cork oak adult trees under cork production. *Forest Ecology and Management*, 175(1-3): 239-246.
- David, T.S. et al., 2007. Water-use strategies in two co-occurring Mediterranean evergreen oaks: surviving the summer drought. *Tree Physiology*, 27(6): 793-803.
- Dickson, R.E., 1989. Carbon and nitrogen allocation in trees. *Annales Des Sciences Forestieres*, 46: S631-S647.
- Dubbert, M. et al., 2014. Influence of tree cover on herbaceous layer development and carbon and water fluxes in a Portuguese cork oak woodland. *Acta Oecologica*, In press
- Escudero, A. and Mediavilla, S., 2003. Decline in photosynthetic nitrogen use efficiency with leaf age and nitrogen resorption as determinants of leaf life span. *Journal of Ecology*, 91(5): 880-889.
- Eugster, W. and Senn, W., 1995. A Cospectral correction model for measurement of turbulent NO<sub>2</sub>

- flux. *Boundary-Layer Meteorology*, 74(4): 321-340.
- Evangelista, M., 2010. Relatório da caracterização da fileira florestal 2010. Associação para a competitividade da indústria da fileira florestal, Portugal, 80 pp.
- Foken, T. and Wichura, B., 1996. Tools for quality assessment of surface-based flux measurements. *Agricultural and Forest Meteorology*, 78(1-2): 83-105.
- Giorgi, F. and Lionello, P., 2008. Climate change projections for the Mediterranean region. *Global and Planetary Change*, 63(2-3): 90-104.
- Ho, L.C., 1992. Fruit growth and sink strength. In: C. Marshall and J. Grace (Editors), *Fruit and Seed Production. Aspects of Development, Environmental Physiology and Ecology*. Cambridge University Press, New York, pp. 101-124.
- Hollinger, D.Y. et al., 1994. Carbon-dioxide exchange between an undisturbed old-growth temperate forest and the atmosphere. *Ecology*, 75(1): 134-150.
- Ibrom, A., Dellwik, E., Larsen, S.E. and Pilegaard, K., 2007. On the use of the webb pearman-leuning theory for closed-path eddy correlation measurements. *Tellus B*, 59(5): 937-946.
- IPCC, 2003. Good practice guidance for land use, land-use change and forestry. Intergovernmental panel on climate change - section 3.2. Institute for Global Environmental Strategies (IGES) for the IPCC, Kanagawa, JP.
- Knohl, A. and Baldocchi, D., 2008. Effects of diffuse radiation on canopy gas exchange processes in a forest ecosystem. *Journal of Geophysical Research-Biogeosciences*, 113(G2).
- Kolle, O. and Rebmann, C., 2007. Eddysoft - documentation of a software package to acquire and process eddy-covariance data. Technical Reports. Max-Planck-Institute for Biogeochemistry 10, Jena, DE.
- Kurz-Besson, C. et al., 2006. Hydraulic lift in cork oak trees in a savannah-type Mediterranean ecosystem and its contribution to the local water balance. *Plant and Soil*, 282(1-2): 361-378.
- Limousin, J.M. et al., 2009. Long-term transpiration change with rainfall decline in a Mediterranean *Quercus ilex* forest. *Global Change Biology*, 15(9): 2163-2175.
- Ma, S., Baldocchi, D.D., Xu, L. and Hehn, T., 2007. Inter-annual variability in carbon dioxide exchange of an oak/grass savanna and open grassland in California. *Agricultural and Forest Meteorology*, 147(3-4): 157-171.
- Mauder, M. and Foken, T., 2011. Documentation and Instruction Manual of the Eddy-Covariance Software Package TK3. Universitt Bayreuth Abt. , Mikrometeorologie.
- Misson, L. et al., 2011. Phenological responses to extreme droughts in a Mediterranean forest. *Global Change Biology*, 17(2): 1036-1048.
- Montserrat-Marti, G. et al., 2009. Summer-drought constrains the phenology and growth of two coexisting Mediterranean oaks with contrasting leaf habit: implications for their persistence and reproduction. *Trees-Structure and Function*, 23(4): 787-799.
- Morin, X., Roy, J., Sonie, L. and Chuine, I., 2010. Changes in leaf phenology of three European oak species in response to experimental climate change. *New Phytologist*, 186(4): 900-910.
- Niinemets, U., Cescatti, A., Rodeghiero, M. and Tosens, T., 2005. Leaf internal diffusion conductance limits photosynthesis more strongly in older leaves of Mediterranean evergreen broad-leaved species. *Plant Cell and Environment*, 28(12): 1552-1566.
- Oliveira, G., Correia, O., Martinsloucao, M. and Catarino, F.M., 1994. Phenological and growth-patterns of the Mediterranean oak *Quercus suber* L. *Trees-Structure and Function*, 9(1): 41-46.
- Ono, K., Terashima, I. and Watanabe, A., 1996. Interaction between nitrogen deficit of a plant and nitrogen content in the old leaves. *Plant and Cell Physiology*, 37(8): 1083-1089.
- Otieno, D.O. et al., 2007. Regulation of transpirational water loss in *Quercus suber* trees in a Mediterranean-type ecosystem. *Tree Physiology*, 27(8): 1179-1187.
- Papale, D. et al., 2006. Towards a standardized processing of Net Ecosystem Exchange measured with

- eddy covariance technique: algorithms and uncertainty estimation. *Biogeosciences*, 3(4): 571-583.
- Paulo, J. and Tomé, M., 2006. Equações para estimação do volume e biomassa de duas espécies de carvalhos: *Quercus suber* e *Quercus ilex*. Publicações do GIMREF; RC1/2006, Instituto Superior de Agronomia. Departamento de Engenharia Florestal, Lisboa.
- Penuelas, J. et al., 2004. Complex spatiotemporal phenological shifts as a response to rainfall changes. *New Phytologist*, 161(3): 837-846.
- Pereira, J.S., Beyschlag, G., Lange, O.L., Beyschlag, W. and Tenhunen, J.D., 1987. Comparative phenology of four Mediterranean shrub species growing in Portugal. In: J.D. Tenhunen, F.M. Catarino, O.L. Lange and O.L. Oechel (Editors), *Plant Response to Stress*. Springer-Verlag, Berlin Heidelberg, pp. 503-512.
- Pereira, J.S., Chaves, M.M., Caldeira, M.C. and Correia, A.V., 2006. Water availability and productivity. In: J.I.L. Morrison and D. Morecroft (Editors), *Plant growth and climate change*. Blackwell Publishers, London, pp. 118-145.
- Pereira, J.S., Kurz-Besson, C. and Chaves, M.M., 2009. Coping with drought. Part II. Scientific Bases for restoration and management. In: J. Aronson, J.S. Pereira and J.G. Pausas (Editors), *Cork oak woodlands on the edge: ecology, adaptive management, and restoration*. Island Press, Washington, DC, pp. 73-80.
- Pereira, J.S. et al., 2007. Net ecosystem carbon exchange in three contrasting Mediterranean ecosystems - the effect of drought. *Biogeosciences*, 4(5): 791-802.
- Perez-Ramos, I.M., Ourcival, J.M., Limousin, J.M. and Rambal, S., 2010. Mast seeding under increasing drought: results from a long-term data set and from a rainfall exclusion experiment. *Ecology*, 91(10): 3057-3068.
- Pinto, C.A. et al., 2012. Drought-induced embolism in current-year shoots of two Mediterranean evergreen oaks. *Forest Ecology and Management*, 285: 1-10.
- Pinto, C.A. et al., 2011. Phenology and growth dynamics in Mediterranean evergreen oaks: Effects of environmental conditions and water relations. *Forest Ecology and Management*, 262(3): 500-508.
- Rebmann, C. et al., 2012. *Eddy Covariance: A Practical Guide to Measurement and Data Analysis*. Ch. Data Acquisition and Flux Calculations. Springer, Dordrecht.
- Reichstein, M. et al., 2013. Climate extremes and the carbon cycle. *Nature*, 500(7462): 287-295.
- Reichstein, M. et al., 2005. On the separation of net ecosystem exchange into assimilation and ecosystem respiration: review and improved algorithm. *Global Change Biology*, 11(9): 1424-1439.
- Richardson, A.D. et al., 2010. Influence of spring and autumn phenological transitions on forest ecosystem productivity. *Philosophical Transactions of the Royal Society B-Biological Sciences*, 365(1555): 3227-3246.
- Ryel, R.J., Leffler, A.J., Ivans, C., Peek, M.S. and Caldwell, M.M., 2010. Functional Differences in Water-Use Patterns of Contrasting Life Forms in Great Basin Steppelands. *Vadose Zone Journal*, 9(3): 548-560.
- Sachs, L., 1992. *Angewandte Statistik: statistische Modelle und ihre Anwendungen*. Springer, 552 pp.
- Sanz-Perez, V., Castro-Diez, P. and Valladares, F., 2009. Differential and interactive effects of temperature and photoperiod on budburst and carbon reserves in two co-occurring Mediterranean oaks. *Plant Biology*, 11(2): 142-151.
- Saxe, H., Cannell, M.G.R., Johnsen, B., Ryan, M.G. and Vourlitis, G., 2001. Tree and forest functioning in response to global warming. *New Phytologist*, 149(3): 369-399.
- Schotanus, P., Nieuwstadt, F.T.M. and Debruin, H.A.R., 1983. Temperature-measurement with a sonic anemometer and its application to heat and moisture fluxes. *Boundary-Layer Meteorology*,

- 26(1): 81-93.
- Sinclair, T.R. and Muchow, R.C., 1999. Radiation use efficiency. *Advances in Agronomy*, Vol 65, 65: 215-265.
- Thomas, C., Foken, T. and Ams, A.M.S., 2002. Re-evaluation of integral turbulence characteristics and their parameterisations, 15th Symposium on Boundary Layers and Turbulence.
- Tyree, M.T. and Sperry, J.S., 1988. Do woody-plants operate near the point of catastrophic xylem dysfunction caused by dynamic water-stress - Answers from a model. *Plant Physiology*, 88(3): 574-580.
- Unger, S. et al., 2009. Partitioning carbon fluxes in a Mediterranean oak forest to disentangle changes in ecosystem sink strength during drought. *Agricultural and Forest Meteorology*, 149(6-7): 949-961.
- Vaz, M. et al., 2010. Drought-induced photosynthetic inhibition and autumn recovery in two Mediterranean oak species (*Quercus ilex* and *Quercus suber*). *Tree Physiology*, 30(8): 946-956.
- Vilagrosa, A., Bellot, J., Vallejo, V.R. and Gil-Pelegrín, E., 2003. Cavitation, stomatal conductance, and leaf dieback in seedlings of two co-occurring Mediterranean shrubs during an intense drought. *Journal of Experimental Botany*, 54: 2015-2024.
- Werner, C. and Correia, O., 1996. Photoinhibition in cork-oak leaves under stress: Influence of the bark-stripping on the chlorophyll fluorescence emission in *Quercus suber* L. *Trees-Structure and Function*, 10(5): 288-292.
- Wilczak, J.M., Oncley, S.P. and Stage, S.A., 2001. Sonic anemometer tilt correction algorithms. *Boundary-Layer Meteorology*, 99(1): 127-150.



## **7. STUDY VII: DROUGHT IMPACT ON CARBON AND WATER CYCLING IN A MEDITERRANEAN *QUERCUS SUBER* L. WOODLAND DURING THE EXTREME DROUGHT EVENT IN 2012**

Arndt Piayda<sup>1, ✉</sup>; Maren Dubbert<sup>2</sup>; Corinna Rebmann<sup>1</sup>; Olaf Kolle<sup>3</sup>; Filipe Costa  
e Silva<sup>4</sup>; Alexandra C. Correia<sup>4</sup>; Joao S. Pereira<sup>4</sup>; Christiane Werner<sup>2</sup>; and  
Matthias Cuntz<sup>1</sup>

<sup>1</sup>Department of Computational Hydrosystems, UFZ Helmholtz Centre for Environmental Research, Permoserstr.  
15, 04318 Leipzig, Germany

<sup>2</sup>Agroecosystem Research, BayCEER, University of Bayreuth, Universitätsstr. 30, 95447 Bayreuth, Germany

<sup>3</sup>Field Experiments & Instrumentation, Max Planck Institute for Biogeochemistry, Hans-Knoll-Str. 10, 07745  
Jena, Germany

<sup>4</sup>Department of Forestry, Instituto Superior de Agronomia, Technical University of Lisbon, Tapada da Ajuda,  
1349-017 Lisbon, Portugal

✉ Corresponding author: Arndt Piayda ([arndt.piayda@ufz.de](mailto:arndt.piayda@ufz.de))



## 7.1. Abstract

Savannah-type ecosystems account for 26–30 % of global gross primary productivity *GPP* with water being one of the major driving factors. In Europe, savannah-type woodlands cover an area of about 1.5 million ha. Here, the recent past has shown a significant decrease of precipitation *P* in winter and spring as well as decrease of total annual precipitation. Strong effects on local water balance and carbon sink strength have thus been reported due to changes in precipitation regime.

The objective of this study is to quantify the impact of the extreme drought event in 2012 on the water balance, gross primary productivity and carbon sink strength of a typical Portuguese cork-oak woodland (*montado*) compared to the wet year 2011. Physiological responses of the dominant tree species *Quercus suber* (L.) are disentangled, employing combined photosynthesis and stomatal conductance modelling.

Precipitation effectiveness *ET/P* increased from 86 % in 2011 to 122 % in the dry year 2012 due to deep soil or ground water access of the *Q. suber* trees leaving no water for ground water replenishment. Understorey and overstorey *GPP* were strongly reduced by 53 % and 28 %, respectively, in 2012 compared to 2011 due to the late onset of the autumn rains in 2011 and an additional severe winter/spring drought. However, the ecosystem was still a carbon sink in both years but with a 38 % reduced sink strength under extreme drought in 2012 compared to 2011. The combined photosynthesis-stomatal conductance model yielded best results if it was allowed to adjust photosynthetic and stomatal parameters simultaneously. If stomatal response was modelled with the Leuning approach, which allows for a different sensitivity to vapour pressure deficit, the stomatal model parameters were highly coupled. A change in either of the parameters needed to be compensated by the other to guarantee a stable sensitivity of stomatal conductance to assimilation, independently from variations in vapour pressure deficit. The *Q. suber* trees showed a 31 % reduced stomatal conductance during the drought period 2012 compared to 2011 due to water supply limitations. In response to reduced leaf internal CO<sub>2</sub> availability, the trees strongly reduced apparent maximum carboxylation rate by 39 % in 2012 compared to 2011. Unexpectedly, the optimum temperature of maximum electron transport rate decreased during the drought period, enhancing the susceptibility of the trees to high temperature stress during the summer.

Our results suggest that, if the trend of decreasing annual precipitation and changed precipitation pattern on the Iberian Peninsula continues, sustained effects on local ground water reservoirs, understorey species composition and tree mortality have to be expected in the long term. To successfully model the effect of drought on the *montado* ecosystem, variable apparent maximum carboxylation rate, stomatal conductance parameter  $m$  and vapor pressure deficit sensitivity parameter need to be incorporated in photosynthesis-stomatal conductance modelling.

## 7.2. Introduction

One of the typical semi-arid ecosystem in Europe is a savannah-type woodland (*montado*), consisting of a sparse overstorey tree layer and a herbaceous understorey layer. During the biomass peak of the herbaceous plants in spring, the understorey layer can provide a large contribution to the whole ecosystem water and carbon balance and thus, can play a significant role in the annual carbon and water budgets (Unger et al., 2009, Paco et al., 2009, Dubbert et al., 2014). However, each layer responds differently to changes in precipitation depending on their life form (chamaephyte or therophyte) and access to different water reservoirs throughout the year Paco et al. (2009) including deep soil or ground water David et al. (2004).

*Montado* ecosystems (span.: *dehesa*) cover an area of about 1.5 million ha in Europe (Bugalho et al., 2011) and contribute together with savannah-type ecosystems on other continents about 30 % to global gross primary productivity *GPP* (Beer et al., 2010, Grace et al., 2006). The major driving factor of *GPP* in *montado* ecosystems is water (Vargas et al., 2013, Pereira et al., 2007, David et al., 2004), since annual precipitation patterns show periodical summer droughts and evapotranspiration losses are high (Krishnan et al., 2012, Huxman et al., 2005).

In the recent past, precipitation shows a significant decrease of rain amount in February and March as well as a decrease of total annual rainfall on the Iberian Peninsula (Guerreiro et al., 2013, Garcia-Barron et al., 2013, Mourato et al., 2010, Paredes et al., 2006). A trend towards extreme events in the form of droughts is observed due to a more heterogeneous distribution of precipitation throughout the year (Garcia-Barron, et al., 2013). These type of changes in precipitation regime have been reported to



strongly affect local water balance (Rodrigues et al., 2011, Vaz et al., 2010, Grant et al., 2010) and carbon sink strength (Perez-Ramos et al., 2013, Pereira et al., 2007, Granier et al., 2007, Ciais et al., 2005) of ecosystems in semi-arid regions and are expected to increase with proceeding climate change (Bussotti et al., 2013, Guerreiro et al., 2013).

Species in semi-arid environments have developed vast structural and functional adaptations to regulate carbon assimilation and respiratory water loss (e.g. Tenhunen et al., 1987, Werner et al., 1999). Considerable knowledge has been acquired on leaf-level physiological processes in the last three decades (e.g. Beyschlag et al., 1986, Sala et al., 1996, Tenhunen, et al., 1985, Tenhunen et al., 1990, Werner et al., 2001), emphasizing the role of ecophysiological adaptations to seasonality and summer drought in Mediterranean climate conditions. In these environments lack of precipitation often interacts with excessive irradiance and high temperature further constraining leaf carbon fixation through photoinhibition during drought (Werner et al., 2001, Werner et al., 2002). Cork oaks strongly reduce transpirational water loss by stomatal closure in response to drought to avoid a critical level of dehydration and hydraulic failure (Oliveira et al., 1992, Tenhunen et al., 1984, Tenhunen et al., 1987, Werner et al., 1996, Kurz-Besson et al., 2006).

To investigate the influence of drought on carbon sink strength at the ecosystem level, combined stomatal conductance-photosynthesis models can be used in order to disentangle regulatory processes from effects of micro-climatic variations. Different descriptions of the underlying processes exist in the literature, though. For example, stomatal conductance can be modelled either reacting to relative humidity Ball et al. (1987) or to vapour pressure deficit Leuning et al. (1995). Also the determination of parameters in individual descriptions is different among different authors. The sensitivity of stomatal conductance to vapor pressure, for example, is often taken as a fixed value while determining only the other parameters in the coupled stomatal conductance-photosynthesis model time-variant, although the sensitivities of stomatal conductance to photosynthesis and to vapour pressure are highly correlated. Recent studies could consequently demonstrate that changes of one single parameter, e.g. only maximum carboxylation rate or only stomatal conductance sensitivity, does not explain drought-induced reductions in both *GPP* and *T* simultaneously (Egea et al., 2011, Reichstein et al., 2003, Zhou et al., 2013). Further, different temperature dependencies of e.g. maximum carboxylation or electron

transport rate have been proposed (Medlyn et al., 2002, von Caemmerer et al., 2000, June et al., 2004). In the present study, we report on drought effects on a Portuguese *montado* ecosystem using the unique opportunity of two consecutive years of very contrasting hydrological conditions: 2011 being a wet year with regular drought pattern occurring in summer, and 2012 being an extremely dry year with strongly reduced precipitation amount. Particularly, 2012 showed a severe additional winter/spring drought characteristic for precipitation pattern changes in recent past on the Iberian Peninsula (2nd driest year since 1950, Costa et al., 2012, Santos et al., 2013, Trigo et al., 2013). This study is focussing on: (1) quantifying the effects of drought on the local ecosystem water balance, overstorey and understorey *GPP*, as well as differences in net ecosystem carbon exchange *NEE* between both years. (2) Identifying physiological responses in the drought year 2012 of the *Q. suber* trees using a combined photosynthesis-stomatal conductance model and testing the model performance with different process descriptions.

### 7.3. Material and methods

#### 7.3.1. Site description

The study was conducted at the savannah-type flux observation site 'PT-Cor' (Fig. 1) of the European integrated carbon observation system ICOS ca. 100 km north-east of Lisbon, Portugal (latitude: 39° 8 0 20.7 00 N, longitude: 8° 20 0 3.0 00 W, altitude: 162 m a.s.l.). The site is planted with evergreen *Quercus suber* (L.) trees (209 individuals ha<sup>-1</sup>) on a cambisol soil (Jongen et al., 2011). The tree canopy has a leaf area index *LAI* of  $1.05 \pm 0.07$  m<sup>2</sup> leaf m<sup>-2</sup> ground, a midday gap probability  $P_{gap}$  (0) of  $0.76 \pm 0.03$  and an average tree canopy height of 9.7 m (Piayda et al., in review). The *Q. suber* trees have access to deep soil layers and the ground water table is relatively shallow at this site (between 2 and 3 m). Native annual grasses and herbs build the understorey vegetation (Dubbart et al., 2014; Jongen et al., 2013a), which emerges after the first rains in autumn, has a peak growth period in spring (Mar - Apr) and becomes senescent at the beginning of the summer period (May-June). The understorey vegetation density and *LAI* are spatially highly variable due to the heterogeneous topography and hence, differences in soil moisture regime. The whole region is under forest

management.

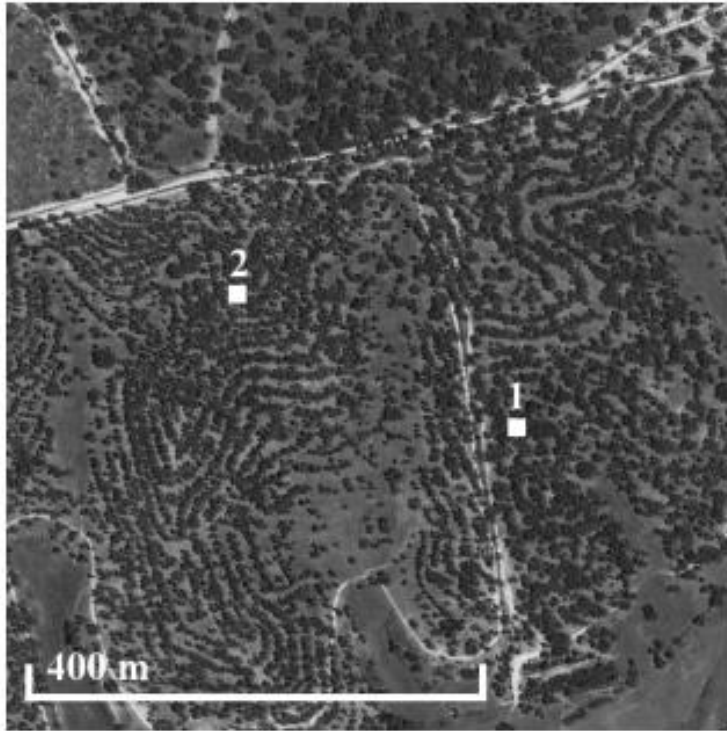


**Figure 1:** Satellite image of the study site (© Google Maps, 2013). 1: position of the overstorey tower. 2: position of the understorey tower.

### 7.3.2. *Climate conditions*

The site is characterised by a Mediterranean climate with moist and mild winters and dry and hot summers. The long term mean annual temperature is about 15.9 °C and the annual sum of precipitation is about 680 mm (Jongen et al., 2013), with a characteristic annual pattern of high winter precipitation (November to January) and summer drought during June to September (Paredes et al., 2006). The relevance of the winter precipitation for the Portuguese hydrological cycle can be easily explained by the prevailing Mediterranean-type climate that concentrates most of precipitation during the winter half of the year, with little to no precipitation in summer. Hence, the following data treatment is based on the hydrological year beginning with first autumn precipitation (October to September).

### 7.3.3. *Overstorey tower eddy covariance measurements*

The overstorey tower (Fig. 1, point 1) is set up with a Gill R3A-50 ultrasonic anemometer (Gill Instruments Ltd., Lymington, UK) in combination with a LI-7000 closed path CO<sub>2</sub> /H<sub>2</sub>O analyzer (LI-COR, Lincoln, USA). The inlet tube has a length of 8.5 m, is attached to one of the anemometer arms

and operated with an average flow rate of ca. 8 l/min. The reference cell is flushed with N<sub>2</sub>. The measurement height is about 23.5 m above ground. Data is continuously acquired and processed live on a field laptop with the eddy-covariance data acquisition and processing software package EddyMeas (meteotools, Jena, DE; Kolle and Rebmann, 2007).

At a height of 20 m above ground, two up- and downward facing LI-190 Quantum sensors (LI-COR, Lincoln, USA) and a NR-LITE net radiometer (Kipp & Zonen, Delft, NL) are attached. A radiation shielded HMP 155 probe measures air temperature  $T$  and relative humidity  $rH$  (Vaisala, Helsinki, FI). Precipitation  $P$  is measured with an ARG100 aerodynamic rain gauge (Environmental Measurements Ltd., North Shields, UK) at the tower top. The meteorological parameters are logged on a CR10X datalogger (Campbell Scientific, Logan, USA).

#### 7.3.4. *Understorey tower eddy covariance measurements*

The understorey tower was located about 286 m north-west of the overstorey tower (Fig. 1, point 2). It was equipped with a Gill R3-50 ultrasonic anemometer (Gill Instruments Ltd., Lymington, UK) in combination with a LI-7500A open path CO<sub>2</sub> /H<sub>2</sub>O analyzer (LI-COR, Lincoln, USA). The gas analyzer was tilted at 45° from the vertical and the sensor separation was about 30 cm. The measurement height of both sensors was 3.15 m above ground. EddyMeas was used for data acquisition here as well.

At 2 m height above ground, two PAR LITE quantum sensors facing up- and downward were attached to a CNR1 net radiometer (Kipp & Zonen, Delft, NL). Air temperature  $T$  and relative humidity  $rH$  were measured with a HMP 155 probe covered by a radiation shield and atmospheric pressure  $p$  was measured with a PTB 110 barometer at 1.5 m above ground (Vaisala, Helsinki, FI). The meteorological parameters were logged on a CR1000 datalogger (Campbell Scientific, Logan, USA).

A third eddy covariance system consisting of an Gill R3-50 ultrasonic anemometer in combination with a LI-7500A open path analyzer was used to test comparability of over- and understorey tower systems. For a period of one week each it was mounted on the overstorey and the understorey tower and measured in parallel. Both systems showed high Bravais–Pearson correlation coefficients of 0.78

to 0.91 as well as small normalized root mean squared errors of 0.01 to 0.06 for water and carbon fluxes in comparison with the portable eddy system.

#### 7.3.5. *Soil temperature and moisture*

Soil temperature  $T_s$  and soil moisture  $\theta$  were measured at open and a tree shaded locations between the two towers.  $T_s$  was measured with thermo-couples in 2, 4, 8, 16, 30, and 60 cm depth, two replicates each (PT100 PRT Temperature Probe, Campbell Scientific).  $\theta$  was measured with 10hs sensors (Decagon Devices, Inc., Washington, USA) at 5, 15, 30 and 60 cm depth, four replicates each. The meteorological parameters were stored on CR1000 dataloggers (Campbell Scientific, Logan, USA).

#### 7.3.6. *Data treatment*

Eddy flux data was post-processed using EddySoft and Python 2.7. Half-hourly means were calculated by block-averaging the 20 Hz data, time lags between  $\text{CO}_2/\text{H}_2\text{O}$  signals and vertical wind velocity were determined via cross correlation analysis following Aubinet et al. (1999). Whenever the cross correlation failed for the closed path analyzer signals of the overstorey tower, the dependency on  $rH$  was used to determine the lag for the  $\text{H}_2\text{O}$  signal according to Ibrom et al. (2007) and Rebmann et al. (2012). High frequency losses were compensated with the use of inductances derived from 140 co-spectral analysis (Eugster and Senn, 1995). The sectorial planar fit method was used for the coordinate rotation of wind vectors (Rebmann et al., 2012; Wilczak et al., 2001). For both towers the moisture and cross wind correction according to Schotanus et al. (1983) was applied and the WPL correction for flux density fluctuations was used for the  $\text{CO}_2/\text{H}_2\text{O}$  signals of the open path understorey sensor only (Leuning, 2007; Webb et al., 1980). The storage term of  $\text{CO}_2$  was calculated after Hollinger et al. (1994) and added to the turbulent  $\text{CO}_2$  flux.

For the purpose of quality control, flags were determined for every half-hourly flux value including the following tests: the 20 Hz data was scanned for exceeded physical limits, change rates and variances. The stationary test of Foken and Wichura (1996) was applied to the high frequency data based upon a 50% deviation criterion. On a half-hourly basis, the integral turbulence characteristics (ITC) were

calculated following Thomas and Foken (2002) with a 30% deviation criterion. For the understorey tower, the parameterization of the ITC was recalculated according to the observations. A spike detection routine was used on the half-hourly data based on the absolute median deviation (Papale et al., 2006). All quality control tests were summed up in a simplified flag system referring to Mauder and Foken (2011).

The partitioning of the net  $\text{CO}_2$  fluxes  $NEE$  into gross primary production  $GPP$  and ecosystem respiration  $R_{eco}$  followed Lasslop et al. (2010) and the flux gap-filling was made according to Reichstein et al. (2005). Gaps were only filled up to a maximum gap length of 6 days.

$T_s$  and  $\theta$  were integrated over the respective depths and the replicates of each site (open and shaded) are averaged. To calculate ecosystem representative  $T_s$  and  $\theta$ , the open and the shaded site were weighted using time-dependent  $P_{gap}$ , modelled from the daily course of sun inclination angle and the view zenith angle distribution of  $P_{gap}$  (Piayda et al., in review). The soil heat flux  $G$  was calculated from the averaged  $T_s$  profiles. To estimate the energy balance closure of the towers, the storage terms due to changes in  $T$ ,  $rH$  were added to the energy balance equation and plotted against the turbulent energy fluxes for daytime values with global radiation  $R_g > 20 \text{ W/m}^2$  (Foken, 2008; Mauder et al., 2013; Twine et al., 2000). The ratio was used to correct sensible heat  $H$ , latent heat  $\lambda E$  and evapotranspiration  $ET$  flux with the Bowen ratio being preserved.

#### 7.3.7. *Photosynthesis and stomatal conductance modelling*

The Farquhar model for photosynthesis (Farquhar et al., 1980) combined with the Leuning model for stomatal conductance (Leuning, 1995) was used to model gross primary production  $GPP_o$  and evapotranspiration  $ET_o$  measured at the overstorey tower for the summer months May to September of 2011 and 2012. The model was fitted to a 31 day long moving window of  $GPP_o$  and  $ET_o$  to gain stable, median daily cycles. These were cropped to the time from sunrise to midday. Model fitting was done using a Nelder-Mead simplex algorithm (Nelder and Mead, 1965) with a higher order multi objective cost function for  $GPP_o$  and  $ET_o$  according to Duckstein (1981) under varying apparent maximum carboxylation rate  $V_{cmax}$  (no separate modelling of mesophyll conductance), stomatal conductance

parameter  $m$  and vapour pressure deficit sensitivity parameter  $D_0$ . See Appendix B for detailed model equations.

## 7.4. Results and discussion

Ecosystem fluxes for the hydrological years 2011 and 2012 (October 2010 to September 2012) are discussed in the following. Flux time series are only compared when data availability is given for both hydrological years, but not on an annual sum basis.

The dominant wind direction changes during the season. Absolute values of flux measurements of the overstorey tower are thus not directly comparable to the absolute values of the understorey tower due to changing footprint area and the heterogeneity of the ecosystem. However, comparisons of the intra-annual pattern of ecosystem fluxes between both towers and inter-annual changes between both years 2011 and 2012 are possible and conducted in the following.

### 7.4.1. *Meteorological and environmental conditions*

Water scarcity is the most important factor for ecosystem productivity in savannah-type ecosystems. Drought stress severity and its impact on the vegetation depends on timing as well as on the amount of precipitation  $P$  (Penuelas et al., 2004). In this context, the hydrological years 2011 and 2012 mark exceptional years on the Iberian Peninsula. Compared to the long term average precipitation of about 680 mm,  $P$  was 34% higher in 2011 and 39% lower in 2012 (Fig. 2a,b) compared to the long term average of precipitation of about 680 mm (Jongen et al., 2013b). In particular, the winter 2011/2012 was very dry over Soutwestern Iberia, with only about 20 % of the long term precipitation Santos2013, Trigo2013. 2012 was the second driest year since 1950. The last negative  $P$  anomaly of comparable severity occurred in the drought year 2004/2005 (Paredes et al., 2006, Santos et al., 2007).

The intra-annual pattern of precipitation has especially changed in 2012. Total annual reduction to the previous year 2011 was 495 mm of which 68 % occurred during a long drought event in winter and early spring (December–March). The beginning of autumn precipitation was also delayed by almost a month in 2012. Winter precipitation is the most important for replenishing the soil and ground water

reservoirs after the summer drought. But the winter precipitation period was shortened and interrupted for about four months in the hydrological year 2012. These phenomena, i.e. reduced annual  $P$ , additional winter/spring drought, and prolonged summer drought, are characteristic for observed  $P$  extremes in the last decades (e.g. Guerreiro et al., 2013, Paredes et al., 2006).

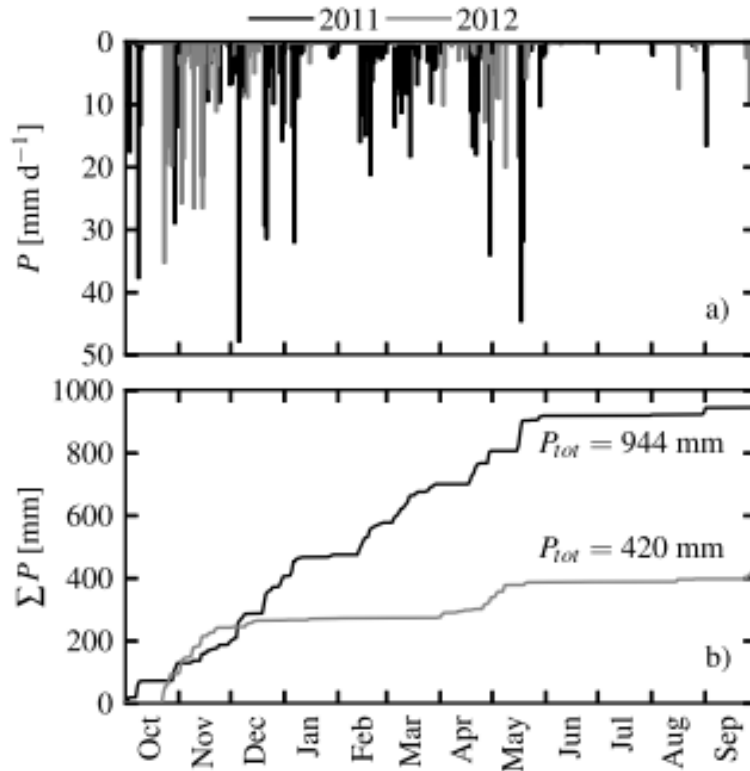


**Figure 2:** a) Daily sum of precipitation  $P$  for 2011 (black) and 2012 (grey). b) Cumulative precipitation  $P$  for 2011 (black) and 2012 (grey) based on half hourly data.

We address first the question of changes in environmental and climatic components between both years, which may have caused significant changes in ecosystem functioning. The distributions of most relevant climatic and environmental variables for plant functioning are therefore analysed in quantile-quantile (Q-Q) plots in Fig. 3. Air temperature (Fig. 3a) and incoming photosynthetically active radiation  $PAR$  (data not shown) showed only minor changes between the two years so that plant available energy in both years was comparably high. In contrast, moisture related variables showed large deviations from the on-to-one line in the Q-Q plots (Fig. 3b–d). All precipitation  $P$  intensities of 2012 stayed well below the ones in 2011 (Fig. 3b). Air vapour pressure deficit  $vpd$  was considerably increased at high deficits in 2012 compared to 2011 (Fig. 3c). This comes from lower absolute



humidity because air temperature did not change substantially. Possible reasons are either diminished local ecosystem evapotranspiration  $ET$ , due to diminished soil moisture (Fig. 3d) and plant transpiration or less air moisture input by incoming air masses from the ocean. Soil moisture was significantly decreased in 2012 compared to 2011 (Fig. 3d), which is exhibited especially in the missing medium soil moisture amounts. The contribution of local  $ET$  to the observed reduction in  $vpd$  was estimated by approximating the average contribution of local  $ET$  to absolute humidity of the atmospheric boundary layer. 50 % of absolute humidity reduction in 2012 compared to 2011 could be explained by a reduced contribution of local  $ET$ . This illustrates the strong influence of  $ET$  on local hydrological conditions and the reinforcement of plant drought stress due to increased  $vpd$ .

The ecosystem, therefore, faced increased transpirational demand from higher atmospheric  $vpd$  combined with strongly decreased soil water availability, which resulted in high water stress for the trees but also for understorey vegetation in 2012 compared to 2011. In the following, the effect of decreased water availability on the ecosystem water budget is discussed.

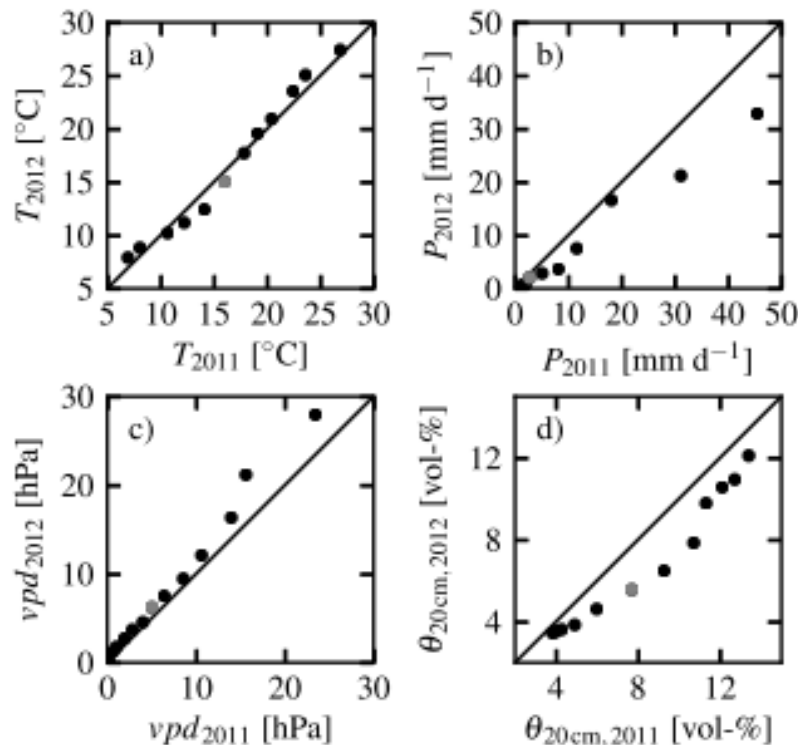


**Figure 3:** Quantile-quantile plot of important climate and environmental parameters for the years 2011 and 2012 based on daily averages. Black dots represent the 0.01, 0.05, 0.1, 0.2, 0.3, 0.4, 0.6, 0.7, 0.8, 0.9, 0.95, and 0.99 quantiles of the respective distribution. Grey dots represent the 0.5 quantile. a) air temperature  $T$ , b) precipitation  $P$ , and c) vapour pressure deficit of the air  $vpd$ , each measured at 20 m height above ground. d) soil moisture in the first 20 cm  $\theta_{20cm}$  (root zone of understorey vegetation).

#### 7.4.2. Drought influence on ecosystem water balance

Evapotranspiration  $ET$  is the major component of total water efflux in Mediterranean ecosystems on annual basis (Huxman et al., 2005). A comparably small amount of precipitation is left for ground water recharge and runoff.  $ET$  usually peaks in May before the onset of drought in the beginning of June in Mediterranean ecosystems (Vargas et al., 2013). But ecosystem evapotranspiration measured here at the overstorey tower (Fig. 4b) peaked within the summer drought period in June to July in 2011. This behaviour is typical for *montado* ecosystems with ground water access of the trees (Paco et al., 2009, Pereira et al., 2007, David et al., 2007, David et al., 2004).

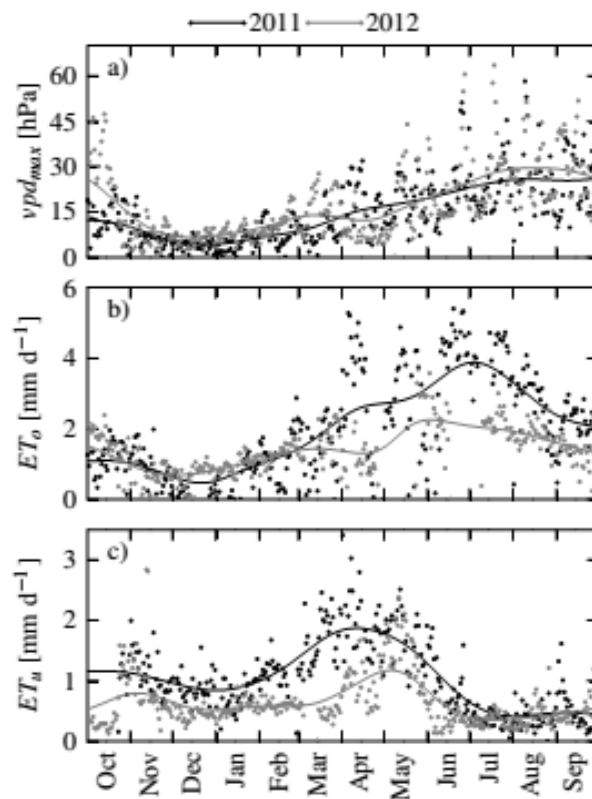


**Figure 4:** a) Maximum daily vapour pressure deficit  $vpd_{max}$ , b) daily sum of ecosystem evapotranspiration  $ET_o$  and c) daily sum of understorey transpiration + soil evaporation  $ET_u$  for 2011 (black) and 2012 (grey). Lines mark kernel regressions.

In 2012  $ET_o$  showed a slight peak shift towards spring in 2012 and was diminished by 26 % compared to 2011. The major decrease occurred in late spring and summer (March to September) although the major reduction in precipitation  $P$  occurred in winter and early spring (December to March) (Fig. 4b). When atmospheric demand (Fig. 4a) and energy input into the system increased in spring 2012, the  $Q$ .

*suber* trees were not able to maintain transpiration  $T$  as high as in 2011. This indicates, that most likely the deep soil and/or ground water reservoirs were not refilled after summer 2011 due to the dry winter as displayed by soil moisture observations in 60 cm depth (Fig. 5b). However, the strongly diminished transpiration  $T$  led to a non-significant increase in maximum daily leaf temperature of only 1.7 °C during the summer period of 2012. The small influence of the reduced transpirational cooling on leaf temperature could be attributed to the high aerodynamic conductance in this open canopy, enabling a comparably high energy transport by sensible heat.

Evapotranspiration measured at the understorey tower ( $ET_u$ ) peaked in March to April 2011 before the beginning of the summer die back of the understorey vegetation, which is rather typical in savannah-type ecosystems (e.g. Paco et al., 2009).  $ET_u$  was reduced, though, by 38 % in 2012 compared to 2011. The peak was slightly delayed under drought conditions in 2012, in contrast to ecosystem  $ET$ . The late onset of autumn precipitation  $P$  in October and additionally the missing recharge of upper soil moisture in winter (Fig. 5a) had an immediate impact on  $ET_u$  inhibiting plant growth and herbaceous transpiration (see Sect. 3).  $ET_o$ , on the other hand, was influenced from March onwards only. The precipitation events occurring in April and March 2012 (Fig. 2a) were not able to increase  $ET$  up to the level of 2011 even though the atmospheric demand was slightly higher in 2012 (Fig. 4c). This can be explained on the one hand by very low soil moistures up to 20 cm depth in October and from March onwards (Fig. 5a), which prevented soil evaporation, and on the other hand, by the strong reduction in plant cover leading to a reduced contribution of herbaceous plant transpiration to ecosystem  $ET$  (see Sect. 3).

Precipitation effectiveness indicates the amount of total precipitation  $P$  used for actual ecosystem evapotranspiration.  $ET/P$  was 86 % in 2011, which is high but comparable to other studies (Sala et al., 1996, Pinol et al., 1991). However, the strong reduction of ecosystem evapotranspiration of 26 % in 2012 was vastly exceeded by the reduction in precipitation  $P$  of 54 %. This confirms recent results from Besson et al. (2014) showing a certain resilience of *Q. suber* tree transpiration to annual water shortages. This led to  $ET/P$  of 122 % in 2012, which is to our knowledge, the highest value reported for *montado* ecosystems so far. Hence more water evaporated from the soil and was transpired by the trees than was brought into the ecosystem by precipitation. This was possible due to the deep soil or

ground water access of the trees maintaining a relatively high transpiration rate throughout the summer. But it left also no water for ground water replenishment or runoff generation (cf. Sala et al., 1996).

Ecosystem productivity was markedly changed in 2012 due to the strong alterations in the water balance, which will be discussed in the following.

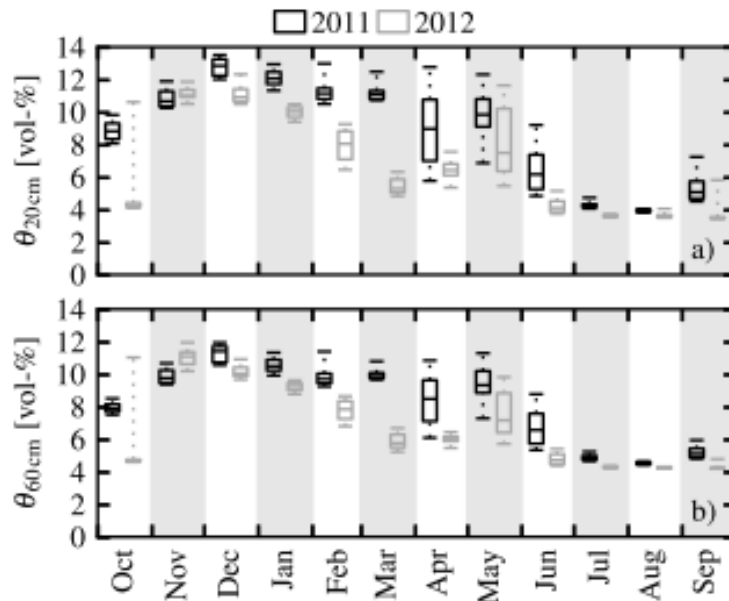


**Figure 5:** Box plot of monthly volumetric soil moisture a) down to 20 cm depth  $\theta_{20\text{ cm}}$  (root zone of understorey vegetation) and b) down to 60 cm depth  $\theta_{60\text{ cm}}$  for the years 2011 (black) and 2012 (grey). Central line marks the median, box marks the 0.25 and 0.75 quantiles. Dashed lines mark the 0.05 and 0.95 quantiles. Data within a two day interval after a rain event were excluded.

#### 7.4.3. Understorey growth inhibition

The local understorey vegetation consists of native annual grasses and herbs (Jongen et al., 2013, Dubbert et al., 2014). The species are adapted to regular summer droughts by seed formation in spring before the onset of the summer droughts. They survive the dry periods as seeds and germinate again at the onset of autumn precipitation. Species abundance during spring depends thus on the amount of previous winter precipitation (Figueroa et al., 1991). The timing of the first autumn rains and rewetting of the soils is thereby of great importance for germination success, number of individuals and plant productivity (Jongen et al., 2013a, DiosMiranda et al., 2009).

The understorey showed a typical annual cycle of gross primary productivity in 2011 (Fig. 6c) for

savannah-type understorey vegetation with the growth onset at the end of October (Ma et al., 2007). Carbon uptake peaked in February to March and ended with the complete die back at the end of May.  $GPP_u$  was strongly reduced by 53 % in 2012 compared to 2011. A small  $GPP_u$  peak occurred along with precipitation  $P$  in April and May (Fig. 6). The reduction of  $GPP_u$  can be explained by the very low soil moisture during October 2011 (Fig. 5a) due to the late onset of autumn precipitation  $P$  inhibiting seed germination.  $GPP_u$  was lower during the entire year 2012 in comparison to 2011, particularly over the main growth period of the understorey vegetation from January to April. It was up to 52 % lower in March 2012, inhibiting further growth during winter/spring and probably caused higher seedling mortality. Dubbert et al. (2014) reported a maximum understorey vegetation cover in this ecosystem of about 80 % for 2011 that was reduced to about 25 % during the same period in 2012 (data for 2012 not shown). Similar effects on seedling germination and mortality were shown by others (Peco et al., 1994, Espigares et al., 1995, Espigares et al., 1993) under artificial rainfall treatments and could be shown here under natural conditions.

#### 7.4.4. *Ecosystem productivity reduction*

Most European, Mediterranean savannah-like ecosystems show a severe drop in gross primary productivity during summer (June to August) framed by a major peak in early spring (April to May) and a minor peak at the onset of autumn rain (Baldocchi et al., 2009).

In our ecosystem, gross primary productivity measured at the overstorey tower showed an in this respect atypical annual behaviour with a very late peak during June–July (Fig. 6b). The amount of carbon gained was also higher compared to other Mediterranean evergreen woodlands in particular during the drought period in summer (Baldocchi et al., 2009, Ma et al., 2007). This annual pattern is rather characteristic for temperate than semi-arid ecosystems. The *Q. suber* trees must have deep soil water or ground water access in “regular” hydrological years, as shown in Sect. 2. This enabled them to maintain high productivity during the summer period despite high atmospheric water demand and low topsoil soil moisture.

Gross primary productivity  $GPP$  showed almost the same seasonal timing in 2012 compared to 2011

but was strongly reduced by 28 % (Fig. 6b). The major reduction took place in spring and summer (April to September) together with the reduction in evapotranspiration (Fig. 6b) when atmospheric demand was high and the emptied deep soil and ground water reservoirs were unable to supply sufficient water (see Sect. 2) in 2012 compared to a regular year. This confirms the results of Pereira et al. (2007) who showed that drought effects on sclerophyllous trees became apparent only after the depletion of the deep soil and ground water reserves. Despite a delayed bud burst in spring, a significant difference in leaf area index *LAI* could not be observed during the summer period by long-term leaf area index observations of (Costa e Silva et al., unpubl.). Reductions in *GPP* and *ET* can hence be attributed solely to leaf physiological responses discussed in Sect. 6.

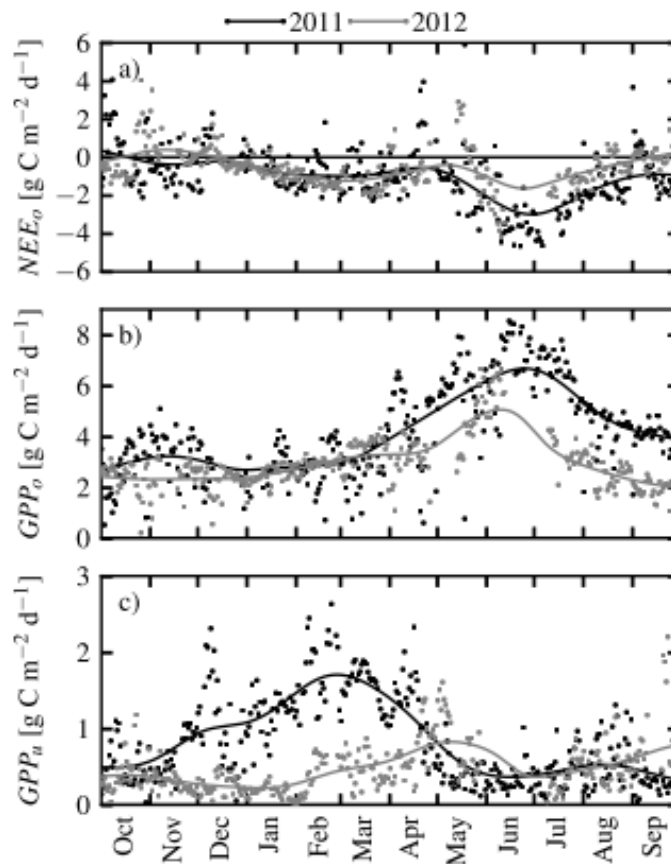


**Figure 6:** a) Ecosystem net carbon exchange  $NEE_o$ , b) ecosystem gross primary production  $GPP_o$ , c) understorey gross primary production  $GPP_u$  for 2011 (black) and 2012 (grey). Dots mark daily sums, lines are kernel regressions.

#### 7.4.5. *Net ecosystem carbon exchange reduction*

The net ecosystem carbon flux  $NEE$  was strongly reduced by 38 % in the drought year 2012 compared to the wet year 2011 (Fig. 6a). The ecosystem was, however, a carbon sink in both years on annual basis even though reductions in precipitation  $P$  (Fig. 6) and gross primary productivity (Fig. 6b) were severe in 2012. Pereira et al. (2007) found a similar behaviour in another montado ecosystems in Portugal. It still demonstrates here once more that precipitation is the dominant environmental variable for inter-annual change of  $NEE$  in semi-arid ecosystems even in ecosystems with ground water access. The reduction in carbon sink strength took place mainly in summer (May to September) along with the strongest reduction in gross primary productivity (Fig. 6b) caused by the lack of water availability for the *Q. suber* trees (cf. Sect. 2).  $GPP_o$  exhibited a reduction of 28 % in 2012 compared to 2011 while  $R_{eco}$  showed only a reduction of 16 %.  $R_{eco}$  is mainly reduced in summer (July to September, data not shown) where soil moisture in the upper soil layer is low in both years due to the regular summer drought (Fig. 5a) and inter-annual differences are small.  $NEE_o$  is therefore much more driven by  $GPP_o$  than by  $R_{eco}$  in the ecosystem studied here. Reichstein et al. (2002) hypothesized that gross primary productivity should be less affected by drought than ecosystem respiration in ecosystems with large subsoil water reservoirs because Reco depends on soil moisture and soil temperature. But it is hot and dry almost every summer in the Mediterranean so that the lack of soil moisture in the upper soil inhibits soil respiration during summer and reduces largely the contribution of  $R_{eco}$  to inter-annual variations (e.g. Unger et al., 2009). This could also be the reason for the controversial findings of Valentini et al. (2000) that  $R_{eco}$  becomes less important for variations of  $NEE$  with decreasing latitude on the Northern Hemisphere. It is, however, clear that vastly different  $GPP_o$  and  $R_{eco}$  cannot be sustained over long time;  $R_{eco}$  base rates have to adapt in the long-term.

#### 7.4.6. Drought impact on tree physiology

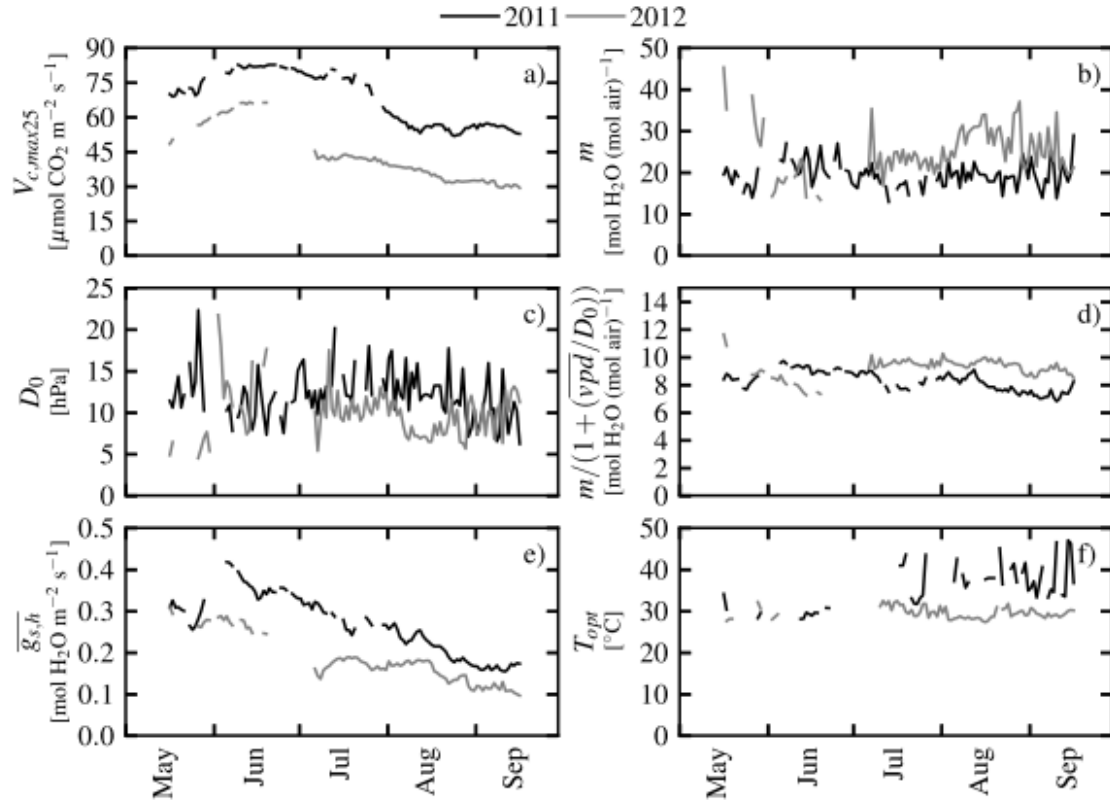


**Figure 7:** a) Apparent maximum carboxylation rate  $V_{c,max}$ , b) stomatal conductance parameter  $m$ , c) vapour pressure deficit sensitivity parameter  $D_0$ , d) fraction  $m/(1 + (vpd/D_0))$  relating assimilation  $A$  and stomatal conductance  $g_s$ , e) daily median stomatal conductance for water vapour  $g_{s,h}$  and f) optimal temperature of carboxylation  $T_{opt}$ . The model is fitted to median daily cycles of gross primary production  $GPP_o$  and evapotranspiration  $ET_o$  of the *Q. suber* trees in a day long moving window for the summer period of 2011 (black) and 2012 (grey).

Multiple physiological mechanisms of plant responses to drought, excessive irradiance and high temperatures have been recognized on the leaf-level such as reduction of exposed leaf area or leaf shedding (Beyschlag et al., 1986, Sala and Tenhunen, 1996, Tenhunen et al., 1985, Tenhunen et al., 1990, Werner et al., 2001). To avoid hydraulic failure or photodamage, carboxylation efficiency  $V_{c,max}$  and/or stomatal conductance  $g_s$  can be down-regulated restricting water loss and carbon assimilation and hence increasing photorespiration as a protective electron sink (Farquhar et al., 1982, Cowan et al., 1977, Tenhunen, et al., 1987, Matthews et al., 1984, Ehleringer et al., 1984). The photosynthesis apparatus can further adapt to altered environmental conditions by changing the



rigidity of the membranes altering thus the temperature optimum of, for example, electron transport rates (Kattge and Knorr, 2007, von Caemmerer et al., 2000, Berry and Björkmann, 1980).

There are different levels of complexity on how to describe photosynthesis in the literature. We focus here on Farquhar-type models of photosynthesis (Farquhar et al., 1980). There are three mechanisms that differ strongly between the different models of vegetation-atmosphere exchange: (1) the reactions to soil water stress, (2) the formulations used for the description of stomatal conductance and (3) the reactions to heat stress. How plants react to water stress is probably the least well-described mechanism in photosynthesis models. The different ecosystem and land surface models differ strongly on how they react to soil water stress. The widely used community land model CLM, for example, reduces apparent carboxylation efficiency  $V_{cmax}$  under drought (Oleson et al., 2010), which then indirectly reduces stomatal conductance as well, while the land surface scheme ORCHIDEE down-regulates stomatal conductance directly leaving  $V_{cmax}$  unchanged (Krinner et al., 2005, Verbeeck et al., 2011).

There is also a great variety of descriptions of stomatal conductance (cf. Damour et al., 2010). Most large-scale models apply the formulation of Ball et al. (1987) though, the so called Ball–Berry or sometimes Ball–Woodrow–Berry model (cf. Eq. B11). Leuning (1995) argued that stomata under controlled conditions react to vapour pressure deficit rather than relative humidity and proposed an alternate form of the Ball–Berry model (cf. Eq. B10), the so-called Leuning model or sometimes Ball–Berry–Leuning formulation. But the photosynthesis models also differ in their reactions to heat stress. It is still discussed in the physiological literature if heat is only changing thylakoid membrane properties limiting electron transport (von Caemmerer et al., 2000, June et al., 2004) or if heat is also inhibiting enzyme activities, i.e. also carboxylation rates (Medlyn et al., 2002, Kattge and Knorr, 2007).

Gross primary productivity  $GPP_o$  and evapotranspiration  $ET_o$  were modelled here for the period May to September to investigate drought impact on *Q. suber* tree physiology on the ecosystem scale and further test different model formulations described above. Differences between both years were most prominent during May to September, understorey vegetation had already vanished and soil evaporation was low compared to tree transpiration (Fig. 4c).

The following discussion includes (1) whether a down-regulation of only carboxylation efficiency  $V_{cmax}$  or only stomatal sensitivity  $m$  is sufficient to describe the ecosystem behaviour in both years. (2) It evaluates the performance of the two prominent stomatal conductance formulations. (3) It compares different representations of photosynthetic temperature dependencies. (4) It discusses possible reasons for down-regulation of stomatal conductance  $g_s$  and carboxylation  $V_{cmax}$ . (5) disentangling the causes for down-regulation of stomatal conductance  $g_s$ . (6) The unexpected change in optimal temperature  $T_{opt}$  between the two years is discussed.

First,  $GPP_o$  and  $ET_o$  were modelled with either allowing the model to adapt each day only  $V_{cmax}$  or only the slope  $m$  of the Ball–Berry stomatal conductance formulation (Ball et al., 1987, Eq. B11). The model was not able to reproduce the observations with sufficient performance in both cases, especially in 2012. The goodness of fit to the observed data steadily decreased with ongoing summer drought.  $GPP_o$  and  $ET_o$  could be successfully modelled if both,  $V_{cmax}$  and  $m$  were allowed to adapt daily to changing environmental conditions, leading to constantly high Nash–Sutcliffe model efficiencies of  $\overline{\varepsilon GPP_o} = 0.88$  and  $\overline{\varepsilon ET_o} = 0.95$  for 2011 and  $\overline{\varepsilon GPP_o} = 0.84$  and  $\overline{\varepsilon ET_o} = 0.90$  for 2012.

Second, the same model calibration experiment was performed with the Leuning model of stomatal conductance (Leuning, 1995, Eq. B10). The Leuning model has, however, an additional model parameter  $D_0$  which describes the sensitivity of the stomata to changes in vapour pressure deficit  $vpd$ . The Leuning model showed comparable high model performances to the Ball–Berry model in both years. When the Leuning model was used in earlier studies (e.g. Wang et al., 1998),  $D_0$  was fixed to a constant value. This implies that stomatal conductance sensitivity to  $vpd$  needs to change always similar to the sensitivity to assimilation. Model performance decreased considerably if  $D_0$  was fixed here. This is because  $m$  and  $D_0$  are highly correlated in the Leuning model (cf. Fig. 7b and c). This strict coupling is likely incorrect here since daily maximum  $vpd$  during the summer drought period was not significantly different between both years (only 1.3 hPa increase on average) but a strong decrease in  $V_{cmax}$  could be observed (see below). Consequently, a decrease in model performance occurred, when  $D_0$  was set constant. Enabling the *Q. suber* trees to regulate stomatal response to  $vpd$  and assimilation  $A$  separately was necessary to explain observed  $GPP_o$  and  $ET_o$ .

The two first points illustrate that the plants needed to regulate their potency of possible carbon assimilation but wanted to increase how swift stomata react to changes. The reduction in maximum carboxylation rate  $V_{cmax}$ , though, was about 37 % while the increase in the slope  $m$  was about 13 % or 30 % whether calculation followed Ball et al. (1987) or Leuning (1995), respectively. This led to an overall decrease in stomatal conductance  $g_s$  of about 31 %.

Third, the temperature dependency of photosynthetic activity has generally been attributed to two different processes in previous publications. Medlyn et al. (2002) and Kattge and Knorr (2007) described the temperature dependency of both, maximum carboxylation rate  $V_{cmax}$  of the Rubisco enzyme and maximum electron transport rate  $J_{max}$  by a peaked function, according to Johnson et al. (1942) (Eq. B6). An increase in enzyme activity with temperature is followed by a decrease above an optimum temperature  $T_{opt}$  due to enzyme deactivation (Case 1). Von Caemmerer (2000), among others, attributed possible decrease of activity of the photosynthetic apparatus at high temperatures rather to thylakoid membrane properties only, limiting electron transport, thus changing with leaf temperature. So only  $J_{max}$  is down-regulated above an optimum temperature  $T_{opt}$  (Eq. B6), but  $V_{cmax}$  increases monotonically with a typical Arrhenius-type function (Eq. B5, Case 2). This was simplified by June et al. (2004) using a gaussian temperature dependency instead of the original formulation (Eq. B8, Case 3). Here all cases showed comparable model performances and no apparent differences in  $GPP_o$  and  $ET_o$  could be noticed. Thus, neither Case 1 nor Case 2 could be falsified here. Case 1 to case 3, however, show a decreasing demand for parametrization (Case 1: 6, Case 2: 4, and Case 3: 3 parameters). Despite the entropy factors of carboxylation and electron transport (Case 1 and Case 2) and optimum temperature  $T_{opt}$  (Case 3), all parameters were fixed to literature values (Table 1). Case 3, although containing only one parameter for optimization like Case 2, showed a more robust computational performance with fastest optimization by the Nelder–Mead algorithm (Nelder and Mead, 1965) among all cases.

Fourth, multiple reasons for down-regulation of photosynthesis under drought conditions are known, ranging from damage of involved enzymes due to high leaf temperatures, inhibition of the photosynthetic apparatus to avoid excess energy in the leaves, to insufficient availability of nitrogen inside the leaves (Tenhunen et al., 1987, Werner et al., 1999). But protection of the photosynthetic

apparatus during environmental stress comes at the cost of reduced carbon sequestration (Tenhunen et al., 1990, Werner et al., 1999, Werner et al., 1996). Excessive radiation and high temperatures provide the risk of photoinhibition and photodamage under reduced CO<sub>2</sub> supply due to stomatal closure and low water potentials (Werner et al., 2002). Stomatal conductance  $g_s$  was strongly reduced by 31 % in 2012 compared to 2011 (Fig. 7e) although differences in daily maximum  $v_{pd}$  during the summer drought period were not significant (only 1.3 hPa increase on average) between both years (Fig. 4a). It is thus very likely that the trees suffered from depleted deep soil or groundwater reservoirs due to the missing recharge by winter precipitation, since upper soil water content values were comparable during summer (Fig. 5a and b). This is an evidence that plant water status of *Q. suber* trees is strongly influenced by access to groundwater here and a down-regulation of transpiration occurred to avoid hydraulic failure (David et al., 2007, Oliveira et al., 1992). Although transpirational cooling of leaves should have been reduced due to limited stomatal conductance, the daily maximum leaf temperature increased by only 1.7 °C in 2012 compared to 2011 (Sect. 1) so that a temperature-based damage of enzymes relevant for photosynthesis is unlikely. The CO<sub>2</sub> influx into the leaves was, however, heavily reduced under the drought conditions in 2012. Energy utilization is thus limited while incoming photosynthetically active radiation  $PAR$  in 2012 was comparably high to 2011 (see Sect. 1). It is therefore very likely that the main cause for the *Q. suber* trees to down-regulate maximum carboxylation rate  $V_{cmax}$  by 37 % (Fig. 7a) was to avoid over-excitation and photodamage (Demmig-Adams et al., 1992, Long et al., 1994, Werner et al., 2002). However, this effect may have been enforced by a decreased nitrogen availability during the leaf development phase in late spring caused by reduced soil water, and thus nitrogen solubility in 2012 (Fig. 5a and b) potentially changing leaf nitrogen status and permanently reducing photosynthetic capacity in 2012 compared to 2011 (Vaz et al., 2010). A possible indication for a permanent reduction of  $V_{cmax}$  is that  $g_s$  tends to converge to the same value at the end of the drought period in both years (Fig. 7e) so that leaf internal CO<sub>2</sub> availability should have approached comparable values as well.  $V_{cmax}$  remained, however, down-regulated permanently. A simultaneous reduction of  $V_{cmax}$  by 37 % (Fig. 7a) and an increase of  $m$  (13 % or 30 % whether  $g_s$  was calculated following Ball (1987) or Leuning (1995, Fig. 7b) was observed. In case of a drought spell like 2012, the *Q. suber* trees responded with both, stomatal limitation as well as down-

regulation of assimilation strongly altering entire ecosystem functioning, which was observed in different semi-arid ecosystems before (Reichstein et al., 2003, Egea et al., 2011, Zhou et al., 2013).

Fifth, the use of the Leuning (1995) model with variable  $D_0$  allowed to disentangle the different impacts on  $g_s$ . Intra-annually, stomatal conductance showed a much stronger sensitivity to  $vpd$  (Fig. 7c) than to variations in assimilation (Fig. 7d). Between both years,  $m/(1 + (\overline{vpd}/D_0))$  increased only slightly by 6 % as a consequence of a slightly stronger reduction in  $V_{cmax}$  than in  $g_s$  (37 % and 31 %, respectively). This displays the strong resilience of sclerophyllous tree species like *Q. suber* to drought, maintaining a water use efficiency comparable to regular years (Zhou et al., 2013). The impact of  $vpd$  on  $g_s$  was, however, weakened in 2012 (reduction of  $D_0$  by 14 %) since  $g_s$  was generally reduced at comparable  $vpd$ .  $m$  compensated fluctuations in  $D_0$  (Fig. 7b) to yield the observed robustness to assimilation. The observed high intra-annual robustness indicates that these Mediterranean species are adapted to maintain a stable operational point (Werner and Maguas, 2010).

Sixth, all three model descriptions (Case 1–3) showed a decrease in the optimum temperature of photosynthesis  $T_{opt}$  by 4–8 °C from 2011 to 2012 (Fig. 7f). Leaf renewal in 2012 occurred under strong drought conditions due to the additional winter drought and under increased temperatures due to the bud burst occurring more than one month later than in 2011 (Costa e Silva et al., unpubl.). So carbon uptake in 2012 was further weakened due to a higher susceptibility of the photosynthesis apparatus to high temperatures in addition to the already discussed reduction of carboxylation efficiency  $V_{cmax}$  by 37 %. Kattge et al. (2007) and Caemmerer et al. (2000), among others, showed for different plant species the opposite trend of increasing  $T_{opt}$  with increasing growth temperature. A possible explanation is that not only growth temperature but also nutrient availability and plant water status have changed strongly here affecting thylakoid membrane properties more than growth temperature.

In summary, the *Q. suber* trees responded to the drought year 2012 with a down-regulation of carboxylation efficiency and a decreased optimal temperature of photosynthesis. They counteracted this reduced carbon sequestration with a better responsiveness of the stomata. These plant responses were caused neither by a higher vapour pressure deficit nor by leaf temperatures nor by a depletion of upper soil moisture. But they were most probably triggered by a strong depletion of deep soil or

ground water due to the additional winter drought.

The combined model of photosynthesis and stomatal conductance was unable to reproduce the observed carbon assimilation and evapotranspiration if only one reaction was considered, i.e. either in the photosynthetic apparatus or in stomatal conductance. It needed to adapt parameters in both sub-modules, i.e. a strong reduction in carboxylation efficiency and a smaller increase in stomatal sensitivity. Earlier model-data approaches had shown that combined photosynthesis-stomatal conductance models need to adapt both parts in times of drought but they always predicted decreases in carboxylation efficiency and stomatal sensitivity. However, the modelling performed here could not distinguish between different model formulations found in the literature, i.e. the stomatal conductance formulations of Ball–Berry vs. Leuning and the different formulations of optimal photosynthetic temperatures.

#### *7.4.7. Future development*

It is expected that the trend of decreasing total annual precipitation and alteration of precipitation patterns on the Iberian Peninsula, namely occurrences of additional winter/spring droughts, will continue with proceeding climate change (Bussotti et al., 2013, Guerreiro et al., 2013, Hulme et al., 1999). Such severe drought periods might occur at higher frequency (Field et al., 2012, Heimann et al., 2008, Granier et al., 2007, Miranda et al., 2002) thereby affecting the ecosystem water balance and productivity (Chaves et al., 2002, Fischer et al., 2002). If precipitation patterns similar to 2012 will occur more often then a sustainable depletion of local ground water reservoirs as well as water storage basins might be expected. This will affect strongly local agriculture that relies on ground water for the deep-rooted cork-oak trees and otherwise uses irrigation water from storage basins. The soil seed bank of native understorey plants may also deplete on the long term due to a shorter life cycle and reduced seed formation (Jongen et al., 2013a, Penuelas et al., 2002, Penuelas et al., 2004, Gordo et al., 2005). A shift of species composition is likely (DiosMiranda et al., 2009) but could not be observed in this ecosystem in a study by Dubbert et al. (2014; 2012 data not shown) during the drought year 2012 itself. However, some effects such as tree mortality may only be evident in the long term after

multiple, consecutive drought years (David et al., 2004, Bussotti et al., 2013).

## 7.5. Conclusions

We reported on the ecosystem fluxes of a savannah-type cork oak woodland under extreme hydrological conditions and altered precipitation  $P$  pattern. We analyzed the effects of drought in the year 2012 compared to the wet year 2011 on evapotranspiration and gross primary productivity of a *montado* ecosystem and its overstorey and understorey components. We additionally analyzed physiological reactions of the *Q. suber* trees.

We conclude the following results: (1) the precipitation effectiveness increased up to 122 % in the dry year 2012 possible due to the ground water access of *Q. suber* trees leaving no water for ground water replenishing and runoff generation. If trends of decreasing annual  $P$  continue, sustainable effects on local ground water reservoirs and storage basins may be expected. (2) The understorey gross primary productivity and the overstorey gross primary productivity were reduced by 53 % and 28 %, respectively, in 2012 compared to 2011 due to a late onset of 2011 autumn rains and an additional severe winter/spring drought. Long term changes in understorey species composition and tree productivity are likely if prolonged summer droughts and additional winter/spring droughts become more frequent. (3) A combined photosynthesis and stomatal conductance model worked best if it was able to adapt the apparent maximum carboxylation rate and the stomatal conductance parameters simultaneously. The slope  $m$  of the stomatal conductance model had to be increased to compensate partly for the strong decrease in carboxylation rate. The model adjusted also the sensitivity of the stomata to vapour pressure deficit  $vpd$  in the Leuning model because both stomatal parameters,  $m$  and  $D_0$  are strongly correlated. The model performance was similar to the Ball–Berry approach. (4) The combined photosynthesis and stomatal conductance model also adjusted the optimum temperature of electron transport to lower values. This decreases carbon sequestration under higher temperatures but makes the photosynthetic apparatus also more vulnerable to heat stress in dry years. (5) The ecosystem was a carbon sink in both years with a 38 % reduced sink strength in the dry year 2012 compared to 2011. Gross primary productivity  $GPP$  was thereby a much stronger driver than ecosystem respiration of the inter-annual variations of the carbon sink.

## 7.6. Appendix A – Nomenclature

$b$	[mol H <sub>2</sub> O m <sup>-2</sup> s <sup>-1</sup> ] Leuning model parameter (offset)
$D_0$	[hPa] Leuning model parameter ( <i>vpd</i> fraction denominator)
$ET_o$	[mm d <sup>-1</sup> ] evapotranspiration measured at the overstorey tower
$ET_u$	[mm d <sup>-1</sup> ] evapotranspiration measured at the understorey tower
$ET_o/P$	[%] precipitation effectiveness ratio
$\overline{\varepsilon GPP_o}$	[-] average Nash-Suttcliff model efficiency for $GPP_o$
$\overline{\varepsilon ET_o}$	[-] average Nash-Suttcliff model efficiency for $ET_o$
$GPP$	[g C m <sup>-2</sup> d <sup>-1</sup> ] gross primary production
$GPP_o$	[g C m <sup>-2</sup> d <sup>-1</sup> ] gross primary production measured at the overstorey tower
$GPP_u$	[g C m <sup>-2</sup> d <sup>-1</sup> ] gross primary production measured at the understorey tower
$g_{sh}$	[mol H <sub>2</sub> O m <sup>-2</sup> s <sup>-1</sup> ] stomatal conductance for water vapour
$g_{sc}$	[mol CO <sub>2</sub> m <sup>-2</sup> s <sup>-1</sup> ] stomatal conductance for carbon
$LAI$	[m <sup>2</sup> leaf m <sup>-2</sup> ground] leaf area index
$m$	[mol H <sub>2</sub> O mol air <sup>-1</sup> ] Leuning model parameter (slope)
$NEE$	[g C m <sup>-2</sup> d <sup>-1</sup> ] net ecosystem carbon exchange
$NEE_o$	[g C m <sup>-2</sup> d <sup>-1</sup> ] net ecosystem carbon exchange measured at the overstorey tower
$NEE_u$	[g C m <sup>-2</sup> d <sup>-1</sup> ] understorey + soil net carbon exchange
$P$	[mm] precipitation
$p$	[hPa] atmospheric pressure
$PAR$	[μmol m <sup>-2</sup> s <sup>-1</sup> ] photosynthetically active radiation
$P_{gap}$	[-] tree canopy gap probability
$R_{eco}$	[g C m <sup>-2</sup> d <sup>-1</sup> ] ecosystem respiration
$rH$	[%] relative air humidity
$\theta$	[%] soil moisture
$T$	[°C] air temperature
$T_s$	[°C] soil temperature



$V_{cmax}$	$[\mu\text{mol m}^{-2} \text{s}^{-1}]$ apparent maximum carboxylation rate
$vpd$	$[\text{hPa}]$ air vapour pressure deficit

## 7.7. Appendix B Photosynthesis model

Appendix B Photosynthesis - stomatal conductance model

Carbon assimilation  $A$   $[\text{mol m}^{-2} \text{s}^{-1}]$  was modelled using the model of Farquhar et al. (1980) modified by a smooth minimum function:

$$A = \min\{J_C; J_E; \eta\} - R_d \quad (\text{B1})$$

with Rubisco-limited  $\text{CO}_2$  assimilation rate  $J_C$   $[\text{mol m}^{-2} \text{s}^{-1}]$ , Ribulose-1,5-bisphosphate (RuBP)-limited  $\text{CO}_2$  assimilation rate  $J_E$   $[\text{mol m}^{-2} \text{s}^{-1}]$  and mitochondrial respiration  $R_d$   $[\text{mol m}^{-2} \text{s}^{-1}]$ . The smoothing parameter  $\eta$  was set to 0.9. The Rubisco-limited rate  $J_C$  was described by:

$$J_C = V_{c,max} \frac{C_i - \Gamma_*}{C_i + K_C \left(1 + \left(\frac{O_i}{K_O}\right)\right)} \quad (\text{B2})$$

with maximum carboxylation rate  $V_{c,max}$   $[\text{mol m}^{-2} \text{s}^{-1}]$ , stomatal cavity  $\text{CO}_2$  concentration  $C_i$   $[\text{mol CO}_2 \text{mol}^{-1} \text{air}]$ ,  $\text{CO}_2$  compensation point  $\Gamma_*$   $[\text{mol CO}_2 \text{mol}^{-1} \text{air}]$  (set to leaf temperature  $T_l$   $1.7^{-6}$ ), Michaelis-Menten coefficients of Rubisco activity for  $\text{CO}_2$   $K_C$   $[\text{mol CO}_2 \text{mol}^{-1} \text{air}]$  and  $\text{O}_2$   $K_O$   $[\text{mol O}_2 \text{mol}^{-1} \text{air}]$ , respectively.  $O_i$   $[\text{mol O}_2 \text{mol}^{-1} \text{air}]$  is the stomatal cavity  $\text{O}_2$  concentration. The RuBP-limited  $\text{CO}_2$  assimilation rate  $J_E$  was described by:

$$J_E = J \frac{C_i - \Gamma_*}{4(C_i + 2\Gamma_*)} \quad (\text{B3})$$

with the rate of electron transport  $J$   $[\text{mol m}^{-2} \text{s}^{-1}]$  as:

$$J = J_{max} \frac{\alpha PAR}{\sqrt{J_{max}^2 + \alpha^2 PAR^2}} \quad (B4)$$

with maximum electron transport rate  $J_{max}$  [mol m<sup>-2</sup> s<sup>-1</sup>], quantum yield of electron transport  $\alpha$  and incident photosynthetically active photon flux density  $PAR$  [mol m<sup>-2</sup> s<sup>-1</sup>]. The temperature dependencies of  $K_c$ ,  $K_o$  and  $R_d$  were modelled using Arrhenius function like:

$$f(T_l) = K_{25} \exp\left(\frac{E_{K_{25}}(T_l - 25)}{298R(T_l + 273)}\right) \quad (B5)$$

with the base rates  $K_{C25}$  [mol CO<sub>2</sub> mol<sup>-1</sup> air],  $K_{O25}$  [mol O<sub>2</sub> mol<sup>-1</sup> air],  $R_{d25}$  [mol m<sup>-2</sup> s<sup>-1</sup>] and activation energies  $E_{C25}$ ,  $E_{O25}$ ,  $E_{Rd25}$  [J mol<sup>-1</sup>] at 25 °C, respectively.  $T_l$  [°C] is leaf temperature and  $R$  [J mol<sup>-1</sup> K<sup>-1</sup>] is universal gas constant. According to Medlyn et al. (2002) and Kattge and Knorr (2007), the temperature dependencies of maximum carboxylation rate  $V_{cmax}$  and maximum electron transport rate  $J_{max}$  were modelled with a modification of the Arrhenius function showing a peak at optimum temperature followed by a decline with increasing leaf temperatures  $T_l$ :

$$f(T_l) = K_{max25} \exp\left(\frac{E_{K_{max25}}(T_l - 25)}{298R(T_l + 273)}\right) \frac{1 + \exp\left(\frac{298\Delta S_K - Hd_K}{298R}\right)}{1 + \exp\left(\frac{(T_l + 273)\Delta S_K - Hd_K}{(T_l + 273)R}\right)} \quad (B6)$$

with the base rates  $V_{cmax25}$ ,  $J_{max25}$  [mol m<sup>-2</sup> s<sup>-1</sup>] and activation energies  $E_{Vcmax25}$ ,  $E_{Jmax25}$  [J mol<sup>-1</sup>] at 25 °C, respectively.  $\Delta S_V$ ,  $\Delta S_J$  [J mol<sup>-1</sup> K<sup>-1</sup>] are the entropy factors and  $Hd_V$ ,  $Hd_J$  [J mol<sup>-1</sup>] are the deactivation energies of  $V_{cmax}$  and  $J_{max}$ , respectively. Leaf surface CO<sub>2</sub> concentration  $C_s$  [mol CO<sub>2</sub> mol<sup>-1</sup> air] and H<sub>2</sub>O concentration  $W_s$  [mol H<sub>2</sub>O mol<sup>-1</sup> air] were calculated via:

$$C_s = C_a - \frac{A}{g_a} \quad (\text{B7})$$

$$W_s = W_i - \frac{ET_{mod}}{g_{s,h}} \quad (\text{B8})$$

with the atmospheric CO<sub>2</sub> concentration  $C_a$  [mol CO<sub>2</sub> mol<sup>-1</sup> air], aerodynamic conductivity  $g_a$  [mol m<sup>-2</sup> s<sup>-1</sup>], stomatal cavity H<sub>2</sub>O concentration  $W_i$  [mol H<sub>2</sub>O mol<sup>-1</sup> air], modelled transpiration  $ET_{mod}$  [mol m<sup>-2</sup> s<sup>-1</sup>] and stomatal conductivity for water vapour  $g_{s,h}$  [mol m<sup>-2</sup> s<sup>-1</sup>].

Stomatal conductance for water vapour  $g_{s,h}$  was calculated with the equation of Leuning (1995):

$$g_{s,h} = m \frac{A}{(C_s - \Gamma_*) \left(1 + \frac{W_i - W_s}{D_0}\right)} + b \quad (\text{B9})$$

with stomatal conductivity slope parameter  $m$  [mol H<sub>2</sub>O mol<sup>-1</sup> air], vapour pressure deficit sensitivity parameter  $D_0$  [hPa] and stomatal conductivity offset parameter  $b$  [mol m<sup>-2</sup> s<sup>-1</sup>]. Canopy conductance for CO<sub>2</sub> and H<sub>2</sub>O were then derived by:

$$g_{c,c} = \frac{1}{\left(\frac{1.56}{g_{s,h}} + \frac{1}{g_a}\right)} \quad (\text{B10})$$

$$g_{c,h} = \frac{1}{\left(\frac{1}{g_{s,h}} + \frac{1}{g_a}\right)} \quad (\text{B11})$$

Hence, stomatal cavity CO<sub>2</sub> concentration was calculated via:

$$C_i = C_a - \frac{A}{g_{c,c}} \quad (\text{B12})$$

and finally, modelled transpiration  $ET_{mod}$  [mol m<sup>-2</sup> s<sup>-1</sup>] and gross primary production  $GPP_{mod}$  [mol m<sup>-2</sup> s<sup>-1</sup>] could be derived by:

$$ET_{mod} = g_{c,h}(W_i - W_a) \quad (B13)$$

$$GPP_{mod} = g_{c,c}(C_a - C_i) \quad (B14)$$

The entire calculation was iterated with initial values for  $ET_{mod} = 0$ ,  $g_{s,h} = 1$  and  $C_i = 0.8C_a$ , until a conversion of  $C_i$  was achieved for every time step. The model was fitted against measured  $ET$  and  $GPP$  under variation of  $V_{cmax25}$ ,  $\Delta S_V$ ,  $\Delta S_J$ ,  $m$  and  $D_0$ . Constant relationships of  $J_{max25} = 1.67V_{cmax25}$  and  $R_{d25} = 0.011V_{cmax25}$  were assumed (Medlyn et al., 2002; Kattge and Knorr, 2007). All other parameters used can be found in Table 1.

**Table 1:** Parameters used in the photosynthesis - stomatal conductance model. Parameters with the source 'site average' were estimated with an optimization on the entire data set.

parameter	value	unit	source
$K_{C_{25}}$	$460^{-6}$	$[\text{mol}_{\text{CO}_2} \text{mol}_{\text{air}}^{-1}]$	(Farquhar et al., 1980)
$K_{O_{25}}$	0.33	$[\text{mol}_{\text{O}_2} \text{mol}_{\text{air}}^{-1}]$	(Farquhar et al., 1980)
$O_i$	0.21	$[\text{mol}_{\text{O}_2} \text{mol}_{\text{air}}^{-1}]$	(Farquhar et al., 1980)
$\alpha$	0.28	[-]	(Beerling and Quick, 1995)
$E_{C_{25}}$	59356	$[\text{J mol}^{-1}]$	(Farquhar et al., 1980)
$E_{O_{25}}$	35948	$[\text{J mol}^{-1}]$	(Farquhar et al., 1980)
$E_{R_{d25}}$	50967	$[\text{J mol}^{-1}]$	(Collatz et al., 1992)
$Hd_V$	204286	$[\text{J mol}^{-1}]$	site average
$Hd_J$	213596	$[\text{J mol}^{-1}]$	site average
$E_{V_{c,max25}}$	61045	$[\text{J mol}^{-1}]$	site average
$E_{J_{max25}}$	37030	$[\text{J mol}^{-1}]$	site average
$b$	$3937^{-6}$	$[\text{mol m}^{-2} \text{s}^{-1}]$	site average

## 7.8. Acknowledgements.

We thank the Herdade da Machoqueira do Grou the permission to establish our field site. We thank Tino Rau for providing data processing code and Sebastian Gimper for technical support. We thank Juliane Mai for help with mathematics. This study was funded by the Deutsche Forschungsgemeinschaft (WATERFLUX Project: # WE 2681/6-1; # CU 173/2-1) and kindly

supported by Helmholtz Impulse and Networking Fund through Helmholtz Interdisciplinary Graduate School for Environmental Research (HIGRADE) (Bissinger and Kolditz, 2008).

## 7.9. References

- Aubinet, M., Grelle, A., Ibrom, A., Rannik, U., Moncrieff, J., Foken, T., Kowalski, A., Martin, P., Berbigier, P., Bernhofer, C., Clement, R., Elbers, J., Granier, A., Grünwald, T., Morgenstern, K., Pilegaard, K., Rebmann, C., Snijders, W., Valentini, R., and Vesala, T.: Estimates of the Annual Net Carbon and Water Exchange of Forests: The EUROFLUX Methodology, vol. 30 of *Advances in Ecological Research*, pp. 113 – 175, Academic Press, 1999.
- Baldocchi, D. D., Ma, S., Rambal, S., Misson, L., Ourcival, J.-M., Limousin, J.-M., Pereira, J., and Papale, D.: On the differential advantages of evergreenness and deciduousness in mediterranean oak woodlands: a flux perspective, *Ecological Applications*, 20, 1583–1597, 2009.
- Ball, J.T.: An analysis of stomatal conductance, PhD, Stanford, 88pp., 1988.
- Beer, C., Reichstein, M., Tomelleri, E., Ciais, P., Jung, M., Carvalhais, N., Rodenbeck, C., Arain, M. A., Baldocchi, D., Bonan, G. B., Bondeau, A., Cescatti, A., Lasslop, G., Lindroth, A., Lomas, M., Luyssaert, S., Margolis, H., Oleson, K. W., Rouspard, O., Veenendaal, E., Viovy, N., Williams, C., Woodward, F. I., and Papale, D.: Terrestrial Gross Carbon Dioxide Uptake: Global Distribution and Covariation with Climate, *Science*, 329, 834–838, 2010.
- Beerling, D. and Quick, W.: A new technique for estimating rates of carboxylation and electron transport in leaves of C3 plants for use in dynamic global vegetation models, *Global Change Biology*, 1, 289–294, 1995.
- Berry, J. and Bjorkman, O.: Photosynthetic Response and Adaptation to Temperature in Higher Plants, *Annual Review of Plant Physiology*, 31, 491–543, 1980.
- Besson, C. K., do Vale, R. L., Rodrigues, M. L., Almeida, P., Herd, A., Grant, O. M., David, T. S., Schmidt, M., Otieno, D., Keenan, T. F., Gouveia, C., M´eriaux, C., Chaves, M. M., and Pereira, J. S.: Cork oak physiological responses to manipulated water availability in a Mediterranean woodland, *Agricultural and Forest Meteorology*, 184, 230–242, 2014.
- Beyschlag, W., Lange, O.L., Tenhunen, J.D.: Photosynthesis and water relations of the Mediterranean sclerophyll *Arbutus unedo* L. Throughout the year at a site in Portugal. 1. Diurnal courses of CO<sub>2</sub> gas exchange and transpiration under natural conditions, *FLORA*, 178, 409–444, 1986.
- Bissinger, V. and Kolditz, O.: Helmholtz Interdisciplinary Graduate School for Environmental Research (HI-GRADE), *GAIA*, 1, 71–73, 2008.
- Bugalho, M.N., Caldeira, M.C., Pereira, J.S., Aronson, J. and Pausas, J.G.: Mediterranean cork-oak savannas require human use to sustain biodiversity and ecosystem services. *Frontiers in Ecology and the Environment*, 9(5): 278–286, 2011.
- Bussotti, F., Ferrini, F., Pollastrini, M., and Fini, A.: The challenge of Mediterranean sclerophyllous vegetation under climate change: From acclimation to adaptation, *Environmental and Experimental Botany*, 2013.
- Chaves, M. M., Pereira, J. S., Maroco, J., Rodrigues, M. L., Ricardo, C. P. P., Os´orio, M. L., Catvalho, I., Faria, T., and Pinheiro, C.: How Plants Cope with Water Stress in the Field? Photosynthesis and Growth, *Annals of Botany*, 89, 907–916, 2002.
- Ciais, P., Reichstein, M., Viovy, N., Granier, A., Ogee, J., Allard, V., Aubinet, M., Buchmann, N., Bernhofer, C., Carrara, A., Chevallier, F., De Noblet, N., Friend, A. D., Friedlingstein, P., Grünwald, T., Heinesch, B., Keronen, P., Knohl, A., Krinner, G., Loustau, D., Manca, G., Matteucci, G., Miglietta, F., Ourcival, J. M., Papale, D., Pilegaard, K., Rambal, S., Seufert, G.,

- Soussana, J. F., Sanz, M. J., Schulze, E. D., Vesala, T., and Valentini, R.: Europe-wide reduction in primary productivity caused by the heat and drought in 2003, *Nature*, 437, 529–533, 2005.
- Collatz, G. J., Ribas-Carbo, M., and Berry, J. A.: Coupled Photosynthesis-Stomatal Conductance Model for Leaves of C4 Plants, *Functional Plant Biol.*, 19, 519–538, 1992.
- Costa, A. C., Santos, J. A., and Pinto, J. G.: Climate change scenarios for precipitation extremes in Portugal, *Theoretical and Applied Climatology*, 108, 217–234, 2012.
- Costa e Silva, F., Correia, A. C., Correia, A. V., Piayda, A., Dubbert, M., Werner, C., David, J. S., and Pereira, J. S.: *Quercus suber* phenological adjustments to seasonal water availability: influence on net ecosystem exchange, unpubl.
- Cowan, I.: *Stomatal Behaviour and Environment*, Academic Press, 1977.
- Damour, G., Simonneau, T., Cochard, H., and Urban, L.: An overview of models of stomatal conductance at the leaf level, *Plant, Cell & Environment*, 33, 1419–1438, 2010.
- David, T. S., Henriques, M. O., Kurz-Besson, C., Nunes, J., Valente, F., Vaz, M., Pereira, J. S., Siegwolf, R., Chaves, M. M., Gazarini, L. C., and David, J. S.: Water-use strategies in two co-occurring Mediterranean evergreen oaks: surviving the summer drought, *Tree Physiology*, 27, 793–803, 2007.
- de Dios Miranda, J., Padilla, F. M., and Pugnaire, F. I.: Response of a Mediterranean semiarid community to changing pattern of water supply, *Perspectives in Plant Ecology, Evolution and Systematics*, 11, 255 – 266, 2009.
- Demmig-Adams, B. and Adams, W. W.: Photoprotection and other responses of plants to high light stress, *Annual review of plant biology*, 43, 599–626, 1992.
- Dubbert, M., Cuntz, M., Piayda, A., Maguas, C., and Werner, C.: Partitioning evapotranspiration – Testing the Craig and Gordon model with field measurements of oxygen isotope ratios of evaporative fluxes. *Journal of Hydrology*, 2013.
- Dubbert, M., Mosen, A., Piayda, A., Cuntz, M., Correia, A., Pereira, J. S., and Werner, C.: Influence of tree cover on herbaceous layer development and carbon and water fluxes in a Portuguese cork oak woodland, *Acta Oecologica*.
- Duckstein, L.: Multiobjective Optimization in Structural Design: The Model Choice Problem, in: *New Directions in Optimum Structural Design*, edited by Atrek, E., John Wiley, 1981.
- Egea, G., Verhoef, A., and Vidale, P. L.: Towards an improved and more flexible representation of water stress in coupled photosynthesis–stomatal conductance models, *Agricultural and Forest Meteorology*, 151, 1370 –1384, 2011.
- Ehleringer, J. R. and Cook, C. S.: Photosynthesis in *Encelia farinosa* Gray in Response to Decreasing Leaf Water Potential, *Plant Physiology*, 75, 688–693, 1984.
- Espigares, T. and Peco, B.: Mediterranean Pasture Dynamics: The Role of Germination, *Journal of Vegetation Science*, 4, pp. 189–194, 1993.
- Espigares, T. and Peco, B.: Mediterranean Annual Pasture Dynamics: Impact of Autumn Drought, *Journal of Ecology*, 83, pp. 135–142, 1995.
- Eugster, W. and Senn, W.: A cospectral correction model for measurement of turbulent NO<sub>2</sub> flux, *Boundary-Layer Meteorology*, 74, 321–340, 1995.
- Farquhar, G., Caemmerer, S., and Berry, J.: A biochemical model of photosynthetic CO<sub>2</sub> assimilation in leaves of C3 species, *Planta*, 149, 78–90, 1980.
- Farquhar, G. D. and Sharkey, T. D.: Stomatal Conductance and Photosynthesis, *Annual Review of Plant Physiology*, 33, 317–345, 1982.
- Field, C., Barros, V., Stocker, T., Qin, D., Dokken, D., Ebi, K., Mastrandrea, M., Mach, K., Plattner, G.-K., Allen, S., Tignor, M., and Midgley, P., eds.: *Managing the Risks of Extreme Events and Disasters to Advance Climate Change Adaptation*, IPCC Special Reports, Cambridge University

- Press, Cambridge, 2012.
- Figuerola, M. E. and Davy, A. J.: Response of Mediterranean Grassland Species to Changing Rainfall, *Journal of Ecology*, 79, pp. 925–941, 1991.
- Fischer, G., van Velthuisen, H., Shah, M., and Nachtergaele, F., eds.: *Global Agro-ecological Assessment for Agriculture in the 21st Century: Methodology and Results*, International Institute for Applied Systems Analysis, 2002.
- Foken, T.: The Energy Balance Closure Problem: An Overview, *Ecological Applications*, 18, 1351–1367, 2008.
- Foken, T. and Wichura, B.: Tools for quality assessment of surface-based flux measurements, *Agricultural and Forest Meteorology*, 78, 83 – 105, 1996. 515
- Garcia-Barron, L., Morales, J., and Sousa, A.: Characterisation of the intra-annual rainfall and its evolution (1837–2010) in the southwest of the Iberian Peninsula, *Theoretical and Applied Climatology*, pp. 1–13, 2013.
- Gordo, O. and Sanz, J. J.: Phenology and climate change: a long-term study in a Mediterranean locality, *Oecologia*, 146, 484–495, 2005.
- Grace, J., Jose, J. S., Meir, P., Miranda, H. S., and Montes, R. A.: Productivity and carbon fluxes of tropical savannas, *Journal of Biogeography*, 33, 387–400, 2006.
- Granier, A., Reichstein, M., Bréda, N., Janssens, I., Falge, E., Ciais, P., Grünwald, T., Aubinet, M., Berbigier, P., Bernhofer, C., Buchmann, N., Facini, O., Grassi, G., Heinesch, B., Ilvesniemi, H., Keronen, P., Knohl, A., Kostner, B., Lagergren, F., Lindroth, A., Longdoz, B., Loustau, D., Mateus, J., Montagnani, L., Nys, C., Moors, E., Papale, D., Peiffer, M., Pilegaard, K., Pita, G., Pumpanen, J., Rambal, S., Rebmann, C., Rodrigues, A., Seufert, G., Tenhunen, J., Vesala, T., and Wang, Q.: Evidence for soil water control on carbon and water dynamics in European forests during the extremely dry year: 2003, *Agricultural and Forest Meteorology*, 143, 123 – 145, 2007.
- Grant, O. M., Tronina, u., Ramalho, J. C., Kurz Besson, C., Lobo-do Vale, R., Santos Pereira, J., Jones, H. G., and Chaves, M. M.: The impact of drought on leaf physiology of *Quercus suber* L. trees: comparison of an extreme drought event with chronic rainfall reduction, *Journal of Experimental Botany*, 61, 4361–4371, 2010.
- Guerreiro, S. B., Kilsby, C. G., and Serinaldi, F.: Analysis of time variation of rainfall in transnational basins in Iberia: abrupt changes or trends?, *International Journal of Climatology*, 2013.
- Heimann, M. and Reichstein, M.: Terrestrial ecosystem carbon dynamics and climate feedbacks, *Nature*, 451, 289–292, 2008.
- Hollinger, D. Y., Kelliher, F. M., Byers, J. N., Hunt, J. E., McSeveny, T. M., and Weir, P. L.: Carbon Dioxide Exchange between an Undisturbed Old-Growth Temperate Forest and the Atmosphere, *Ecology*, 75, pp. 134–150, 1994.
- Hulme, M., Mitchell, J., Ingram, W., Lowe, J., Johns, T., New, M., and Viner, D.: Climate change scenarios for global impacts studies, *Global Environmental Change*, 9, Supplement 1, S3 – S19, 1999.
- Huxman, T. E., Wilcox, B. P., Breshears, D. D., Scott, R. L., Snyder, K. A., Small, E. E., Hultine, K., Pockman, W. T., and Jackson, R. B.: Ecohydrological implications of woody plant encroachment, *Ecology*, 86, 308–319, 2005.
- Ibrom, A., Dellwik, E., Larsen, S. E., and Pilegaard, K.: On the use of the Webb-Pearman-Leuning theory for closed-path eddy correlation measurements, *Tellus B*, 59, 937–946, 2007.
- Johnson, F. H., Eyring, H., and Williams, R. W.: The nature of enzyme inhibitions in bacterial luminescence: Sulfanilamide, urethane, temperature and pressure, *Journal of Cellular and Comparative Physiology*, 20, 247–268, 1942.
- Jongen, M., Pereira, J. S., Aires, L. M. I., and Pio, C. A.: The effects of drought and timing of

- precipitation on the inter-annual variation in ecosystem-atmosphere exchange in a Mediterranean grassland, *Agricultural and Forest Meteorology*, 151, 595 – 606, 2011.
- Jongen, M., Lecomte, X., Unger, S., Pint’o-Marijuan, M., and Pereira, J. S.: The impact of changes in the timing of precipitation on the herbaceous understorey of Mediterranean evergreen oak woodlands, *Agricultural and Forest Meteorology*, 171-172, 163–173, 2013a.
- Jongen, M., Unger, S., Fangueiro, D., Cerasoli, S., ao Silva, J., and Pereira, J. S.: Resilience of montado understorey to experimental precipitation variability fails under severe natural drought, *Agriculture, Ecosystems & Environment*, 178, 18 – 30, 2013b.
- June, T., Evans, J. R., and Farquhar, G. D.: A simple new equation for the reversible temperature dependence of photosynthetic electron transport: a study on soybean leaf, *Functional Plant Biol.*, 31, 275–283, 2004.
- Kattge, J. and Knorr, W.: Temperature acclimation in a biochemical model of photosynthesis: a reanalysis of data from 36 species, *Plant, Cell and Environment*, 30, 1176-1190, 2007.
- Knorr, W.: Annual and interannual CO<sub>2</sub> exchanges of the terrestrial biosphere: process-based simulations and uncertainties, *Global Ecology and Biogeography*, 9, 225–252, 2000.
- Kolle, O. and Rebmann, C.: EddySoft Documentation of a Software Package to Acquire and Process Eddy-covariance Data, Technical Reports 10, Max-Planck-Institut für Biogeochemie, Jena, 2007.
- Krinner, G., Viovy, N., de Noblet-Ducoudré, N., Ogée, J., Polcher, J., Friedlingstein, P., Ciais, P., Sitch, S., and Prentice, I. C.: A dynamic global vegetation model for studies of the coupled atmosphere-biosphere system, *Global Biogeochemical Cycles*, 19, n/a–n/a, 2005
- Krishnan, P., Meyers, T. P., Scott, R. L., Kennedy, L., and Heuer, M.: Energy exchange and evapotranspiration over two temperate semi-arid grasslands in North America, *Agricultural and Forest Meteorology*, 153, 31–44, 2012.
- Kurz-Besson C., Otieno D., Lobo-do-Vale R., Siegwolf R., Schmidt M., David T., Soares David J., Tenhunen J., Pereira J. S., and Chaves M.: Hydraulic lift in cork-oak trees in a savannah-type Mediterranean ecosystem and its contribution to the local water balance, *Plant and Soil*, 282: 361-378, 2006.
- Lasslop, G., Reichstein, M., Papale, D., Richardson, A. D., Arneth, A., Barr, A., Stoy, P., and Wohlfahrt, G.: Separation of net ecosystem exchange into assimilation and respiration using a light response curve approach: critical issues and global evaluation, *Global Change Biology*, 16, 187–208, 2010.
- Leuning, R.: A critical appraisal of a combined stomatal-photosynthesis model for C<sub>3</sub> plants, *Plant, Cell & Environment*, 18, 339–355, 1995.
- Leuning, R.: The correct form of the Webb, Pearman and Leuning equation for eddy fluxes of trace gases in steady and non-steady state, horizontally homogeneous flows, *Boundary-Layer Meteorology*, 123, 263–267, 2007.
- Long, S., Humphries, S., and Falkowski, P. G.: Photoinhibition of photosynthesis in nature, *Annual review of plant biology*, 45, 633–662, 1994.
- Ma, S., Baldocchi, D. D., Xu, L., and Hehn, T.: Inter-annual variability in carbon dioxide exchange of an oak/grass savanna and open grassland in California, *Agricultural and Forest Meteorology*, 147, 157 – 171, 2007.
- Matthews, M. A. and Boyer, J. S.: Acclimation of Photosynthesis to Low Leaf Water Potentials, *Plant Physiology*, 74, 161–166, 1984.
- Mauder, M. and Foken, T.: Documentation and Instruction Manual of the Eddy-Covariance Software Package TK3, Universität Bayreuth Abt. Mikrometeorologie, 2011.
- Mauder, M., Cuntz, M., Drue, C., Graf, A., Rebmann, C., Schmid, H. P., Schmidt, M., and Steinbrecher, R.: A strategy for quality and uncertainty assessment of long-term eddy-



- covariance measurements, *Agricultural and Forest Meteorology*, 169, 122 – 135, 2013.
- Medlyn, B.E., Loustao, D., and Delzon, S.: Temperature response of parameters of a biochemically based model of photosynthesis. I. Seasonal changes in mature maritime pine *Pinus pinaster* Ait.), *Plant, Cell and Environment*, 25, 1155–1165, 2002.
- Miranda, P., Coelho, F., Tome, A.R. and, V. M., Carvalho, A., Pires, C., Pires, H., Pires, V. C., and Ramalho, C.: *Climate Change in Portugal: Scenarios, Impacts and Adaptation Measures (SIAM Project)*, chap. 20<sup>th</sup> century Portuguese Climate and Climate Scenarios, pp. 23–83, Gradiva, 2002.
- Mourato, S., Moreira, M., and Corte-Real, J.: Interannual variability of precipitation distribution pattern in Southern Portugal, *International Journal of Climatology*, 30, 1784–1794, 2010.
- Nelder, J. A. and Mead, R.: A Simplex Method for Function Minimization, *The Computer Journal*, 7, 308–313, 1965.
- Oleson, K. W., Lawrence, D. M., Bonan, G. B., Flanner, M. G., Kluzek, E., Lawrence, P. J., Levis, S., Swenson, S. C., and Thornton, P. E.: Technical Description of version 4.0 of the Community Land Model (CLM), Tech. rep., NATIONAL CENTER FOR ATMOSPHERIC RESEARCH, 2010.
- Oliveira, G., Correia, O.A., Martins Loucao, M.A., and Catarino, F.M.: Water relations of cork-oak (*Quercus suber* L) under natural conditions, *Vegetatio*, 100, 199–208, 1992.
- Paco, T. A., David, T. S., Henriques, M. O., Pereira, J. S., Valente, F., Banza, J., Pereira, F. L., Pinto, C., and David, J. S.: Evapotranspiration from a Mediterranean evergreen oak savannah: The role of trees and pasture, *Journal of Hydrology*, 369, 98 – 106, 2009.
- Papale, D., Reichstein, M., Aubinet, M., Canfora, E., Bernhofer, C., Kutsch, W., Longdoz, B., Rambal, S., Valentini, R., Vesala, T., and Yakir, D.: Towards a standardized processing of Net Ecosystem Exchange measured with eddy-covariance technique: algorithms and uncertainty estimation, *Biogeosciences*, 3, 571–583, 2006.
- Paredes, D., Trigo, R. M., Garcia-Herrera, R., and Trigo, I. F.: Understanding Precipitation Changes in Iberia in Early Spring: Weather Typing and Storm-Tracking Approaches, *J. Hydrometeorol*, 7, 101–113, 2006.
- Penuelas, J., Filella, I., and Comas, P.: Changed plant and animal life cycles from 1952 to 2000 in the Mediterranean region, *Global Change Biology*, 8, 531–544, 2002.
- Penuelas, J., Filella, I., Zhang, X., Llorens, L., Ogaya, R., Lloret, F., Comas, P., Estiarte, M., and Terradas, J.: Complex spatiotemporal phenological shifts as a response to rainfall changes, *New Phytologist*, 161, 837–846, 2004.
- Peco, B. and Espigares, T.: Floristic fluctuations in annual pastures: the role of competition at the regeneration stage, *Journal of Vegetation Science*, 5, 457–462, 1994.
- Pereira, J. S., Mateus, J. A., Aires, L. M., Pita, G., Pio, C., David, J. S., Andrade, V., Banza, J., David, T. S., Paco, T. A., and Rodrigues, A.: Net ecosystem carbon exchange in three contrasting Mediterranean ecosystems - the effect of drought, *Biogeosciences*, 4, 791–802, 2007.
- Perez-Ramos, I. M., Rodriguez-Calcerrada, J., Ourcival, J. M., and Rambal, S.: *Quercus ilex* recruitment in a drier world: A multi-stage demographic approach, *Perspectives in Plant Ecology, Evolution and Systematics*, 15, 106 – 117, 2013.
- Pinol, J., Lledo, M. J., and Escarre, A.: Hydrological balance of two Mediterranean forested catchments (Prades, northeast Spain), *Hydrological Sciences Journal*, 36, 95–107, 1991.
- Rebmann, C., Kolle, O., Heinesch, B., Queck, R., Ibrom, A., and Aubinet, M.: Eddy-covariance: A Practical Guide to Measurement and Data Analysis, chap. Data Acquisition and Flux Calculations, pp. 59 – 84, Springer, Dordrecht, 2012.
- Reichstein, M., Tenhunen, J. D., Rouspard, O., Ourcival, J.-m., Rambal, S., Miglietta, F., Peressotti, A., Pecchiari, M., Tirone, G., and Valentini, R.: Severe drought effects on ecosystem CO<sub>2</sub> and

- H<sub>2</sub>O fluxes at three Mediterranean evergreen sites: revision of current hypotheses?, *Global Change Biology*, 8, 999–1017, 2002.
- Reichstein, M., Tenhunen, J., Rouspard, O., Ourcival, J.-M., Rambal, S., Miglietta, F., Peressotti, A., Pecchiari, M., Tirone, G., and Valentini, R.: Inverse modeling of seasonal drought effects on canopy CO<sub>2</sub>/H<sub>2</sub>O exchange in three Mediterranean ecosystems, *Journal of Geophysical Research: Atmospheres*, 108, 2003.
- Reichstein, M., Falge, E., Baldocchi, D., Papale, D., Aubinet, M., Berbigier, P., Bernhofer, C., Buchmann, N., Gilmanov, T., Granier, A., Grunwald, T., Havrankova, K., Ilvesniemi, H., Janous, D., Knohl, A., Laurila, T., Lohila, A., Loustau, D., Matteucci, G., Meyers, T., Miglietta, F., Ourcival, J.-M., Pumpanen, J., Rambal, S., Rotenberg, E., Sanz, M., Tenhunen, J., Seufert, G., Vaccari, F., Vesala, T., Yakir, D., and Valentini, R.: On the separation of net ecosystem exchange into assimilation and ecosystem respiration: review and improved algorithm, *Global Change Biology*, 11, 1424–1439, 2005.
- Rodrigues, A., Pita, G., Mateus, J., Kurz-Besson, C., Casquilho, M., Cerasoli, S., Gomes, A., and Pereira, J.: Eight years of continuous carbon fluxes measurements in a Portuguese eucalypt stand under two main events: Drought and felling, *Agricultural and Forest Meteorology*, 2011.
- Sala, A. and Tenhunen, J.: Simulations of canopy net photosynthesis and transpiration in *Quercus ilex* L. under the influence of seasonal drought, *Agricultural and Forest Meteorology*, 78, 203 – 222, 1996.
- Santos, J., Corte-real, J., and Leite, S.: Atmospheric large-scale dynamics during the 2004/2005 winter drought in Portugal, *International Journal of Climatology*, 27, 571–586, 2007.
- Santos, J. A., Woollings, T., and Pinto, J. G.: Are the Winters 2010 and 2012 Archetypes Exhibiting Extreme Opposite Behavior of the North Atlantic Jet Stream?, *Mon. Wea. Rev.*, 141, 3626–3640, 2013.
- Schotanus, P., Nieuwstadt, F., and Bruin, H.: Temperature measurement with a sonic anemometer and its application to heat and moisture fluxes, *Boundary-Layer Meteorology*, 26, 81–93, 1983.
- Tenhunen, J.D., Lange, O.L., Gebel, J., Beyschlag, W., and Weber, J.A.: Changes in photosynthetic capacity, carboxylation efficiency, and CO<sub>2</sub> compensation point associated with midday stomatal closure and midday depression of net CO<sub>2</sub> exchange of leaves of *Quercus suber*, *PLANTA*, 162, 193–203, 1984.
- Tenhunen, J.D., Lange, O.L., Harley, P.C., Beyschlag, W., and Meyer, A.: Limitations due to water-stress on leaf net photosynthesis of *Quercus coccifera* in the Portuguese evergreen scrub, *Oecologia*, 67, 23–30, 1985.
- Tenhunen, J.D., Pearcy, R.W., and Lange, O.L.: diurnal variations in leaf conductance and gas exchange in natural environments, in *Stomatal function: Meeting Honolulu, Hawaii, USA, April 1983*, edited by Zeiger, E., Farquhar, G.D., Cowan, I.R., Stanford University press, California, USA, 1987.
- Tenhunen, J.D., Serra, A.S., Harley, P.C., Dougherty, R.L., Reynolds, and J.F., Factors influencing carbon fixation and water-use by Mediterranean sclerophyll shrubs during summer drought, *Oecologia*, 82, 381–393, 1990.
- Thomas, C. and Foken, T.: Re-evaluation of integral turbulence characteristics and their parameterisations, 15<sup>th</sup> Conference on Boundary Layer and Turbulence, 2002.
- Trigo R. M., Juan A. Añel, David Barriopedro, Ricardo García-Herrera, Luis Gimeno, Raquel Nieto, Rodrigo Castillo, Myles R. Allen, and Neil Massey. THE RECORD WINTER DROUGHT OF 2011–12 IN THE IBERIAN PENINSULA. AMERICAN METEOROLOGICAL SOCIETY, BAMS, S41, 2013.
- Twine, T., Kustas, W., Norman, J., Cook, D., Houser, P., Meyers, T., Prueger, J., Starks, P., and Wesely, M.: Correcting eddy-covariance flux underestimates over a grassland, *Agricultural and*

- Forest Meteorology, 103, 279 – 300, 2000.
- Unger, S., Maguas, C., Pereira, J. S., Aires, L. M., David, T. S., and Werner, C.: Partitioning carbon fluxes in a Mediterranean oak forest to disentangle changes in ecosystem sink strength during drought, *Agricultural and Forest Meteorology*, 149, 949 – 961, 2009.
- Valentini, R., Matteucci, G., Dolman, A. J., Schulze, E.-D., Rebmann, C., Moors, E. J., Granier, A., Gross, P., Jensen, N. O., Pilegaard, K., Lindroth, A., Grelle, A., Bernhofer, C., Grunwald, T., Aubinet, M., Ceulemans, R., Kowalski, A. S., Vesala, T., Rannik, U., Berbigier, P., Loustau, D., Guðmundsson, J., Thorgeirsson, H., Ibrom, A., Morgenstern, K., Clement, R., Moncrieff, J., Montagnani, L., Minerbi, S., and Jarvis, P. G.: Respiration as the main determinant of carbon balance in European forests, *Nature*, 404, 861–865, 2000.
- Vargas, R., Sonnentag, O., Abramowitz, G., Carrara, A., Chen, J., Ciais, P., Correia, A., Keenan, T., Kobayashi, H., Ourcival, J.-M., Papale, D., Pearson, D., Pereira, J., Piao, S., Rambal, S., and Baldocchi, D.: Drought Influences the Accuracy of Simulated Ecosystem Fluxes: A Model-Data Meta-analysis for Mediterranean Oak Woodlands, *Ecosystems*, pp. 1–16, 2013.
- Vaz, M., Pereira, J., Gazarini, L., David, T., David, J., Rodrigues, A., Maroco, J., and Chaves, M.: Drought-induced photosynthetic inhibition and autumn recovery in two Mediterranean oak species (*Quercus ilex* and *Quercus suber*), *Tree Physiology*, 30, 946–956, 2010.
- Verbeeck, H., Peylin, P., Bacour, C., Bonal, D., Steppe, K., and Ciais, P.: Seasonal patterns of CO<sub>2</sub> fluxes in Amazon forests: Fusion of eddy covariance data and the ORCHIDEE model, *Journal of Geophysical Research: Biogeosciences*, 116, 2011.
- von Caemmerer, S.: *Biochemical Models of Leaf Photosynthesis*, CSIRO Publishing, 2000.
- Wang, Y.-P. and Leuning, R.: A two-leaf model for canopy conductance, photosynthesis and partitioning of available energy I: Model description and comparison with a multi-layered model, *Agricultural and Forest Meteorology*, 91, 89 – 111, 1998
- Webb, E. K., Pearman, G. I., and Leuning, R.: Correction of flux measurements for density effects due to heat and water vapour transfer, *Quarterly Journal of the Royal Meteorological Society*, 106, 85–100, 1980.
- Werner, C. and Correia, O.: Photoinhibition in cork-oak leaves under stress: Influence of the bark stripping on the chlorophyll fluorescence emission in *Quercus suber* L. *Trees – Structure and Function*, 10: 288–292, 1996.
- Werner, C., Correia, O., and Beyschlag, W.: Two different strategies of Mediterranean macchia plants to avoid photoinhibitory damage by excessive radiation levels during summer drought, *Acta Oecologia*, 20, 15–35, 1999.
- Werner, C., Ryel, R., Correia, O., and Beyschlag, W.: Effects of photoinhibition on whole-plant carbon gain assessed with a photosynthesis model. *Plant, Cell and Environment*, 24: 27–40, 2001.
- Werner, C., Correia, O., and Beyschlag, W.: Characteristic pattern of chronic and dynamic photoinhibition of different functional groups in a Mediterranean ecosystem. *Functional Plant Biology*, 29: 999–1011, 2002.
- Werner, C. and Maguas, C.: Carbon isotope signals as a tracer of functional traits in a Mediterranean macchia plant community, *Functional Plant Biology*, 37, 2010.
- Wilczak, J., Oncley, S., and Stage, S.: Sonic Anemometer Tilt Correction Algorithms, *Boundary-Layer Meteorology*, 99, 127–150, 2001.
- Zhou, S., Duursma, R. A., Medlyn, B. E., Kelly, J. W., and Prentice, I. C.: How should we model plant responses to drought? An analysis of stomatal and non-stomatal responses to water stress, *Agricultural and Forest Meteorology*, 2013.

## CURRICULUM VITAE AND PUBLICATIONS

Stand: 23.9.2014

M. Sc. Maren Dubbert

Date of birth 04.06.1984  
Place of birth Lemgo, Germany  
Nationality German  
Marital Status unmarried partners  
Postal address Frankenwaldstr. 2, 95448 Bayreuth  
E-Mail address [maren.dubbert@uni-bayreuth.de](mailto:maren.dubbert@uni-bayreuth.de)  
[maren-dubbert@gmx.de](mailto:maren-dubbert@gmx.de)  
Mobile +49 17663754620



### Professional appointment

Since 7/12 Scientific co-worker at the chair of AgroEcosystem Research at the University of Bayreuth  
1/10 – 6/12 Scientific co-worker at the chair of Experimental and Systems Ecology at the University of Bielefeld  
10/06 – 12/09 Partially contracted as student and scientific co-worker at the chair of Experimental and Systems Ecology at the University of Bayreuth  
8/03 – 7/04 Freiwilliges Ökologisches Jahr (FÖJ) at the Umweltzentrum Heerser Mühle, Bad Salzuflen

### Academic Record

10/04 – 12/09 Student of biology at the University of Bielefeld, Bachelor and Masters Degree in biology (1.1 and 1 (6-1))  
10/08 – 5/09 ERASMUS student at the University of Lisbon  
1/10 – 6/12 PhD student at the University of Bielefeld, Germany  
7/12 – 7/14 PhD student at the University of Bayreuth, Germany (continuation within the same research project)

### Education

2000 – 2003 secondary school (Marianne-Weber-Gymnasium) in Lemgo  
1994 – 2000 secondary school (Bürgermeister-Gräfer-Realschule) in Lemgo  
1990 – 1994 primary school (Ostschule) in Lemgo

### Grants and prizes

2008-2009 ERASMUS scholarship  
2009-2010 scholarship University Bielefeld, Dep. Of Biology fund for advancement of woman  
2011 Best poster award at the annual meeting of the Arbeitsgemeinschaft stabiler Isotope (ASI)

Publications

Peer-reviewed Journals:

- Dubbert, M., Rascher, K. G., Werner, C. (2012) Species specific differences in temporal and spatial variation in  $\delta^{13}C$  of plant carbon pools and dark-respired CO<sub>2</sub> under changing environmental conditions. *Photosynthesis Research* (DOI 10.1007/s11120-012-9748-3).
- Dubbert, M., Cuntz, M., Piayda, A., Maguas, C., Werner, C. (2013) Partitioning evapotranspiration – Testing the Craig and Gordon model with field measurements of oxygen isotope ratios of evaporative fluxes. *Journal of Hydrology* (DOI 10.1016/j.jhydrol.2013.05.033).
- Dubbert, M., Piayda, A., Cuntz, M., Werner, C. (2014a) Oxygen isotope signatures of transpired water vapor – the role of isotopic non-steady-state transpiration in different seasons under natural conditions. *New Phytologist*.
- Dubbert, M., Mosena, A., Piayda, A., Cuntz, M., Correia, A., Pereira, J. S., Werner, C. (2014b) Influence of tree cover on understory grassland productivity, species development and longevity in a Portuguese cork-oak woodland. *Acta Oecologica*, 59: 35-45.
- Dubbert, M., Piayda, A., Cuntz, M., Correia, A., Costa e Silva, F., Pereira, J. S., Werner, C. (2014c) Stable oxygen isotope and flux partitioning demonstrates understory of an oak savanna contributes up to half of ecosystem carbon and water exchange. *Frontiers in Plant Science*, in press.
- Piayda, A., Dubbert, M., Rebmann, C., Kolle, O., Costa e Silva, F., Correia, A., Pereira, J. S., Werner, C., Cuntz, M. (2014a) Drought impact on carbon and water cycling in a Mediterranean *Quercus suber* L. woodland during the extreme drought event in 2012. *Biogeosciences discussions*.
- Piayda, A., Dubbert, M., Werner, C., Correia A. V., Pereira, J. S., Cuntz, M., (2014b) Influence of wooden tissue and leaf clumping on vertically resolved leaf area index and angular gap probability estimates. Under review *Ecology*.
- Costa e Silva, F., Correia, A.C., Piayda, A., Dubbert, M., Werner, C., Cuntz, M., David, J.S., Pereira, J.S. (2014) Extreme dry winter effects on a *Q. suber* woodland: net ecosystem exchange and tree phenology adjustments. Under review *Agricultural and Forest Meteorology*.

Conference proceedings:

- Rascher, K.G., Máguas, C., Dubbert, M., Müller, M., Werner, c. (2010) Species specific fractionation factors and environmental conditions determine phloem sap  $\delta^{13}C$  signatures. SIBAE, Monte Verità, Switzerland, poster.
- Dubbert, M., Piayda, A., Cuntz, M., Pereira J.S., Werner, C. (2011) Impact of understory and tree vegetation on infiltration and redistribution of rain water in soil of a Mediterranean cork-oak forest (montado). Medecos, Los Angeles, USA, poster.
- Unger, S., Dubbert, M., Mosena, A., Pereira, J.S. Máguas, C., Soares David, T., Aires, L.M., Piayda, A., Cuntz, M., Werner, C. (2011) Understory plays a dominant role determining changes in carbon and water fluxes in a cork-oak woodland (montado). Medecos, Los Angeles, USA, oral presentation.
- Mosena, A., Dubbert, M., Piayda, A., Cuntz, M., Pereira, J.S., Máguas, C., Werner, C. (2011) Dynamics of understory plant composition and diversity in Mediterranean cork-oak forests in correlation to small scale microclimatic changes. Medecos, Los Angeles, USA, poster.
- Dubbert, M., Mosena, A., Cuntz, M., Werner, C. (2011) Impacts of a rain-pulse on short-term dynamics of evapotranspiration and  $\delta^{18}O_{ET}$ . GfÖ Jahrestagung, Oldenburg, Germany, poster.
- Dubbert, M., Piayda, A., Cuntz, M., Werner, C. (2011) Seasonal dynamics in understory evapotranspiration (ET) and soil evaporation (E) and  $\delta^{18}O_{ET}$  and  $\delta^{18}O_E$  in a Mediterranean cork-oak forest. Jahrestagung der Arbeitsgemeinschaft stabiler Isotope – GASIR, Villigen, Switzerland, poster.
- Dubbert, M., Piayda, A., Cuntz, M., Maguas, C., Pereira, J.S., Werner, C. (2012) Partitioning evapotranspiration using stable oxygen isotopes – A field approach with high-frequency Cavity Ring-Down Spectroscopy measurements. JESIUM, Leipzig, poster.
- Piayda, A., Dubbert, M., Cuntz, M., Werner, C., Pereira, J.S. (2012) A comparison of open soil chamber and understory Eddy-covariance measurements of  $CO_2$  and  $H_2O$  exchange in a savannah-type cork-oak stand in Portugal, JESIUM, Leipzig, poster.
- Dubbert, M., Rascher, K.G., Werner, C. (2012) Species specific differences in temporal and spatial variation in  $\delta^{13}C$  of plant carbon pools and dark-respired  $CO_2$  under changing environmental

conditions. JESIUM, Leipzig, poster.

Dubbert, M., Cuntz, M., Piayda, A., Pereira, J.S., Maguas, C., Werner, C. (2012) Using  $\delta^{18}O$  signatures to trace evapotranspiration and partition ecosystem water fluxes, BayCeer workshop, Bayreuth, oral presentation.

Dubbert, M., Rascher, K.G., Maguas, C., Werner, C. (2012) Species-specific differences in temporal and spatial variation in  $\delta^{13}C$  of carbon pools under changing environmental conditions, BayCeer workshop, Bayreuth, poster.

Piayda, A., Dubbert, M., Cuntz, M., Werner Pinto, C., Pereira, J. S., 2012. Leaf area index in a Mediterranean ecosystem, HIGRADE Fall Conference, Leipzig, oral presentation.

Piayda, A., Cuntz, M., Dubbert, M., Werner, C., Pereira, J. S. (2013) Comparison of vertical resolved LAI measurements in a savannah-type cork-oak forest, TR32-HOBE, Bonn, poster.

Dubbert, M., Cuntz, M., Piayda, A., Pereira, J. S., Maguas, C., Werner, C. (2013) Partitioning evapotranspiration – Testing the Craig and Gordon model with field measurements of oxygen isotope ratios of evaporative fluxes, EGU, Wien, oral presentation.

Piayda, A., Cuntz, M., Dubbert, M., Werner, C., Pereira, J. S. (2013) Comparison of vertical resolved leaf area index measurements in an open canopy savannah-type forest, EGU, Wien, oral presentation.

Dubbert, M., Cuntz, M., Piayda, A., Maguas, C., Werner, C., (2013) Partitioning evapotranspiration in a Mediterranean oak savannah – Validating the Craig and Gordon model with field measurements of oxygen isotope ratios of evaporative fluxes. GfÖ, Potsdam, poster.

Dubbert, M., Mosena, A., Piayda, A., Cuntz, M., Correia, A., Perreira, J.S., Werner, C. (2013) Influence of tree cover on herbaceous layer productivity, species development and longevity in a Portuguese cork-oak woodland. GfÖ, Potsdam, oral presentation.

Nay-Htoon, B., Dubbert, M., Ko, J., Gebauer, G., Werner, C. (2013) Partitioning Evapotranspiration of rain-fed dryland rice (*Oryza sativa* L) based on oxygen isotope ratio of evaporative fluxes. BayCeer workshop, Bayreuth, poster.

Piayda, A., Dubbert, M., Rebmann, C., Kolle, O., Costa e Silva, F., Correia, A., Pereira, J.S., Werner, C., Cuntz, M. (2013) Water balance and carbon sink strength of a European savannah-type

woodland during the drought year 2012. BayCeer workshop, Bayreuth, poster.

Dubbert, M., Piayda, A., Pereira, J.S., Cuntz, M., Werner, C. (2013) Linking water and carbon fluxes in a Mediterranean cork-oak woodland using a combined flux and  $\delta^{18}O$  partitioning approach. BayCeer workshop, Bayreuth, poster.

Dubbert, M., Piayda, A., Cuntz, M., Werner, C. (2013) Validating the Craig and Gordon model with field measurements of oxygen isotope ratios of evaporative fluxes. BayCeer workshop, Bayreuth, poster.

Dubbert, M., Piayda, A., Pereira, J.S., Cuntz, M., Werner, C. (2013) Linking water and carbon fluxes in a Mediterranean oak woodland using a combined flux and  $\delta^{18}O$  partitioning approach. AGU 2013, San Francisco, oral presentation.

Piayda, A., Dubbert, M., Rebmann, C., Kolle, O., Costa e Silva, F., Correia, A., Pereira, J.S., Werner, C., Cuntz, M. (2013) Water balance and carbon sink strength of a European savannah-type woodland during the drought year 2012, AGU 2013, San Francisco, poster.

Dubbert, M., Piayda, A., Costa e Silva, F., Correia, A., Pereira, J.S., Cuntz, M., Werner, C. (2014) Partitioning water fluxes and the link to ecosystem productivity using stable oxygen isotopes in a Mediterranean oak woodland. EGU, Vienna, oral presentation.

Dubbert, M., Piayda, A., Cuntz, M., Werner, C. (2014) Oxygen isotope signatures of transpired water vapor - the role of isotopic non-steady-state transpiration of Mediterranean cork-oaks (*Quercus suber* L.) under natural conditions. EGU, Vienna, poster.

Piayda, A., Dubbert, M., Rebmann, C., Kolle, O., Costa e Silva, F., Correia, A., Pereira, J.S., Werner, C., Cuntz, M. (2014) Drought influence on carbon and water cycling in a Mediterranean *Quercus suber* L. woodland during the drought year 2012. EGU, Vienna, poster.

Theses:

Dubbert, M. (2007) Untersuchung zur Ammonium- und Nitrataufnahmeeffizienz verschiedener Arten im Ökosystem Binnendünen mit Hilfe von  $^{15}N$ -Labelling. Bachelor thesis University Bielefeld (together with S. Jerrentrup).

Dubbert, M. (2009) Species-specific differences in photosynthetic and post-photosynthetic fractionation processes, altering  $\delta^{13}C$  on temporal and spatial scales. Master thesis University Bielefeld.





## **DECLARATION**

(Eidesstattliche) Versicherungen und Erklärungen

(§5 Nr. 4 PromO)

Hiermit erkläre ich, dass keine Tatsachen vorliegen, die mich nach den gesetzlichen Bestimmungen über die Führung akademischer Grade zur Führung eines Doktorgrades unwürdig erscheinen lassen.

(§8 S. 2 Nr. 5 PromO)

Hiermit erkläre ich mich damit einverstanden, dass die elektronische Fassung meiner Dissertation unter Wahrung meiner Urheberrechte und des Datenschutzes einer gesonderten Überprüfung hinsichtlich der eigenständigen Anfertigung der Dissertation unterzogen werden kann.

(§8 S. 2 Nr. 7 PromO)

Hiermit erkläre ich eidesstattlich, dass ich die Dissertation selbständig verfasst und keine anderen als die von mir angegebenen Quellen und Hilfsmittel benutzt habe. Ich habe die Dissertation nicht bereits zur Erlangung eines akademischen Grades anderweitig eingereicht und auch nicht bereits diese oder eine gleichartige Doktorprüfung endgültig nicht bestanden.

(§8 S. 2 Nr. 9 PromO)

Hiermit erkläre ich, dass ich keine Hilfe von gewerblichen Promotionsberatern bzw. –vermittlern in Anspruch genommen habe und auch künftig nicht nehmen werde.

---

Maren Dubbert

Bayreuth, März 2014